THE CHARACTERISTICS AND ORIGIN OF THE HOIDAS LAKE REE DEPOSIT

A Thesis Submitted to the College of
Graduate Studies and Research
In Partial Fulfillment of the Requirements
for the Degree of
Master of Science
in the
Department of Geological Sciences
University of Saskatchewan
Saskatoon

By

Kimberley Michelle Halpin

PERMISSION TO USE

In presenting this thesis in partial fulfillment of the requirements for a Postgraduate degree from the University of Saskatchewan, I agree that the Libraries of this University may make it freely available for inspection. I further agree that permission for copying of this thesis in any manner, in whole or in part, for scholarly purposes may be granted by the professor or professors who supervised my thesis work or, in their absence, by the Head of the Department or the Dean of the College in which my thesis work was done. It is understood that any copying, publication, or use of this thesis or parts thereof for financial gain shall not be allowed without my written permission. It is also understood that due recognition shall be given to me and to the University of Saskatchewan in any scholarly use which may be made of any material in my thesis.

Requests for permission to copy or to make other use of material in this thesis in whole or part should be addressed to:

Head of the Department of Geological Sciences
University of Saskatchewan
Saskatoon, Saskatchewan
S7N 5E2

ABSTRACT

The Hoidas Lake Rare Earth Element (REE) Deposit is one of several REE showings which are spatially associated with a regional-scale fault system that cuts through the Rae Province in northern Saskatchewan. The showings occur along the Hoidas-Nisikkatch fault, believed to be a subsidiary of the Black Bay Fault, and consist of multiple REE-enriched veins. Surface outcrops and drilling have delineated a vein system, called the JAK zone, which extends for over 1 km along strike, with the system remaining open both along strike and down dip. The majority of the REE are hosted by fluorapatite and allanite-(Ce), although there are also minor amounts of monazite, bastnaesite and chevkinite which can contain significant concentrations of REE. The veins are dominantly LREE-enriched, specifically La, Ce, and Nd.

The mineralization at Hoidas Lake is complex, with the chemical and mineralogical compositions changing with each vein generation. The earliest veins consist of REE-bearing allanite and chevkinite which occur in association with clinopyroxene, titanite, and hyalophane. The allanite-rich veins are followed by veins dominated by red or green apatite, both of which are typically brecciated. Finally, there is a late apatite which crosscuts all previous vein generations. Each of the distinct apatite generations shows discrete chemical variations, particularly in their light rare earth element content, with the total rare earth oxide content ranging from approximately 1.5% in the oldest apatite to as much as 5% in the green apatite.

The majority of the apatite and allanite crystals are strongly zoned, reflecting the chemical changes in the mineralizing system through time and, particularly in the earliest vein generations, there are signs of hydrothermal alteration. The early apatite generations typically show the development of monazite inclusions which suggests interaction with hydrothermal fluids, as do the REE-poor rims and bastnaesite alteration observed in the majority of the allanites.

The veins are fault controlled and are interpreted to be late magmatic-hydrothermal in origin, with the fluid derived from a magmatic source at depth. Although the exact source of the fluids remains uncertain, the high concentration of REE, as well as Sr and Ba, and a relative depletion in high field strength elements suggests that the mineralization may be related to either an alkali or carbonatitic source.

ACKNOWLEDGEMENTS

I owe a huge amount of gratitude to Dr. Ansdell for his guidance, support and particularly for his patience and encouragement throughout this experience. The numerous, often impromptu, discussions greatly enhanced the thesis. I would also like to thank Dr. Yuanming Pan and Dr.Tom Kotzer for their advice, comments and suggestions. John Pearson, with Great Western Minerals, also provided valuable insight and encouragement during this project, and is also thanked for his flexibility during the transitional period as I finished my thesis and started work.

Financial and logistical support for this project was graciously provided by Great Western Minerals. Additional financial support was provided by the Society of Economic Geologists, NSERC and the University of Saskatchewan in the form of a Student Research Grant, Canadian Graduate Scholarship and Graduate Scholarship, respectively. The NSERC Discovery Grant and the University of Saskatchewan Department Head's Research Grant, both awarded to Dr. Ansdell, provided additional financial support.

Field assistance was provided by Jillian Christman, Doug Engdahl and Adam Engdahl and I would like thank them for their help, especially as they often worked under less than ideal conditions without complaint. I am also grateful for the technical support I received from Blaine Novakovski, Tom Bonli, Jim Rosen, and Jianzhong Fan at the University of Saskatchewan and Reid MacDonald and Richard Hogan at Great Western Minerals.

Finally, I would like to thank my family and friends for all their love and support, not only during the development of my thesis, but throughout my many years at University. To my friends who kindly pretended to be interested in my rambling discussions about my thesis, and who provided distractions when necessary, and to my family whose love, support, and encouragement has always made life easier.

TABLE OF CONTENTS

PERMISSION TO USE ..... **i**
ABSTRACT ..... **ii**
ACKNOWLEDGEMENTS ..... **iii**
TABLE OF CONTENTS ..... **iv**
LIST OF TABLES ..... **viii**
LIST OF FIGURES ..... **ix**

CHAPTER 1 INTRODUCTION **1**
1.1 PURPOSE OF THESIS 1
1.2 OBJECTIVES 2
1.3 METHODOLOGY 2
1.4 SAMPLING TECHNIQUE 3
1.5 LOCATION AND ACCESSIBILITY 4
1.6 PREVIOUS GEOLOGICAL WORK 5
1.7OVERVIEW OF THE HOIDAS LAKE DEPOSIT 6
1.8 LAYOUT OF THESIS 7

CHAPTER 2 CURRENT UNDERSTANDING OF REE DEPOSITS **8**
2.1 INTRODUCTION 8
2.2 HISTORIC EMPHASIS OF RESEARCH 8
2.3 REE DEPOSIT TYPES AND GEOLOGIC SETTING 9
2.4 THE DEBATE OVER THE ORIGINS OF REE DEPOSITS 14
2.5 REE IN MAGMATIC SYSTEMS 14
2.5.1 ORTHOMAGMATIC FLUIDS 15
2.6 REE BEHAVIOR IN HYDROTHERMAL SETTINGS 16
2.6.1 COMPLEXATION OF REE 16
2.6.2 INFLUENCES OF TEMPERATURE AND PRESSURE 17
2.6.3 INFLUENCES OF pH AND FLUID COMPOSITION 18
2.7 REE BEHAVIOR IN METAMORPHIC ENVIRONMENTS 21
2.8 ENRICHMENT OF REE IN HYDROTHERMAL SYTSEMS 21
2.9 AREAS REQUIRING FURTHER RESEACH 23

CHAPTER 3 GEOLOGICAL SETTING **24**
3.1 INTRODUCTION 24
3.2 REGIONAL GEOLOGY 26
3.2.1 ARCHEAN CRATONS AND PALEOPROTEROZOIC OROGENS 26
3.2.2 POST-COLLISIONAL SEDIMENTATION, MAGMATISM AND DEFORMATION 29
3.3 LOCAL GEOLOGICAL SETTING 31
3.3.1 ECONOMIC POTENTIAL OF THE SOUTHERN RAE 32

CHAPTER 4 DEPOSIT GEOLOGY **34**
4.1 INTRODUCTION 34
4.2 JAK ZONE GEOLOGY 34

4.2.1 STRUCTURE 39
4.2.2 METAMORPHISM 43
4.3 REE SHOWINGS 44
4.3.1 JAK ZONE MINERALIZATION 44
4.3.1.1 DIOPSIDE – ALLANITE VEINS 46
4.3.1.2 RED APATITE BRECCIA 48
4.3.1.3 GREEN APATITE BRECCIA 49
4.3.1.4 COARSE RED APATITE 51
4.3.2 ADDITIONAL REE SHOWINGS IN THE HOIDAS LAKE AREA 52
4.3.2.1 HOIDAS SOUTH SHOWINGS 52
4.3.2.2 NISIKKATCH SHOWINGS 54
4.4 PARAGENESIS OF THE HOIDAS LAKE DEPOSIT 56

CHAPTER 5 HOST ROCK CHARACTERISTICS 60
5.1 INTRODUCTION 60
5.2 MINERALOGICAL AND PETROGRAPHIC FEATURES 60
5.2.1 TONALITE 60
5.2.2 GRANODIORITE 62
5.2.3 MONZOGRANITE 63
5.2.4 PEGMATITES 65
5.2.5 LAMPROPHYRES 68
5.3 WHOLE ROCK GEOCHEMISTRY 68
5.3.1 XRF RESULTS 70
5.3.2 MAJOR ELEMENT CONCENTRATIONS 70
5.3.2.1 GRANITOIDS 70
5.3.2.2 PEGMATITES 71
5.3.2.3 LAMPROPHYRES 74
5.3.3 TRACE ELEMENT CONCENTRATIONS 75
5.3.3.1 GRANITOIDS 75
5.3.3.2 PEGMATITES 75
5.3.3.3 LAMPROPHYRES 76
5.4 RELATION OF THE HOIDAS LAMPROPHYRES TO THE DUBAWNT LAMPROPHYRES 78
5.5 POTENTIAL RELATION OF THE HOST ROCKS TO THE MINERALIZATION AT HOIDAS LAKE 82

CHAPTER 6 MINERALOGY AND CHEMISTRY OF THE VEINS 84
6.1 INTRODUCTION 84
6.2 MINERALOGICAL AND PETROGRAPHIC FEATURES 85
6.2.1 DIOPSIDE-ALLANITE VEINS 85
6.2.2 RED APATITE BRECCIA 90
6.2.3 GREEN APATITE BRECCIA 92
6.2.4 COARSE RED APATITE 93
6.3 CHEMICAL COMPOSITION OF THE REE-BEARING MINERALS 94
6.3.1 ALLANITE 94
6.3.2 APATITE 100
6.3.2.1 RED APATITE BRECCIA 100

6.3.2.2 GREEN APATITE BRECCIA 103
6.3.2.3 COARSE RED APATITE 105
6.3.2.4 COMMON FEATURES TO ALL APATITES 106
6.3.3 TITANITE AND CHEVKINITE 108
6.3.4 MONAZITE 112
6.3.5 REE CARBONATES 114
6.4 CHEMICAL COMPOSITION OF THE GANGUE MINERALS 114
6.4.1 CLINOPYROXENE 114
6.4.2 AMPHIBOLE 116
6.4.3 FELDSPAR 116
6.5 SUMMARY 118

CHAPTER 7 CONSTRAINTS ON THE ORIGIN OF THE MINERALIZATION AND THE SOURCE OF THE RARE EARTH ELEMENTS 120
7.1 INTRODUCTION 120
7.2 EXISTING THEORIES ON THE ORIGIN OF THE HOIDAS LAKE MINERALIZATION 121
7.3.1 GRANITIC ROCKS 123
7.3.2 PEGMATITES 124
7.3.3 MAFIC OCCURENCES IN THE ENA DOMAIN 125
7.3.4 RELATION TO OTHER ROCK TYPES 128
7.4 VEIN COMPOSITIONAL AND TEXTURAL CONSIDERATIONS 130
7.4.1 CHEVKINITE 131
7.4.2 HYALOPHANE 131
7.4.3 DIOPSIDE 133
7.4.4 ALLANITE 135
7.4.5 TITANITE 138
7.4.6 APATITE 139
7.5 EVOLUTION OF THE MINERALIZING SYSTEM 142
7.5.1 COMPOSITIONAL VARIATIONS IN THE MINERALIZING SYSTEM 143
7.5.2 CHANGE IN REDOX CONDITIONS 145
7.5.3 TRANSPORTATION OF THE REE 145
7.5.4 TEMPERATURE OF FORMATION 146
7.6 KEY CHARACTERISTICS OF THE HOIDAS LAKE REE MINERALIZATION 147
7.6.1 LATE MAGMATIC-HYDROTHERMAL MINERALIZATION 147
7.6.2 IMPORTANCE OF STRUCTURES 148
7.6.3 POTENTIAL RELATION TO MANTLE-DERIVED MAGMATISM 148
7.7 ORIGINS OF THE HOIDAS LAKE MINERALIZATION 151
7.8 RELATION TO OTHER REE SHOWINGS IN THE REGION 152

CHAPTER 8 SUMMARY 154
8.1 CONCLUSIONS 154
8.2 RECOMMENDATIONS FOR FURTHER RESEARCH 155
8.2.1 REGIONAL GEOLOGICAL MAPPING 155
8.2.2 GEOCHRONOLOGY 155
8.2.3 FLUID COMPOSITION 156

REFERENCES **158**
APPENDIX A PETROGRAPHIC DESCRIPTIONS **A-1**
APPENDIX B ANALYTICAL TECHNIQUES **B-1**

LIST OF TABLES

Table 2.1 REE Deposits 11
Table 5.1 Summary of Host Rock XRF Results 71
Table 5.2 Summary of XRF and ICPMS Results for Pegmatites and Lamprophyres 73
Table 5.3 Major element composition of the average Dubawnt Lamprophyre compared to the Hoidas Lake Lamprophyres 80
Table 6.1 Representative EPMA data from the recognized apatite generations 102

LIST OF FIGURES

Figure 2.1 Global rare earth element production from 1950 to 2000. 9
Figure 2.2 Setting of REE Deposits 13
Figure 2.3 REE Speciation 19
Figure 3.1 Regional geological map of the western portion of the Canadian Shield 25
Figure 3.2 Domains of the southern Rae Province 32
Figure 4.1 Geological map of the Hoidas Lake area 36
Figure 4.2 Examples of some of the pegmatites in the Hoidas Lake area. 37
Figure 4.3 Two examples of outcropping lamprophyre 40
Figure 4.4 Alteration present at the contact between the lamprophyre and the surrounding granodiorite gneiss 41
Figure 4.5 Historical REE showings 45
Figure 4.6 Diopside-allanite vein 47
Figure 4.7 Close up of the vein from figure 4.6 48
Figure 4.8 Alteration of a large pyroxene crystal to amphibole 48
Figure 4.9 Examples of the red apatite breccia 50
Figure 4.10 Green apatite breccia 51
Figure 4.11 Small vein of coarse red apatite in a diopside-allanite vein 52
Figure 4.12 Surface expression of the Hoidas-Nisikkatch fault 53
Figure 4.13 Deformed veins at Hoidas South 55
Figure 4.14 Narrow boudinaged diopside-allanite vein 57
Figure 4.15 Preliminary paragenesis of the Hoidas Lake REE vein system 59
Figure 5.1 Outcrop samples locations 61
Figure 5.2 Example of granodiorite from sample HL0709-4 62
Figure 5.3 Monzogranite from samples HL0709-3 and HL0709-7 64
Figure 5.4 Image of the HS-Pegm 66
Figure 5.5 Granitic pegmatites 67
Figure 5.6 Lamprophyre in thin section 69
Figure 5.7 Element variation diagrams 72
Figure 5.8 Shand's Index 74
Figure 5.9 Trace elements variations plotted against SiO_2 76
Figure 5.10 Discrimination diagrams 77
Figure 5.11 REE plot of selected samples 78
Figure 5.12 MORB-normalized spider diagram comparing the Hoidas Lake and Dubawnt lamprophyres 81
Figure 5.13 Chondrite normalized REE plot of the Hoidas Lake and Dubawnt lamprophyres 82
Figure 6.1 Examples of the variation observed in the Diopside-Allanite veins 86
Figure 6.2 Large allanite crystal from sample 782076 87
Figure 6.3 Examples of chevkinite in allanite 89
Figure 6.4 Two examples of the red apatite breccia 91
Figure 6.5 Image of the green apatite breccia 93
Figure 6.6 Image of the coarse red apatite 94
Figure 6.7 Compositional variations observed in the Hoidas Lake allanites 95
Figure 6.8 REE distribution of the Hoidas Lake allanite 96
Figure 6.9 Example of the decrease in REE content from the core to rim an allanite 98
Figure 6.10 Back scattered electron (BSE) images of allanites 99

Figure 6.11 BSE image of a red apatite breccia 101
Figure 6.12 Variation between total REE content and Ce oxide between the four zones of red apatite 101
Figure 6.13 BSE of green apatite 103
Figure 6.14 BSE image of green apatite 104
Figure 6.15 REE Composition of the green apatite 104
Figure 6.16 Coarse red apatite 105
Figure 6.17 REE composition of the coarse red apatite 106
Figure 6.18 Apatite composition of the Hoidas Lake apatites 107
Figure 6.19 Substitution of REE into the apatite structure 107
Figure 6.21 Titanite (Ti) crystal surrounded by zoned, altered allanite 109
Figure 6.22 Zoned chevkinite crystal surround by allanite 110
Figure 6.23 Chevkinite-Perrierite Discrimination 111
Figure 6.24 Example of monazite inclusions in a clast from the red apatite breccia 113
Figure 6.25 Example of monazite (Mz) with the green apatite 113
Figure 6.26 Compositional variation of the REE-carbonates 115
Figure 6.27 Composition of the clinopyroxene 115
Figure 6.28 Typical clinopyroxene from the diopside-allanite vein generation 116
Figure 6.29 Composition of the feldspar 117
Figure 6.30 Hyalophane altering to Ba-Sr Sulphate 118
Figure 7.1 REE content of the veins compared to the paralkaline pegmatite and lamprophyre. 126
Figure 7.2 Apatite discrimination plot 130
Figure 7.3 Composition of the feldspar 133
Figure 7.4 Compositional variations observed in the Hoidas Lake allanites 136
Figure 7.5 Variation in REE and Ti content of the Hoidas Lake apatites 137
Figure 7.6 Monazite inclusions in apatite 142
Figure 7.7 Trace element composition of the REE-bearing vein generations 150
Figure 7.8 Potential origin of the mineralization at Hoidas Lake 151

CHAPTER 1
INTRODUCTION

1.1 PURPOSE OF THESIS

Significant concentrations of rare earth elements (REE) are found only occasionally, as suggested by the limited number of REE mines. The key issue is that, although the mineralogy of the REE is quite extensive, there are only a limited number of minerals which are capable of hosting major quantities of REE, and these minerals are only rarely found in significant economic concentrations (Mariano, 1989). Traditionally, economic concentrations of REE were found predominantly in monazite-bearing placer deposits, or in association with carbonatites, and therefore the emphasis of most REE deposit research has focused on these two deposit types, to the detriment of other potentially economic sources of REE mineralization (Giere, 1996). Even for some of the most well known and thoroughly researched REE deposits conjecture still remains as to the details of the genesis of many of these unusual deposit types.

The Hoidas Lake REE Deposit is an interesting, instructive deposit with economic potential. The mineralogy found at Hoidas Lake is unique, as reconnaissance investigations indicate that the REE are hosted mainly by allanite and apatite, as opposed to the more typical monazite or bastnaesite host minerals. The unusual mineralogy observed at Hoidas Lake, and the multiple vein generations, provides a valuable opportunity to enhance the available knowledge about the formation and evolution of REE deposits. There is also the potential to add to the existing knowledge about the unusual minerals which host the REE.

In addition to its academic value, the Hoidas Lake REE Deposit has significant economic potential; should the site be brought into production it will be the only currently operating rare earth element mine in North America. This may be extremely significant for the Canadian economy as rare earth elements are crucial components in many high-technology products. Economic rare earth element deposits are rare, and therefore the results of this research will assist in developing new potential targets for mineral exploration, which will help meet the global demand for REE as technology advances.

1.2 OBJECTIVES

The overall objective of this project was to provide constraints on the genesis and evolution of the Hoidas Lake REE Deposit, which will aid in the development of a petrogenetic model for this unique deposit type. Of particular interest are the source of the REE, the timing of the mineralization, and the controlling factors for mineralization. The focus of this project was therefore a detailed examination of the vein system in order to understand the mineralogical and geochemical variations through time. To achieve the desired objectives a multifaceted approach was required, involving the examination of mineralogical, petrological, and geochemical relationships within the Hoidas Lake REE Deposit by means of geological mapping, petrography, geochemistry, and electron-probe microanalysis.

1.3 METHODOLOGY

Geological mapping and core logging of selected drill holes which intersect the mineralization provided basic information on the geologic framework of the area, and provided familiarity with the various styles of mineralization. Fieldwork helped to determine the number of vein generations and their respective mineralogy. Samples from both outcrop and drill core were used to establish the macroscopic relationships, with the most instructive samples being selected for more detailed analysis.

The compositional and textural relationships between minerals in the deposit were examined using transmitted light microscopy and electron microprobe analysis. Microscopic and back-scattered electron analysis was used to resolve the relative timing of mineral growth which aided in determining the petrogenetic history of the vein system. Specific minerals, particularly apatite and allanite, were analyzed using electron microprobe wavelength dispersive analysis to ascertain their chemical composition, and thus identify chemical changes in the vein system with time. Finally, the information contained in the mineralogical, textural, and geochemical data sets were combined to construct a genetic model for this unique deposit type.

1.4 SAMPLING TECHNIQUE

Since 2001 one hundred and twenty-four drill holes have been completed on the property, in addition to number of shallow surface trenches. The drill holes have been evenly distributed along a grid system which covers the JAK zone, the main zone of mineralization discovered to date at Hoidas Lake. In addition to the extensive drilling in the JAK zone there are also a number of surface showings. Although there is only moderate exposure of the vein system at surface, the veins can often be traced along strike for several meters. The exposure of the vein system at surface has been enhanced in fourteen locations by systematic trenching, in some instances allowing a three dimensional view of the vein system. Finally, there is also a 5 m by 3 m bulk sample pit which has only been partially refilled, allowing a more complete view of the vein system at surface than that found in the smaller trenches.

In the summer of 2006 the preliminary field work involved the selection of nineteen representative holes from along the JAK zone based on information obtained from the existing drill logs. Initially, holes which recorded good vein intersections with a variety of vein types were selected. Consideration was also given to holes with other anomalous features, such as features showing relative age relationships, or holes which contained high grade assay results. One of the key problems encountered at this stage was that in many of the holes the mineralized interval had been entirely removed, if not the entire hole taken, for analysis needed for the ongoing pre-feasibility study being conducted by Great Western Minerals, the owner of the property. Despite this obstacle, consistent coverage of the mineralized zone was still possible, with no more than 75m between the holes sampled along strike. From each of the sampled holes representative samples of the various vein types were collected, as well as samples which contain evidence of the relationships between vein generations. Selected samples of unusual mineralogy or alteration were taken when they occurred. Finally, altered and unaltered representative samples of the host rocks were selected.

During the 2007 field season additional samples of the vein material were collected from fresh, unsplit core to help characterize the relationships and contacts between the various vein generations. In selected cases where there was a particularly informative vein intersection, which clearly shows the transitions or cross cutting

relationships between the vein generations, entire boxes of core were taken. Outcrop samples for geochronology and geochemistry were collected from the pegmatites and lamprophyres in the surrounding area. Outcrop samples of the host rock were taken perpendicular to the strike of the vein systems up to 500 m away from the main zone of mineralization. The spacing of the sampling along these lines is somewhat erratic, as it was dictated by the location of the outcrop.

Additional samples of vein material were taken from the mineralized showings at both Hoidas South, which is approximately 3 km south of the JAK zone, and Nisikkatch Lake, which is approximately 10 km south of the JAK zone. These samples were obtained in an attempt to check for potential changes in either the style or chemistry of the mineralization along the strike of the vein system. No samples of the vein system north of the JAK zone were collected as previous attempts to locate historic showings in this area were unsuccessful.

The aim of the fieldwork was to assess the nature of the host rocks and their relation to the vein system, the distribution and geometry of the veins, and to document vein characteristics, including macroscopic structural, textural, and composition relationships both within individual vein generations and in the system as a whole. The veins were initially grouped into categories, or generations, based on their compositional and morphological features; major mineralogical and textural features were established in the field and later refined through more detailed petrographic and geochemical analysis.

1.5 LOCATION AND ACCESSIBILITY

The Hoidas Lake Project is located on the northwestern shore of Hoidas Lake in northern Saskatchewan. Hoidas Lake is located 60 km northeast of Uranium City, Saskatchewan. The project area is accessible year-round by scheduled flights from major cities in southern Saskatchewan to either Stony Rapids, which is approximately 130 km southeast of Hoidas Lake, or Uranium City, which is 56 km southwest of Hoidas Lake, and then by float or ski-equipped aircraft to Hoidas Lake . There is also an all-weather road to Stony Rapids with winter road access to Uranium City. Due to active uranium mining and exploration in the area, both Stony Rapids and Uranium City have extensive infrastructure in

place including power, commercial and charter aircraft service.

1.6 PREVIOUS GEOLOGICAL WORK

The earliest mapping of the region was carried out by C. Camsell in 1916 during a reconnaissance mapping project which extended from Lake Athabasca in Saskatchewan to Great Slave Lake in the Northwest Territories. Camsell proposed the term “Tazin Series” for the metamorphosed and deformed Precambrian sedimentary and volcanic rocks as well as for the subsequent intrusions. In 1936 F.J Alcock conducted systematic reconnaissance mapping of the area north of Lake Athabasca up to the Northwest Territories border (Koster, 1965). Alcock modified the concept of Camsell’s “Tazin Series” to separate the metasedimentary rocks from the intrusions by proposing that the metasedimentary rock be named the “Tazin Group” and the younger granitoids by referred to as the “post-Tazin” plutons (Alcock, 1936). More recent regional mapping was completed in the early 1960’s by Koster, with the Hoidas Lake area mapped in 1965 (Koster, 1965).

The REE showings at Hoidas Lake were discovered in 1950 as a result of post-World War Two uranium exploration. In 1950 Jack Lane discovered the allanite showing at Hoidas Lake and staked the JAK claims to cover the showings and also the surrounding area. A sample from the main allanite showing at the north end of Hoidas Lake assayed by the Chief Mineral Resources Division in Ottawa ran: 2% Th, 0.5% Y, 6.0% La, 7.0% Ce and 0.1% Gd. Trenching of the main allanite showing was carried out by Lane, but few details were filed for assessment purposes.

The veins were next examined by D.D. Hogarth of McGill University, Montreal, Quebec, in 1953 during work done by the Geological Survey of Canada. Various samples were collected at this time, including a sample of allanite from one of the Hoidas Lake showings that ran 12.03% REE, predominantly Ce (Hogarth, 1957). This work, combined with the results obtained from an airborne radiometrics and electromagnetic survey flown by Canadian Areo Service Limited in 1961, lead Goble Exploration Syndicate to stake six claims in 1965 to cover the main allanite showings. A ground survey completed at that time reported that the allanite showings varied between 2 meters to 5 meters in width and had an approximate exposed strike length of 425 meters.

In 1980 Kintla Explorations Limited obtained the six claims to explore for

uranium and thorium. After a brief prospecting period, the property laid dormant until 1996 when Daren Industries Ltd. staked claim S-10987 to cover the main allanite showing on Hoidas Lake. This was the first time a claim was staked for the purpose of exploring for an economic deposit of REE. A sample taken from the main showing ran 14.58% REE, with 7.12% being Ce and 3.7% La. Daren Industries Ltd. carried out preliminary metallurgical testing of the allanite samples and the results showed that recovery of 97.6% of the REEs hosted by allanite was possible using gravimetric separation followed by a cold acid leach.

The Hoidas Lake property was optioned by Great Western Gold Corp., which is now Great Western Minerals Group Ltd., from Daren Industries Ltd. in 1999. Shortly after acquiring the property a sampling and trenching program was carried out on the main allanite showing, the JAK Zone. The preliminary results indicated multiple mineralized zones which contained significant concentrations of REE. In 2001 the preliminary work was followed up by a 16 hole, 1,100 meter drill program to delineate the JAK Zone. Additional assaying and metallurgical testing was completed on the samples obtained from the drilling. To date over one hundred and twenty four drill holes have been completed on the property, as well as various regional prospecting programs and bulk sampling of the JAK Zone.

1.7 OVERVIEW OF THE HOIDAS LAKE DEPOSIT

The Hoidas Lake REE deposit is an anastomosing vein system hosted by intrusive rocks of granitic to tonalitic composition. The vein system consistently dips eastward and parallels the Hoidas-Nisikkatch fault, a subsidiary of the regional scale Black Bay Fault. The REE are hosted predominantly by apatite and allanite, although there are minor amounts of chevkinite, bastnaesite, and monazite. The JAK zone is one of 26 REE showings along the Hoidas-Nisikkatch fault system and to date it is the only zone which has been delineated by drilling. As confirmed by drilling, the JAK zone extends for 1000 m along strike and has an approximate width of 75m, although the vein system remains open both along strike and down dip. The veins are enriched in light rare earth elements, specifically La, Ce, and Nd, and are also enriched in Ba, Sr, and Y. Grades reported from whole rock assays average from between 2% and 4% Total Rare

Earth Oxide (TREO) with higher grade intersections averaging between 5% and 6%TREO (Pearson, 2006).

1.8 LAYOUT OF THESIS

The basic layout of the thesis will consist of a brief review of the current understanding of REE deposits (Chapter 2) to provide a general framework for the Hoidas Lake REE Deposit. The review of the current state of knowledge is followed by a detailed description of the features of the Hoidas Lake Deposit, progressing from the large scale, regional setting of the deposit (Chapter 3) to the local geological features (Chapter 4) to the detailed mineralogical and chemical features of the mineralization (Chapters 5 and 6). Finally, theories on the origins of the mineralization at Hoidas Lake will be discussed (Chapter 7), as well as the recommendations for further research (Chapter 8).

CHAPTER 2
CURRENT UNDERSTANDING OF REE DEPOSITS

2.1 INTRODUCTION

Rare earth element deposits occur in a wide range of geologic settings and can be either epigenetic or syngenetic. The variety of geological associations, when combined with the limited number of deposits which have been researched in detail, make exploration for these deposits exceedingly difficult (Neary and Highly, 1984). Knowledge of the known economic, as well as non-economic, sources of REE is an essential component in attempting to understand the origin and distribution of these deposits. The link between geological features, of all scales, and the occurrence of a mineral deposit is essential for resource identification and exploration.

2.2 HISTORIC EMPHASIS OF RESEARCH

The emphasis of much of the REE deposit research to date has focused on either placer or carbonatite deposits, to the detriment of other potentially economic REE sources (Giere, 1996). Historically, these two deposits types have been the main economic sources of REE production, with monazite placer deposits as the dominant source of REE until the mid-1960. After 1964 the carbonatite at Mountain Pass, USA became the main source of REE production, and from this point onwards carbonatites or carbonatite associated deposits have accounted for the majority of REE production. In the late 1980's to early 1990's China surpassed the USA as the main REE producer (Fig. 2.1) (Haxel et al., 2002).

The monazite, or more rarely xenotime, placer deposits which accounted for most of the early REE production were appealing for a number of reasons. One of the key features of these deposits is often the ease of mining, as opposed to high REE content (Jackson and Christiansen, 1993). The REE content of many of these deposits is actually quite low, with monazite composing between 0.1 and 2% of the placer deposit (Morteani, 1991). In many placer deposits the REE are often found in conjunction with other forms of mineralization; in these cases it possible to recover REE as a by-product, enabling economic recovery despite the low REE concentrations (Wu et al., 1996). A

necessary consideration in this sort of production is that the economics of REE production is dependent on the continued economic production of another commodity.

Since the development of Mountain Pass, carbonatites have remained the main source of REE production. These deposits can contain wt.% levels of REE and are typically strongly enriched in LREE. Although in many cases the REE enrichment observed in carbonatites is of primary igneous origin, such as the bastnaesite at Mountain Pass, there are also several examples where the REE enrichment associated with the carbonatites is the result of either hydrothermal or supergene processes, further enhancing the REE potential of carbonatites (Rankin, 2005; Orris and Grauch, 2002).

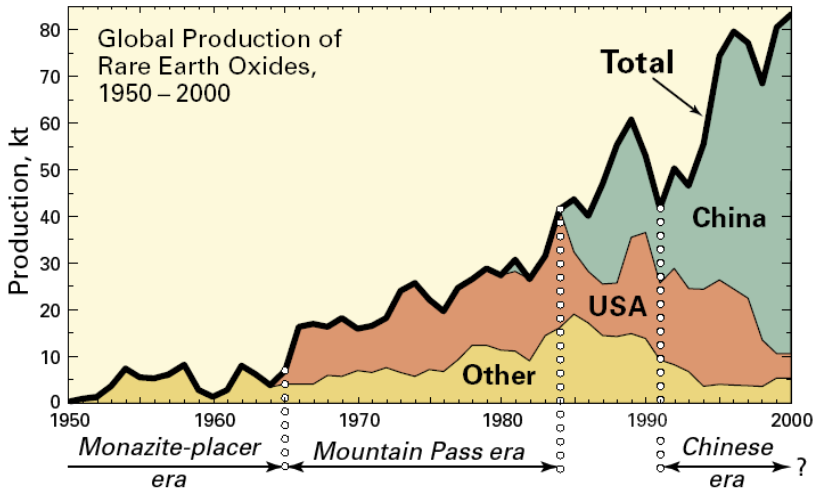

Figure 2.1 Global rare earth element production from 1950 to 2000. Four main periods of production are evident, starting with the monazite-placer era, which began in the late 1800's and continued on until 1964 when production from these sources was surpassed by the carbonatite deposit at Mountain Pass. The Mountain Pass era started in 1965 and continued to dominate REE-production until about 1984. This was followed by a short, transitional, period with USA production levels decreasing and China's REE production increasing. After about 1991 the Chinese dominate REE production, with carbonatites still accounting for much of the production (adapted from Haxel et al., 2002).

2.3 REE DEPOSIT TYPES AND GEOLOGIC SETTING

Although carbonatites and placer deposits account for the majority of the historic REE production, the style and setting of REE rich occurrences are actually quite diverse: the historic focus on carbonatites and placers was largely due to the grade and ease of mining. This does not exclude other types of deposits from being potentially economic, although there is a significant variation in both grade and tonnage even between similar

types of deposits (Table 2.1). Although carbonatite or carbonatite affiliated REE deposits have received the most attention there are several other varieties of REE deposit types which deserve mention.

Alkaline igneous complexes are capable of hosting significant concentrations of REE as is observed in many of the alkaline ultramafic rocks of the Kola Peninsula, Russia, and the Ilimaussaq Complex, Greenland (Salvi and Williams-Jones, 2005; Belolipetskii and Voloshin, 1996). The REE deposits associated with alkaline rocks can be either HREE or LREE dominant; it is also possibly to have U mineralization, or variety of other possible metals, associated with the REE mineralization (Pollard, 1995). In most instances the REE alone are not economic to mine from these alkaline associated sources; if associated with another commodity the REE may be recovered as a by-product (Wu et al., 1996; Salvi and Williams-Jones, 2005).

Another common, although often overlooked, source of REE mineralization are igneous affiliated occurrences such as pegmatites or hydrothermal veins (Mariano, 1989). REE mineralization can occur in some rare element pegmatites, especially in pegmatites associated with calc-alkali granitic magmatism or with syenitic intrusions. The REE mineralization seen in most pegmatites tends to be the result of magmatic factors and forms as an integral part of the primary crystallization, not the result of later alteration (Pollard, 1995). The major REE minerals found in pegmatites tend to be minerals which are enriched in HREE, such as xenotime (Morteani, 1991).

Historically, the potential for REE mineralization related to hydrothermal processes has been ignored as REE were assumed to be immobile elements, which recently has proved to be untrue (e.g. Rolland et al., 2003). Many deposits which have previously been classified as having a magmatic origin may actually have experienced significant REE enrichment by the alteration of the primary minerals due to their interaction with late to post magmatic fluid flow (Salvi and Williams-Jones, 2005). Some of the most important REE deposits in the world are now believed to have a hydrothermal component in their petrogenesis, including Bayan Obo and Miaoniuping deposits, China, the Mary Kathleen deposit, Australia, and the Gallinas Mountain deposit, USA (Huang et al., 2006; Samson and Wood, 2005 and references

Table 2.1 REE Deposits

Deposit Name	Type	REE Mineralogy	Grade (% REO)	Tonnage (Mt)	Status
Bayan Obo	Carbonatite/Hydrothermal	Bastnaesite, Monazite	4.1	750	Current Producer
Mountain Pass	Carbonatite	Bastnaesite, Parisite, Monazite	5	90	Current Producer
Thor Lake	Alkaline Igneous	Bastnaesite	0.42	1.5	Potential Resource
Ilimaussaq Complex	Alkaline Igneous	Eudailyte	3	6.6	Potential Resource
Strange Lake	Alkaline Igneous/Hydrothermal	Gadolinite, Bastnaesite, Kainosite	0.54	52	Potential Resource
Lovozero	Peralkaline Syenite	Loparite, Eudailyte, Rinkite	1.2	1000	Current Producer
Brockman	Volcanic	Bastnaesite, Xenotime	0.22	9.3	Potential Resource
Mary Kathleen	Metamorphic	Allanite	4	6.8	Past Producer
Mount Weld	Laterite	Monazite	11.2	15.4	Potential Resource
Araxa	Laterite	Monazite	1.8	8.1	Potential Resource
Longnan	Ion Adsorption	Clay	0.1	1	Current Producer
Karonge	Vein	Bastnaesite, Monazite	1.59	0.06	Past Producer
Maoniuping	Vein	Bastnaesite	2	0.4	Current Producer
Steenkampskraal	Vein	Monazite, Apatite	12.5	0.2	Past Producer
Nolan's Bore	Vein	Apatite, Allanite	4	3.8	Potential Resource
Hoidas Lake	Vein	Apatite, Allanite	2.4	2.5	Potential Resource

Note that the above list represents a selection designed to show some of the variety of deposit types and is by no means exhaustive. For a more complete listing see Orris and Grauch (2002). REE Mineralogy lists only the main REE bearing minerals and is not a complete list of the REE minerals present. Grade, Tonnage and the Status of the deposit are largely taken from Orris and Grauch (2002), with additional values from Castor (2008). Hoidas Lake information is from Great Western Minerals Group.

therein; Smith et al., 2000; Oliver et al., 1999; Giere, 1996 and references therein). These deposits show that REE are not only mobile in hydrothermal fluids, but also that they can reach significant concentrations (Haas et al., 1995). Although in the past hydrothermal REE deposits have been overlooked, they represent a potentially significant economic source of REE (Giere, 1996).

One of the most important predictive characteristics, and therefore the most useful for exploration purposes, is the geological or tectonic setting of the various deposit types (Fig. 2.2)(Barton, 1993). Associated with many of these deposits is a predictable tectonic or geological setting. As would be expected from the wide range of deposit types and style of mineralization, REE deposits can occur in a wide variety of settings. The geologic setting of REE deposits is as diverse as the REE deposits themselves. Despite this diversity some patterns do emerge. For example, the frequent association of carbonatites and, to a lesser extent, alkali complexes with extensional settings suggests that such environments would represent an important primary target for REE mineralization. The carbonatites also tend to be spatially related to major faults and a common feature is the concentration of carbonatite occurrences at the intersection of major faults (Woolley, 1989; Salvi and Williams-Jones, 2005). Smaller scale structures are also important, particularly for deposits which may have a hydrothermal component, as these open structures facilitate fluid movement.

Age distribution of the mineralized occurrences may be a further area of interest. Although the actual distribution of occurrences is fairly evenly split between the Proterozoic, Phanerozoic and Cenozoic, there appears to be a distinct difference in the economic potential of the deposits (Orris and Graunch, 2002). REE occurrences of Proterozoic age seem to contain economic concentrations of REE much more frequently than similar Phanerozoic deposits. Although the data set used for this observation is by no means complete, it is interesting to note and would be an interesting avenue of further research.

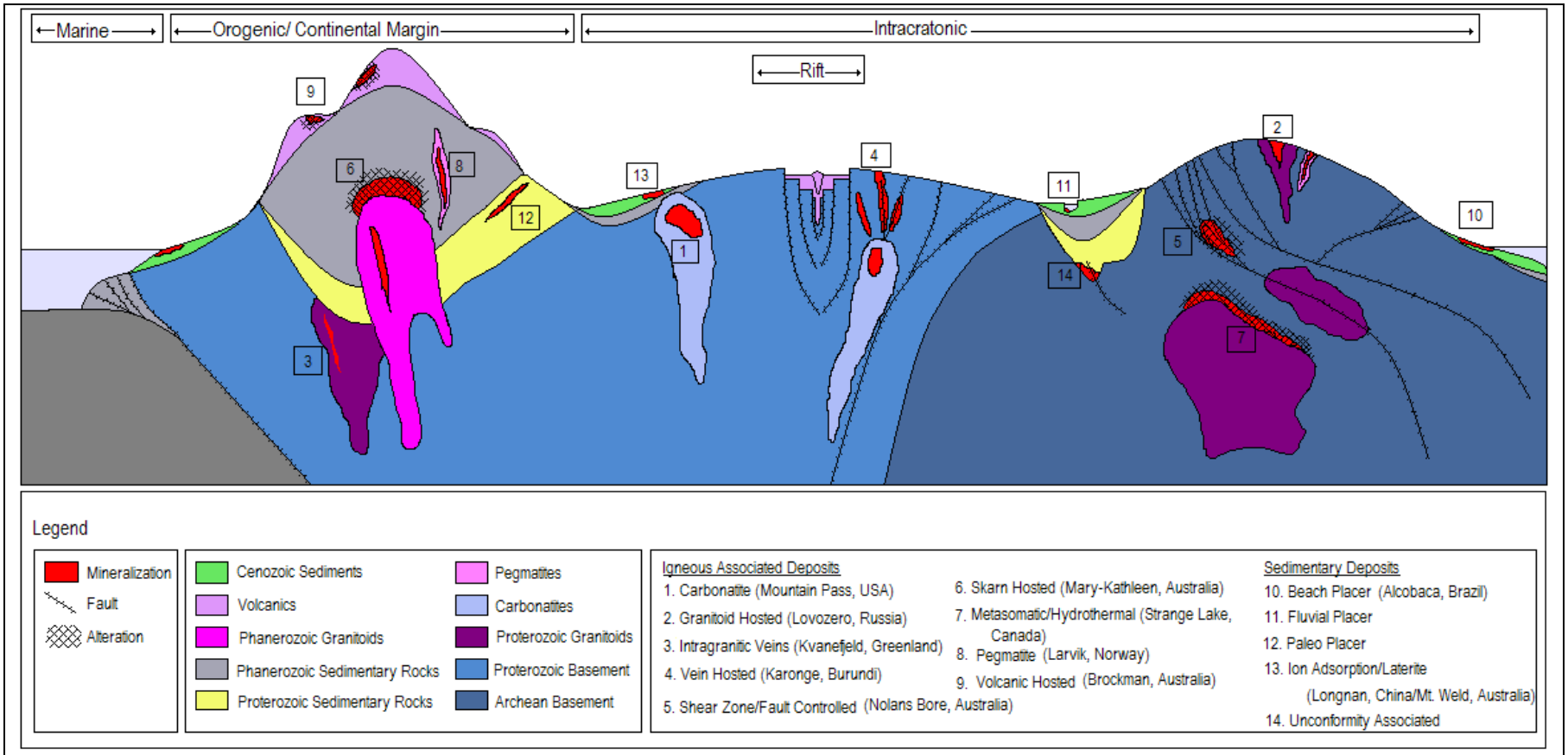

Figure 2.2 Setting of REE Deposits. A simplified illustration of the tectonic, or geologic, settings of the major types of REE Deposits. Please note that the above illustration is not drawn to scale in order to show the relevant features, which are often relatively small in scale. In the brackets following the deposit type on the diagram is deposit which is analogous to that deposit style. References for the analogous deposits are as follows 1. Mariano, 1989; 2. Salvi and Williams-Jones, 2005; 3. Salvi and Williams-Jones, 2005; 4. Mariano, 1989; 5. Hussey, 2003; 5. Giere, 1996; 7. Salvi and Williams-Jones, 2005; 8. Larsen, 1996; 9. Ramsden et al., 1993; 10. Neary and Highley, 1984; 13. Wu et al., 1996/Morteani and Preinfalk, 1996; 14. Harper, 1987.

2.4 THE DEBATE OVER THE ORIGINS OF REE DEPOSITS

Although the previous discussion on the variety of REE deposit types may imply that the origin of these deposits are easily determined this is not always the case. For many deposits there is intense debate over the origin of the deposit; in some cases this controversy is largely a result of lack of available information and could be resolved with additional research. However there are a number of well characterized and thoroughly researched deposits whose origins are the subject of ongoing controversy. One of the best examples of this is the Bayan Obo deposit which, despite being one of the largest and thoroughly researched deposits, is still one of the most enigmatic.

Since its discovery in 1927 the genesis of this deposit has been a hotly contested subject, without any definite consensus to date, despite numerous, detailed geological studies (Yang and Le Bas, 2004). Everything from the origins of the host rocks to the timing and source of the mineralization has been disputed. There is little to no agreement on whether the host rocks are igneous or sedimentary in origin, let alone on the origins of the mineralization. Speculation on the origins of the mineralization has ranged from syngenetic ores related to exhalative fluids to epigenetic mineralization transported by metasomatic or hydrothermal fluids.

Even within these two broad camps there is dissention over the features of the mineralization. For example the derivation of the fluids is a highly contested subject, with some favoring a subduction-related fluid source, while others believe the fluid to be linked to nearby granitic plutons and still others argue for a carbonatitic fluid source. One of the few features acknowledged by most authors is that the deposit formed by multiple mineralization events (Campbell and Henderson, 1997).

2.5 REE IN MAGMATIC SYSTEMS

The REE have a low mineral-melt partition coefficient in most magmas due to their large ionic radii, which prevents their entry into most of the common minerals. As a result, the REE behave as incompatible elements, becoming concentrated in the remaining melt. Only minerals with large cation sites, and

relatively flexible structures, can incorporate the REE. Minerals that accept the REE as substitutions, such as apatite, zircon, and garnet, and minerals which contain REE as essential components, such as allanite, monazite or bastnaesite, concentrate the REE quite effectively and therefore often account for much of the REE content in the rock (Henderson, 1996). In primary magmatic deposits it is this concentration of the REE in the residual phases which leads to the development of economic concentrations of REE, particularly in carbonatitic or alkaline intrusions which tend to have higher REE concentrations than most other magmas (Salvi and Williams-Jones, 2005; Mariano, 1989).

2.5.1 ORTHOMAGMATIC FLUIDS

More common than purely magmatic enrichments are those which result from a combination of magmatic and hydrothermal processes. For example, the REE-bearing pegmatites, skarns and veins of the Grenville province formed from a combination of magmatic and hydrothermal processes. Both the formation of pyroxene bearing skarns in reactive wall rock and the apatite veins are believed to have formed from fluids related to vapor-phase saturation of the pegmatites in the region. This results in a complex mineralization ranging from magmatic in the pegmatites to metasomatic in the skarns to hydrothermal in the apatite veins (Lentz, 1991). This is just one of many examples where the observed REE enrichment is the result of transportation and precipitation from orthomagmatic fluids (Hou et al., 2009; Salvi and Williams-Jones, 2005 and references therein; Wall and Mariano, 1996; Samson and Wood, 2005 and references therein).

Vapor-liquid immiscibility during late stage crystallization in magmatic-hydrothermal systems can serve to enrich the REE content in fluids. As a vapor phase boils off the remaining fluid will be a highly saline brine, which is much more favorable for the complexation of REE. Aqueous fluid with high Cl and F contents are much more successful at fractionating the REE, in addition to other lithophile elements such as Ba and Sr, from melts and therefore these fluids are significant to the transport and deposition of magmatically derived REE deposits (de Hoog and van Bergen, 2000). Typically, there is a multistage devolatilization which is

responsible for REE liberation from magmas, with the REE mobilized only during the later stages of fluid evolution, not in the initial fluid release (de Hoog and van Bergen, 2000).

In many fluids exsolving from magmas, water is an important component, as well as CO_2, SO_2, H_2S, HCl, and possibly HF. The REE typically remain in the melt as compared to an aqueous fluid phase, in the absence of strong complexing agents. This is partially explained by the preponderance of the F remaining in the melt, although the partitioning is dependent on not only the melt composition, but also the prevailing temperature and pressure. However, the concentration of possible ligands does have an effect on the partioning of the REE between phases. For example, since the majority of aqueous REE species involve complexation with various ligands, with increasing ligand content the partitioning of the REE into aqueous fluids increases. This is demonstrated best by the LREE at high salinities, which preferentially partition into the aqueous fluid. The HREE tend to have lower partition coefficients than the LREE and as a result it is possible to obtain a fluid which is enriched in LREE relative to the melt (Samson and Wood, 2005).

2.6 REE BEHAVIOR IN HYDROTHERMAL SETTINGS

The degree of mobility of the REE in any aqueous environment is controlled by a number of factors including; ligand availability, pH, temperature, and pressure (Giere, 1996; Haas et al., 1995). Other important factors are the fluid rock ratios, reaction kinetics, and various other crystal-chemical influences. Unfortunately, detailed analysis of many of these factors is still somewhat lacking in the literature (Rolland et al., 2003).

2.6.1 COMPLEXATION OF REE

The REE tend to exist as complexes in all but the most acidic or very dilute solutions and at the lowest temperatures. In cool, highly dilute or very acidic solutions the REE exist primarily as unassociated cations, with the LREE occurring preferentially. However, solutions of this nature are unlikely to occur in most geological settings. As the pH, as well as temperature and pressure, increase the

proportion of REE^{3+} in solution decline sharply and therefore the tendency for REE to form aqueous complexes increases with rising temperature, pressure, and pH. For this reason REE complexes are important as, at the conditions found in most geological environments, they are likely the predominant species (Haas et al, 1995).

With the exception of the aforementioned conditions, where REE can be transported as hydrated ions, the formation of aqueous complexes is required for the transportation of REE. The strongest complexes are formed with ligands such as F^-, $SO_4^{2-}CO_3^{2-}$, PO_4^{3-}, and OH^- . The REE may also complex with Cl^-; this complex is somewhat weaker than those formed with the previously listed ligands, although it seems to be important in some basinal brines (Samson and Wood, 2005; Quirt et al., 1991). Speciation is not only influenced by the prevailing temperature and pressure conditions; it is also very sensitive to both concentration and availability of anions, as well as the pH of the solution (Haas et al., 1995).

2.6.2 INFLUENCES OF TEMPERATURE AND PRESSURE

The exact effects of temperature and pressure on REE complexation are difficult to anticipate due to the lack of thermodynamic data (Smith et al., 1999). The predicted behavior of the REE at certain temperatures and pressures varies somewhat depending on the ligands species; there are several distinct behaviors shown by REE complexes with increasing temperatures and pressures. The most straight forward behavior, exhibited by REE complexed with Cl^{2+}, Cl_2^+, F^{2+}, F_2^+, HCO_3^+, and $H_2PO_4^+$, involves a progressive increase in association with increasing temperature and pressure (Haas et al., 1995). Although this is only one possible option, the REE are often erroneously assumed to exhibit this behavior regardless of the complex composition.

Though the previous pattern is the simplest, it is not the most commonly observed behavior. At low temperatures and pressures the REE may also complex with sulfates and carbonates instead of the more typical chlorine, fluorine, and hydroxide complexes (Smith et al., 2000). REE complexes with CO_3^+, and SO_4^+, as well as higher order Cl ligands such as Cl_3 or Cl^-_4, F_3, and all OH complexes, initially increase with increasing temperature and pressure. At some point in each of

these cases the stability begins to decrease, despite the rising temperature and pressure. In the final pattern, as demonstrated by $REEF_4^-$, there is an inverse relationship between temperature and complex stability; as the temperature increases the stability drops (Haas et al, 1995).

In fluids with more complex composition, which more closely mimic those found in natural systems, increasing the temperature and pressure has a slight influence on the relative stabilities of the various REE complexes (van Middlesworth and Wood, 1998). In this situation the relative stability field of Cl and OH complexes increases with increasing temperature and pressure at the expense of F stability range, relative to pH. The amount to which the F stability decreases is also somewhat dependent on the relative concentrations of the ligands. The lower the concentration of F, the more reduced the range of pH conditions at which it is the predominant, stable species (Haas et al, 1995). Despite the effects that changes in temperature and pressure can have on REE systematics, the wide range of temperatures associated with the formation of REE minerals, even within a single deposit or occurrence, may indicate that the fluid composition plays a more dominant role (Smith et al., 1999).

2.6.3 INFLUENCES OF pH AND FLUID COMPOSITION

The initial control on the fluid chemistry or composition is the fluid source itself (Smith et al., 1999). In many cases the exact origin of the high salinity fluids which are often associated with REE minerals remains unclear, and the numerous possibilities are often strongly dependent on the local geology. For example, a late stage fluid release from magma, dissolution of evaporites, as well as dehydration or mineral break down reactions are all possible fluid sources depending on the geologic history of a region (Oliver et al., 1999).

One of the most important considerations is the pH of the fluid. The concentration of REE in a fluid depends largely upon the fluids pH, as does the species of REE complex that will form (van Middlesworth and Wood, 1998). Under acidic conditions, complexes with Cl are predominant, while at a more neutral pH F will be favored and, in more basic fluids, OH complexes will become the principal

complex type (Fig. 2.3). Although the exact pH range at which a certain complex type dominates varies somewhat, the changes in complex type with changing pH hold true regardless of changing temperature and pressure conditions (Haas et al., 1995). The pH of a fluid not only influences the solubility of the REE, but also what mineral species precipitates (Smith et al., 1999).

The species of REE complex which forms in a given system is also influenced by the relative availability of the potential ligands, a factor which is strongly influenced by the total ligand concentration in solution. Elevated

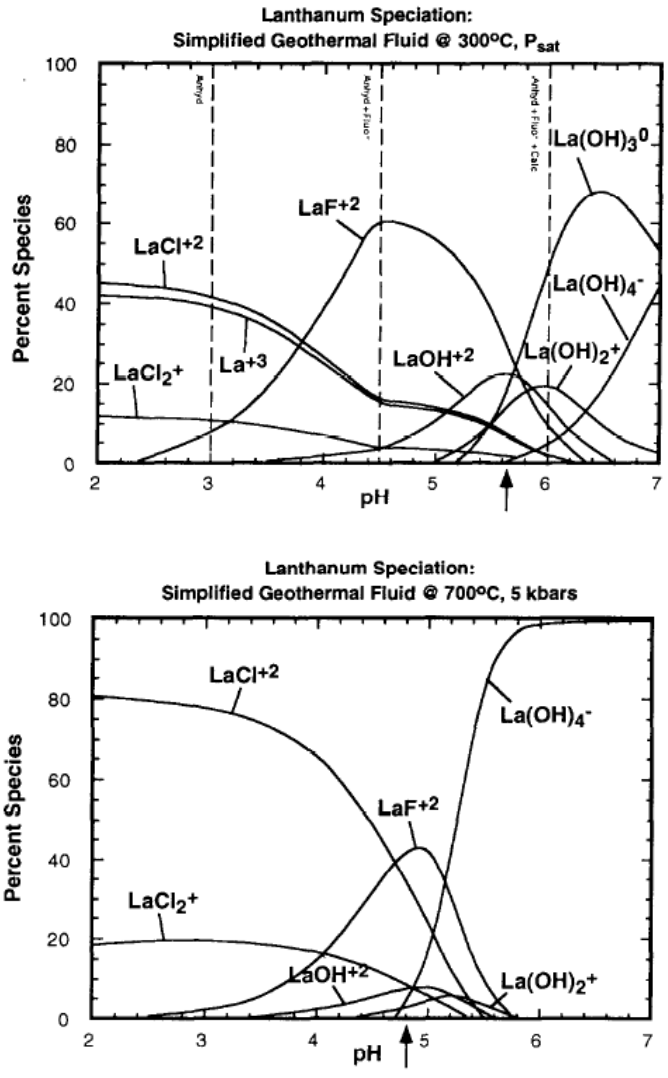

Figure 2.3 REE Speciation. Results of speciation of REE complexes at various temperature, pressures and pH. The percent of each REE complex type is plotted against the pH of the fluid. The arrow under the abscissa indicates the point of neutral pH at the given pressure and temperature conditions. From Haas et al., 1995.

concentrations of select ligands such as F, CO_2, or SO_2, may stimulate REE mobility under less severe pH and temperature conditions than otherwise necessary (van Middlesworth and Wood, 1998). In the case of carbonate and hydroxide complexes, the pH of the solution does influence the availability; in low pH fluids there will be a reduced availability of CO_3^{2-} and OH^-. A further consideration is the influences of other trace elements, as well as the major rock forming elements, since the presence of competing cations in a system may limit the mobility of the REE (Haas et al, 1995).

There may also be differences in REE transport depending on whether the fluid is dominantly aqueous or carbonic. There is controversy regarding the effects of CO_2 in fluids (Smith et al, 1999; Samson and Wood, 2005), with a number of studies claiming that in CO_2 rich fluids, as compared to H_2O dominant fluids, there is an increase in the solubility of REE and that the LREE in general have a higher solubility than the HREE (Smith et al., 2000; Rolland et al., 2003). This result is debatable, as other investigations indicate only limited REE solubility in higher temperature, CO_2 rich fluids (Pan and Fleet, 1996; Samson and Wood, 2005). The problem of H_2O rich fluids compared to CO_2 rich fluids is important, as there are many natural fluids which have a high CO_2 component, though as of yet this debate is unresolved. An understanding of the methods of complexation and transport are particularly lacking for CO_2 dominant fluids and deserve further investigation due to their potential importance in natural systems (Smith et al., 1999).

Yet another potential influence is possible fluid rock interactions, as fluids may be buffered by interactions with the wall rocks. The extent to which fluid rock interactions influence the mobility of REE is controlled by both the reactivity of the wall rocks and also by the fluid to rock ratios. One possible factor which should be considered is that interactions with the wall rock may trigger the formation of ligand-rich minerals which can initiate the precipitation of REE-rich mineral species, as low ligand activity will destabilize the REE complexes in the fluid (Smith et al., 1999).

2.7 REE BEHAVIOR IN METAMORPHIC ENVIRONMENTS

In the past, REE have been assumed to be relatively immobile during metamorphism, however, there is emerging evidence that this may not be true in all metamorphic events (de Jong et al., 1998). In the past it was assumed that REE were only mobile under low grade, fluid rich metamorphic conditions and were unaffected by high grade metamorphism, although the relative mobility of REE was a subject of much debate (Grauch, 1989 and references therein). More recent investigations, such as those by Pan and Fleet (1996), indicate that the mobility of REE may occur under a much broader range of conditions than previously recognized.

As in hydrothermal environments, the mobility or immobility of the REE in a metamorphic setting is controlled by the fluid composition, including the pH, oxygen fugacity, and the concentration of the ligands in the fluids. The stability and abundance of REE bearing phases, as well as the temperature and pressure, must also be considered (Rolland et al., 2003). The available data indicates that there is a correlation between LREE, V, and Y mobility during both prograde or retrograde regional metamorphism and the activity of Cl and F in the associated metamorphic fluids (de Jong et al., 1998). Precipitation of REE minerals can occur as a result of changes in fluid composition due to a number of processes including fractional crystallization, fluid rock reaction, or fluid mixing processes (Rolland et al., 2003).

REE mobility in metamorphic environments is most common in areas adjacent to major fault or shear zones, which can act as conduits to focus fluid flow (de Jong et al., 1998). One relationship which must be distinguished is whether the enrichment in REE is the result of precipitation of REE rich minerals or the loss of more mobile major elements (Rolland et al., 2003).

2.8 ENRICHMENT OF REE IN HYDROTHERMAL SYTSEMS

Although the evidence suggests that it is possible for REE to be transported in fluids, the concentration of REE carried by these fluids is still quite low in comparison to most other elements in the fluids; the highest recorded total REE content from an ancient hydrothermal system is 1290 ppm (Banks et al., 1994). The REE content of most hydrothermal fluids is typically between 5 ppm to 200ppm

(van Middlesworth and Wood, 1998; Giere, 1996). As a result of this, there must be a mechanism to further concentrate the REE if the formation of hydrothermal deposit is to be a viable option. To form significant concentration of REE the fluid must be either heavily enriched in REE, which is not typically the case, or the environment of deposition must be exceptionally efficient at stripping the REE from the fluid (Samson and Wood, 2005).

The predominant ways in which this can occur are quite similar to the various factors which influence the solubility, and transport, of REE. The most significant factors are probably changes in pressure and temperature. The role of temperature in REE solubility is complex and varies depending upon the mineral in question (Samson and Wood, 2005). An added difficulty is that there is little agreement on solubility of even the well known REE minerals (Giere, 1996).

The effects of pressure are also strongly mineral dependent; for example monazite solubility decreases as pressure decreases, while apatite's solubility increases as pressure drops. The influence of pressure changes on REE solubility suggest that structures may play an important role in controlling the location of deposition of REE minerals (Giere, 1996). There is often a strong structural control in the deposition of REE deposits as the sudden drop in pressure can result in fluid immiscibility and subsequent mineral precipitation (Oliver et al., 1999). This is reinforced by the number of REE deposits which seem to have a structural control; many occur in breccias, fractures, or other open cavities in the host rock (Samson and Wood, 2005).

As shown above, fluid composition will greatly affect the ability of a fluid to transport REE. Other influences which may act to concentrate the REE into a particular location are the interactions with wall rocks, fluid mixing, or the crystallization of gangue minerals (Giere, 1996). In general, factors which alter the fluid can change the equilibrium of a system to allow for the formation of REE rich minerals. The key problem is that the systems are quite complex, with a variety of influencing forces, and behavior of REE at high temperatures is not well understood. Due to these limiting factors, determining the exact mechanism responsible for the

enrichment of REE in particular settings can be difficult, if not impossible (Oliver et al., 1999)

2.9 AREAS REQUIRING FURTHER RESEACH

As many REE deposits have at least some hydrothermal component an understanding of the role of hydrothermal processes in concentrating REE to economic levels is necessary to fully understand these deposits. This requires an understanding of the processes responsible for the acquisition, transportation and deposition of REE in hydrothermal solutions; something which is still somewhat lacking in the literature. Although significant progress has been made, particularly in the last decade, further research examining REE mineral solubilities, the stability of various REE complexes and even the partitioning of the REE between hydrothermal solutions, minerals and melts of various compositions at geologically relevant temperatures and pressures is still needed.

CHAPTER 3
GEOLOGICAL SETTING

3.1 INTRODUCTION

The Hoidas Lake REE deposit is located in the southern portion of the Rae Province in Northern Saskatchewan, Canada. The Rae Province, which is part of the larger Churchill Province, has experienced a complex and protracted evolutionary history involving numerous periods of deformation, plutonism and metamorphism during the Archean and Paleoproterozoic. As a result of its complex thermotectonic history the Rae Province is predominantly granite–greenstone terrane characterized by northeast-trending linear greenstone belts with intervening gneissic and granitic rocks which are variably reworked (Fig. 3.1) (Mahan et al., 2003).

The southwestern portion of the Churchill Province is composed of Archean granitoid basement rocks and Paleoproterozoic to Neoarchean supracrustal rocks, intruded by abundant Paleoproterozoic granites (Hartlaub et al., 2005). In Saskatchewan the Rae Province typically consists of very high-grade, midcrustal complexes ranging from ultramafic to tonalitic to granitic in composition. These mid crustal gneisses, along with the minor supracrustal gneisses, are intruded by granodioritic to tonalitic igneous bodies, mafic dikes, and pegmatites (Orrell et al., 1999).

An examination of the regional tectonic setting will provide the geological framework into which the Hoidas Lake deposit fits. This is essential as the regional scale evolution likely forms an integral part in the formation of the deposit. Understanding how the REE deposit fits with respect to this complex series of events may aid in determining the factors which influence the timing and location of the mineralization. Also, an understanding of the regional geological history may provide additional insight into the deformational history and paragenesis of the deposit and aid in the identification of other prospective regions.

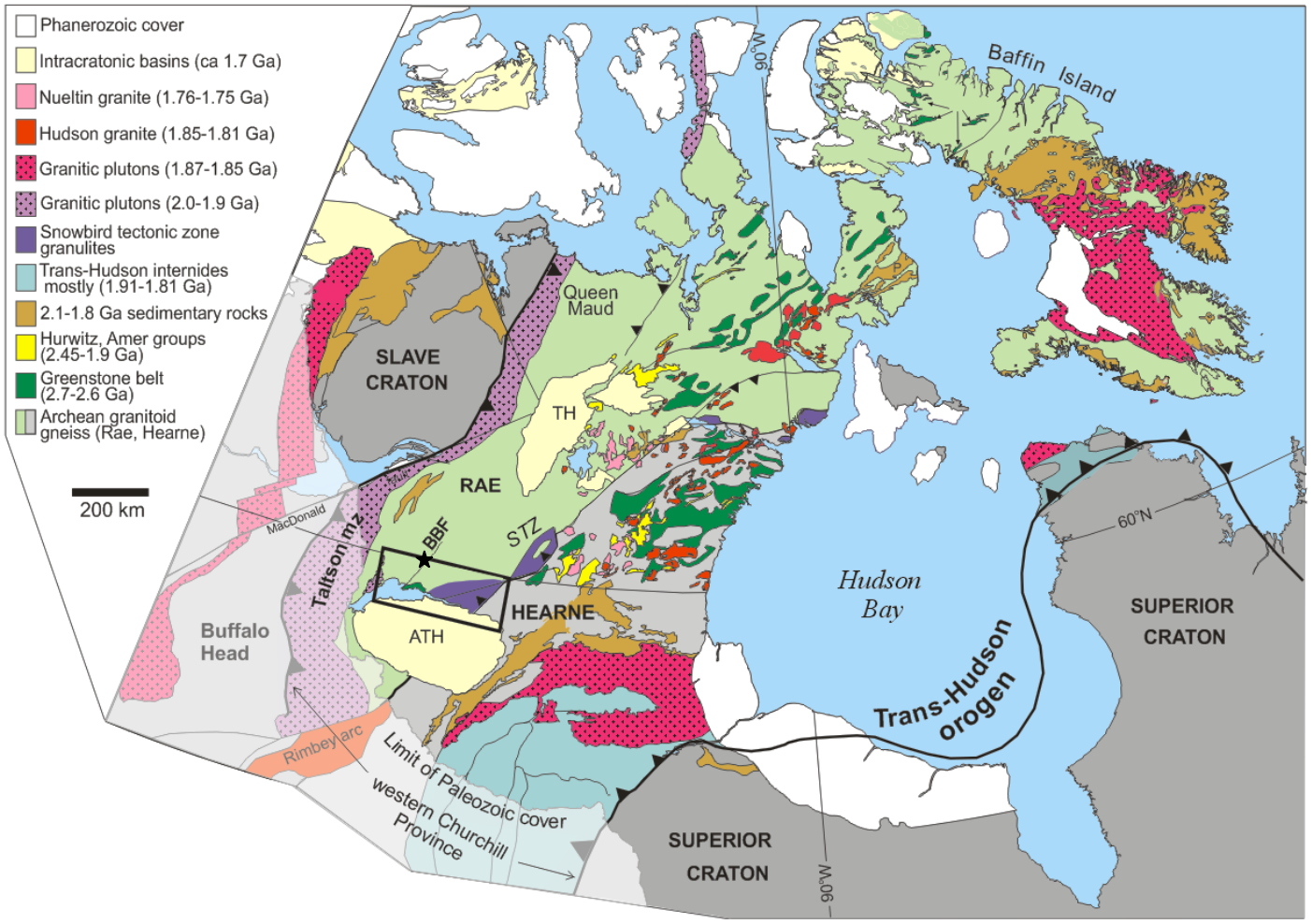

Figure 3.1 Regional geological map of the western portion of the Canadian Shield. ATH, Athabasca basin; BBF, Black Bay Fault; TH, Thelon basin; STZ, Snowbird Tectonic Zone. Rectangle indicates area shown in Fig. 3.3, with the star showing the location of Hoidas Lake. Modified after Pehrsson and van Breemen, 1994.

3.2 REGIONAL GEOLOGY

3.2.1 ARCHEAN CRATONS AND PALEOPROTEROZOIC OROGENS

The Rae Province of northwestern Canada is an extensive area of Archean crust which extends from Saskatchewan and Alberta, northeast to Baffin Island and is often classified as the northwestern portion of the larger Churchill Structural Province (Crocker et al., 1993). It extends westward from the Snowbird tectonic zone, which separates the two portions of the Churchill Province into the Rae and the Hearne, to the Taltson magmatic zone in Alberta and the Northwest Territories. During the assembly of Laurentia, the Rae and Hearne Provinces formed the central component to which the Slave and Superior cratons were welded (Fig.3.1) (Aspler et al.,2002)

The Rae Province in Saskatchewan largely consists of Archean rocks with 2.8 to 2.65 Ga granite-greenstone belts and 2.6 Ga granitic to dioritic intrusions being the dominant lithologies, although there are some 3.0 Ga or older gneisses (Hartlaub et al., 2005). The Archean igneous rocks are overlain by a number of supracrustal units, some of which are indicative of extensional, or rift, environments. The Prince Albert, Woodburn Lake, and the Mary River groups, all of which are approximately 2.7 Ga in age, are considered to indicate continental extension in the northern Rae Province. Recently it has been suggested that the Murmac Bay Group, southern Rae Province, may also represent an extensional environment, although it is slightly younger at 2.3 Ga (Hartlaub et al., 2004; Heaman et al., 2003). The presence of continental sedimentary rocks which have been cross cut by mafic dikes and overlain by volcanic material, as is observed in the Murmac Bay Group, is similar to what is commonly observed in modern rift environments (Hartlaub et al., 2004). The Murmac Bay Group is dominated by quartzites, basalts, and pelitic to psammitic sedimentary rocks, all of which have been metamorphosed to amphibolite facies (Ashton et al., 2001).

These Archean rocks are overprinted by the 2.4 to 2.26 Ga Arrowsmith Orogen which was accompanied by voluminous magmatism (Berman et al., 2005). The emplacement of the magmatic rocks is broadly synchronous with widespread deformation and metamorphism which occurred at approximately 2.3 Ga. The magmatic

rocks cover a wide range of compositions, from mafic to felsic, and are believed to have been emplaced in a syn- to postcollisional setting. Although the majority of the magmatism at this time is believed to be related to a collision along the western margin of the Rae Province, the accreted terrane has not been definitively identified. The Arrowsmith Orogen is only one of several episodes of thermotectonic activity in the Rae Province and is therefore largely obscured by the younger episodes (Hartlaub et al., 2007).

The Snowbird tectonic zone, which is defined by a northeast trending gravity anomaly spanning almost 3000 km, divides the Churchill Province into the Rae Province to the northwest and Hearne Province to the southeast (Hoffman, 1990) and represents a major, crustal scale feature in this region of the Canadian Shield (Baldwin et al., 2003; MacLachlan et al., 2005; Flowers et al., 2006). The origin and age of this structure is a source of contention, with a number of different theories currently under debate.

The Snowbird tectonic zone has been interpreted as a Paleoproterozoic suture between the Rae and Hearne provinces by many authors, including Hoffman (1988), and more recently by Berman et al. (2007), although this theory has been debated by others such as Hanmer et al. (1995) who suggest that the Churchill Province was a discrete tectonic entity by approximately 2.6 Ga and that the Snowbird tectonic zone represents a late Archean intracontinental shear zone which experienced only limited Paleoproterozoic reworking. The controversy surrounding origins of the Snowbird tectonic zone continues in more recent interpretations, with Flowers et al. (2006) suggesting that the Snowbird tectonic zone was the site of an incipient intracontinental rift within an older orogenic zone, while Mahan and Williams (2005) attribute the Snowbird tectonic zone to the interactions of Proterozoic intracontinental thrust and strike-slip shear zones. Although general consensus on the nature or origin of the Snowbird tectonic zone is lacking, it is clear that the Snowbird tectonic zone has a complex, polyphase history (MacLachlan et al., 2005).

The southeastern portion of the Churchill Province, the Hearne Province, shares many similarities to the Rae Province, although there are some distinct differences. Like the Rae Province, the Hearne is composed primarily of Archean

rocks which are structurally overlain by Archean to Proterozoic metasedimentary rocks and intruded by Paleoproterozoic granitoids (Hoffman, 1988; Ansdell, 2005; Orrell et al., 1999). The Hearne is dominated by juvenile Neoarchean crust consisting of a mixed assemblage of calc-alkaline to tholeitic basalts as well as some intermediate to felsic volcanics and sedimentary rocks (Davis et al., 2004). One key difference observed between the Rae and Hearne is the metamorphic grade attained. In the Rae Province the metamorphic grade varies from upper amphibolite to granulite facies, while in the Hearne Province the dominant metamorphic grade tends to be greenschist to amphibolite facies (Davis et al., 2004; Martel et al., 2008).

To the northwest, the Churchill Province is separated from the Slave craton by the Thelon Orogen and Taltson Magmatic Zone, collectively referred to as the Taltson-Thelon Orogen, and the Great Slave Lake Shear Zone (Ross, 2002). The Great Slave Lake Shear Zone is associated with the convergence of the Slave and the Rae provinces, and constitutes a right-lateral continental transform with the age of the ductile motion along the fault being ca. 2.0 to 1.9 Ga (Ross and Eaton, 2002; McNicoll et al., 2000). The ductile deformation has been overprinted by younger brittle deformation which is assumed to have occurred between 1.84 and 1.72 Ga (Ross and Eaton, 2002).

The Taltson-Thelon Orogen is also the result of the dextral-oblique collision of the Slave Craton, a granite-greenstone terrain which served as the foreland for the Taltson-Thelon orogen, and the Rae Province. The Rae Province acted as a relatively rigid hinterland to which additional crustal elements were accreted (Ross and Eaton, 2002). The Thelon tectonic zone, the northern portion of the orogenic belt, is composed of highly deformed granitic to dioritic orthogneiss. The southern portion of the belt is composed of the Taltson magmatic zone, which is interpreted as a continental magmatic arc and a collisional orogenic belt. Overall, the Taltson-Thelon orogen consists of a 3.2–2.9 Ga reworked basement complex, 2.4–1.9 Ga metasedimentary rocks and 2.0–1.9 Ga granitic intrusions.

The magmatic arcs, which occurred between 2.0 and 1.9 Ga, are the result of the subduction of the Slave Craton along an eastward-dipping subduction zone (Hoffman, 1988). The subduction related magmatism in the western portion of the

Rae was long lived; the oldest intrusions in this belt are granodiorites with an I-type, calc-alkaline geochemical signature, while the younger plutons are moderately to strongly peraluminous. The emplacement of these plutons coincides with the oblique plate convergence between the Slave and Rae Provinces. This represents a subduction system which evolved into a collisional orogen (McNicoll et al., 2000; Ross and Eaton, 2002).

The metamorphic evolution of the Taltson–Thelon Orogen is characterized by granulite-facies peak metamorphic conditions, followed by amphibolite and greenschist facies retrograde metamorphism. The observed metamorphism is attributed to a combination of both mantle-derived magmatism and tectonic thickening resulting from collision of the Slave and Rae Cratons (Grover et al., 1997).

To the southeast the Churchill is separated from the Superior Craton by the 500 km wide Trans-Hudson Orogen, which extends from Greenland through Canada, and into the north-central portion of the United States. The Trans-Hudson Orogen is the result of the collision between the Churchill and Superior Provinces, with the Superior Province as the foreland and the Hearne as the hinterland (Hoffman, 1988; Ansdell, 2005). The Trans-Hudson Orogen is composed of Paleoproterozoic arc rocks, reworked portions of the bounding Superior and Hearne province, and continental margin metasedimentary rocks. Deformation along the margin of the Hearne began as early as 1.87 Ga with the accretion of arc rocks. Emplacement of the Wathaman Batholith, a continental margin batholith, occurred between ca. 1.86 and 1.85 Ga, with terminal collision occurring between 1.83 and 1.77 Ga (Meyer et al., 1992).

3.2.2 POST-COLLISIONAL SEDIMENTATION, MAGMATISM AND DEFORMATION

The result of these orogenic events was intense Paleoproterozoic reworking of the intervening Archean rocks of the Rae Province, including the development of numerous supracrustal units. One of the oldest of these units is the Paleoproterozoic Thluicho Lake Group, at 1.93 to 1.82 Ga. The Thluicho Lake Group is dominated by

siliciclastic rocks which have been interpreted as syn- to post-orogenic molasse formed by the exhumation and erosion of the Taltson-Thelon and the Trans-Hudson Orogens and deposited in a strike-slip pull-apart basin. The Thluicho Lake Group is variably deformed and metamorphosed, to at least greenschist facies (Bethune et al., 2006).

There is also evidence of tectonic escape along a system of E to NE trending dextral shear zones, which were active during the period between approximately 1.9 to 1.83 Ga (Peterson et al., 2002). The Black Bay Shear Zone is a major, northeast trending structure which displays a protracted deformational history ranging from early ductile to late brittle episodes of movement. Although the exact timing of the movement along the Black Bay Shear Zone is not well constrained, the entire deformational history occurred between approximately 2.3 and 1.7 Ga, with the transition from ductile to brittle conditions occurring before 1.83 Ga (Bergeron, 2001).

Other siliciclastic basinal successions in the Rae Province, including those of the Martin Group and the Baker Lake Group, contain contemporaneous mafic igneous rocks, named the Gillies Channel Formation and the Christopher Island Formation, respectively (Peterson et al., 2002; Morelli et al., 2009). The Baker Lake Group, the lowermost member of the Dubawnt Supergroup, was deposited in a series of fault-bounded, northeast-striking elongated troughs and is believed to record the initial deposition within an intracontinental rift basin. The Baker Lake Group mainly consists of continental redbeds and the ultrapotassic volcanic rocks of the Christopher Island Formation (Rainbird et al., 2003; Rainbird et al., 2006). The Martin Group, which also contains coarse continental redbed deposits and mafic volcanics, is considered by some to be an equivalent of the Baker Lake Group, although the volcanics in the Martin Group have a more basaltic composition (Rainbird et al., 2006; Morelli et al., 2009).

Accompanying the volcanism of the Christopher Island Formation was the emplacement of the Dubawnt minettes, a regionally extensive 1.83 Ga lamprophyre dyke suite (Peterson et al., 2002). Broadly contemporaneous with the dyke suite are other late syn- to post-orogenic igneous rocks such as the 1.84 to 1.81 Ga Hudson

granitoids. The Hudson granitoid plutons tend to be elongated, NE-SW, suggesting emplacement along pre- to syn-magmatic structures (Fig. 3.1) (Peterson et al., 2002; van Breeman et al., 2005). These were followed at approximately 1.75 Ga by the Nueltin rapakivi granite (Peterson et al., 2002).

Continued brittle downfaulting and crustal sagging allowed for the formation of the younger Wharton and Barrensland Groups, which together with the Baker Lake Group form the approximately 1.84 to 1.7 Ga Dubawnt Supergroup (Peterson et al., 2002; Rainbird et al., 2003). The Thelon basin is a large erosional remnant of this sag basin and, although the original extent of this basin is unknown, the Athabasca basin is thought by some to be another remnant (Rainbird et al., 2003; Peterson et al., 2002). The 1.74 to 1.66 Ga Athabasca Group consists of essentially flat lying, unmetamorphosed quartz-rich sandstone which unconformably overlies the older rocks of the Rae Province (Rainbird et al., 2007; Ashton et al., 2001).

3.3 LOCAL GEOLOGICAL SETTING

Internally, the Rae Province in Saskatchewan has been subdivided into a number of lithostructural domains based on inferred differences in lithological makeup, structural character, and metamorphic grade (Fig. 3.3) (Macdonald 1987; Ashton and Card, 1998). In many cases the complex history makes definitive identification of protoliths difficult, if not impossible, and therefore the nomenclature of the Rae Province is largely descriptive. The result is a large area of Precambrian Shield in Saskatchewan for which very little is known about the original rock types, ages, geological relationships, tectonic history, and mineral potential (Ashton and Card, 1998).

The Hoidas Lake property lies within the Rae Province, but specifically within the Ena Domain, near its boundary with the Train Lake Domain (see Fig. 4.1). The Ena Domain is dominated by gneissic granodiorites, with minor amounts of more mafic gneisses, and amphibolites which have been intruded by granites. The typical metamorphic grade observed in the Ena Domain is upper amphibolite to lower granulite (Ashton et al., 2005). The rocks of the Ena Domain are believed to be Archean to Paleoproterozoic in age (Ashton et al., 2007).

The boundary which separates the Ena domain from the Train Lake domain is the Black Bay Fault, a major brittle-ductile structure which extends for over 100 km in strike length from the west side of the Crackingstone Peninsula, on the north shore of Lake Athabasca, north east into the Northwest Territories (Harvey et al., 2002). The Black Bay Shear Zone is several kilometers wide and the early components of this major shear zone may represent a suture between Paleoarchean to Mesoarchean crust in the Beaverlodge Domain and Neoarchean crust to the west of the shear zone (Bergeron, 2001; Ashton et al., 2005; Hartlaub et al., 2005).

The REE-enriched vein system at Hoidas Lake is associated with the Hoidas – Nisikkatch Fault, a subsidiary of the Black Bay Fault. The Hoidas-Nisikkatch Fault roughly parallels the Black Bay Fault and likely shares the complex history of the Black Bay Fault, including multiple periods of reactivation and deformation.

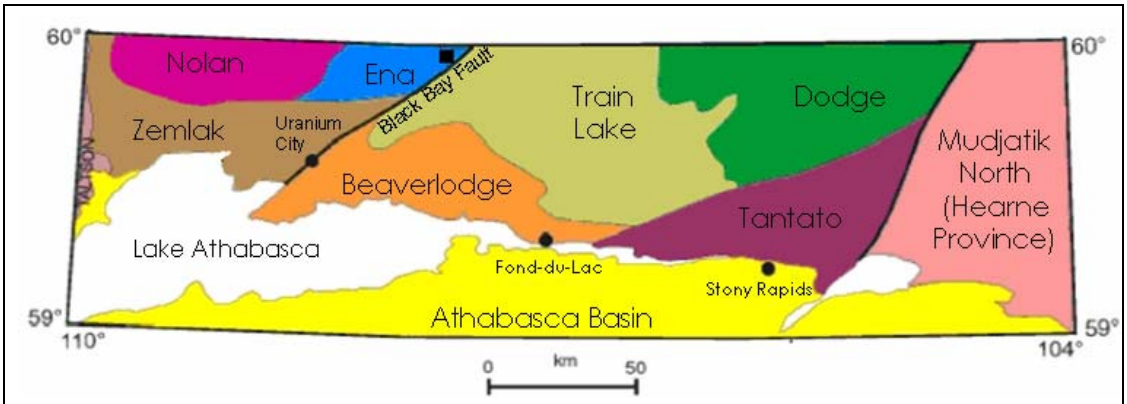

Figure 3.2 Domains of the southern Rae Province. Black square to the west of the Black Bay Fault denote the location of the Hoidas Lake REE Deposit (Modified from Ashton and Card, 1998).

3.3.1 ECONOMIC POTENTIAL OF THE SOUTHERN RAE

This portion of the Rae Province is best known for its uranium potential as the Athabasca Basin hosts many world class unconformity uranium deposits and due to its highly prospective nature is the site of extensive ongoing uranium exploration (Jefferson et al., 2007). Just north of the Athabasca Basin, in the area immediately around Uranium City, there are a number of vein type uranium deposits, some of which were mined during the period between 1953 and 1982. The majority of these

economic occurrences are found in the Beaverlodge Domain, although additional uranium showings can be found on the western side of the Black Bay fault in the Zemlak Domain (Ashton et al., 2001).

In addition to uranium occurrences there are also a number of gold and copper showings in the region, with historic gold production from the Box and Athona Mines (Ashton et al., 2001; Ashton and Hunter, 2003). Although relatively rare there are also a minor number of nickel showings, with the most significant being the Dinty Lake nickel deposit, in the northern portion of the Beaverlodge Domain, which reportedly contains 1.5 million tons grading 0.6% Ni. There has also been some speculation on the tin-tungsten potential of the Train Lake Domain as anomalous tungsten concentrations were recorded during regional sediment surveys (Ashton and Card, 1998).

CHAPTER 4
DEPOSIT GEOLOGY

4.1 INTRODUCTION

The JAK zone, which is located on the northwestern shore of Hoidas Lake, is the main focus of this study, although additional samples were collected from the showings at both Hoidas South and Nisikkatch South for comparison. The JAK zone was selected as the main sampling location due to the abundance of available information. It has been extensively delineated by drilling, with over 124 drill holes evenly distributed over the grid system on the property. Drilling has confirmed that the zone has a minimum continuous strike length of 1 km, with the total width being approximately 75m; individual veins vary from 1 to 11 m thick, although the average vein intersection is approximately 3 m wide. As defined by drilling, the veins display an anastomosing geometry and are continuous up to 300 m depth. To date, the system remains open both along strike and down dip.

4.2 JAK ZONE GEOLOGY

In the JAK Zone there are two dominant lithologies, a variably deformed rock of monzogranitic composition and a granodioritic to tonalitic gneiss, both of which are believed to be Paleoproterozoic to Archean in age (Ashton et al., 2005; Ashton et al., 2007)(Fig. 4.1). The dominant rock type adjacent to the JAK Zone veins is a variably deformed pale pink to light grey monzogranite, which becomes progressively less deformed as the distance from the Hoidas-Nisikkatch fault increases. These rocks typically display a gneissic texture, although rare lower strain zones do exist. The monzogranite gneiss is typically medium grained and moderately foliated, and may contain up to 10 % hornblende, biotite, and magnetite. Local partial melting of the monzogranite has resulted in the formation of a K-feldspar rich leucosome which contains a minimum of 10% hornblende and magnetite.

In close proximity to the mineralized veins the host rocks appears to be overprinted by potassic and hematitic alteration characterized by the increasingly pinkish coloration of the host rocks immediately adjacent to the veins. This alteration causes some uncertainty in defining contacts, as the margins of the alteration are

typically quite gradational. For example, in places the gneiss seems to grade from a monzogranite immediately adjacent to the veins, to granite, to almost a granodiorite in composition. From the observed relationships in the field it is unclear if the change in composition is the result of a gradational contact between separate rock types, or if it is simply pervasive alteration affecting a granodiorite.

In the northwest portion of the grid the tonalitic gneiss is the dominant lithology. The tonalite most commonly occurs as meter to decimeter scale blocks, boudins, and schlieren in the younger, monzogranite intrusions (Gunning and Card, 2005). Like the granitic gneisses, the tonalite is typically medium-grained and is moderately to strongly foliated. It is compositionally banded, with plagioclase and hornblende-biotite rich zones defining the foliation and gneissosity. The tonalite tends to be moderately to strongly magnetic due to the presence of accessory magnetite. In addition to its presence in the extreme western portion of the JAK zone grid, the tonalitic gneiss is also the dominant lithology to the east of the Hoidas-Nisikkatch Fault (Harvey et al., 2002). It should be noted that in many cases the boundaries seem to be fairly gradational, and even within a given unit the rock may grade back and forth between tonalite and granodiorite.

Although amphibolite is a common constituent in the gneisses of the Ena Domain, it is volumetrically insignificant in the Hoidas Lake area. Amphibolite in the Hoidas Lake area is found as meter scale angular blocks and schlieren in the tonalities and granites, and in rare instances the amphibolite bands form coherent units up to 8 km long (Gunning and Card, 2005). The amphibolite is typically fine to medium grained, equigranular, and contains up to 50% clinopyroxene and hornblende with minor chloritized biotite. The presence of minor centimeter to meter scale compositional layering in the amphibolite implies a supracrustal protolith (Gunning and Card, 2005).

Rare dioritic to gabbroic dikes can also be found in the region. Both types of dikes are mildly magnetic due to the presence of accessory magnetite. In outcrop the diorite dikes tend to be fairly narrow, typically under a meter in width, and feature sharp

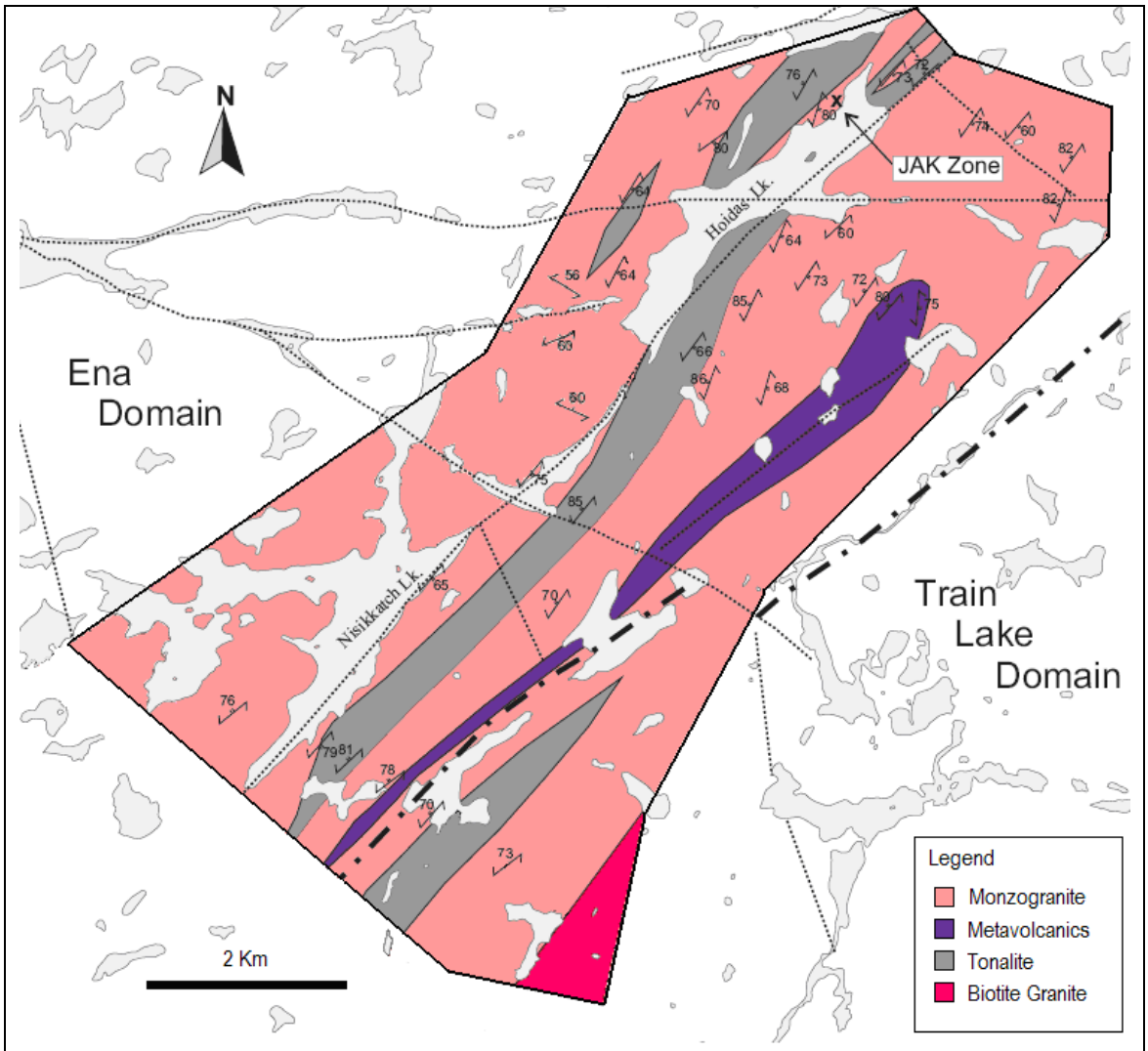

Figure 4.1 Geological map of the Hoidas Lake area (adapted from Gunning and Card, 2005). Bold dashed line marks major faults, fine dotted line marks air photo lineaments.

linear contacts with the surrounding gneisses (Fig. 4.2(a)). Although the strike of these dikes varies in each occurrence they all tend to dip steeply to the east. In many, although not all cases, the diorite dikes show a sub-parallel alignment with the structural grain in the host rocks, resulting in a broadly northeastern strike. The diorite dikes are fine to medium grained and are typically a medium grey color. The more mafic, or gabbroic dikes, are not observed at surface and are only rarely encountered in the drill core. The gabbroic dikes also tend to be quite narrow, with distinct contacts.

Late pegmatite dikes are very common in the JAK zone, and are among the youngest rocks in the region. From the numerous cross cutting relationships observed in

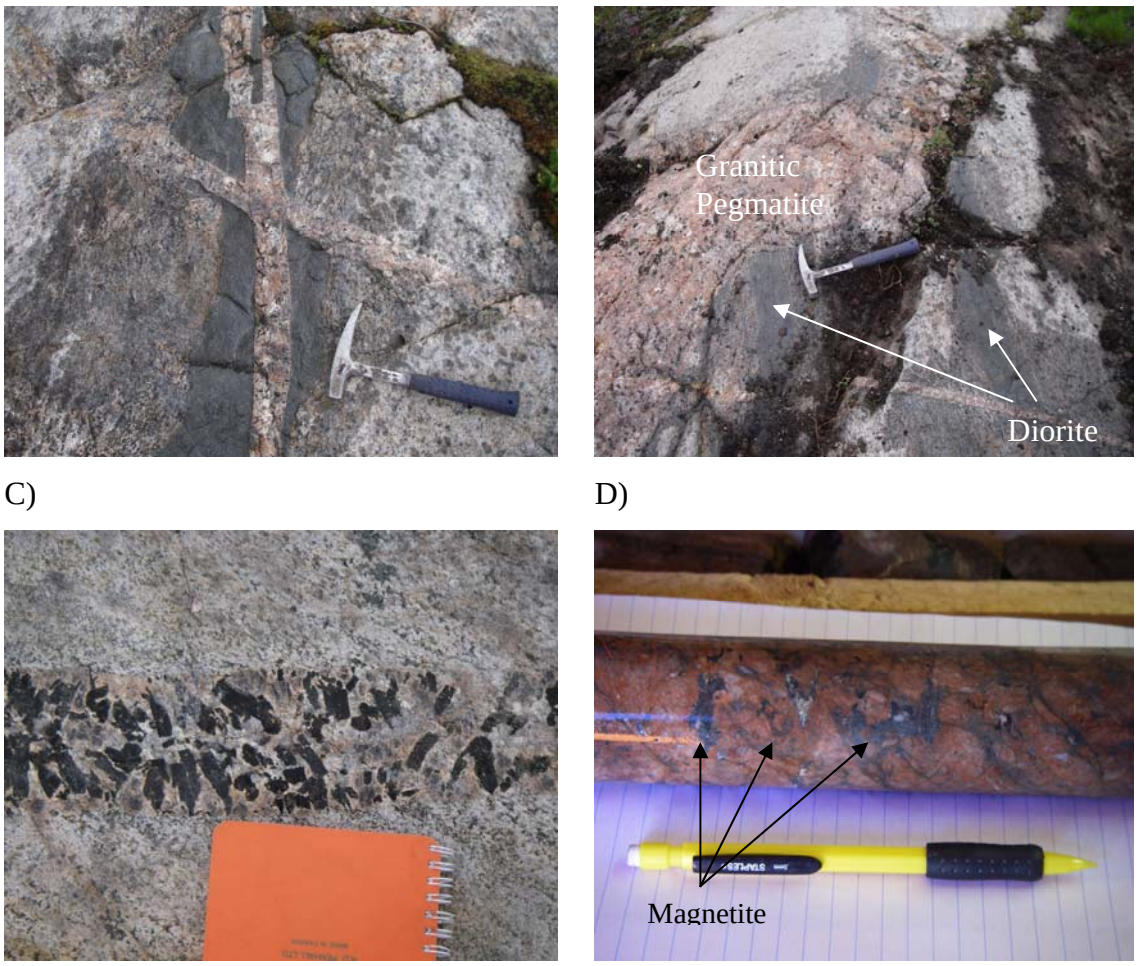

Figure 4.2 Examples of some of the pegmatites in the Hoidas Lake area. A) A small diorite dike crosscut by two pegmatite generations. The younger pegmatite, which runs from top to bottom in the photo, is slightly more syenitic than the older, more granitic pegmatite. Hammer head is aligned N-S. B) Granitic pegmatite with slightly gradational boundaries cross cutting small diorite dikes. Hammer head is aligned N-S C) Close up of a small hyalophane rich pegmatite with abundant amphibole. Bottom of the field notebook is aligned N-S. D) Example of magnetite rich pegmatite.

the field it is clear that there are multiple pegmatite generations (Fig. 4.2(a)). The majority of these dikes are sharp sided and steeply dipping, many with a subparallel alignment to the prevailing northeast trending structural grain. Quartz ribbons within some of the pegmatites are parallel to the foliation, at variable angles to the orientation of the contact, indicating that the oldest pegmatites were intruded prior to the last ductile shear event. It should be noted that although there does appear to be a preferred

orientation to the dikes as a whole, the orientation of individual dikes can be somewhat erratic. In addition to the typical straight sided dikes there are also some more amoeboid intrusions, often with gradational boundaries, which can be found throughout the area (Fig. 4.2(b)).

The pegmatites also show a wide range of compositions, with the composition somewhat related to the geometry of the dike. Most of the pegmatites have a fairly typical, granitic composition and essentially consist of K-feldspar and quartz with minor biotite and plagioclase. The more amoeboid intrusions have diffuse boundaries and appear to have formed in situ from partial melting of the host gneisses. The few deformed pegmatite dikes also tend to have a granitic composition, often with trace amounts of amphibole or biotite present.

There are, however, a number of pegmatites which have a more unusual composition; these pegmatites contain abundant hornblende and hyalophane, a Ba-rich feldspar, and are relatively quartz poor. In the JAK Zone these more unusual pegmatites are essentially undeformed, and tend to be less than a meter in width. The hyalophane pegmatites are consistently sharp sided, steeply dipping and, although the strike is variable, the majority of these dikes have a broadly northern strike (Fig. 4.2(c)). A common feature of most of the pegmatite generations is the presence of magnetite, although both the amount and morphology varies; it occurs as very fine disseminated euhedral crystals, centimeter-scale interstitial blebs, and as discontinuous stringers (Fig. 4.2(d)).

While some of the pegmatites may be the result of decompressional melting following the peak metamorphic conditions, others seem to be the result of separate intrusive events. The multiple pegmatite generations, confirmed by crosscutting relationships, suggest that the pegmatites were emplaced during several episodes over an extended period of time. This is further supported by the presence of both deformed and completely undeformed, unmetamorphosed pegmatites on the property. Unfortunately, the pegmatites only crosscut the granitoid host rocks, the diorite dikes and each other making it difficult to determine relative timing between the pegmatites and the mineralization.

Rare lamprophyre dikes up to 2.5 m wide can be found to the west of the Hoidas-Nisikkatch Fault in the Hoidas Lake area. The lamprophyres are porphyritic and are composed of approximately 70 to 80% of a very fine grained grayish to greenish-brown groundmass with 20 to 30% phenocrysts. The phenocrysts are approximately 5 to 8 mm in size and consist of either biotite, or possibly phlogopite, and amphibole. In some cases the large biotite or amphibole phenocrysts show a weak preferred orientation, typically paralleling the contacts of the lamprophyre.

The lamprophyres outcrop in two distinct manners; they either form distinct ridges which rise approximately 0.5 m above the surrounding gneisses or they seem to weather preferentially to form a slight depression (Fig. 4.3). In all cases the lamprophyres appear to be structurally controlled and show sharp, linear contacts with a very steep to vertical dip. The strike of the lamprophyres is quite consistent as compared to the other dikes, although it does vary slightly between approximately 045^{o} and 065^{o}. In rare cases angular xenoliths of the surrounding granitic to tonalitic gneisses can be found near the margins of the lamprophyre.

The age of the lamprophyres in relation to both the veins and many of the pegmatites is uncertain due to the lack of cross-cutting relationships in the field. The lamprophyres are essentially undeformed, and appear to have been emplaced after peak metamorphic conditions were achieved. The gneiss immediately adjacent to the lamprophyres typically displays evidence of potassic alteration, with fracture sets near the lamprophyre preferentially altered. Signs of this alteration extend for up to 5 m away from the lamprophyre contact (Fig. 4.4).

4.2.1 STRUCTURE

The Hoidas Lake area, like much of the Ena Domain, has experienced multiple phases of folding and faulting. At Hoidas Lake three distinct phases of ductile deformation have been recognized, followed by a period of brittle deformation. This protracted deformational history has largely obscured or destroyed any primary features. The earliest recognized deformation (D_1) appeared to be a prolonged event characterized by the development of an early S_1 foliation. The oldest fabric (S_1) is only rarely

A)

B)

Figure 4.3 Two examples of outcropping lamprophyre show (A) those which form a slight rise and (B) those which have weathered preferentially. Contacts identified with a dashed line. Rock hammer for scale.

Figure 4.4 Alteration present at the contact between the lamprophyre and the surrounding granodiorite gneiss. Although the pervasive alteration of the gneiss is somewhat limited, the alteration extends along fractures for several meters away from the contact.

preserved and is mainly encountered in the rare low strain areas of the monzogranite (Gunning and Card, 2005). In most outcrops the S_1 fabric has either been overprinted by the dominant S_2 fabric or rotated into parallelism with the S_2 fabric (Harvey et al., 2002).

The D_2 deformational event is likely associated with shearing along the Black Bay Shear Zone and is responsible for the dominant northeast trending structural grain observed in the Hoidas Lake area (Harvey et al., 2002). The earliest portion of this protracted deformational event created a strong, typically northeast trending, northwest dipping S_2 foliation and formed tight to isoclinal F_2 folds (Normand et al., 2009;Gunning and Card, 2005). The intensity of the S_2 fabric is variable, ranging from

mylonitic near the Hoidas-Nisikkatch Fault, to weakly gneissic in the area west of Hoidas Lake. The folds associated with D_2 range from symmetrical to asymmetrical (Harvey et al., 2002). In the z-limbs and hinges of the asymmetrical folds the foliation dips to the northwest, while in the intervening s-limbs the foliation typically dips to the northeast (Gunning and Card, 2005).

Following the early D_2 foliation and folding intensification of strain, accompanied by an increase in deformation, triggered late shearing (Harvey et al., 2002). This late shearing in D_2 is not only linked to the formation of shear zones in the Hoidas Lake area, but also to the development of the larger Black Bay Shear Zone (Kraus and Ashton, 2000). Locally within the S_2 mylonitic units there are well developed stretching lineations that plunge moderately to steeply to the east-southeast (Harvey et al., 2002).

In some instances the shear zones appear to form a conjugate set consisting of northeast trending dextral shears and north-trending sinistral shears. The orientation of these conjugate sets suggests that the main compressive stress during the formation of the D_2 shear zones was from the west-northwest and east-southeast (Harvey et al., 2002). Evidence of a dextral component to the D_2 deformation can be found both in rare kinematic indicators and in the presence of dikelets which are oriented parallel to the plane of instantaneous extension in a dextral shear system. The orientation of these granite pegmatite dykes at approximately 15 to 20^o clockwise from the dominant foliation suggests that they were emplaced in dilation zones in a dextral system (Gunning and Card, 2005). The rare δ-porphyroclasts also indicate a dextral sense of movement in the shear zones, while the plunge of the lineations suggest a minor oblique-reverse component to the motion in the shear zones (Harvey et al., 2002). Although the kinematic indicators used to draw these conclusions are quite rare in the Hoidas Lake area, the inferred dextral motion is consistent with what is known about the early ductile movement along the Black Bay Shear Zone (Ashton et al., 2001).

The final phase of ductile deformation, D_3, contains both ductile and brittle features. The ductile phase of deformation at the start of D_3 resulted in fairly open F_3 folds which plunge to the northeast or southwest (Normand et al., 2009). Although the F_3 folds are relatively rare, the open interlimb angle, combined with the lack of axial

planar foliation, serves to distinguish them from the more common F_2 folds (Harvey et al., 2002). Steeply dipping meter to decimeter scale D_3 shears zones overprint the original D_2 shear zones. The D_3 shear zones normally parallel the northeast trending S_2 foliation and often feature well developed ribbon mylonites and rare dextral kinematic indicators. The displacement associated with the D_3 shear zones was mostly strike-slip, as indicated by the shallow to moderate doubly plunging stretching lineations. In many cases the early ductile features of D_3 are often overprinted by later, more brittle features (Gunning and Card, 2005).

In addition to the brittle features associated with D_3 there are also a number of other late fault, fractures, and lineaments. In the area immediately surrounding Hoidas Lake the brittle faults have three dominant orientations; northeast, east, and southeast (Harvey et al., 2002). The faults which trend northeast, including the Hoidas-Nisikkatch Fault, are approximately parallel to the Black Bay Fault and may represent subsidiaries of the Black Bay Fault. These faults commonly overprint older shear zones and, due to their geometry, are likely part of the brittle portion of the D_3 event. The east trending faults, one of which dissects Hoidas Lake, are broadly parallel to the larger Tazin River Fault, approximately 15 km southwest of Hoidas Lake, and appear to be part of the same fault set as the Tazin River Fault. Finally, the southeast trending faults, which are not as readily apparent in the Hoidas Lake area, are oriented approximately 30^o clockwise from the more dominant east trending faults and are accompanied by a series of extension fractures which strike at 143^o and typically have a nearly vertical dip (Harvey et al., 2002).

4.2.2 METAMORPHISM

Metamorphism in the Hoidas Lake area is consistent with what is known about the Ena Domain in general (Ashton et al., 2005). Upper amphibolite facies to possibly lower granulite facies metamorphism constitute the peak metamorphic conditions in the area. The mineral assemblage of biotite, hornblende, and magnetite found in most of the tonalites and granites at Hoidas is stable at amphibolite facies. The presence of young granitic pegmatites, or melt segregations, with minimum melt compositions suggests that partial melting occurred in some locations. The intermediate to mafic dikes, which

are essentially undeformed as compared to the tonalites and granites into which they intrude, often have their original pyroxene either partially or completely replaced by amphibole, indicating that the amphibolite facies conditions persisted to or occurred again after their emplacement. The presence of minor chlorite and epidote alteration in most lithologies suggests subsequent retrograde metamorphism.

4.3 REE SHOWINGS

The REE showings, which consist of apatite-allanite-diopside veins, are mainly focused along the northeast trending Hoidas – Nisikkatch Fault (Fig. 4.5). Although the exact length of the Hoidas-Nisikkatch Fault is unknown, it can be traced over a minimum strike length of 10 kilometers, with the showings fairly regularly distributed along this length. The veins are typically found adjacent to the fault, with the strike of the veins essentially paralleling that of the fault. In total there are approximately 30 historical REE showings recorded in the area, although recent attempts to find a few of the historic showings have failed. Of the approximately 26 showings which have been located the JAK zone showings are the only ones to have been drill tested to date.

4.3.1 JAK ZONE MINERALIZATION

The mineralization at the JAK zone is confined to an anastomosing vein system which roughly parallels the Hoidas-Nisikkatch Fault, with an average strike of approximately 045^{o}. Due to the anastomosing nature of the system the strike of individual veins may deviate substantially from this average, although they are remarkably consistent both along strike and down dip. In all cases the veins dip to the east, typically between 70^{o} and 80^{o}. The localization of the mineralization seems to be largely structurally controlled, with the veins hosted by riedel-type dilation zones (Gunning and Card, 2005).

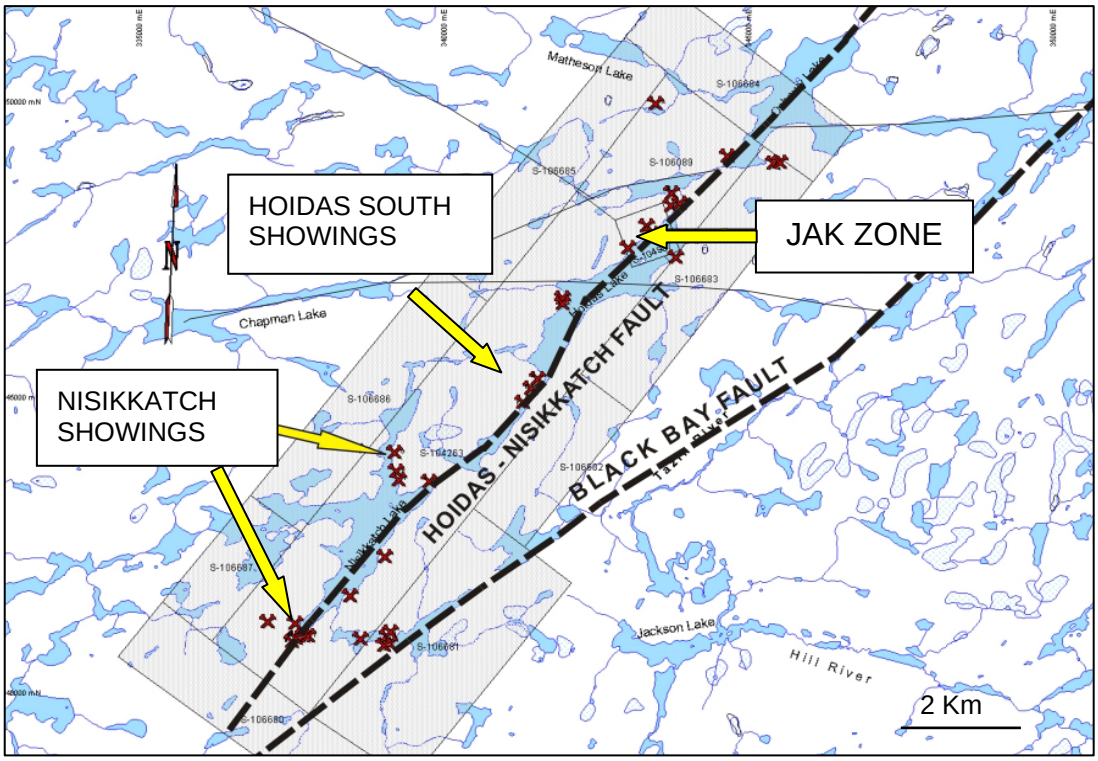

Figure 4.5 Historical REE showings (red crosses) in the Hoidas Lake area. Samples for this study were obtained from the JAK Zone, Hoidas South, and from the showings at the southern end of Nisikkatch Lake. Shaded regions represent the mineral leases controlled by Great Western Minerals at present.

The vein system consists of multiple vein generations, including several macroscopically distinct apatite generations, combined with rather ubiquitous allanite mineralization. The abundant allanite and apatite, combined with relatively minor amounts of monazite, bastnaesite, and chevkinite are the main REE carriers in the veins. Gangue minerals found in the veins are diopside, hornblende, hyalophane, scapolite, calcite, titanite, chloritized biotite and epidote, with minor amounts of pyrite, hematite, and magnetite.

The contact between the veins and host rock is normally quite sharp although slightly gradational contacts, with the gradation occurring over a few centimeters, are also quite common. In some cases the contact shows slight potassic alteration characterized by an increase in potassium feldspar, with minor amounts of sericite and chlorite; when present, evidence of the potassic alteration extends into the wall rock for

less than 1 meter. Also present is a weak hematitic alteration, with late hematite coated fractures more common than pervasive hematitic alteration. In areas with the most intensely altered wall rock there is often minor amounts of late epidote alteration or veinlets which cross cuts the more prevalent alteration types. The contacts between the various vein generations shows a much greater variability than observed between the veins and host rocks; in some instances there is a sharp, cross cutting relationship between vein generations while in others, especially in the various breccias, there is an almost continuous brecciated gradation from one vein type to the next.

Individual vein occurrences can be fairly isolated, consisting of a small vein with simple, often almost monomineralic composition, while the larger veins typically show a zoned pattern with hyalophane, diopside, and allanite at the vein margins and apatites, particularly breccias, occupying the central portion of the vein. Only rarely are all vein generations found in a single vein intersection; most intersections contain only 2 or 3 of the generations of mineralization. In many instances, particularly in the zoned veins, the central portion of the vein is faulted, and all that is recovered by drilling is rubbly core or fault gouge.

4.3.1.1 DIOPSIDE – ALLANITE VEINS

The oldest of the REE bearing veins are the diopside-allanite dominant variety. In outcrop these veins are typically between 30 cm and 2 m in width and are often traceable at surface several meters along strike (Fig. 4.6). The contacts with the host rock are usually quite sharp, although in a minor number of cases there does seem to be a slightly ragged or gradational contact. The gradational contacts are always quite narrow; typically less than 2 cm wide. Also, in a minor number of cases, clasts or xenoliths of the wall rock can be found within the veins.

The proportion of minerals in the diopside-allanite veins is quite erratic or patchy in nature, but each vein consists of a few essential components. The dominant minerals in this vein generation are allanite, diopside, and hornblende; although in most cases the amphibole present in the veins appears to be an alteration product rather than a primary mineral. The concentration of allanite ranges from only a few percent in some locations

Figure 4.6 Diopside-allanite vein showing the sharp, linear contacts typical of this vein generation. Contacts shown by dashed white line. Hammer head is aligned N-S.

to almost 95% in some of the allanite rich sections of the veins (Fig. 4.7). In addition to the dominant minerals, the veins can also contain hyalophane and minor amounts of apatite. The apatite which occurs in this vein generation is mainly small, dark red crystals. There are also a number of accessory minerals which may or may not be present such as pyrite, calcite, biotite, epidote, titanite, hematite, or magnetite.

In contrast to the surrounding rocks, which often show signs of intense ductile deformation, the diopside-allanite veins in the JAK zone lack evidence of significant strain. The relatively fresh, unstrained nature of these veins suggesting a late, post ductile deformational, origin. In some of the diopside-allanite veins there is some minor evidence of brittle deformation, mainly as angular clasts found at the contacts with the younger apatite generations or rare xenoliths of wall rock. Although the veins do not contain evidence of ductile deformation there is evidence of metamorphism, or possibly hydrothermal alteration, in the form of amphibole replacing some of pyroxene crystals in the veins (Fig. 4.8).

It should be noted that although allanite can be found in trace quantities throughout all the vein generations, the vast majority of the allanite is confined to this early vein generation. The majority of allanite in the subsequent breccias occurs as clasts derived from the diopside-allanite vein generation. The early diopside-allanite vein type accounts for approximately 25 percent of the overall vein system.

Figure 4.7 Close up of the vein from figure 4.6 showing the allanite rich nature of the vein.

Figure 4.8 Alteration of a large pyroxene crystal to amphibole from trench # 9 in the JAK Zone. The lighter green in the above photo is pyroxene, while the darker flecks are amphibole.

4.3.1.2 RED APATITE BRECCIA

Volumetrically, the red apatite breccias are the most significant portion of the vein system. There are clearly multiple brecciation events, and in some cases it is possible to observe cross-cutting breccia generations. There are also apatite breccia clasts which suggests more than one generation of breccia formation. The apatite breccias are not the straight-sided veins typical of the earlier diopside-allanite veins; the

apatite breccia veins are much more erratic in strike and amorphous in shape (Fig. 4.9). At the margins of some of the apatite veins there can be a biotite dominant section, in rare instances up to almost meter thick. These biotite-rich sections can be essentially monomineralic or, more typically, contain small amounts of apatite or calcite. In many cases the red apatite breccias occur within the diopside-allanite veins, often with a brecciated, gradational margin between the two vein generations.

The essential component to these breccias is the red apatite crystals and clasts for which this vein generation is named. The apatite or breccia clasts range from sub-angular to sub-rounded. In addition to the apatite, there is often abundant biotite and up to 5% hornblende found in the breccias. There are also sub-angular clasts of both the wall rock and the earlier diopside-allanite present in many of the breccias (Fig. 4.9). The size range of the clasts is generally 5mm to 3 cm, although the complete range in sizes extends from less than 1mm to greater than 10 cm.

The composition of the matrix of the red apatite breccias varies frequently, often within a single vein. The most common components of the matrix include a mix of apatite, calcite, chlorite, scapolite, and hematite, with only the relative proportions of each mineral varying between samples. The breccias range from essentially clast supported breccias to completely matrix supported, with a complete gradation between the two end members.

4.3.1.3 GREEN APATITE BRECCIA

The green apatite ranges from a bright, vivid green to a more muted, grayish color. The green apatite breccias are usually clast supported, although matrix supported varieties do exist, and there is often a gradational contact with the red apatite breccias (Fig. 4.10). Green apatite rims can be found on some of the apatite clasts in the red apatite breccias and there are often small green apatite crystals in the red apatite breccias, suggesting some overlap between the two generations. The matrix composition is relatively simple compared to the variety observed in the red apatite breccias in that it is almost entirely composed of calcite, quartz, and apatite.

A)

B)

Figure 4.9 Examples of the red apatite breccia (A) Large allanite-diopside clasts in a red apatite breccia. Picture shows the west wall of the bulk sample pit. (B) Allanite-Diopside clasts at the contact between the red apatite breccia and the diopside-allanite vein. Northwest edge of the bulk sample pit.

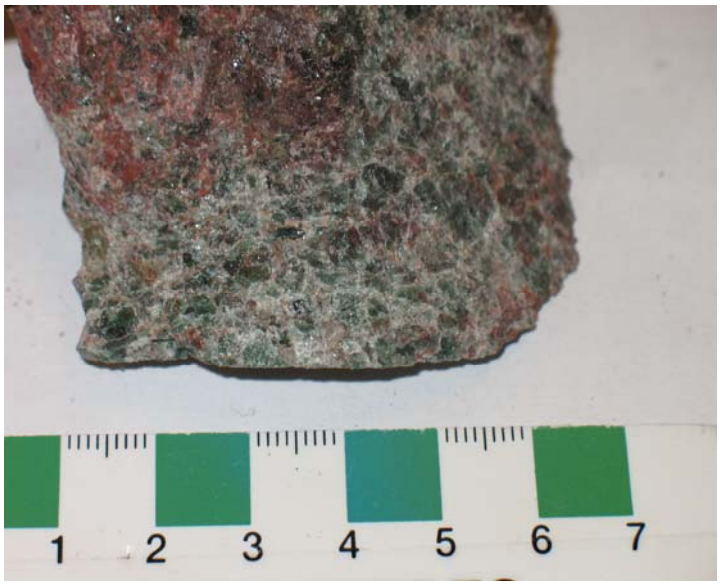

Figure 4.10 Green apatite breccia from DDH HL06-75. Upper left corner of the sample contains moderate amounts of the red apatite breccia grading to the green apatite breccia in the lower right. The matrix in the green portion contains abundant calcite. Scale bar in cm.

The green apatite breccia is relatively rare; there is no surface exposure of the green apatite in the JAK zone and it is only occasionally observed in drill core. The centers of the green apatite breccia veins are often faulted, and all that is recovered during drilling is loose rubble, which makes it difficult to collect representative samples of this rare vein type.

4.3.1.4 COARSE RED APATITE

The coarse red apatite is the youngest of the mineralized vein generations at Hoidas Lake. These veins are essentially monomineralic and cross cut all earlier vein generations (Fig. 4.11). This vein generation is dominated by large, bright red apatite crystals, generally 1 to 2 cm in size, but may also contain trace amounts of allanite, hornblende, pyrite, calcite, and hematite. Most of the accessory minerals in this vein generation occur either as rare euhedral inclusions in the apatite or, more commonly, as small euhedral to anhedral interstitial crystals. A unique feature of these apatite veins is that they lack the brittle deformation features of the earlier vein generations. The coarse red apatite veins are also typically quite narrow; consistently under a meter in total width.

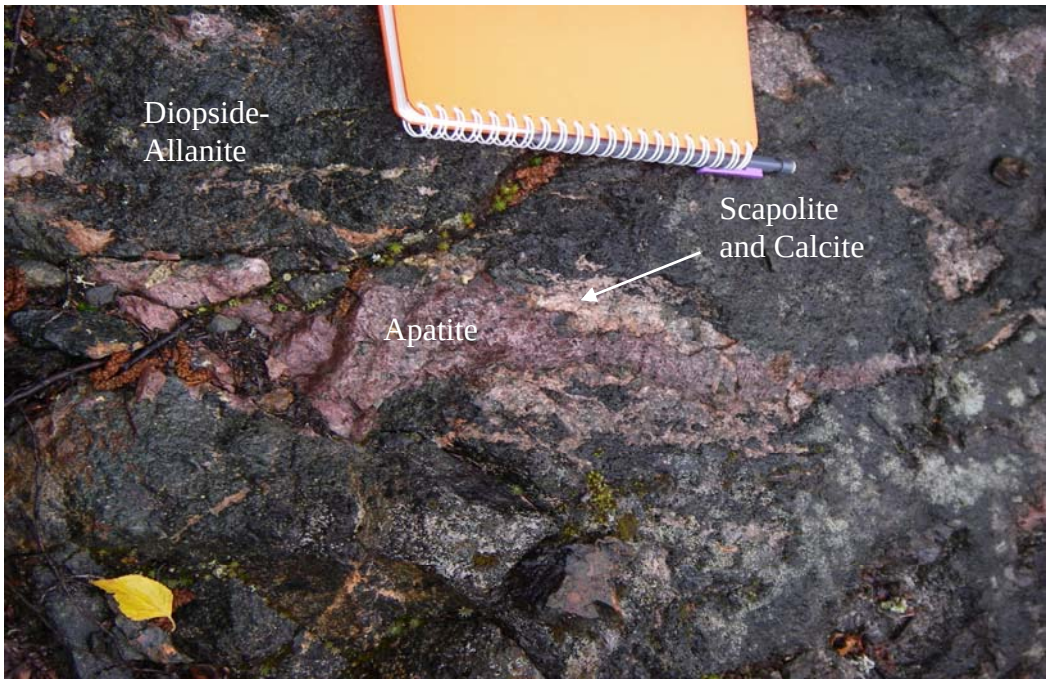

Figure 4.11 Small vein of coarse red apatite in a diopside-allanite vein. Minor amounts of calcite and scapolite are associated with the apatite.

4.3.2 ADDITIONAL REE SHOWINGS IN THE HOIDAS LAKE AREA

In addition to the JAK zone there are approximately 25 other showings concentrated along the Hoidas Nisikkatch fault. Due to the wealth of information available in the JAK zone the majority of the field work focused on this area, however a few of the additional showing were also briefly examined to confirm the extent of the vein system and the consistency of vein characteristics. The additional showings which have been examined include those at the southern end of Hoidas Lake, referred to as the Hoidas South showing, and at the southern tip of Nisikkatch Lake (Fig. 4.5).

4.3.2.1 HOIDAS SOUTH SHOWINGS

The showing examined and sampled at Hoidas South consisted of a single large outcrop which has been blasted and stripped of vegetation to improve the exposure of the veins. The total exposed area measures approximately 14 by 22 m. The host rock in this area is a moderately to strongly deformed granite, with minor intrusions of a hyalophane-rich pegmatite and the occasional diorite dike. Unlike the JAK Zone, the

dikes in this area tend to be ductilely deformed, and are commonly folded. The hyalophane-rich rock appears porphyroclastic, with a mylonitized matrix hosting up to 35% hyalophane porphyroclasts. Associated with the hyalophane porphyroclasts are amphibole, diopside and allanite crystals which are essentially undeformed, suggesting that they may be the result of later alteration. This material typically borders the REE rich zones and often forms a tectonite containing entrained clasts of vein material.

The entire exposed area is sheared and faulted, with the most prominent feature being what appears to be the surface expression of the Hoidas-Nisikkatch Fault, a 1 to 2 m wide zone of intensely fractured rock (Fig 4.12). The brittle features of the fault appear to overprint a large section of ductilely deformed granite, which is typically strongly mylonitized. The granitic mylonite at Hoidas South is similar in appearance to the mylonite observed near the JAK zone veins, with strong quartz ribboning being the most readily apparent feature in the mylonites.

Figure 4.12 Surface expression of the Hoidas-Nisikkatch fault near the Hoidas South REE showings.

The majority of the vein generations found in the JAK zone are also recognizable at Hoidas South, with some minor differences. The youngest apatite generation, the coarse red apatite, does not seem to be as prevalent at Hoidas South, but there are examples of the green apatite breccias in outcrop, something which was not observed in the JAK zone trenches (Fig. 4.13). The diopside-allanite veins typically have very sharp contacts with the host rock, and often have either hyalophane-rich sections or biotite at their contacts with the granitic mylonite. The apatite veins vary from having fairly sharp contacts to a much more gradational, brecciated boundary. Samples of each vein type, as well as the unusual hyalophane-hornblende pegmatite, were obtained for comparison to the samples which were collect from the JAK zone.

The key difference between the mineralization at Hoidas South and that observed in the JAK zone trenches is that the Hoidas South veins contain evidence of ductile deformation, while the JAK zone veins are essentially brittle features. In some places, particularly immediately adjacent to the fault, the veins are isoclinally folded, with slightly thickened hinges and may feature attenuated limbs (Fig. 4.13). Further away from the fault zone the folds are more open. The mineralization mainly occurs in the fold nose, and often consists of disrupted or boudinaged band of hyalophane and apatite in an amphibole-biotite matrix. It tends to be the earliest veins which show the majority of the ductile deformation, with later veins showing only minor ductile or even brittle features indicating that the vein formation occurred over a broad range of conditions. Based on the limited data from Hoidas South it is difficult to fully explain the relationship between the largely brittle features of the JAK Zone compared to the ductile deformation of some of the early veins at Hoidas South. The difference in deformational style may simply be a result of the proximity to the Hoidas-Nisikkatch fault at the Hoidas South showing.

4.3.2.2 NISIKKATCH SHOWINGS

At the southern end of Nisikkatch Lake there are a number of old trenches which expose the REE mineralized veins. Unfortunately, in many cases the trenches have been partially refilled, and in some cases overly enthusiastic blasting resulted in the destruction of the majority of the showing. In these cases the entire surface showing,

A)

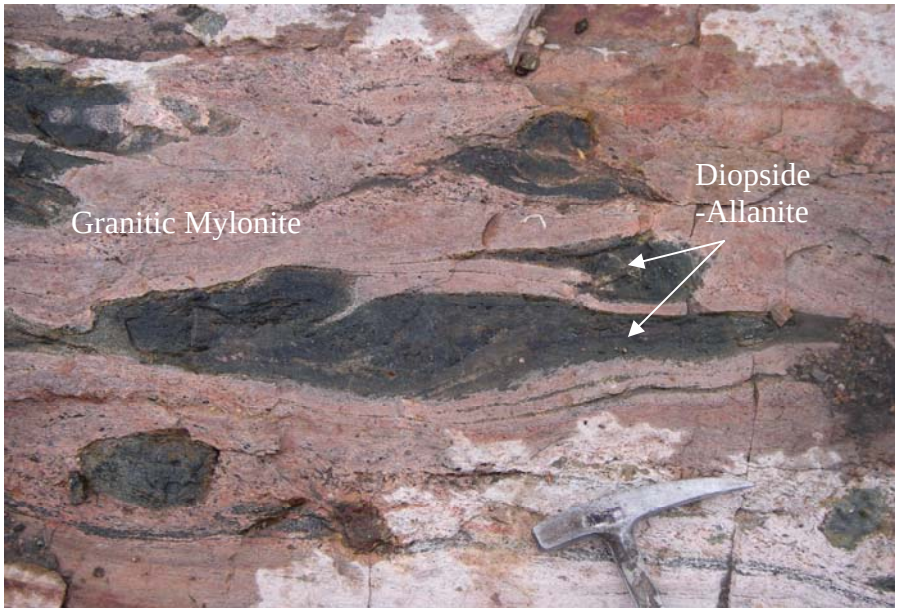

B)

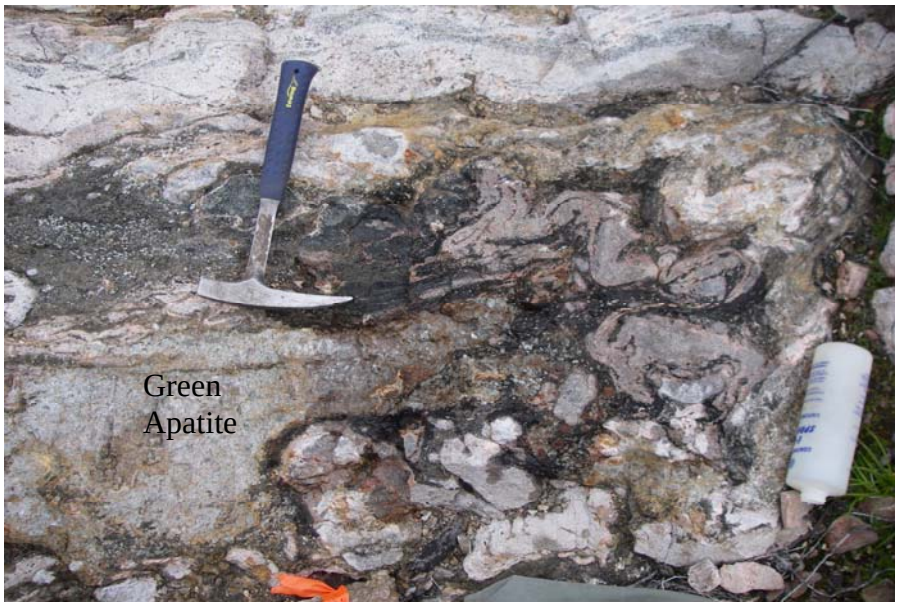

Figure 4.13 Deformed veins at Hoidas South A) Intensely deformed diopside-allanite vein at Hoidas South. Hinges of the folded Diopside-Allanite vein are thickened with attenuated limbs. B) Green apatite occurrence at Hoidas South. The Green apatite in the center of the fold is separated from the folded, deformed granite by a dark layer of biotite with minor allanite and amphibole.

including the contacts to the host rocks, have been destroyed; any continuation at depth is typically buried by the rubble. Examination of the rubble, which is often largely composed of vein material, yields some information about vein composition and relationships.

The key difference between the Nisikkatch showings and those on Hoidas Lake is the apparent absence of the hyalophane-rich pegmatites in the immediate proximity of the Nisikkatch showings. However, further reconnaissance work and mapping at Nisikkatch may reveal additional, currently unrecognized, igneous phases. Another feature which is unique to Nisikkatch is the presence of a number of small, late quartz veinlets and rusty patches of weathered sulfides in the outcrop. The fairly pervasive potassic and hematitic alteration observed at Hoidas Lake is not as consistent at the Nisikkatch showings. In some cases the alteration is essentially absent, while other veins feature strongly altered wall rocks. In the cases where the alteration is present there are usually proximal granitic pegmatites, suggesting that the alteration may be related to pegmatitic activity as opposed to being directly related to the veins themselves.

Continuing down strike from the trenched showings there are a number of small, typically less than 30 cm in width, veins which often exhibit a slightly anastomosing geometry. Similar to the diopside-allanite veins in the JAK zone, these veins display sharp, linear contacts and can be traced along strike for several meters and in most cases show only brittle signs of deformation. In one instance a small, boudinaged diopside-allanite vein was encountered, suggesting that the vein was exposed to ductile conditions at some point after it formed (Fig. 4.14).

4.4 PARAGENESIS OF THE HOIDAS LAKE DEPOSIT

The relative timing of the veins in relation to the some of the magmatic, metamorphic, and deformational events could not be determined by field relationships. It is clear from observed cross cutting relationships that the mineralized veins are younger than the tonalite, diorite, granodiorite and granites of the region, which are considered to be Archean to Paleoproterozoic in age (Ashton et al., 2005; Ashton et al., 2007). The timing of the pegmatites and lamprophyres observed in the area, in relation

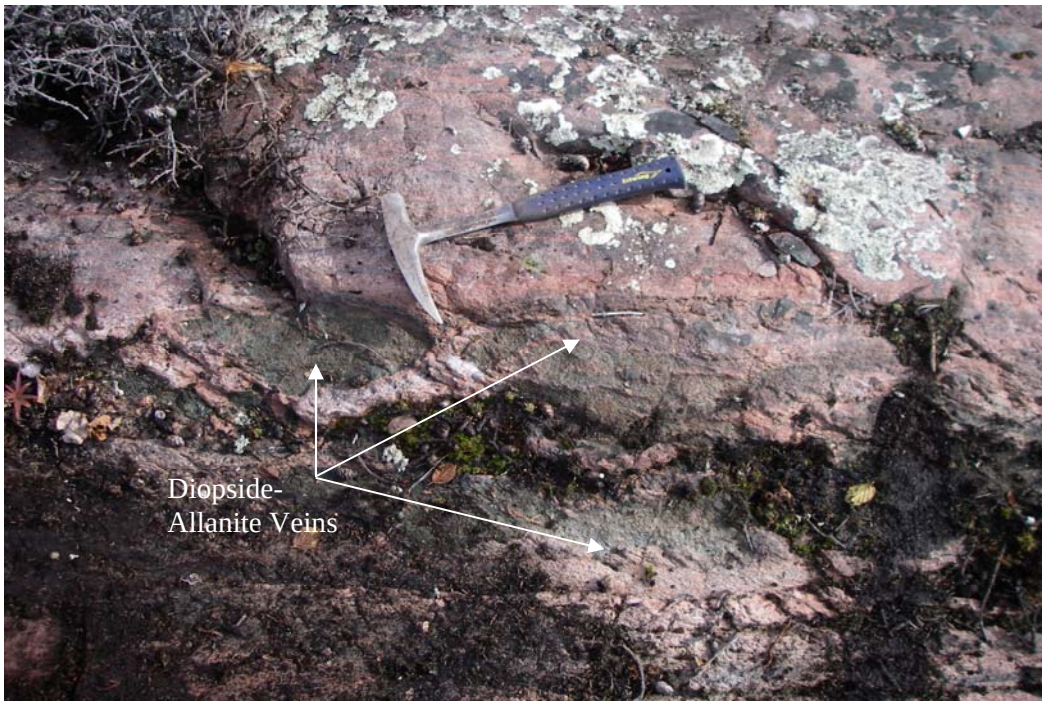

Figure 4.14 Narrow boudinaged diopside-allanite vein south of the trenched Nisikkatch showings. Rock hammer for scale.

to the timing of the veins, cannot be ascertained by field relationships; absolute dating will be required (Fig. 4.15).

However, geochronological data obtained in the region has been used to suggest that the lamprophyres intruded at approximately 1.83 Ga and that the veins formed at approximately 1.87 Ga, although there is some debate about the accuracy of these absolute age determinations (Gunning and Card, 2005). The estimate of 1.83 Ga for the Hoidas Lake lamprophyres assumes that these lamprophyres are contemporaneous with the lamprophyres of the Dubawnt Supergroup, approximately 500 km to the northeast in Nunavut (Peterson et al., 2002). However, the Dubawnt lamprophyres have been difficult to date with certainty due to the lack of appropriate minerals for geochronological studies. The available dates for the Dubawnt lamprophyres are fairly imprecise; the most common age quoted is a U-Pb age 1,832 +/- 30 Ma obtained from monazite and apatite, although additional dates of 1,825 +/- 12 Ma and 1,850+/- 30 Ma have been obtained from these lamprophyres or associated rocks (Peterson and van Breemen, 1999; Peterson et al., 2002). The age of the REE veins at Hoidas is based on a

single, unpublished, U-Pb monazite age determination reported by Gunning and Card (2005), although there is very little additional information provided such as which vein generation the sample was taken from or whether the monazite is a primary or secondary mineral. Currently, the pegmatite generations in the area have not been dated, and have only been observed cross cutting the igneous host rocks of the region.

From the detailed examinations of the vein system it is clear that there are multiple vein generations, with the diopside-allanite veins being the oldest vein generation. Although the diopside-allanite veins are clearly one of the oldest vein generations in the system, allanite mineralization is somewhat ubiquitous, with allanite occurring to some extent in almost every mineralized vein generation, as well as in most of the host rocks in the area as a trace mineral. From the presence of multiple apatite breccia generations it is clear that there were either several discrete episodes of apatite mineralization or that the apatite veins formed over a protracted period of time (Fig. 4.15).

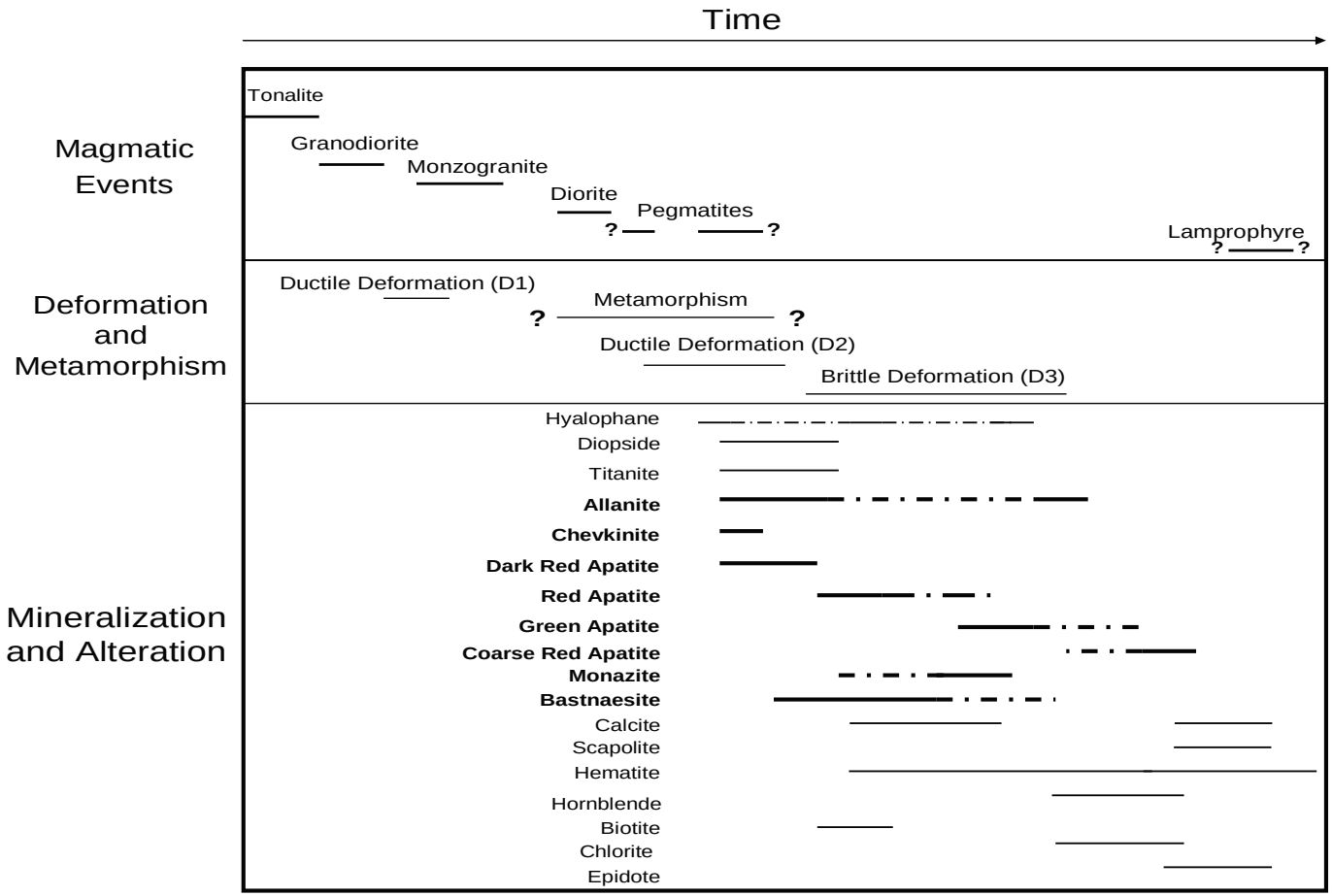

Figure 4.15 Preliminary paragenesis of the Hoidas Lake REE vein system. Although the above diagram is primarily based on information obtained during the examination of the JAK zone, relationships observed at both the Hoidas South and Nisikkatch showings were taken into account during the construction of the diagram. Question marks indicate the lack of necessary information to establish relative relationships and therefore the position on the diagram is tentative at best.

CHAPTER 5
HOST ROCK CHARACTERISTICS

5.1 INTRODUCTION

The veins are hosted by a variety of metamorphosed, dominantly igneous rocks, although there has been no detailed systematic mapping and associated petrographic and geochemical analysis to properly define and characterize these rocks. The aim of this chapter is to provide a preliminary petrographic and geochemical description of the dominant rock types in the area. In order to assess the potential relationships between the host rocks and the REE veins, representative samples of the major host rock types were collected for further analysis. Outcrop samples were taken perpendicular to the strike of the vein system; the spacing of the sampling along these lines is somewhat erratic, as it was dictated by the location of outcrops. Additional samples of the pegmatites and lamprophryes in the surrounding area were also obtained for analysis. A single sample of pegmatite from the Hoidas South showing was obtained due to its similarity to some of the more unusual pegmatites in the JAK Zone area which could not be sampled satisfactorily near the JAK zone.

For each of the samples a polished thin section was made to confirm the field identification and to allow for a detailed examination of the mineralogical and petrographic features. Additional thin sections of the host rock, provided by Great Western Minerals, were also examined. These additional samples were collected from both outcrop and drill core. In addition to the petrographic analysis, the major and trace element concentrations were determined for 11 samples, including three pegmatite samples and three lamprophyre samples, by x-ray fluorescence spectrometry (XRF). Supplemental ICP-MS analyses were obtained for the lamprophyre and pegmatites due to their potential temporal relation to the vein system.

5.2 MINERALOGICAL AND PETROGRAPHIC FEATURES

5.2.1 TONALITE

Petrographic examination of the samples identified as tonalite in the field revealed that although plagioclase is the dominant mineral, typically 60 to 70%, they also contain approximately 15% quartz and up to 15% potassium feldspar. There is also

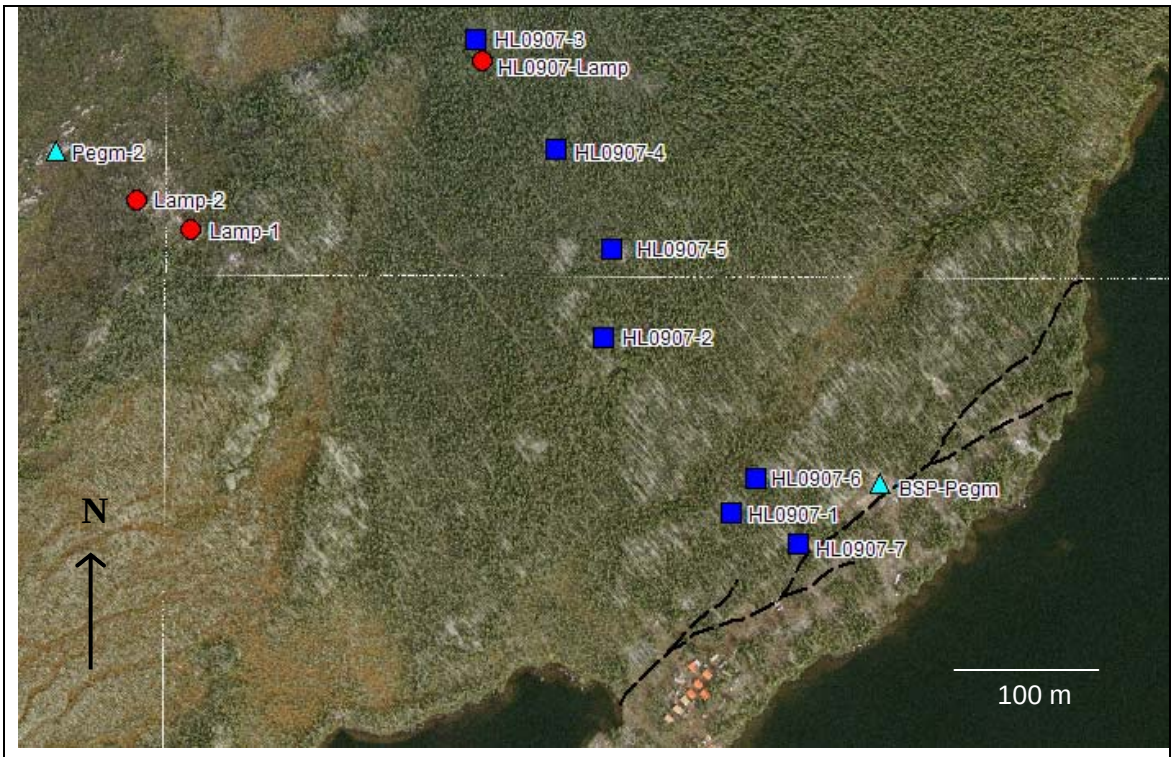

Figure 5.1 Outcrop samples locations. Samples shown were collected perpendicular to the strike of the JAK Zone. Additional samples of the pegmatites and lamprophyres were collected for analysis. Sample HS-Pegm is not shown in the above diagram as it was collect from the showing at Hoidas South. Dashed line indicates the approximate surface trace of the vein.

a variable amount of hornblende, up to 15% in some cases, and therefore many of these samples are more accurately described as granodiorite as opposed to a tonalite. These samples typically contain small amounts of biotite, normally less than 5%, with traces of apatite, zircon, chlorite, epidote and carbonates. The opaques observed in these samples are dominated by magnetite with minor amounts of ilmenite, hematite, and chalcopyrite.

In most samples the feldspars are relatively fresh, although the outcrop samples often show some minor alterations to clays. The plagioclase typically has moderately defined twinning, although in some of the more strained samples deformation twins can be observed. The potassium feldspar ranges from a perthitic variety to a tartan-twinned microcline. The quartz typically displays undulose extinction, and is often riddled with secondary fluid inclusions. The samples are typically moderately foliated, with the

hornblende and other ferromagnesian phases defining the foliation. In most cases the ferromagnesian phases show minor alteration to greenschist facies minerals, suggesting minor retrograde metamorphism.

5.2.2 GRANODIORITE

Plagioclase, typically albite twinned, makes up approximately 45% of these samples while there is around 25% quartz. At the boundary between plagioclase and quartz crystals there is sometimes myrmekite. In addition to the quartz and plagioclase there is also approximately 10% potassium feldspar and up to 15% biotite. Minor amounts of hornblende (up to 5%) and traces of apatite, titanite, carbonate, epidote and chlorite are also found in these samples (Fig. 5.2). The opaque minerals are dominated by magnetite (up to 2 or 3%) with minor amounts of pyrite, hematite and ilmenite.

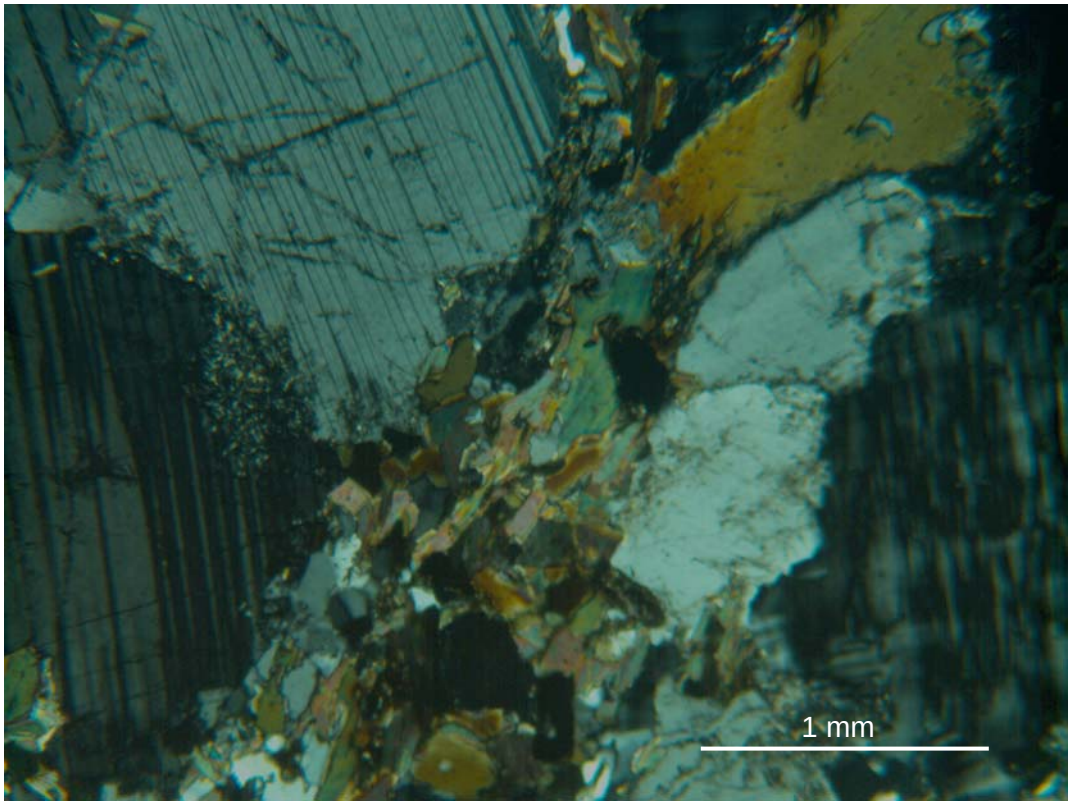

Figure 5.2 Example of granodiorite from sample HL0709-4. Left side of the image is dominated by plagioclase, while the centre and right consists of biotite, quartz and k-feldspar. Image taken under crossed polars.

The intensity of deformation varies slightly between samples, although on average the granodiorites are weakly to moderately foliated, with rare samples showing a distinctly gneissic fabric. The quartz tends to be quite strained and may have a slightly elongate appearance in thin section. The feldspars in these samples are frequently altered, with the most common alteration types being sericitic and hematitic. Minor chloritic alteration can be observed on the biotite, and when present the epidote also appears to be a secondary mineral, suggesting retrograde metamorphism.

5.2.3 MONZOGRANITE

The rocks identified as granites or monzogranites show the most variation in composition, with the granitic mylonite samples typically having a slightly more alkali-granite to syenitic composition. Petrographic analysis indicated that this group of rocks ranges from granites and monzogranite, senso stricto, to quartz syenite and even rare examples of alkali feldspar quartz syenite. The most common mineral in these samples is a slightly turbid potassium feldspar, commonly microcline, which can reach concentrations of up to 80%, although more typically the concentration is between 40 to 65%. In addition to the microcline and other alkali feldspars there can be up to 25% quartz, which often contains inclusions of trace minerals or secondary fluid inclusions. Minor amounts of biotite, amphibole, and plagioclase can be found, along with traces of apatite, zircon, titanite, muscovite, chlorite, epidote and carbonate (Fig. 5.3). These samples also contain relatively rare magnetite, hematite and pyrite.

The fabric in most samples is not as apparent in thin section as it is in hand sample or outcrop, which is likely a function of the scale of the layering, and only rarely can the thin sections be described as gneissic. Overall the granitic samples tend to be weakly foliated, although the quartz is often deformed, displaying moderate to strong undulose extinction, and often has an elongated shape. Clots of biotite and hornblende may also present, and can help to further define the foliation. The prescence of chlorite and epidote in most samples suggest a minor amount of retrograde metamorphism.

The feldspar shows moderate sericitic alteration, although the intensity of the alteration varies. Minor hematitic alteration is common along late fracture sets which cross cut the granite. There also seems to be some correlation between proximity to the

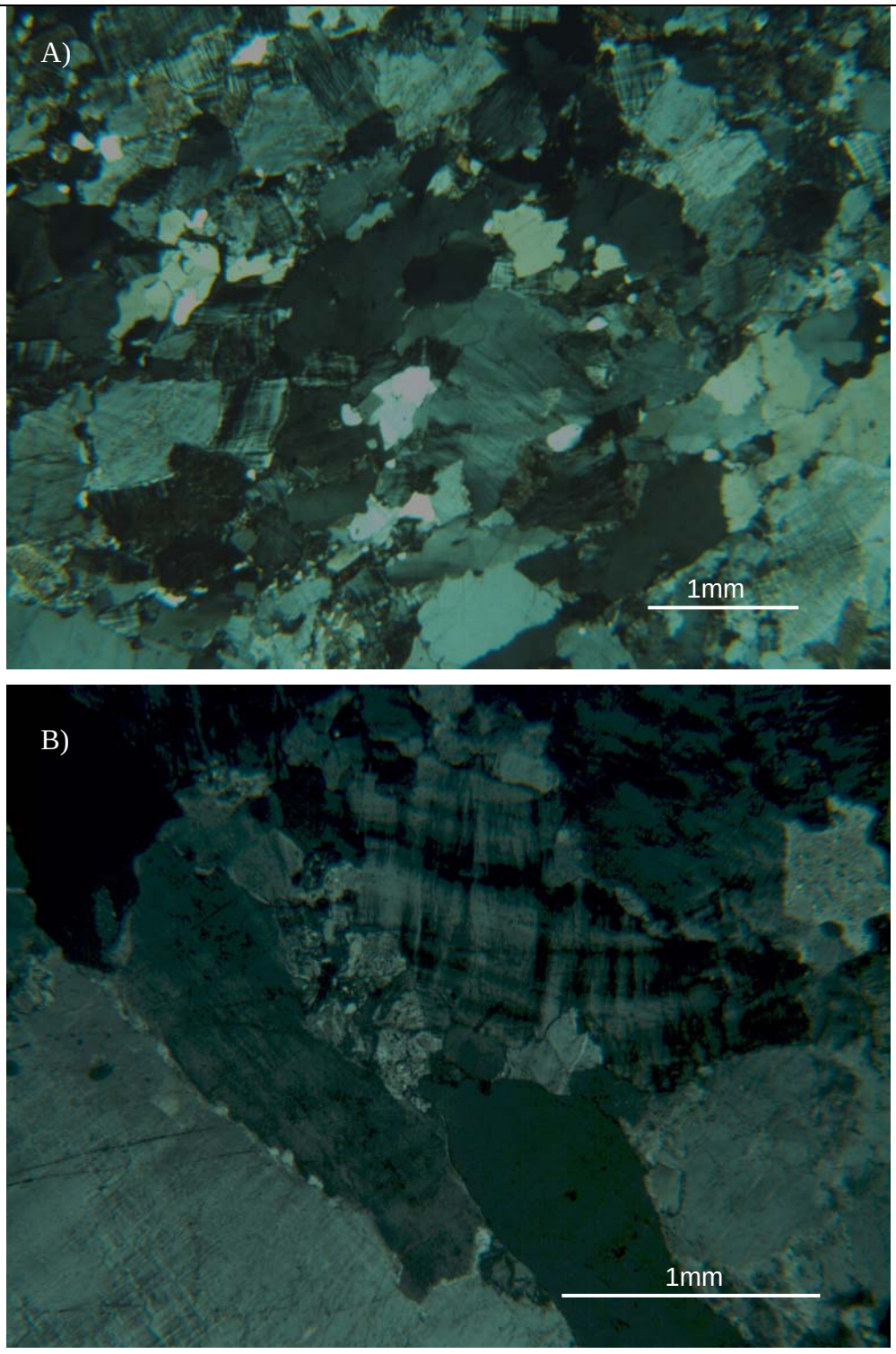

Figure 5.3 Monzogranite from samples HL0709-3 and HL0709-7. Both samples are dominated by k-feldspar with minor amounts of quartz. Image (A) shows Sample HL0709-3 and (B) Sample HL0709-7. Both images taken under crossed polars.

veins and the relative proportions of hematite and magnetite; with increased separation from the veins magnetite becomes more prevalent, while sample adjacent to the veins seem to contain more hematite. In some samples a rim of hematite surrounds the magnetite suggesting this difference may be the result of alteration rather than a primary feature. It is unclear whether this alteration is a result of the vein emplacement or simply represents a late oxidation event.

5.2.4 PEGMATITES

The three pegmatite samples represent some of the most commonly encountered pegmatite compositions found in the Hoidas Lake area. Although there are a number of similarities between the pegmatite types, there are also a number of key differences. Although all samples contain quartz, alkali feldspars and plagioclase, the amounts of each of these minerals can vary substantially from sample to sample. In all three examples the amount of plagioclase is quite low, typically under 5%. The amount of quartz varies from less than 5% in the HS-Pegm to approximately 20% in the BSP-Pegm. The alkali feldspar content is also somewhat variable, ranging from a low of 50% in the BSP-Pegm to up to 85% in Pegm-2. All samples also contain trace amounts of magnetite. Each of the pegmatites displays minor evidence of retrograde metamorphism, with most pegmatites containing minor to trace amounts of chlorite, epidote, and tremolite or actinolite.

The accessory mineral content of the samples is highly variable. In this respect the most unusual pegmatite is the HS-Pegmatite sample which contains up to 10% amphibole as well as minor to trace amounts of clinopyroxene, apatite, titanite, allanite, magnetite and fluorite. The most common amphibole in this sample appears to be hornblende, although in rare instances it seems to have optical properties more typical of an arfvedsonite. There is also a very minor amount of tremolite to actinolite, which appears to be largely an alteration product of the earlier amphiboles. Although the quartz in this sample displays undulose extinction, the sample as a whole is relatively undeformed and only slightly altered (Fig. 5.4).

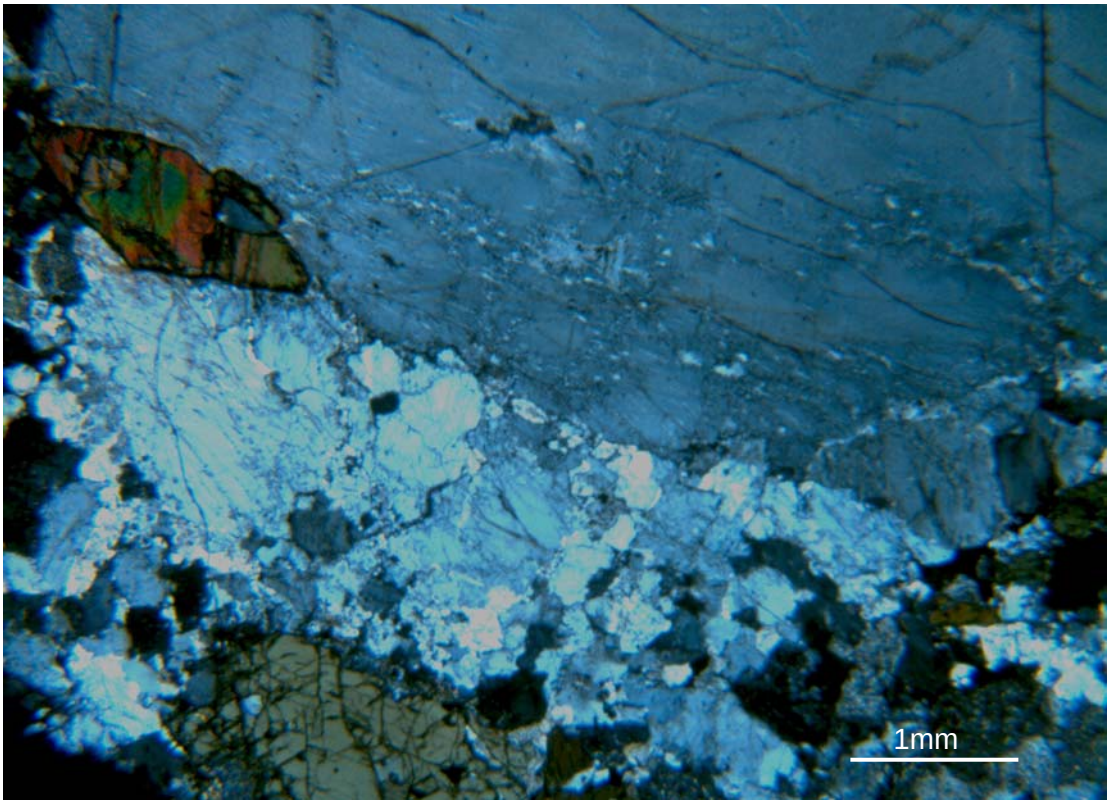

Figure 5.4 Image of the HS-Pegm The majority of the image consist of k-feldspar and quartz with a euhedral titanite in the upper left corner of the image and a subhedral hornblende in the lower left corner. Image taken under crossed polars.

The unusual mineralogy of the HS-Pegm clearly contrasts with the fairly typical mineralogy encountered in Pegm-2. In addition to the abundant quartz and alkali feldspars, Pegm-2 also contains minor amounts of muscovite, epidote, chlorite and traces of hematite, magnetite and chalcopyrite. Of the three pegmatite samples this is the least deformed and least altered (Fig. 5.5 (A)). Sample BSP-Pegm also contains minor amounts of amphibole, pyroxene, and titanite, although in smaller amounts than observed in the HS-Pegm (Fig. 5.5 (B)). Minor to trace amounts of biotite, muscovite, chlorite, epidote and calcite are also present in this sample. The BSP-Pegm is the most intensely deformed of the sampled pegmatites, with strong undulose extinction in the quartz and some indication of a preferred orientation to some of the mafic minerals. Also, in some areas there seems to be a reduction in crystal size related to the intense deformation (Fig. 5.5(B)).

A)

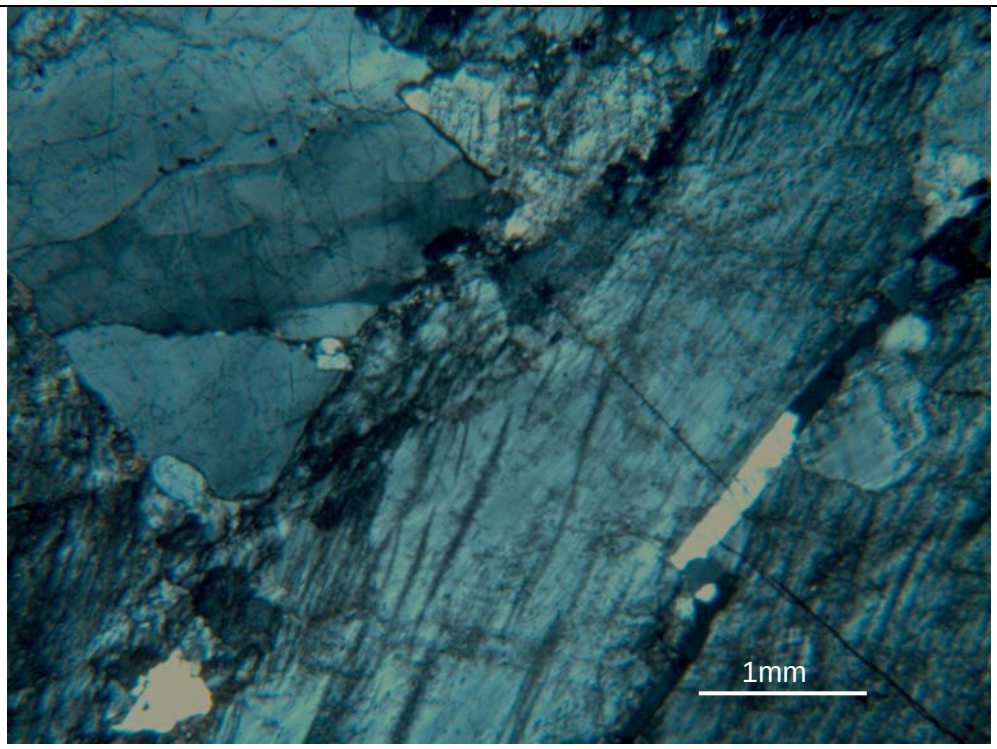

B)

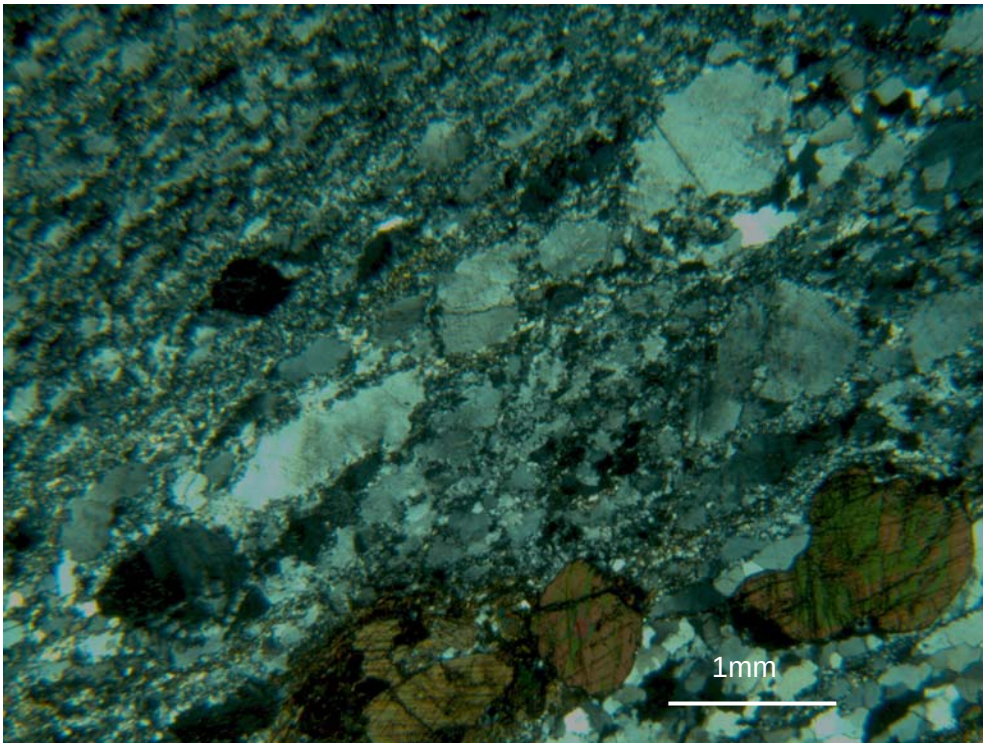

Figure 5.5 Granitic pegmatites Image (A) shows an example of Pegm-2. The upper left of the image shows weakly undulose quartz with the remaining area dominated by k-feldspar. Image (B) shows the highly deformed BSP-Pegm. Majority of the image consists of quartz and k-feldspar, with subhedral titanite in the lower right of the image. Images taken under crossed polars.

5.2.5 LAMPROPHYRES

All the lamprophyres encountered in the Hoidas Lake area are porphyritic, with the most common phenocrysts being biotite and a less common, often altered, amphibole. The groundmass is fine grained, massive and is largely composed of very fine crystals of feldspar; most of the feldspars are slightly perthitic potassium feldspar, although minor amounts of microcline and rare plagioclase can also be observed. In addition to the feldspars, the groundmass contains minor to trace amounts of diopside, olivine, apatite, titanite, epidote and carbonate (Fig. 5.6). Rare opaques can be found in the groundmass; typically magnetite rimmed by hematite, suggesting a secondary change in the oxidation of the system. In some cases there may also be minor amounts of pyrite and traces of chalcopyrite. The composition of these lamprophyres suggests that they can be more accurately named either a minette, or possibly a vogesite, depending on the relative abundances of hornblende and biotite. In almost all cases biotite is the dominant phenocryst, suggesting the composition is closer to that of a minette (Le Maitre, 1989).

The lamprophyres typically lack the deformation observed in most of the other rocks in the Hoidas Lake area, although there is some evidence of minor metamorphism. Minor amounts of alteration have resulted in the formation, at the expense of some of the primary minerals, of actinolite, epidote, and chlorite, suggesting the lamprophyres were exposed to greenschist metamorphic conditions. This is clearly evident in both types of phenocrysts, with chloritic alteration present to varying degrees on the biotite, while the hornblende may be almost completely replaced by a combination of chlorite, tremolite and actinolite. These secondary greenschist facies minerals can also be observed in the groundmass. In at least one of the lamprophyres the groundmass seems to be weakly hematized, predominantly along fracture planes.

5.3 WHOLE ROCK GEOCHEMISTRY

Eleven of the outcrop samples were analyzed by XRF for their major and trace element content. These samples include three representative samples of the visually distinct pegmatites and three lamprophyres. The remaining five samples are of the granitoid host rocks and were collected along a transect perpendicular to the strike of the

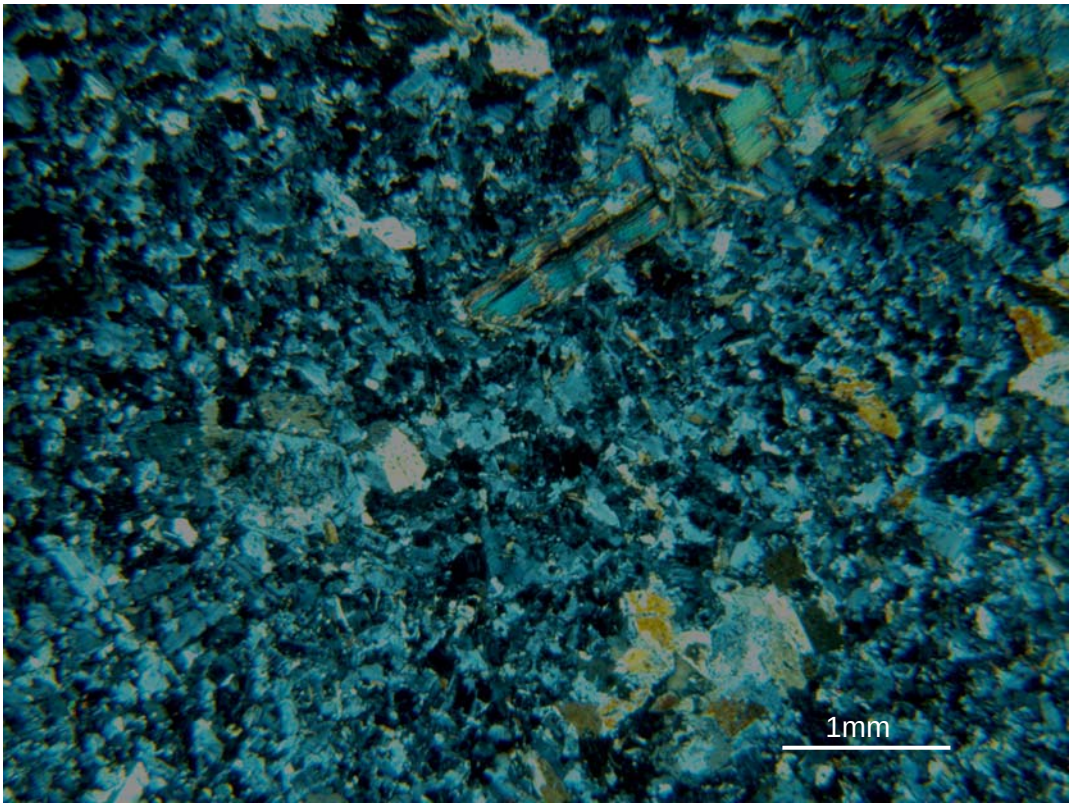

Figure 5.6 Lamprophyre in thin section, from sample Lamp-2, showing the porphyritic nature. Large biotite phenocrysts are present in the upper right of the image. Groundmass is largely composed of K-feldspars with minor amounts of amphibole, diopside and epidote. Image taken under crossed polars.

veins. The granitoid rocks sampled in the field consisted of rocks identified as either granites or granodiorites; due to the relatively restricted nature of the tonalite in the immediate vicinity of the JAK zone it was not encountered during this transect and therefore was not sampled. Overall, the whole rock geochemistry will provide constraints on the character of the host rocks to the deposit and will help assess their potential relationship to the vein system. Finally, the analysis of the lamprophyres will help confirm that all the encountered lamprophyres are of a single generation, based on the similarity of their field and petrographic characteristics. Analyses of the lamprophyre can also be used to compare the Hoidas Lake lamprophyres to those of the Dubawnt group to determine if there is any possibly relation, as suggested by Gunning and Card (2005).

5.3.1 XRF RESULTS

Each of the samples was analyzed for their major element content as well as for their Nb, Zr, Y, Sr, Rb, and Ba contents. Details of the analytical procedure can be found in Appendix B. Results of the XRF analysis are provided in Table 5.1 and 5.2. Two samples of the original eleven were selected for ICP-MS analysis to examine their REE content (Table 5.2). Due to the fairly unremarkable mineralogy and chemistry of the granitoids and some of the pegmatites the decision was made to focus further geochemical analysis on the lamprophyres and the HS-Pegmatite sample. The similar chemical content of the three analyzed lamprophyres in the XRF analysis suggests that additional analysis of the three would likely continue to yield similar results. In light of the previously encountered similarities, a single representative sample of the lamprophyres was selected for the more detailed ICP-MS analysis. Details of the analytical procedure can be found in Appendix B.

5.3.2 MAJOR ELEMENT CONCENTRATIONS

5.3.2.1 GRANITOIDS

The host rocks at Hoidas Lake range in SiO_2 composition from a low of 61 wt.% in sample HL0907- 2 to a high of 73.5 wt. % in sample HL0907-7 (Table 5.1). The total alkalis (Na_2O+K_2O) range from a low of 8.17 wt. % in sample HL0907-2 to a high of 10.68 wt. % in HL0907-7. In all the analyzed granitoids the proportion of K_2O is greater than Na_2O; this is especially apparent in samples near the vein system, HL0907-7 and HL0907-1, which might indicate potassic alteration associated with vein formation (Fig. 5.7). The analyzed samples range from metaluminous to peralkaline in nature (Fig. 5.8). The granitoids which fall into the peralkaline range are samples HL0907-1, HL0907-3, and HL0907-7. These three samples may have experienced some alteration as samples HL0907-1 and HL0907-7 occur in close proximity to the veins and sample HL0907-3 occurs near a lamprophyre.

The majority of the samples display relatively low Fe_2O_3, MgO, TiO_2 and CaO contents, with the highest values being recorded by HL0907-2 (Fig. 5.7). The differences between HL0807-2 and the other granitoid samples is likely the amount of amphibole, biotite and iron bearing opaques present in the sample.

Table 5.1 Summary of Granitoid Host Rock XRF Results

	HL0907-1	HL0907-2	HL0907-3	HL0907-4	HL0907-7
SiO_2	73.4	61.0	72.8	66.9	73.5
Al_2O_3	13.7	17.3	14.1	15.6	13.6
Fe_2O_3	0.98	5.32	2.35	3.54	0.75
MgO	0.09	1.95	0.26	1.16	0.16
CaO	0.33	4.11	0.68	2.52	0.39
Na_2O	2.56	3.47	2.85	3.39	2.11
K_2O	7.44	4.70	6.82	5.05	8.57
TiO_2	0.04	0.73	0.24	0.46	0.01
P_2O_5	0.03	0.21	0.08	0.11	0.07
MnO	0.01	0.08	0.03	0.06	0.02
Cr_2O_3	0.02	0.03	0.02	0.03	0.02
Nb	bdl	11	7	14	bdl
Zr	127	454	309	295	60
Y	5	24	16	22	5
Sr	669	597	240	748	233
Rb	185	134	199	169	148
Ba	3014	2020	627	2172	582

Major oxide concentration given in wt.% and the trace element content in ppm. Bdl. – Below detection limit. See Fig. 5.1 for sample locations.

5.3.2.2 PEGMATITES

The pegmatites have a fairly moderate, restricted range of SiO_2 values which vary from 63 to 68.5 wt. % (Table 5.2). The total alkali content is broadly similar to that observed in the granitoids; the pegmatite values range from a high of 10.35 wt. % to a low of 7.85 wt. %. Again, the proportion of K_2O is greater than Na_2O, as was observed for the granitoids. For most of the major oxides values obtained for the pegmatites fall within the range of variation displayed by the granitoids (Fig. 5.7). An exception to this is the Na_2O content of Pegm-2 which is distinctly lower than the other samples. Sample HS-Pegm, which is the hyalophane bearing pegmatite found adjacent to the mineralization at Hoidas South, is the only peralkaline pegmatite sample, with the other two samples being metaluminous (Fig. 5.8).

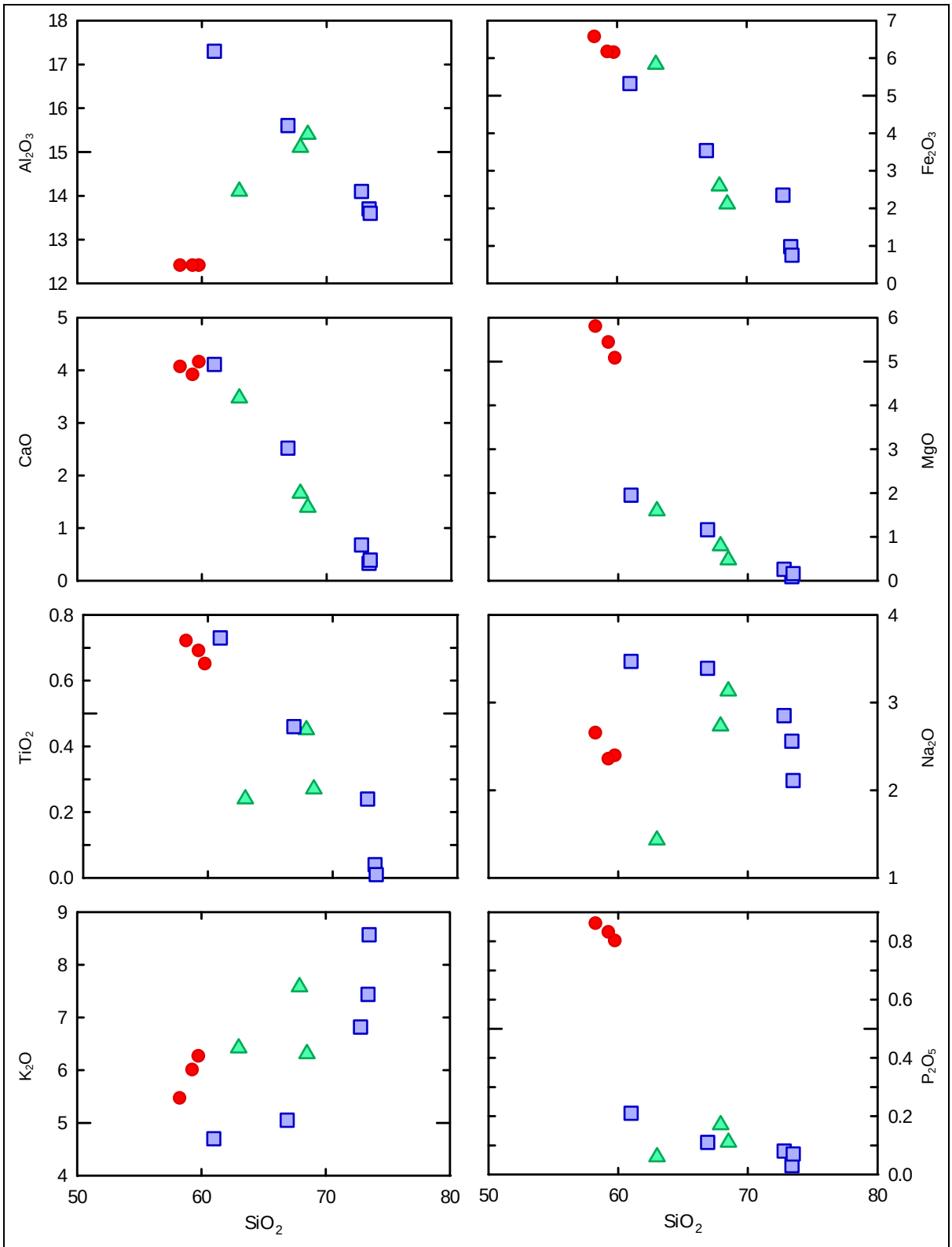

Figure 5.7 Element variation diagrams. All values in the above diagram are in wt %. Lamprophyres shown by red circles, pegmatites by green triangles and granitoids by blue squares.

Table 5.2 Summary of XRF and ICPMS Results for Pegmatites and Lamprophyres.

	HS-Pegm	BSP-Pegm	Pegm-2	Lamp-1	Lamp-2	HL0709-Lamp
SiO_2	67.9	68.5	63.0	59.8	58.3	59.3
Al_2O_3	15.1	15.4	14.1	12.4	12.4	12.4
Fe_2O_3	2.59	2.11	5.83	6.14	6.56	6.16
MgO	0.79	0.47	1.59	5.07	5.79	5.43
CaO	1.66	1.39	3.47	4.15	4.06	3.91
Na_2O	2.73	3.13	1.43	2.39	2.65	2.35
K_2O	7.58	6.31	6.42	6.26	5.46	6.00
TiO_2	0.45	0.27	0.24	0.65	0.72	0.69
P_2O_5	0.17	0.11	0.06	0.80	0.86	0.83
MnO	0.04	0.04	0.08	0.10	0.10	0.09
Cr_2O_3	0.01	0.02	0.01	0.02	0.02	0.02
Nb	16	3	2	12	13	13
Zr	416	497	86	251	281	288
Y	46	13	13	25	24	24
Sr	3482	1499	487	1122	991	1085
Rb	188	154	142	297	230	258
Ba	6345	5313	5631	4674	4209	4205
La	227.7	na	na	50	na	na
Ce	478.1	na	na	97	na	na
Pr	76.1	na	na	13.4	na	na
Nd	292.6	na	na	48.2	na	na
Sm	49.2	na	na	8.5	na	na
Eu	12.8	na	na	1.4	na	na
Gd	27.5	na	na	6.5	na	na
Tb	1.5	na	na	0.6	na	na
Dy	10.2	na	na	3.6	na	na
Ho	1.3	na	na	0.6	na	na
Er	3	na	na	1.5	na	na
Tm	0.3	na	na	0.2	na	na
Yb	1.7	na	na	1.1	na	na
Lu	0.2	na	na	0.1	na	na

Major oxide concentration given in wt.% and the trace element content in ppm. NA. – not available. See Fig. 5.1 for sample locations.

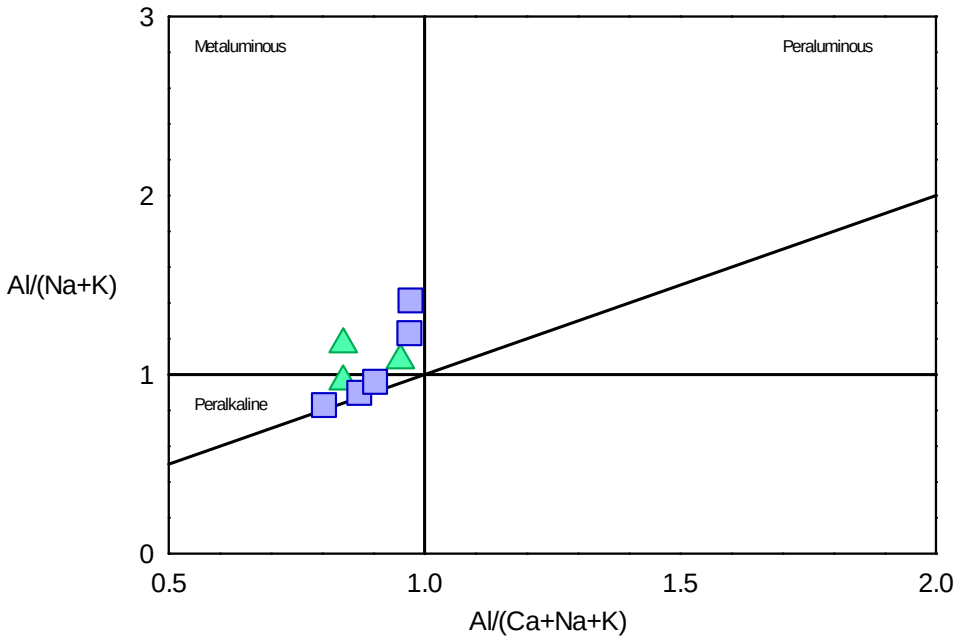

Figure 5. 8 Shand's Index (Maniar and Piccoli, 1989) of the analyzed whole rock samples. Pegmatites are represented by the green triangles and the granitoids by the blue squares.

5.3.2.3 LAMPROPHYRES

In terms of the major, and also the trace elements, the three lamprophyres samples are essentially identical, despite their slight macroscopic or petrological differences (Fig 5.7). Due to the similarity in their chemistry the three lamprophyres found in the JAK Zone likely represent a single event. Based on the whole rock chemistry they are best classified as calc-alkaline lamprophyres. The lamprophyres contain between 58.3 and 59.8 wt. % SiO_2 and, for their SiO_2 content, relatively high alkalis. As would be expected for calc-alkaline lamprophyres the K_2O content is much higher than the Na_2O content and, compared to other varieties of lamprophyre, the TiO_2, P_2O_5 and MnO contents are relatively low (Rock, 1987).

5.3.3 TRACE ELEMENT CONCENTRATIONS

5.3.3.1 GRANITOIDS

Although the host granitoids with the lowest Y content are samples HL0907-1 and HL0907-7, the closest to the mineralized vein system, the presence of the veins appears to have very little influence on the Y content of the host rocks. As was observed in the majority of the major element plots sample HL0907-1 and HL0907-7 typically display similar values for most trace elements, and have identical values for Y, suggesting that there is no reduction of Y, and therefore of the REE in general, due to close proximity to the veins (Fig. 5.9).

There does however, seem to be a reduction in the Ba content of the host rock with increased proximity to the veins as sample HL0907-7 has only a fraction of the Ba content found in HL0907-1. Sample HL0907-3 also has a very low Ba value, although there is no associated feature in outcrop to explain this apparent reduction, suggesting that the apparent fluctuation in Ba content could be due to primary compositional variations of the monzogranites rather than any sort of secondary alteration associated with the mineralization. A similar, although less extreme, pattern is also observed for Sr. All of the granitoids plot within either the collisional or volcanic arc granite fields on the discrimination diagrams proposed by Pearce et al., (1984) (Fig. 5.10).

5.3.3.2 PEGMATITES

An unexpected feature of the Ba plot is that although HS-Pegm contains the highest overall Ba content, is really not that distinct, especially considering the presence of hyalophane in this pegmatite (Fig. 5.9). This suggests that Ba may be a common substitution in the alkali feldspars in the other pegmatite generations. Surprisingly, it is the Y and Sr values which clearly distinguish the HS-Pegm pegmatite from not only the other host rocks, but also from the other pegmatites. Both the BSP- Pegm and Pegm-2 plot with the host granitoids in terms of their Y and Sr, while the concentration in the HS-Pegm is several times higher. Yet another distinct feature of the HS-Pegm is that it is the only sample which plots in the within plate granite field on the discrimination diagrams (Fig. 5.10).

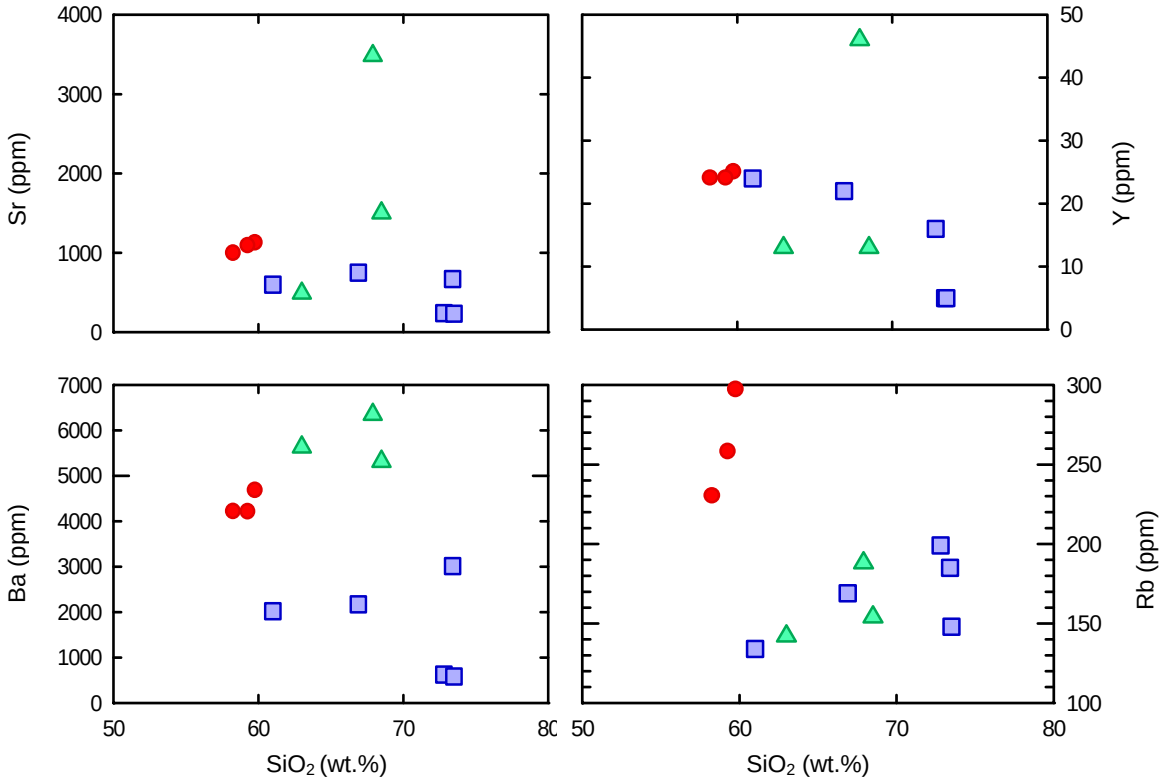

Figure 5.9 Trace elements variations plotted against SiO_2. Trace element content in ppm and SiO_2 is in wt%.

Sample HS-Pegm is LREE enriched, with the chondrite normalized REE plot displaying a negative slope, with a $(La/Yb)_N$ ratio of 134. The slope is not consistent across the full range of REE; the segment from La to Nd is quite flat, with a $(La/Nd)_N$ ratio of approximately 1, while from Sm to Yb is much steeper, with a $(Sm/Yb)_N$ ratio of almost 30 (Fig. 5.11).

5.3.3.3 LAMPROPHYRES

Similar to the major element patterns, the lamprophyres typically plot in a tight cluster in most of the trace element diagrams (Fig. 5.9). However, the Rb content of the lamprophyres is higher than for the granitoids or pegmatites. Overall, the trace element composition of the lamprophyres is fairly unremarkable, as most values are quite close to the average values compiled by Rock (1987). The exception to this is the Ba content

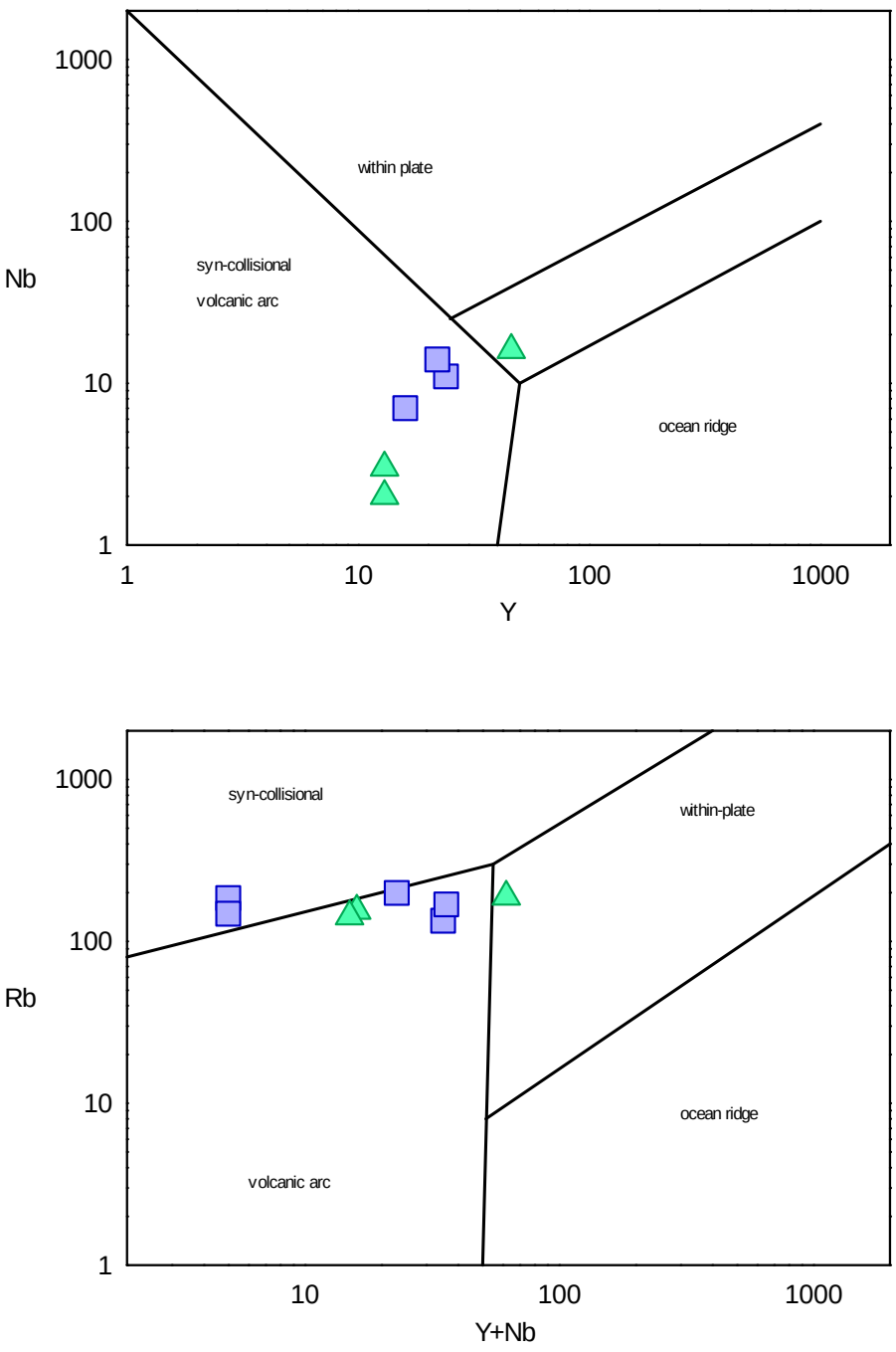

Figure 5.10 Discrimination diagrams as proposed by Pearce et al., 1984. Pegmatites are represented by the green triangles and the granitoids by blue squares.

of the lamprophyres which, at over 4000 ppm, is much higher than the mean of 1900 ppm listed by Rock (1987).

REE content of the lamprophyre is also within the range typically observed for calc-alkaline lamprophyres (Rock, 1987). The Hoidas Lake lamprophyres display a negative slope on the chondrite normalized REE diagram, although they are not as LREE enriched as the HS-Pegm. The $(La/Yb)_N$ ratio of the lamprophyre is 45, although the slope is more consistent than that of the HS-Pegm. Another difference is that the lamprophyre has a slight negative Eu anomaly which was not observed in the pegmatite (Fig. 5.11).

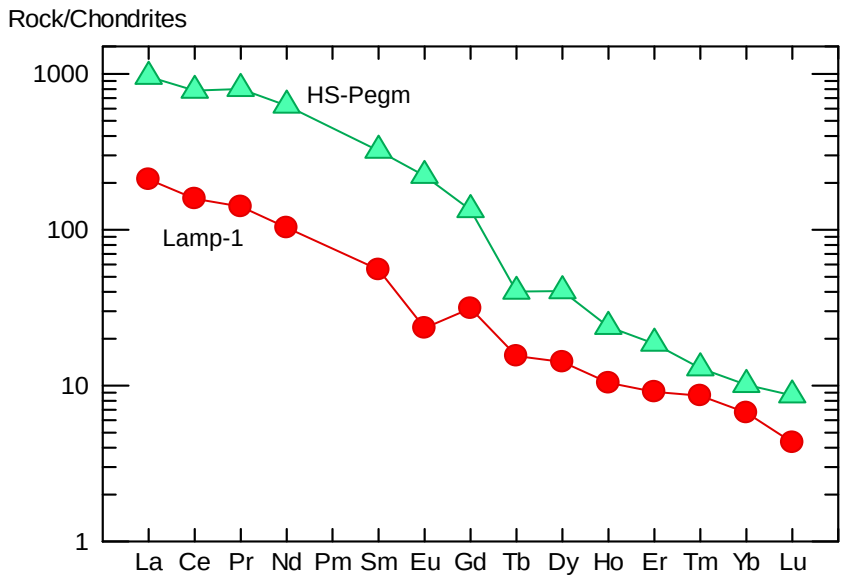

Figure 5.11 REE plot of selected samples. All samples are normalized using the chondrite values from Sun and McDonough (1989). Triangles represent HS-Pegm, circles the lamprophyre.

5.4 RELATION OF THE HOIDAS LAMPROPHYRES TO THE DUBAWNT LAMPROPHYRES

The lamprophyres encountered at Hoidas Lake have previously been assumed to be equivalent to the ultrapotassic minettes found in the Christopher Island Formation of the Dubawnt Supergroup in the Northwest Territories (Gunning and Card, 2005). The Dubawnt minettes are believed to be between 1.85 to 1.80 Ga, although attempts to

accurately date these lamprophyres have been difficult due to the paucity of appropriate minerals for geochronology. The Dubawnt lamprophyres are part of an ultrapotassic dike swarm which are believed to extend as far south as the northern edge of Lake Athabasca, and thus could be found in the Hoidas Lake area (Peterson et al., 2002).

The Dubawnt minettes are highly porphyritic, with the main phenocyrsts consisting of phlogopite, clinopyroxene and apatite, with approximately 25% of the lamprophyres containing olivine phenocyrsts. In all examples the groundmass is dominated by potassium feldspars, which are often rich in Ba, with minor amounts of alkali amphibole, titanite, magnetite and primary carbonates. There may also be rare occurrences of resorbed diopside (Peterson et al., 2002). From a petrographic standpoint the Dubawnt minettes show some similarities to the lamprophyre samples from Hoidas Lake although there are some differences. The key differences are not in the presence or absence of minerals, but as to whether a given mineral occurs as a phenocryst or is restricted to the matrix. For example, in the Hoidas Lake lamprophyres apatite does occur as a phenocryst, although it can also be found in the groundmass, and clinopyroxene phenocrysts are rare, with clinopyroxene mainly restricted to the groundmass. Another difference is the lack of olivine phenocrysts and, as these are only observed in a fraction of the Dubawnt minettes, it is possible that the lack of olivine in the Hoidas Lake samples is a function of the small number of samples examined.

The chemical characteristics of the Dubawnt lamprophyres include an average SiO_2 content of 53 wt. %, although there is a significant amount of variation with values ranging from 43 to 59 wt. % (Table 5.3). There is also some variation observed in the amount of CaO, with an average CaO content around 5.6 wt. %; although this is slightly depleted compared to the average calc-alkaline lamprophyre, which contain 6.6 wt. % CaO, it is still within the accepted range of 4 to 9 wt. % CaO (Rock, 1987; Peterson et al., 1994; Peterson et al., 2002). These lamprophyres typically contain much more K_2O than Na_2O, with a mean K_2O/Na_2O which is greater than 4, and are highly magnesian, with an average Mg/(Mg+Fe) of approximately 0.73. The Al_2O_3 content of the Dubawnt minettes is moderate, around 12%, which is typical of calc-alkaline minettes, however, the low Ca content combined with the high K concentration suggests that they may be

more accurately termed a transitional minette-lamproite (Peterson et al., 1994; Peterson et al., 2002).

The Dubawnt lamprophyres tend to be enriched in LILE and incompatible elements and display a large depletion of HFSE in relation to their K, Rb, Sr, Ba and Th content (Peterson et al., 1994). In particular Ti, Nb, and Ta tend to be strongly depleted in these lamprophyres (Fig. 5.12) (Peterson et al., 2002). These lamprophyres are LREE enriched, displaying a negative slope with a $(La/Yb)_N$ of between 58 and 203 (Fig. 5.13). In most cases the lamprophyres lack an Eu anomaly, although in a small number of instances a slight negative Eu anomaly exists (Peterson et al., 1994).

Table 5.3 Major element composition of the average Dubawnt Lamprophyre compared to the Hoidas Lake Lamprophyres

	Dubawnt Lamprophyres			Hoidas Lake Lamprophyres		
	Average	P97-c32	P97-t138b	Lamp-1	Lamp-2	HL0709-Lamp
SiO_2	53.2	59.6	51.14	59.8	58.3	59.3
Al_2O_3	12.0	12.4	10.33	12.4	12.4	12.4
FeO	6.3	5.17	7.53	6.14	6.56	6.16
MgO	9.2	5.89	9.87	5.07	5.79	5.43
CaO	5.6	5.00	8.03	4.15	4.06	3.91
Na_2O	1.6	3.36	1.46	2.39	2.65	2.35
K_2O	6.9	3.57	4.13	6.26	5.46	6.00
TiO_2	0.8	1.09	1.11	0.65	0.72	0.69
P_2O_5	0.8	1.45	1.55	0.80	0.86	0.83

Major oxide concentration in wt. %. Average composition of the Dubawnt Lamprophyre from Peterson et al., 1994. Examples P97-c32 and P97-t138b are from Peterson et al., 2002.

Examining the geochemistry of the Hoidas Lake lamprophyres there are a number of similarities to the Dubawnt minettes, although there are also some differences. In terms of the major element composition the amount of SiO_2 and Al_2O_3 found in the Hoidas lamprophyres is similar to that observed in the Dubawnt minettes, although the SiO_2 content is at the upper end of what occurs in the Dubawnt lamprophyres (Table 5.3). However, there are differences in the content of the other major elements. The maximum CaO in the Hoidas lamprophyres is 4.15% and the

K_2O/Na_2O is lower at about 2.4. The Mg/(Mg+Fe) is also lower for Hoidas at 0.46 instead of the 0.73 ratio obtained from the Dubawnt lamprophyres.

The Hoidas Lake lamprophyres have the observed enrichment of incompatible and LILE seen in the Dubawnt minettes, as well as relatively depleted Nb, Ta and Ti content, and plot with in the range displayed by the Dubawnt minette on MORB-normalized spider diagrams (Fig. 5.12). The REE plot (Fig. 5.13) shows slightly more variation between the Hoidas Lake lamprophyres and the Dubawnt lamprophyres. The LREE are not as enriched in the Hoidas Lake lamprophyres, falling below the range of the Dubawnt lamprophyres, although the HREE content is a similar. The $(La/Yb)_N$ ratio of the Hoidas Lake lamprophyres, at 45, is similar to what is observed for the Dubawnt lamprophyres. There is a slight Eu anomaly in the Hoidas Lake lamprophyres which is more distinct than the Dubawnt minettes.

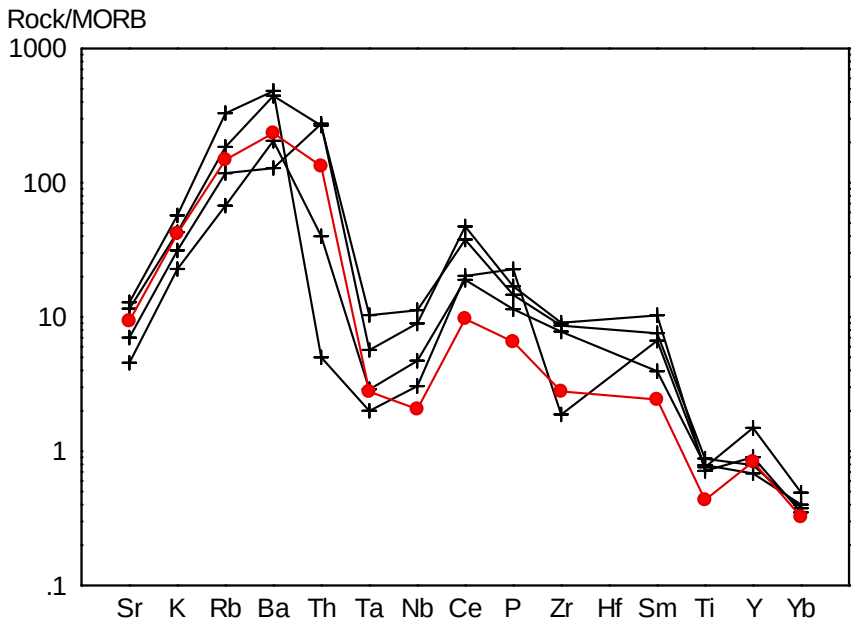

Figure 5.12 MORB-normalized spider diagram comparing the Hoidas Lake and Dubawnt lamprophyres. Hoidas Lake lamprophyres are shown by the red circles and the Dubawnt minettes by the black crosses. All Dubawnt values from Peterson et al., (2002).

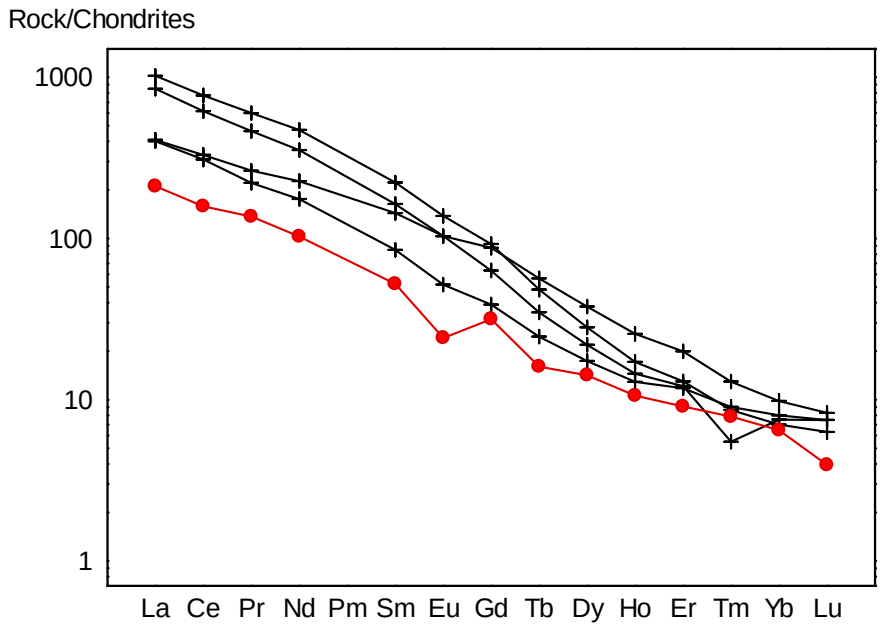

Figure 5.13 Chondrite normalized REE plot of the Hoidas Lake and Dubawnt lamprophyres. Hoidas Lake sample is shown by the red circles and the Dubawnt minettes by the black crosses. Dubawnt REE content from Peterson et al., (2002) and chondrite values from Sun and McDonough (1989).

Although there are many similarities between the Hoidas and Dubawnt lamprophyres there are also a number of differences, making it impossible to confirm their relation by chemistry alone. Many of these apparent differences may be a function of small sample size as opposed to a true difference in chemical composition; for this reason additional geochronological data will aid in assessing the potential relationship of the Hoidas Lake lamprophyres to the Dubawnt lamprophyres.

5.5 POTENTIAL RELATION OF THE HOST ROCKS TO THE MINERALIZATION AT HOIDAS LAKE

The host rock immediately adjacent to the veins does not appear to be a contributing factor to the mineralization. There is little to no visible alteration of the host rocks in the vicinity of the veins, suggesting only limited interaction between the mineralizing system and the wall rocks at any significant scale. This observation is supported by the whole rock geochemistry, which only shows slightly potassic alteration

associated with proximity to the vein system. The mild potassic alteration is restricted to the area immediately adjacent to the contact between the veins and the host rocks, with the evidence of alteration rapidly fading into fresh wall rock within a matter of meters. Rare examples of gradational contacts occur at cm scale, indicating that to fully assess the interaction between the wall rock and the mineralizing system sampling at a much finer scale would be required.

The pegmatites and lamprophyres are potentially more interesting than the host rocks. Although it is difficult to assess their potential relation to the mineralization due to an absence of cross-cutting field relationships the unusual chemistry displayed by the hyalophane-bearing pegmatites and the lamprophyres are intriguing, particularly the enrichment in the REE, Sr and Ba. If nothing else the presence of these igneous rocks indicates the presence of an unusual igneous environment in the region at broadly the time of vein formation.

CHAPTER 6
MINERALOGY AND CHEMISTRY OF THE VEINS

6.1 INTRODUCTION

The REE-rich veins of the JAK zone at Hoidas Lake are part of a 10 km long trend of REE showings centered along the Hoidas-Nisikkatch fault. The anastomosing, eastward dipping vein system contains abundant apatite and allanite, which are the main REE carriers in this deposit, and only minor amounts of monazite and bastnaesite. This is distinctly different than the typical REE deposits in which REE are dominantly found in monazite or bastnaesite.

The vein system at Hoidas Lake is complex, hosting multiple vein generations with a range of mineralogical associations. The earliest veins consist of REE-bearing allanite, titanite, chevkinite, and minor apatite, in association with clinopyroxene and hyalophane. The allanite-rich veins are followed by veins dominated by red or green apatite, both of which are typically brecciated. Finally, there is a late apatite which crosscuts all previous vein generations. Although the macroscopically distinct apatite generations are lower in grade than the allanite they will provide the main source of REE, due to the large volume of apatite present in the vein system.

The initial examination of the veins in both outcrop and drill core resulted in the separation of the veins into distinct generations based on the observed macroscopic relationships. Representative samples of each of the vein types and the various styles of mineralization from both outcrop and drill core were obtained for further petrographic analysis. The majority of the samples were taken from the JAK zone, although a limited number of samples from both the Hoidas South and Nisikkatch showings were also examined.

The initial petrographic analysis consisted of the examination of 25 polished thin sections provided by Great Western Minerals. These samples allowed for a basic review of the mineralogy of the vein system and also provided some evidence of the later alteration. The information obtain from this initial set of samples was supplemented by an additional 45 polished thin sections which were selected to show not only the individual vein generations, but also the relationships between the generations.

From the entire set of 70 polished thin sections 16 samples were selected for electron microprobe analysis (EMPA). The composition of the major minerals found in the veins was analyzed by wavelength dispersive spectrometry (WDS). The main focus of the EMPA was to characterize the chemical composition of the main REE-bearing minerals of the various vein generations and to confirm the composition of the most common gangue minerals. The backscattered electron images obtain also helped to provide further information on the textural relationships between these minerals. Details of the analytical procedure and results can be found in Appendix B.

Following the EMPA analysis a series of whole rock ICP-MS analysis were obtained for each vein generation. In total 13 vein samples were analyzed for their complete REE composition as well as a suite of 34 additional elements. The whole rock samples were selected to be representative of their vein generation and at least one sample from each set has corresponding EMPA data available. Details of the analytical technique and the results can be found in Appendix B.

6.2 MINERALOGICAL AND PETROGRAPHIC FEATURES

6.2.1 DIOPSIDE-ALLANITE VEINS

The earliest vein generation is dominated by diopside and allanite, with varying amounts of hyalophane, titanite, amphibole, dark red apatite and rare chevkinite (Fig. 6.1). There are also traces of biotite, epidote, chlorite, calcite, hematite, magnetite and pyrite present in these samples. The relative proportion of each mineral varies erratically from sample to sample and the presence or absence of the minor minerals is also unpredictable.

The allanite most commonly found in these samples is anhedral to rarely subhedral and very coarsely crystalline, with the large crystals up to several cm in size. Particularly in the larger crystals the allanite is strongly zoned and in several cases displays a dark, likely metamict, core (Fig. 6.1 and 6.2). Petrographically, metamict allanite can be recognized by changes to the optical properties, such as decreased birefringence and pleochroism in partially metamict samples. Fully metamic allanite is isotropic (Giere and Sorensen, 2004). The zones present in the allanite are broadly

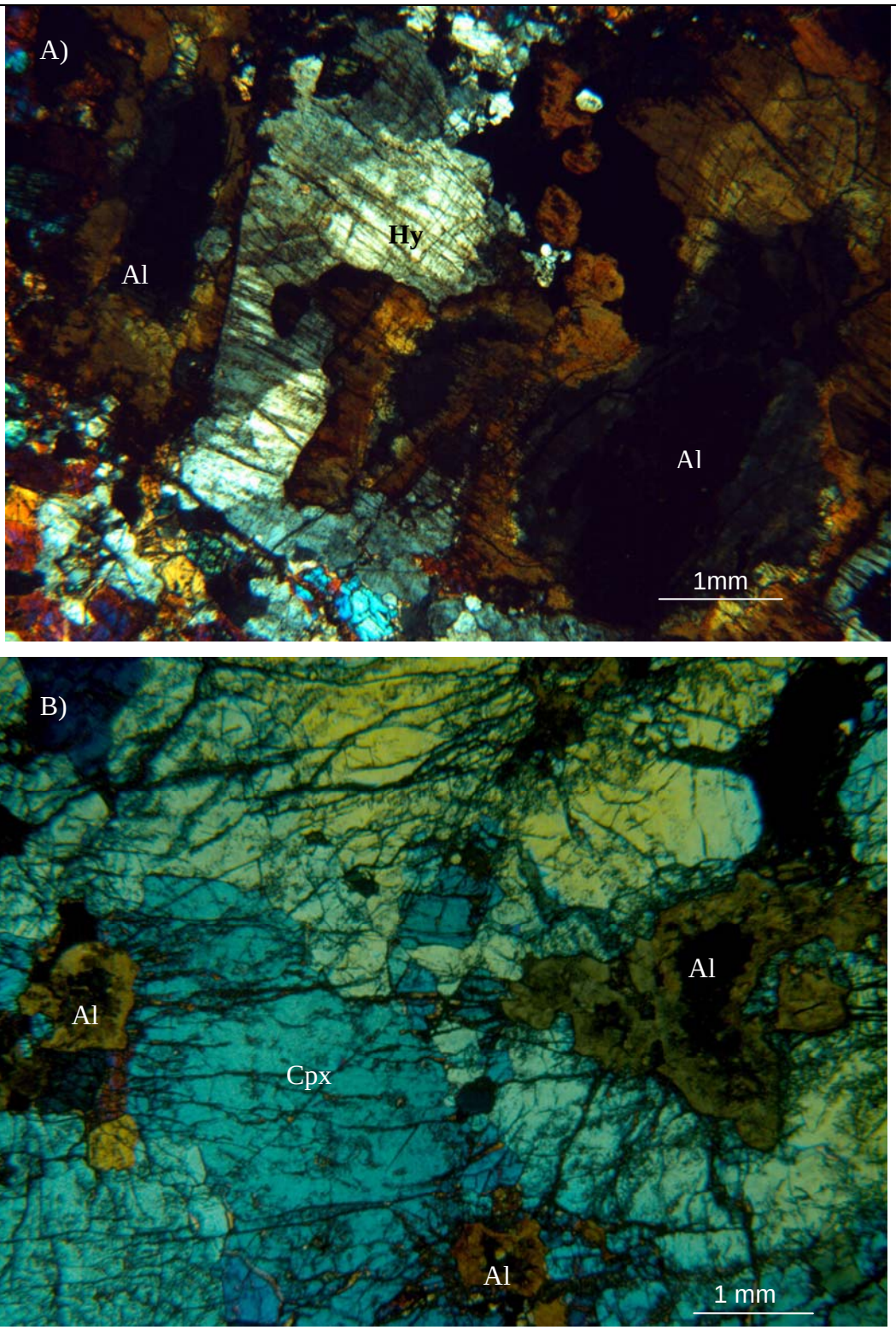

Figure 6.1 Examples of the variation observed in the Diopside-Allanite veins. Image (A) shows a hyalophane-rich vein from sample 782076. Image (B) shows a more typical diopside-allanite vein from sample 881109B. Allanite (Al), Diopside (Cpx), Hyalophane (Hy). Both images are taken under crossed polars.

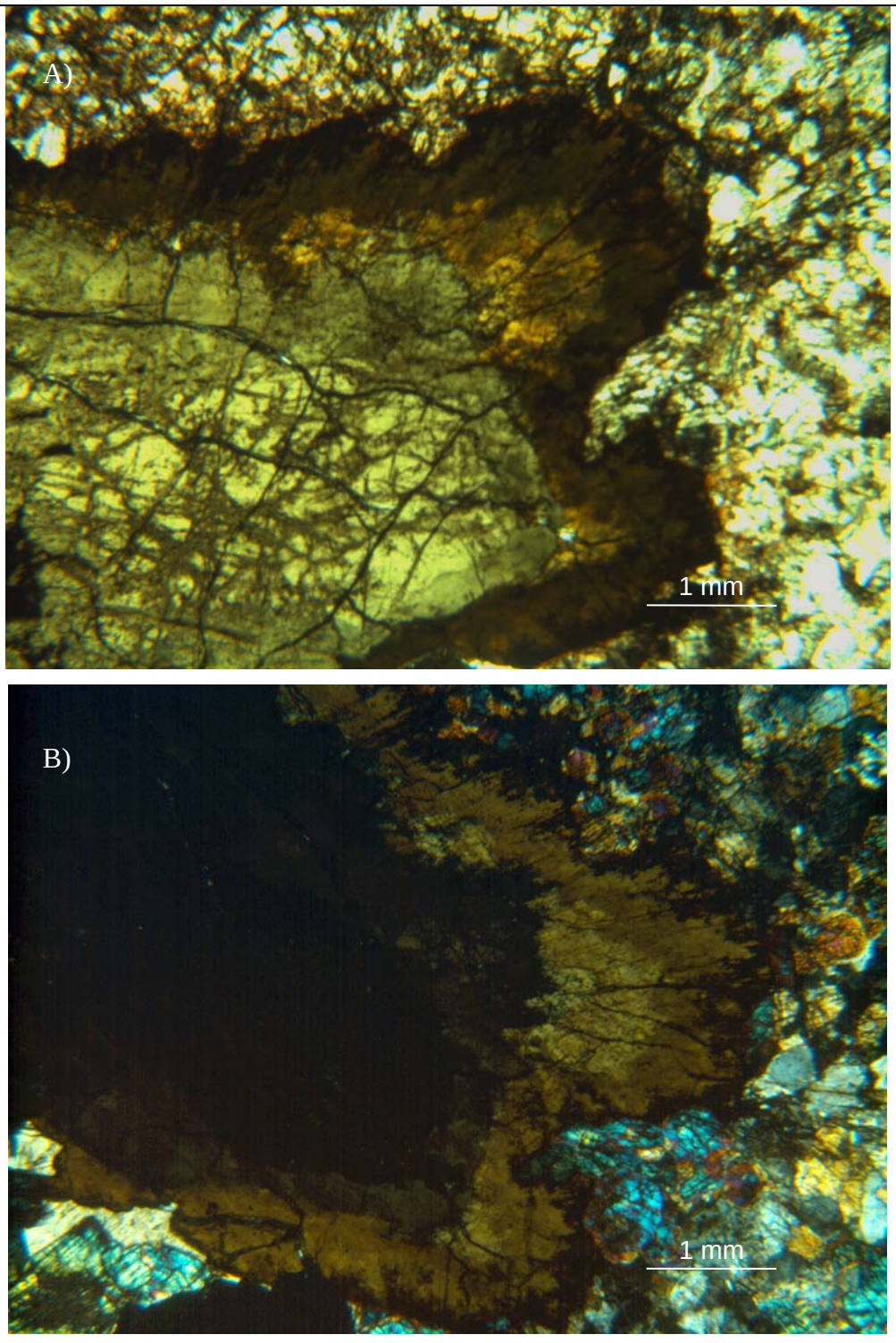

Figure 6.2 Large allanite crystal from sample 782076 displaying the irregular zonation typical of the allanites at Hoidas Lake. The allanite is surrounded by diopside and hyalophane. Image A) is in plane polarized light while B) shows the same image with crossed polars. Image B) is rotated slightly to better display the zonation.

concentric, but the boundaries are ragged and the width of the zones is inconsistent. In some instances the rim of the allanite crystal displays petrographic features characteristic of epidote rather than allanite senso stricto.

Less common than these large, zoned allanites are smaller, subhedral to almost euhedral allanites which can be either zoned or unzoned. If present, the zoning in these allanites is typically concentric, with a much cleaner appearance than the larger crystals. These subhedral to euhedral allanites often occur in masses of small interlocking crystals.

The allanite is generally inclusion free, although in some cases inclusions of both titanite and chevkinite are present. There are also rare inclusions of clinopyroxene, apatite, hyalophane, magnetite and hematite. There is typically some variation in the appearance of the allanite immediately adjacent to these rare inclusions, similar to the zonation observed towards the rim of the crystals. Due to their close association with the allanite many of the other minerals in these samples are intensely fractured. The allanite is often surrounded by anastomosing, radiating cracks caused by the radioactive decay of U or Th which leads to structural damage. This can lead to cracking as a result of a volume change, and potentially additional alteration. In the diopside-allanite vein it is the hyalophane and apatite that are the most strongly affected, although the typical radiating fractures can be found in clinopyroxene crystals as well.

The clinopyroxene and feldspar crystals are typically subhedral to anhedral and may contain small inclusions of allanite. The clinopyroxene crystals range from less than a millimeter to over a centimeter in size and often show minor amounts of alteration to amphiboles. The hyalophane crystals are typically smaller, averaging only a few mm in size, and in most cases are anhedral. Moderate alteration to clays is present in some samples, particularly in those from surface showings. In rare cases very fine exsolution lamella can be observed. More common are hematite-coated fractures which give a pink tint to the hyalophane in both hand sample and thin section.

The titanite and chevkinite are most commonly encountered in close proximity to allanite crystals or, particularly in the case of the chevkinite, as inclusions in the allanite (Fig. 6.3). The titanite crystals are usually large, up to a cm in size, relatively

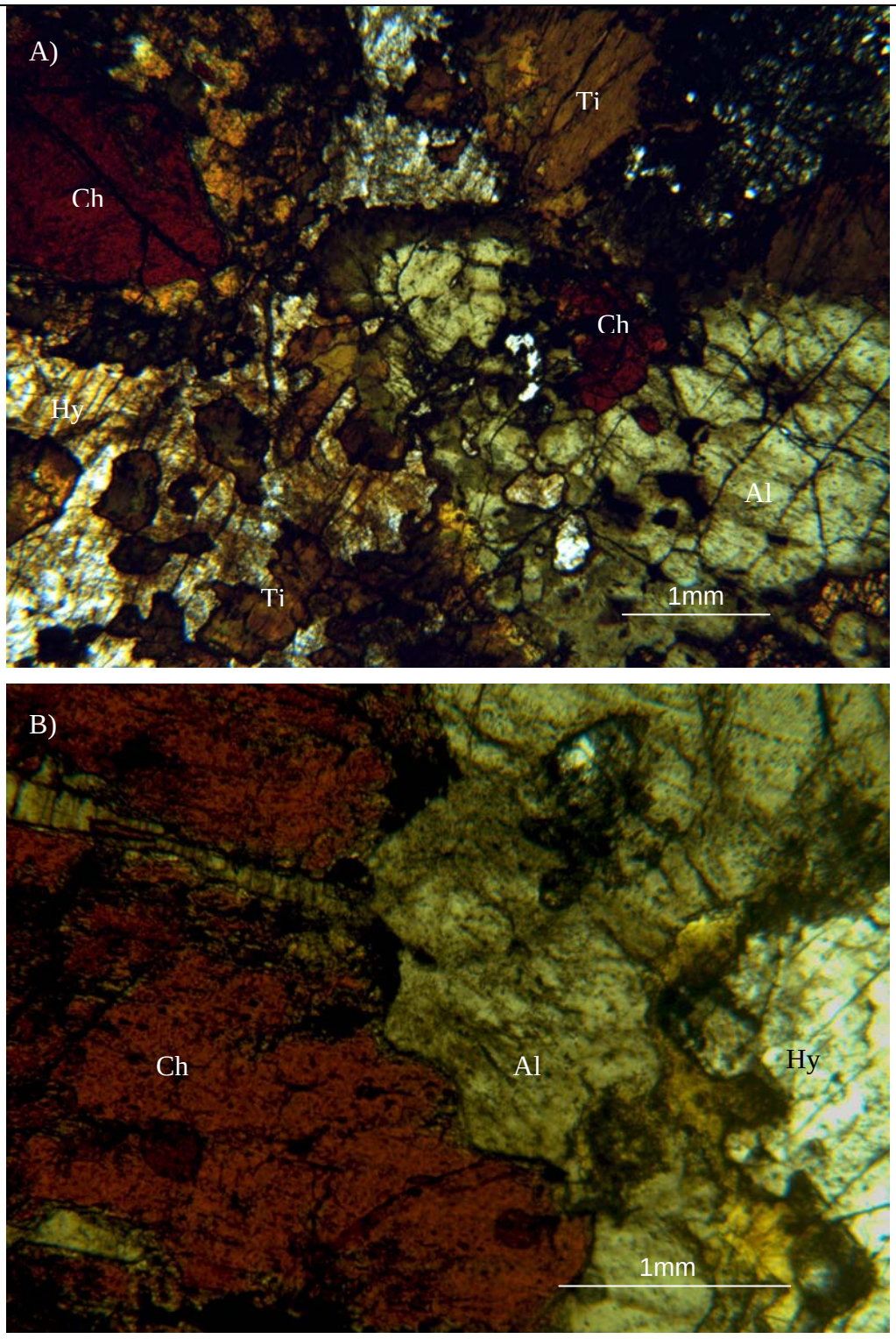

Figure 6.3 Examples of chevkinite in allanite. Image A) shows an example of an allanite (Al), titanite (Ti) and chevkinite (Ch) rich sample of vein with a minor amount of hyalophane (Hy). Image B) is at a higher magnification to better display the chevkinite core in some of the zoned allanites. Both images are in plane polarized light. Both images from sample no. 782076.

inclusion free and are typically subhedral, although rare euhedral crystals can be found. The chevkinite crystals have a similar appearance, but tend to be smaller, only a few mm in size, subhedral to anhedral, and have a deep reddish color. Despite the close proximity of these two minerals to the allanite crystals, they lack the fracturing observed in other minerals of this vein generation.

The amphibole present in these samples is often the result of secondary alteration of the primary minerals and typically consists of hornblende or actinolite. The hornblende is most commonly encountered as small anhedral patches of alteration within the larger diopside crystals. Amphibole can also be found along the margins of late fracture sets, in which case it is often found with chlorite. In very rare instances there are crystals of hornblende which do not appear to be the result of alteration of the diopside and which are subhedral to euhedral.

The most common opaque minerals in this vein generation are magnetite and hematite, with the pyrite typically occurring in late cross-cutting fractures. In most cases the magnetite is rimmed by a narrow mantle of hematite, suggesting later oxidation of the primary magnetite.

6.2.2 RED APATITE BRECCIA

The red apatite breccias tend to occur as brecciated clasts or, more rarely, as masses of small crystals less than 1mm in size. Although apatite is the dominant clast type these breccias are often polymictic as they can contain clasts from both the diopside-allanite veins and the host rocks. The breccias range from being clast-supported to matrix-supported, often within a single vein. All clast types range from sub-rounded to sub-angular in shape. The apatite clasts vary greatly in size, with almost a continuous gradation from the matrix up to large clasts several centimeters in size (Fig. 6.4).

The larger clasts are often riddled with inclusions, particularly in the cores of the crystals. There are two varieties of inclusions observed in these large apatites, the first of which shows strong alignment and the second of which consists of randomly

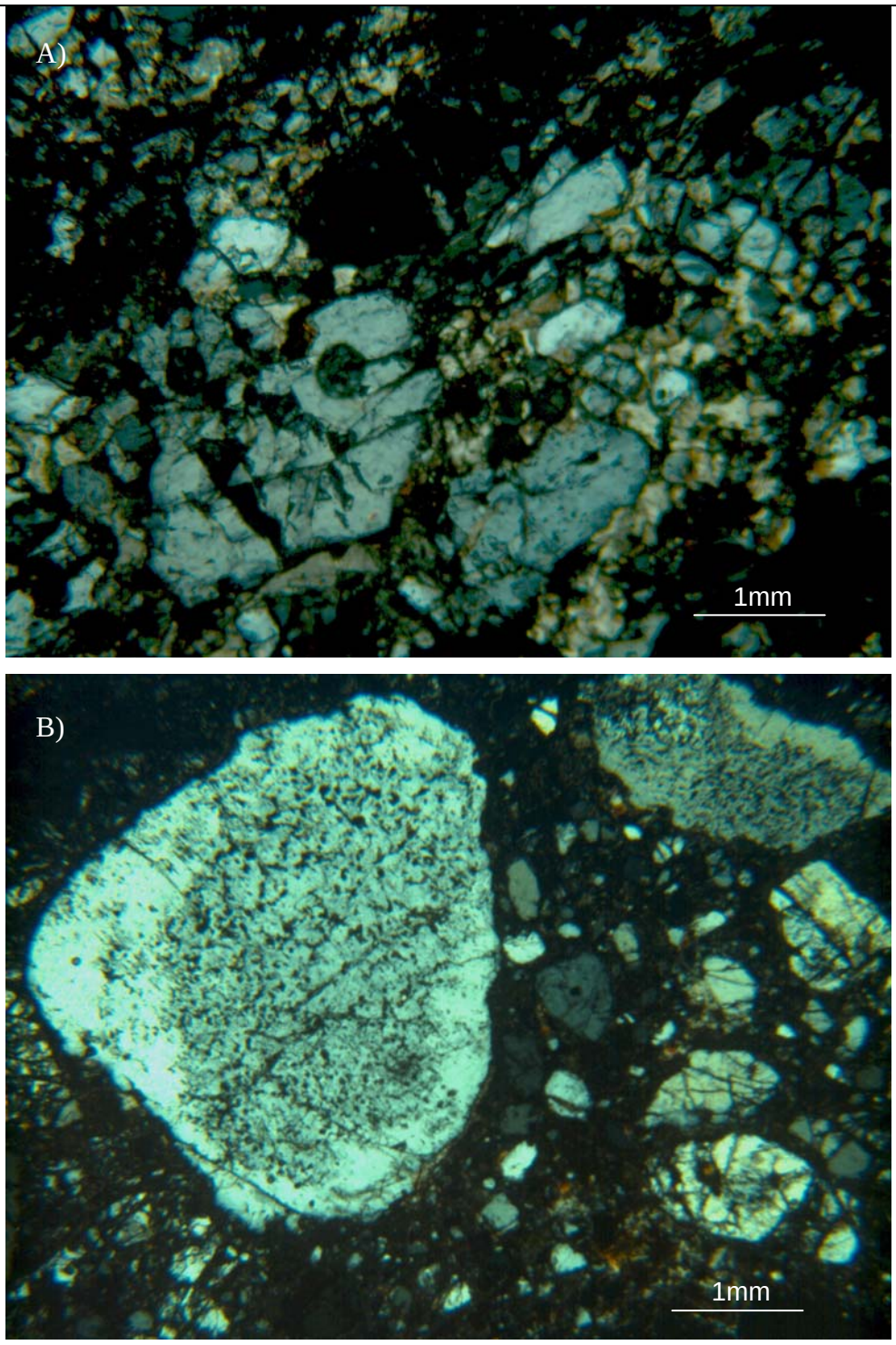

Figure 6.4 Two examples of the red apatite breccia. Image A) shows an apatite breccia with a carbonate rich matrix from sample no. 881318A while image B) shows a similar breccia from sample no. 37903 but the matrix of this sample contains a much higher proportion of hematite. Particularly in image B) the zoned, inclusion rich cores can be observed in the larger clasts. Both images are taken under crossed polars.

oriented opaques, which appear to be either hematite or goethite. The aligned inclusions are typically too fine to identify petrographically with any certainty, although the light yellow color and high birefringence suggest that these inclusions may be monazite. Also, rare inclusions of allanite can be found in a small number of apatite crystals.

The matrix in the red apatite breccias is largely composed of apatite, with variable amounts of associated calcite, hematite, hornblende and biotite (Fig. 6.4). In some cases the matrix also contains minor amounts of quartz, scapolite, chlorite, or pyrite. Another feature encountered in a small number of samples is the presence of open, vuggy spaces in the breccias. These open spaces are often partially filled with calcite and late euhedral pyrite, suggesting that the observed pyrite is younger than other components in the matrix. Hematite occurs not only as inclusions in the apatite and in the matrix, but also as late cross-cutting veinlets. Quartz, scapolite, calcite and chlorite can also be found as discrete, crosscutting veins. Typically these crosscutting veins are essentially monomineralic, although rare quartz-calcite, quartz-scapolite or calcite-scapolite veins can be found.

6.2.3 GREEN APATITE BRECCIA

There is also a relatively rare bright green to grayish green apatite which can be found in the central portion of some of the veins. Occurrences of this apatite generation are relatively rare due to the poor core recovery caused by the highly brecciated, often rubbly and unconsolidated nature of the core. This apatite is most commonly encountered at the margins of open, faulted areas or adjacent to areas of core loss. This apatite is not found at surface in the JAK zone, although there is a single occurrence of green apatite in outcrop at Hoidas South.

The green apatite seems to have formed after the red apatite breccias and before the late coarse red apatite, although the contacts with both the earlier and later apatites are gradational. Like the earlier red apatite, the green apatite most commonly occurs as brecciated clasts in a matrix of apatite, calcite and quartz (Fig 6.5). A key difference is that this apatite breccia lacks the iron oxides, amphiboles and biotite often observed with the red apatite breccias. The green apatite breccias are dominantly matrix supported with the clasts ranging from sub-angular to sub-rounded in shape. The green apatite is

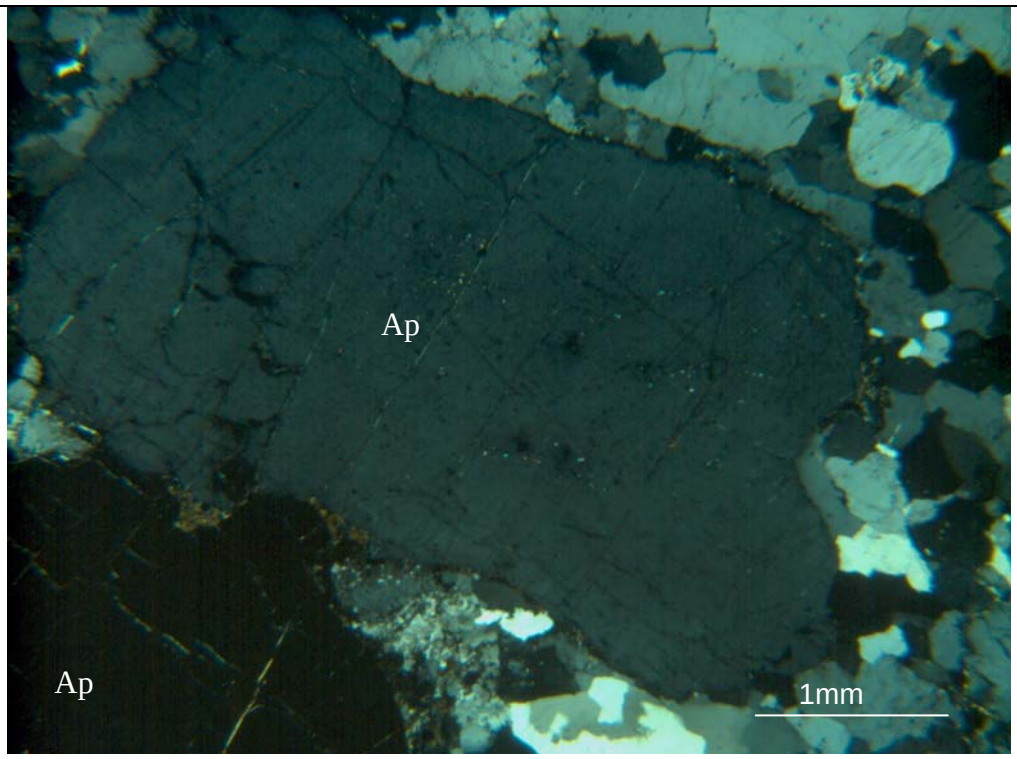

Figure 6.5 Image of the green apatite breccia from sample no. HS-GA. The large apatite (Ap) clasts are in a quartz rich matrix. Note that these clasts lack the inclusion rich nature observed in the red apatite breccia (Fig. 6.4 (B)).

essentially unzoned and inclusion free, although in some cases there is a slight variation in the color of the apatite from core to rim.

6.2.4 COARSE RED APATITE

The coarse red apatite is also typically inclusion free. Macroscopically, this apatite is a deep, bright red color and is coarsely crystalline with cm sized crystals. In contrast to the earlier apatites, the coarse red apatite shows few, if any, signs of deformation or damage. In rare cases veins of the coarse red apatite can be described as a crackle breccia. In these instances the apatite is fractured with the resulting clasts essentially still in place, with no rotation to the clasts (Fig. 6.6). The only inclusions observed in this apatite generation are small clasts of the earlier vein generations which the coarse red apatite crosscuts or rare reddish opaques, which are likely hematite. In some cases there is a thin rim of allanite between this generation of apatite and the older

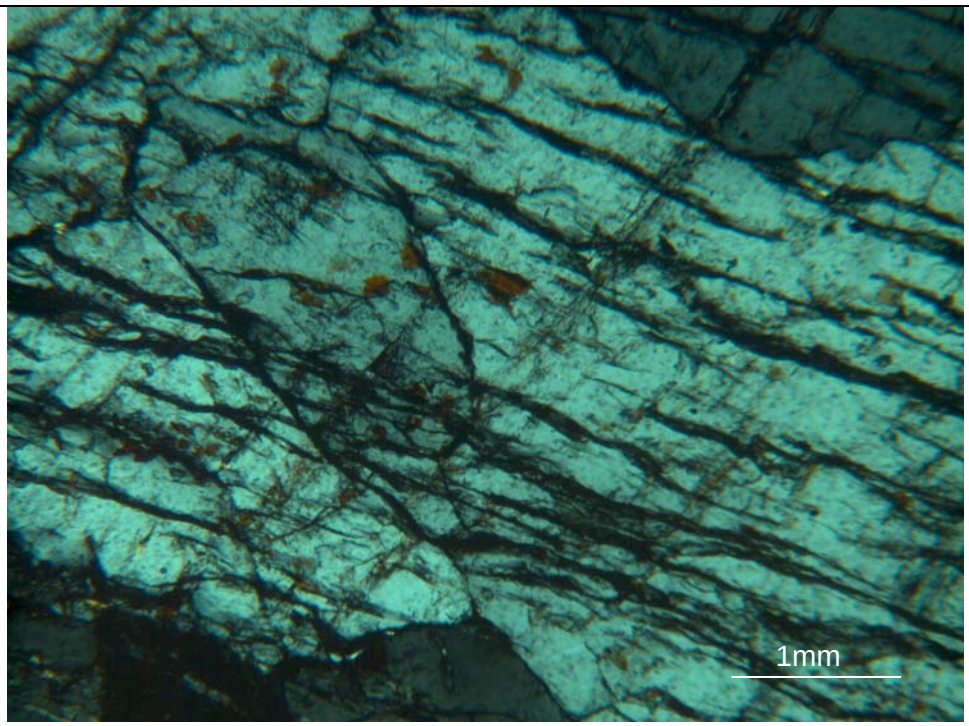

Figure 6.6 Image of the coarse red apatite from sample no. 881257A. Inclusions of a reddish opaque, likely hematite, can be found in this apatite. This vein generation lacks the brecciation associated with the other apatites, although the crystals can be heavily fractured.

veins which it crosses. Later pyrite, as well as scapolite and quartz, can be found as a common fracture fill.

6.3 CHEMICAL COMPOSITION OF THE REE-BEARING MINERALS

6.3.1 ALLANITE

The composition of the allanite from Hoidas Lake ranges from that of allanite, sensu stricto, towards the ferriallanite and epidote end members, although the majority of the analyzed points plot in close proximity to the allanite end member (Fig. 6.7). The composition of the Hoidas Lake allanites plots mainly in the region of overlap between the igneous and hydrothermal allanites of Petrik et al., (1995) (Fig. 6.7). The allanites from Hoidas Lake are LREE-enriched and all analyzed samples are of the Ce-dominant variety, although the total REE content varies between samples depending not only on

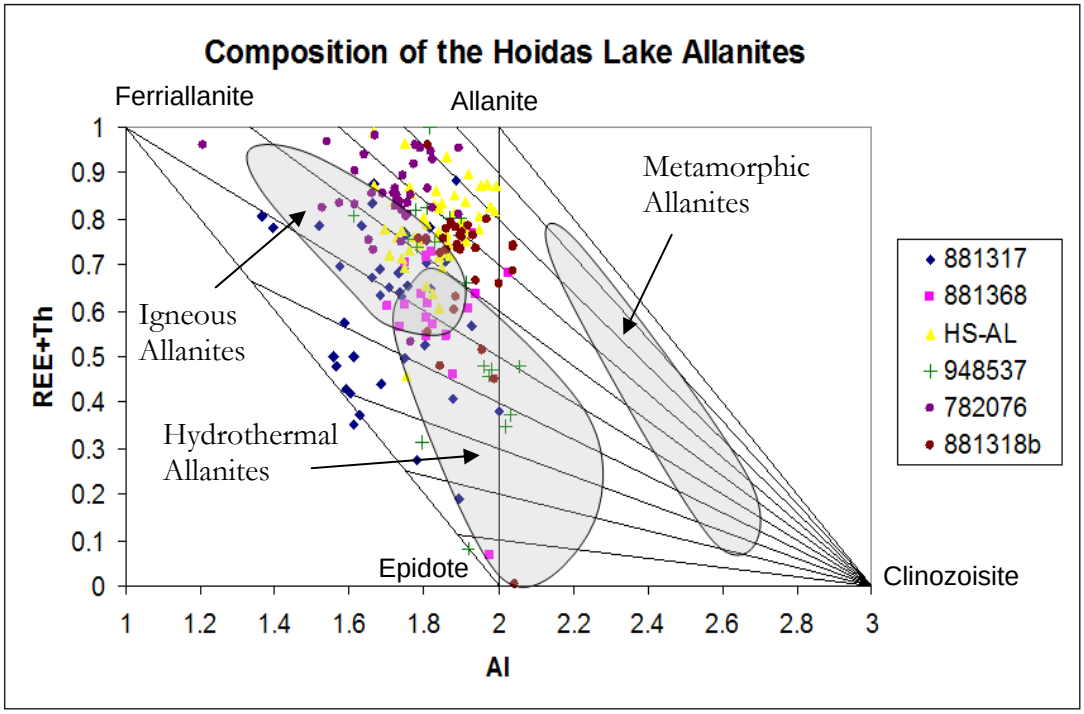

Figure 6.7 Compositional variations observed in the Hoidas Lake allanites. Shaded fields are adapted from Petrik et al. (1995). The majority of the Hoidas Lake allanites plot in or near the region of overlap between the Igneous and Hydrothermal allanite fields. Results in Table B.6 in Appendix B.

the composition of the allanite, but also on the amount of metamictization (Table B.6, Appendix B). The relative order of LREE content in the Hoidas Lake allanites is Ce > La > Nd > Pr > Sm.

The chondrite-normalized REE plot for allanite-rich samples shows a steep negative slope with a $(La/Yb)_N$ ratio of up to 8,642. An interesting feature of these allanites is the lack of an Eu anomaly, as igneous allanites typically display a pronounced negative Eu anomaly, particularly from tonalites, granodiorites and monzogranites. A distinct Eu anomaly is the result of allanite crystallization in association with plagioclase, as is typical in many igneous rocks (Gregory et al., 2006). The lack of an Eu anomaly in allanite may thus suggest a metasomatic or metamorphic source (Giere and Sorensen, 2004). There is an unusual saw-tooth pattern between Tb and Tm which cannot be readily explained (Fig. 6.8). In addition to the REE there are also slight enrichments in both Sc and Y associated with the allanite-rich samples.

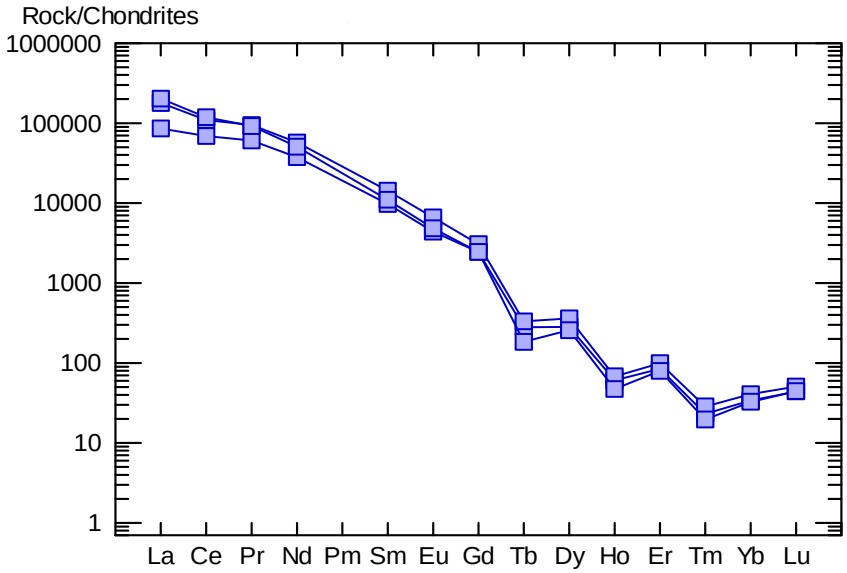

Figure 6.8 REE distribution of the Hoidas Lake allanite normalized to chondrite. Result of ICP-MS analysis of allanite dominant whole rock samples (Table B.13). The Hoidas Lake allanites are extremely LREE enriched and lack both a Ce and Eu anomaly. Chondrite values are from Sun and McDonough, 1989.

Samples of allanite which are not metamict typically contain between 18% and 28% TREO based on the EMPA results, while the samples which are closer to epidote in composition typically contain less than 10% TREO. As is common with allanites, due to their Th and U content, there are several samples from Hoidas Lake which display evidence of metamictization in thin section. This is confirmed by the low analytical totals observed for these allanites, as the radiation damage is often accompanied by hydration of the mineral, which leads to low EPMA oxide totals (Giere and Sorensen, 2004). Although the alteration, and the resulting low analytical totals, in these samples prohibit any detailed, quantitative analysis, the TREO range of the variably metamict samples usually falls between the two extremes of non-metamict allanite and epidote.

In many cases, due to the intense zonation observed in the majority of the Hoidas Lake allanites, a single crystal can show a wide compositional range. Chemical zonation observed in the crystals is quite similar to the zonation observed petrographically; the core of crystals may be metamict and there is frequently a rim of

epidote. In relatively unaltered crystals the core is typically REE-rich, with the REE content decreasing as the edge of the crystal is approached (Fig. 6.9).

As was observed petrographically, the zonation in the back-scattered electron images is roughly concentric, although the composition of the zones is somewhat patchy or mottled in appearance and the boundaries between zones are highly irregular in nature. The chemical variation between zones is largely a function of REE content, although the Fe, Al and Ti content also vary, but not as systematically as the REE. In some cases there is a decrease in Fe content and an increase in Al content towards the rim of the crystal. Only in very rare instances are zones which appear to parallel the boundaries of a euhedral crystal observed, and in these cases the composition within zones is fairly consistent. Again, the zoning is concentric and in some instances oscillatory (Fig 6.10).

In addition to the REE the allanites also contains minor amounts of Sr, Ti, Mn and Mg (See Table B.6 Appendix B). Ti is consistently present, with only the relative amount varying between samples. The TiO_2 content ranges from 0.05 wt. % up to 2.6 wt. %, although the majority of samples contain about 0.77 wt.% TiO_2. The SrO content of the allanites ranges from below the detection limits to as high as 1.6 wt.%. The increase in Sr or Ti is often accompanied by a slight decrease in the amount of Ca, Mg, or Fe present in the samples. Minor amounts of Mg and Mn are found in all the samples, although the highest observed concentration of MgO is only 2.4 wt.% and MnO is less than 0.6 wt. %.

There are also minor amounts of Ba encountered in some of the allanites, with a limited number of allanites containing up to 3.7 wt.% BaO. Higher contents of Ba are encountered in altered samples with low analytical totals, suggesting that some of the Ba enrichment may be a secondary feature and is likely related to alteration rather than the primary allanite composition. However, more moderate amounts of Ba are encountered in relatively unaltered crystals, suggesting that minor to moderate concentrations of Ba can be found as a primary feature in the allanite.

The allanites also contain small amounts of Th and U which are largely responsible for the metamict nature of many of the samples as the α-decay of these

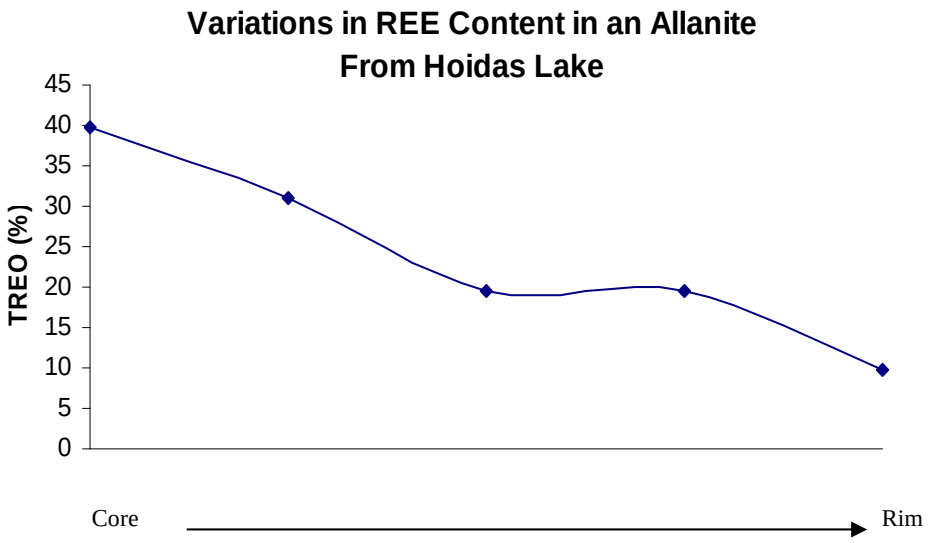

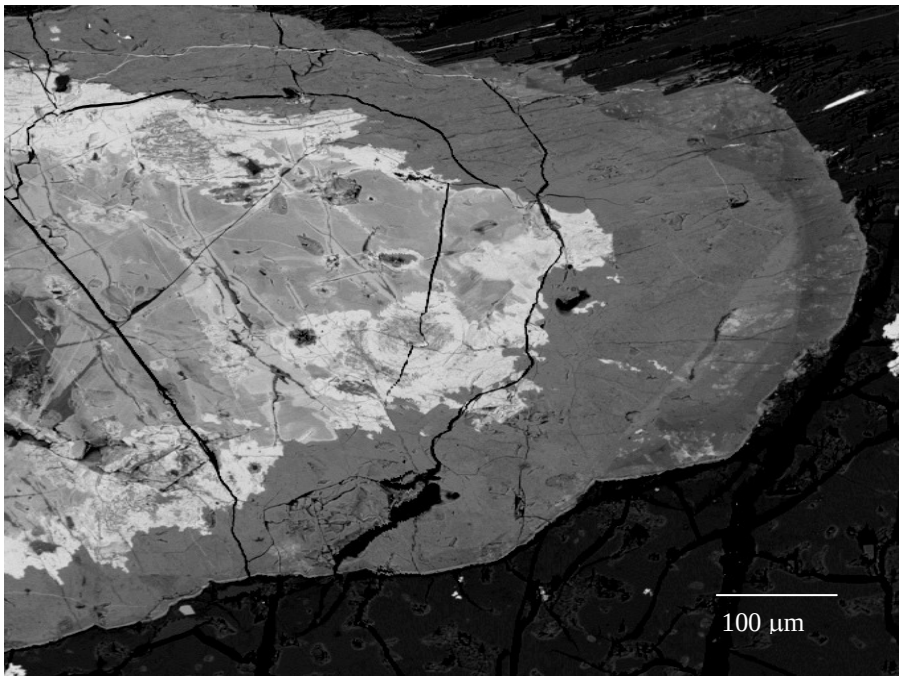

Figure 6.9 Example of the decrease in REE content from the core to rim an allanite crystal in sample no. 948537. Although most crystals show this general pattern, the maximum REE content in the core of the crystals is typically lower.

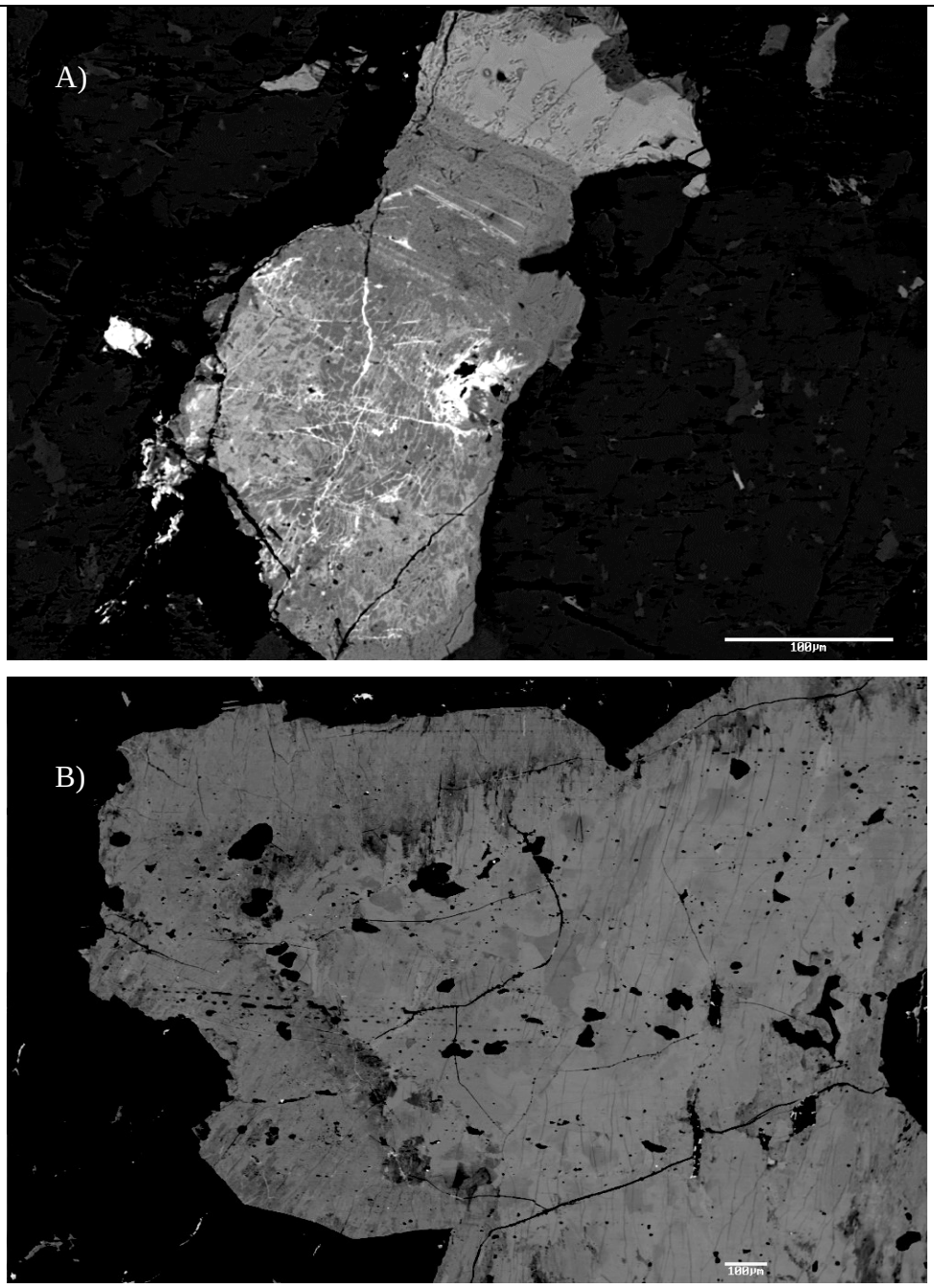

Figure 6.10 Back scattered electron (BSE) images of allanites. Image A) shows a rare example of preserved primary zonation in allanite from sample 881317. Image B) displays the more common irregular zonation, as was typically observed during petrographic analysis. This example is from sample HL-AL The variation in these images is almost entirely controlled by the REE content of the allanite, with high REE areas displayed by the lightest colors and REE-poor areas shown by the darker shades. All scale bars are 100µm.

elements damages the crystal structure (Catlos et al.2000; Giere and Sorensen, 2004). As is typical the Hoidas Lake allanite is more enriched in Th than U, with an average ThO_2 content of 0.4 wt. %. The U content found in allanite-rich samples is consistently under 100 ppm.

6.3.2 APATITE

6.3.2.1 RED APATITE BRECCIA

Although at a macroscopic level the red apatite appears to be homogeneous, the backscattered electron images reveal that there are several distinct zones present within the apatite crystals or clasts. In total, there are four distinct zones in the red apatite breccia, with the oldest zone, referred to as Zone 1, corresponding to the dark red apatite. The apatite in Zone 1 is a dark grey in backscattered images and is typically riddled with monazite inclusions. Zone 2 is a lighter grey in backscattered images, and is also inclusion rich. The inclusions are typically monazite, with minor amounts of thorite and an unidentified REE oxide or carbonate. In both Zones 1 and 2 the area around the inclusions appears mottled in the backscattered images with dark, REE-poor regions surrounding inclusions. Zone 3 is also a light grey in the backscattered images, but it lacks the inclusions of Zone 2. Zone 4, the youngest zone, occurs as a narrow, dark rim on many of the clasts. It is chemically and visually equivalent to the coarse red apatite, the youngest apatite generation (Fig. 6.11).

The four zones recognized in the backscattered images of the red apatite breccias can also be distinguished based on the variations in their chemical composition, primarily by the variation in REE content. The dark red apatite, or Zone 1, tends to be Ce-dominant and has relatively low REE contents, typically around 1.5% TREO. The REE content of Zone 2 and 3 in the red apatite breccia increases to approximately 2% and 4%, respectively (Fig. 6.12). The apatites in Zone 2 and 3 are also of the Ce-dominant variety. The apatite of Zone 4 has the lowest REE content and is Nd-dominant (Table 6.1) (Table B.5 Appendix B).

The presence of monazite inclusions only locally affects the REE content of the apatite, with the REE required to form the monazite derived almost entirely from the

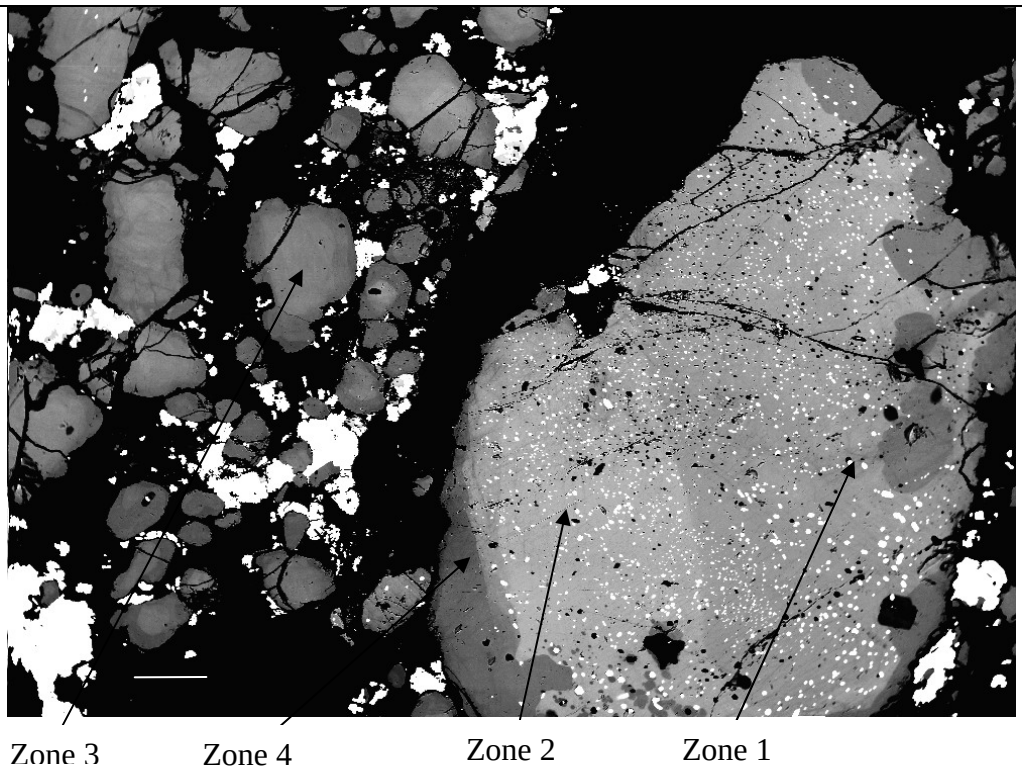

Figure 6.11 BSE image of a red apatite breccia from sample no. 37920. The image to the above shows the four distinct zones. 100 μm scale bar in the lower left corner of the image.

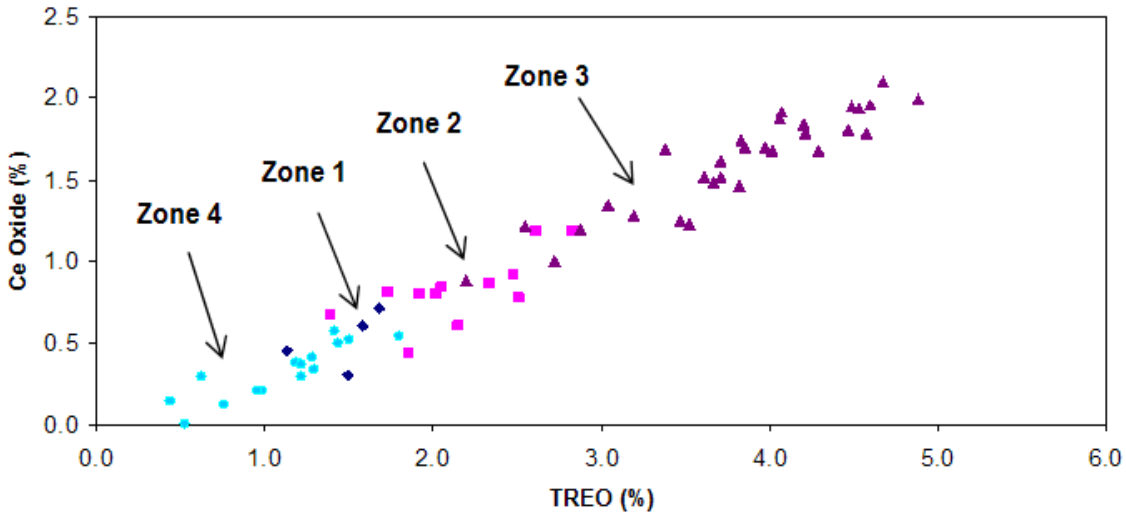

Figure 6.12 Variation between total REE content and Ce oxide between the four zones of red apatite in the Hoidas Lake REE deposit. Similar relationships are obtained for both La and Nd.

Table 6.1 Representative EPMA data from the recognized apatite generations

Oxide (%)	Dark Red Apatite (Zone 1)	Red Apatite (Zone 2)	Red Apatite (Zone 3)	Green Apatite	Coarse Red Apatite (Zone 4)
SiO_2	0.749	1.206	1.465	2.103	0.477
ThO_2	0.133	0.000	0.000	0.338	0.307
Y_2O_3	0.043	0.009	0.091	0.164	0.123
La_2O_3	0.142	0.205	0.392	0.967	0.000
Ce_2O_3	0.716	1.189	1.343	2.440	0.203
Pr_2O_3	0.151	0.173	0.018	0.369	0.161
Nd_2O_3	0.537	0.810	0.978	1.464	0.251
Sm_2O_3	0.074	0.102	0.101	0.022	0.005
Gd_2O_3	bdl	0.010	0.087	0.016	0.042
Dy_2O_3	0.015	0.114	0.032	0.050	0.145
CaO	55.90	53.38	52.46	49.06	53.93
SrO	0.816	0.682	0.655	1.367	0.625
BaO	0.000	0.000	0.098	0.003	0.000
P_2O_5	33.83	38.20	38.29	36.61	40.94
SO_3	0.032	0.059	0.256	0.509	0.078
F	1.80	2.845	2.651	3.570	3.170
Cl	0.143	0.111	0.143	0.286	0.017
	95.09	99.09	99.06	99.34	100.47

altered, relative REE-depleted areas surrounding the inclusions. Away from these altered areas the apatite composition is likely comparable to the original composition in terms of REE content, as experiments conducted by Harlov et al. (2005) suggest that the original REE content remains undisturbed in inclusion free regions of altered crystals. This suggests that the low REE content of both Zone 1 and 2 is a primary feature of these apatites as the calculated TREO content of these apatite generations was based on the composition of the unaltered regions of the crystals.

6.3.2.2 GREEN APATITE BRECCIA

The green apatite breccia lacks both the inclusions and zonation observed in the earlier apatite generations (Fig. 6.13 and 6.14). In addition to these visual distinctions there is also a compositional difference between the green and red apatites; the green apatite is more enriched in REE relative to the red apatites, with an average of 5.5% TREO. As with the first three zones of the red apatite, the green apatite also contains Ce as the main REE. The chondrite normalized REE pattern of this apatite generation reveals a negative sloping, relatively flat pattern with a $(La/Yb)_N$ ratio of 280 and a slight Tb anomaly (Fig. 6.15). The relatively low overall REE content observed in this sample, as compared to the microprobe results, is likely due to dilution of the REE caused by the presence of non-REE-bearing matrix material in the whole rock samples used for the ICP-MS analysis.

This apatite generation also contains minor amounts of SiO_2, up to a maximum of 2.5 wt. %, and lower Ca contents than the other apatites, which is likely due to the REE substitution mechanism (Table B.4 Appendix B). There is also between 0.8 and 1.4 wt % SrO present in this apatite generation. As with the other apatites, the amount of Th and Y present in these samples is some what variable, with values ranging from below the detection limits to a maximum of less than 0.5 wt. %.

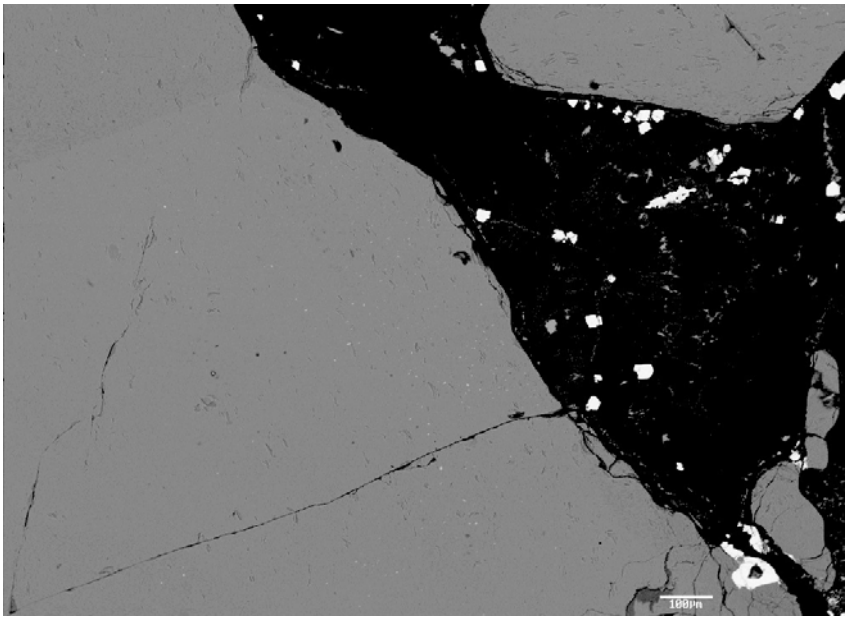

Figure 6.13 BSE image of the green apatite breccia in a quartz matrix from sample HL06-75. The small bright minerals in the matrix are typically monazite, although rare pyrite can also occur. Scale bar is 100μm.

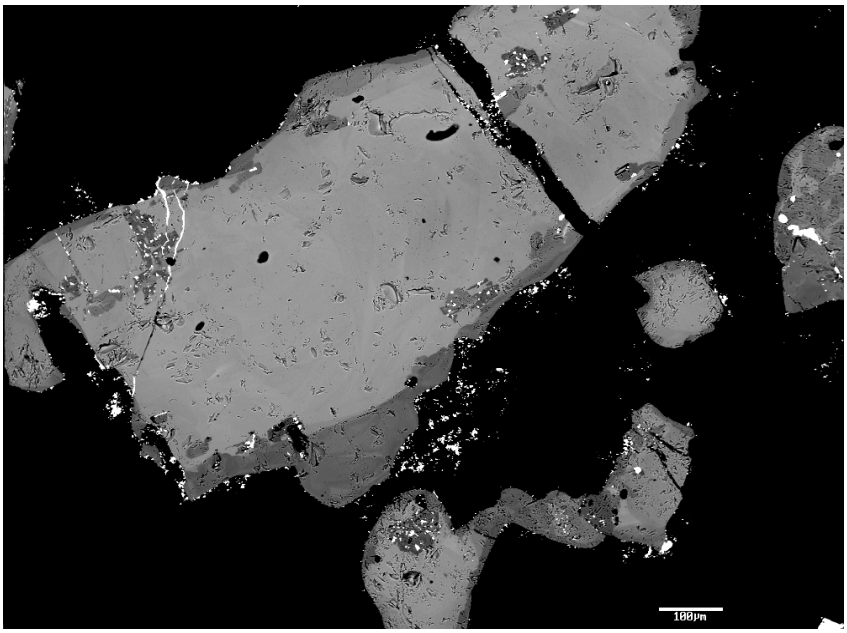

Figure 6.14 BSE image of green apatite (light grey) rimmed by coarse red apatite (darker grey) from sample 37906. Apatite clasts are in a quartz and calcite rich matrix. 100µm scale bar in the lower right corner of the image.

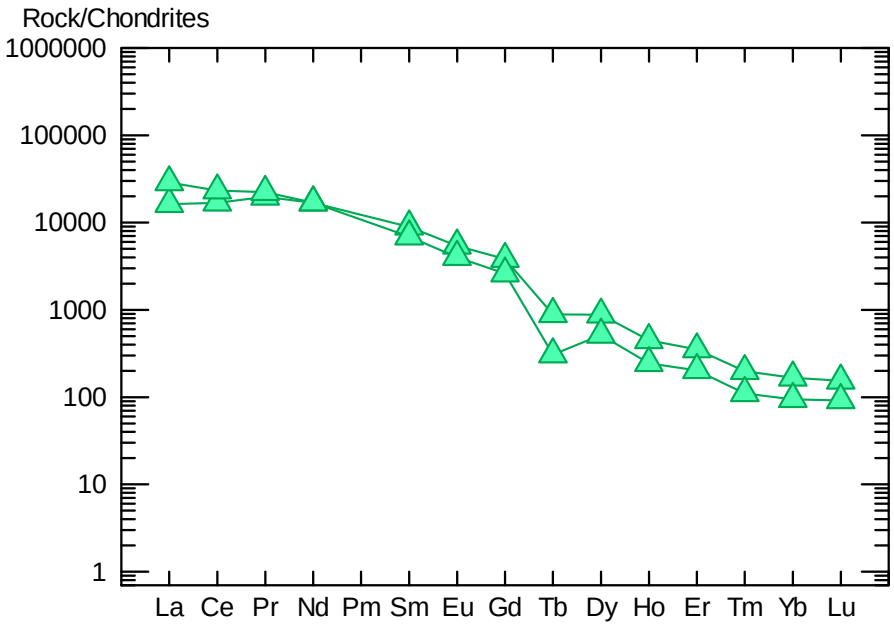

Figure 6.15 REE Composition of the green apatite generation normalized to chondrite. Results are from the ICP-MS analysis of whole rock samples. Low values, as compared to the microprobe results are likely a result of the large amounts of REE-poor matrix in these samples. Chondrite values from Sun and McDonough, 1989.

6.3.2.3 COARSE RED APATITE

The coarse red apatite is another inclusion free apatite with a relatively homogeneous composition. The intense zoning observed in the backscattered images of the earlier red apatite generations is noticeably absent in the coarse red apatite, as are the monazite inclusions (Fig. 6.16). Although from a macroscopic perspective the green apatite appears to be the most distinct, at the chemical level it is the coarse red apatite, which is equivalent to Zone 4 in the apatite breccias, which is the most easily distinguished. Of the analyzed apatites, the coarse red apatite consistently has the highest middle rare earth element (MREE) content, although it also features the lowest overall TREO content (Table B.3 in Appendix B). The MREE account for an average of 33% of the TREO of this apatite generation and it typically features Nd as the dominant REE, as opposed to the more typical Ce-dominant apatite found in the earlier generations. As with the other apatite generations, the chondrite normalized REE pattern shows a slight enrichment of the LREE with a relatively gentle negative slope, with an average $(La/Yb)_N$ ratio of only 181, and lacks an Eu anomaly. Again, there appears to be a slight negative Tb anomaly present (Fig 6.17).

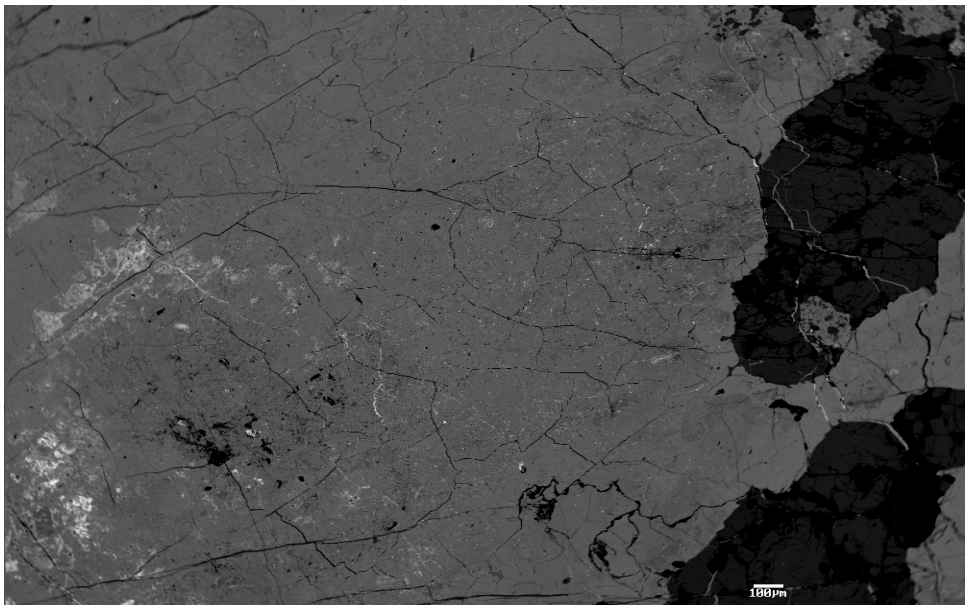

Figure 6.16 Coarse red apatite from sample no. 37933. 100 µm scale bar in the lower right corner of the image.

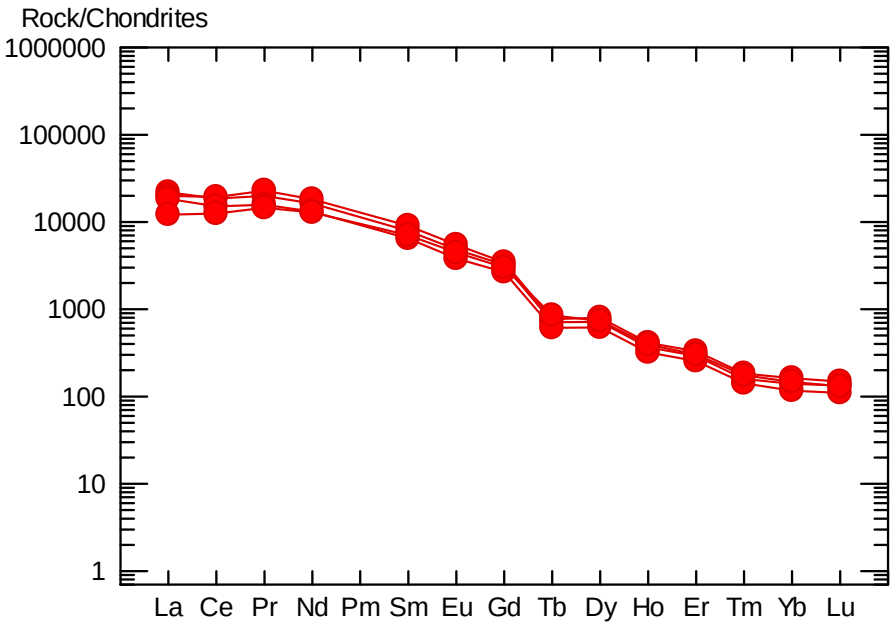

Figure 6.17 REE composition of the coarse red apatite normalized to chondrite. Chondrite values from Sun and McDonough, 1989.

6.3.2.4 COMMON FEATURES TO ALL APATITES

The apatites analyzed are fluorapatite, with a range in composition from fluorapatite to those with about 50% hydroxyl component (Fig. 6.18). This slight variation in the apatite composition appears to vary independently of the apatite generation, with all generations showing some OH content. As the Hoidas Lake apatites are exclusively fluorapatite to hydroxylapatite in composition the REE are likely located in the Ca(2) site of the apatite (Pan and Fleet, 2002).

The dominant mechanism for the incorporation of REE into apatite for all the apatite generations appears to be the coupled substitution of

$$SiO_4^{4-} + REE^{3+} \leftrightarrow Ca^{2+} + PO_4^{3-}$$

(Fig. 6.19). Surprisingly there is little to no evidence of Na in the apatites, as the substation of Na in REE-rich apatite is a common method of maintaining the charge balance. Another common substitution in the Hoidas Lake apatites is that of Sr^{2+} for Ca^{2+} in all apatite generations; like the REE, Sr also shows a preference for the Ca(2)

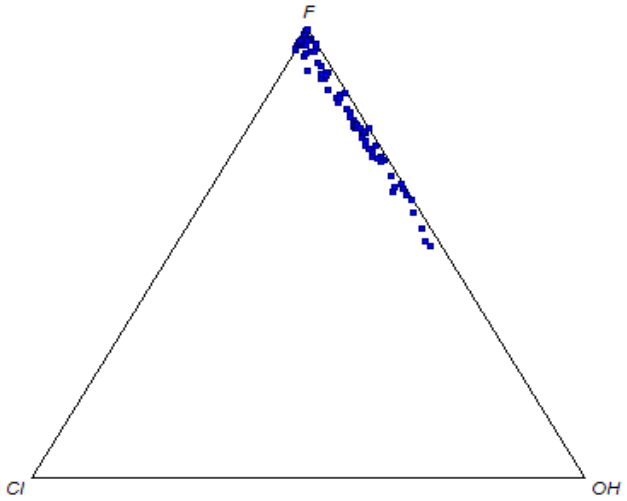

Figure 6.18 Apatite composition of the Hoidas Lake apatites in terms of F, Cl, and OH endmembers. All apatite generations show as range of values between pure fluorapatite and apatite with some OH component. There is no relation of OH content to apatite generation observed.

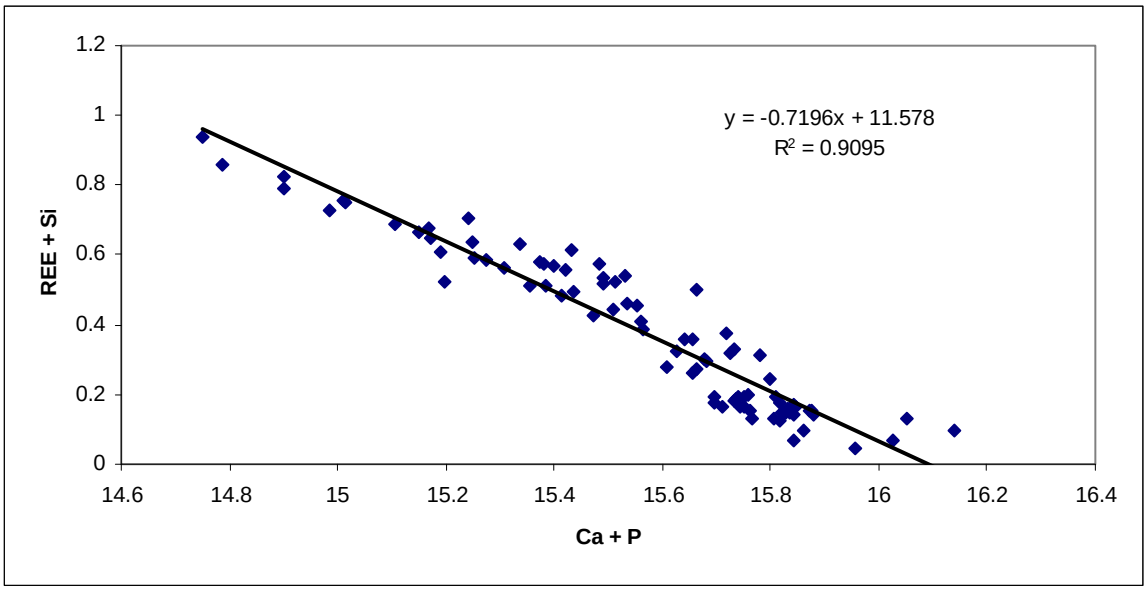

Figure 6.19 Substitution of REE into the apatite structure based on the coupled substitution of

$$SiO_4^{4-} + REE^{3+} \leftrightarrow Ca^{2+} + PO_4^{3-}.$$

site in fluorapatite and hydroxylapatite (Pan and Fleet, 2002) (Fig. 6.20). Although there is some slight variability, the SrO content is quite consistent in the majority of the apatites, with most samples containing around 0.7 wt.%; the exception is the green apatite which normally contains over 1 wt. %.

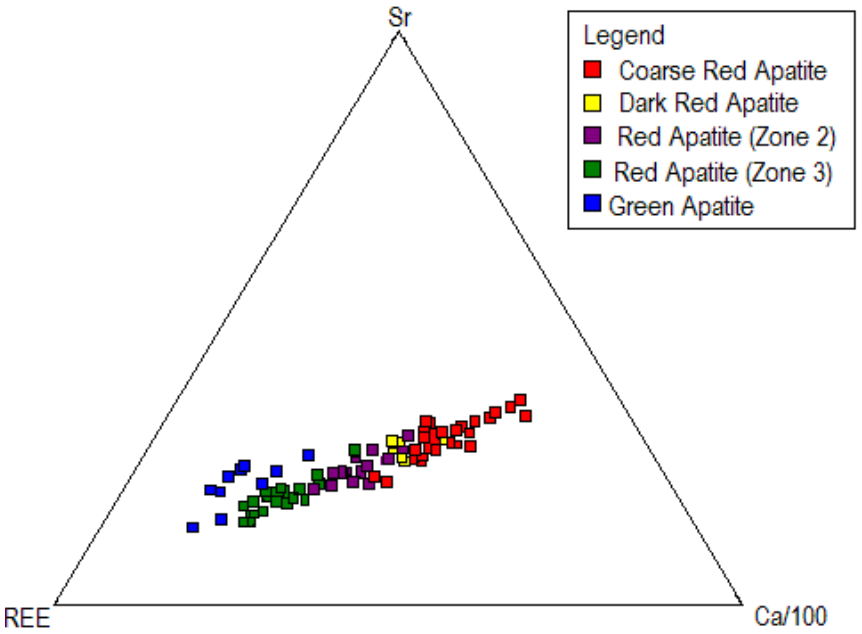

Figure 6.20 Apatite composition on Sr-REE-Ca triangular diagram.

6.3.3 TITANITE AND CHEVKINITE

Associated with the allanite in the diopside-allanite veins is titanite and a minor amount of chevkinite. Although the distribution of the chevkinite in the veins is quite erratic, when present it can reach concentrations of up to 5%. Both of these minerals are REE-bearing; the titanite contains between 3.0 and 6.2 % TREO while the chevkinite contains between 35.6 to 41.7 % TREO. An unusual feature of the titanite is that Nd is the most abundant REE, followed by Ce, Sm, and finally La (Table B.7 Appendix B). This is distinctly different than other REE-bearing minerals in this vein generation which are typically Ce or sometimes La dominant. There is also very little Th in comparison with other minerals in this vein generation, with a maximum ThO_2 content of 0.21 wt %. The titanite contains between 0.89 and 2.3 wt.% FeO and up to 0.8 wt % MgO. In backscattered images the titanite is surprisingly homogeneous in comparison

to the other REE-bearing minerals in the diopside-allanite veins, which are often distinctly zoned (Fig 6.21).

The chevkinite mainly occurs as subhedral to anhedral cores entirely encased in allanite. The relative REE composition of the chevkinite is typically similar to that of the allanite with Ce as the dominant REE, followed by lesser amounts of La and Nd (See Table B.8 in Appendix B). Only traces of REE heavier than Nd are present in the chevkinite. Although only analysis of the LREE is possible with EMPA, the ratio of La/Nd in the allanite and chevkinite is essentially identical; both have a ratio of about 1.5. As observed in the allanite, the chevkinite is strongly zoned in the backscattered images. The zoning in the chevkinite is roughly concentric in most cases, with irregular, ragged boundaries similar to those in allanite. The majority of the zonation observed in the chevkinite is due to the variation in the Ti and REE content, with the highest REE content found in the centers of the crystal decreasing outward to the comparatively REE-poor, Ti-rich rims. This is then mantled by zoned allanite (Fig. 6.22). There is also a minor amount of Th, Mg and Sr found in the chevkinite; up to a maximum of 1.7 wt.% ThO_2, 0.79 wt. % MgO and 0.84 wt.% SrO.

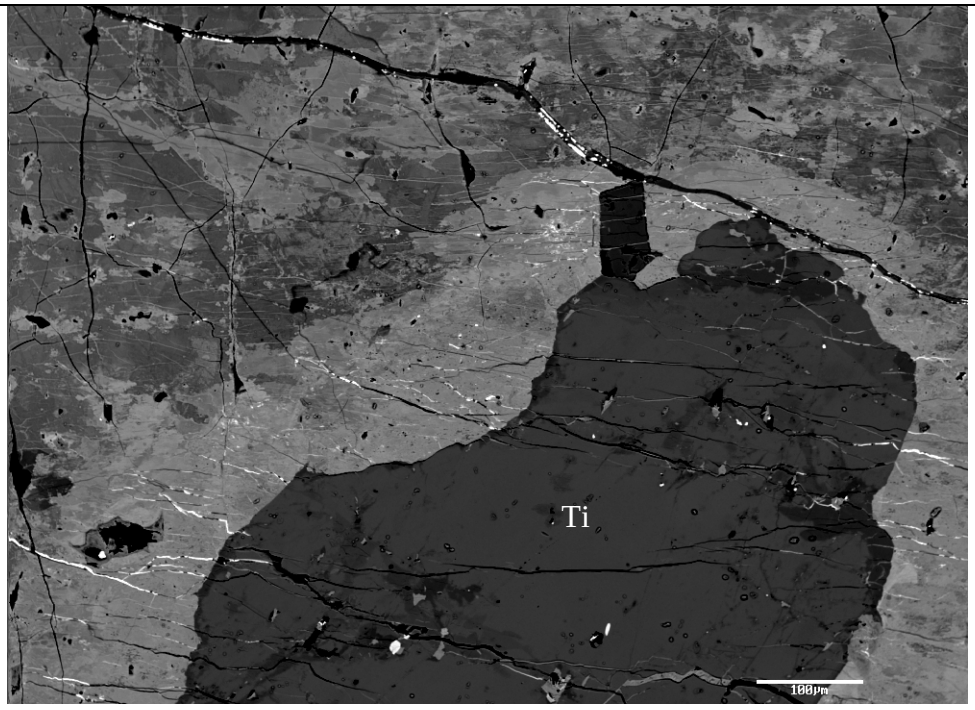

Figure 6.21 Titanite (Ti) crystal surrounded by zoned, altered allanite from sample no. 881237. Scale bar is 100µm.

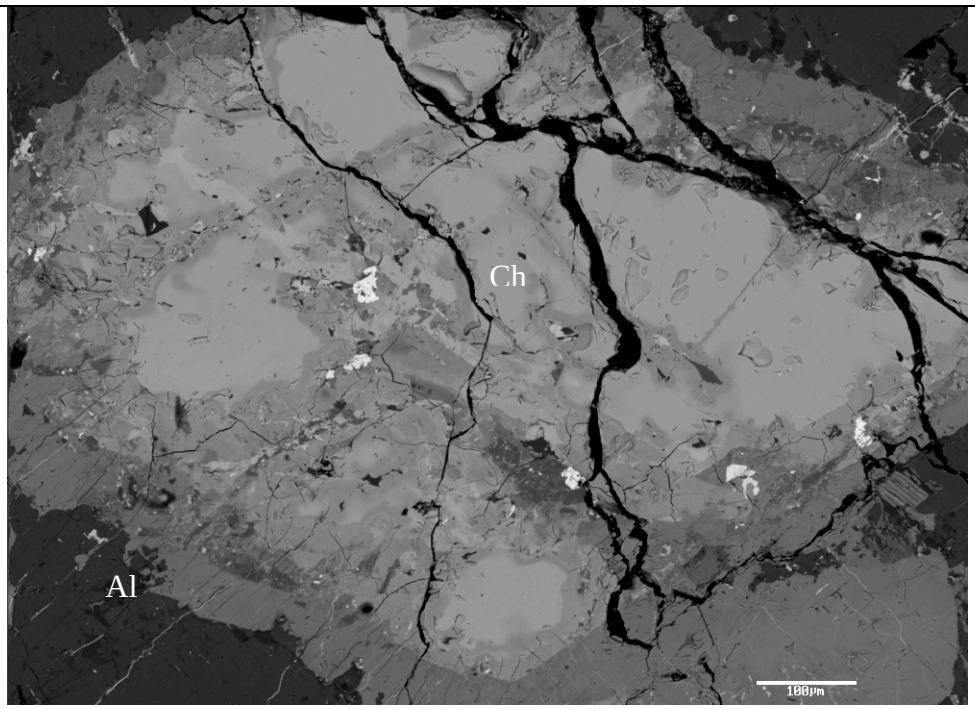

Figure 6.22 Zoned chevkinite crystal surround by allanite in sample no. 782076. The lighter grey (chevkinite (Ch)) distinguishes regions of high REE+Ti content ranging to lower REE+Ti content in the darker grey allanite (Al) regions. Scale bar is 100μm.

It should be noted that the designation of chevkinite is somewhat tentative; the mineral in question may actually be perrierite based on the chemical composition of the mineral. There has been significant debate as to whether chevkinite and perrierite are isomorphous or dimorphous (see MacDonanld and Belkin, 2002). The consensus seems to be that chevkinite and perrierite have very similar, although not identical, chemical compositions and seem to form an extensive solid solution series (Ito, 1967). The composition of both minerals can be expressed by the idealized formula of $A_4BC_2Ti_2Si_4O_{22}$, where A = (REE,Ca,Sr,Th), B = Fe^{2+}, C = (Fe^{2+},Fe^{3+},Ti,Al,Zr). The major compositional differences depend on the amount of Ca, Fe, Al and REE present. These composition variations are reflected in structural differences, particularly the β angle which varies from approximately 100^o in chevkinite to 113^o in perrierite (MacDonald and Belkin, 2002).

A method of chemical discrimination proposed by MacDonald and Belkin (2002), involving the ratio of Fe/(Fe+Al+Ti), has the samples from Hoidas Lake clustering at 0.3 which is the dividing point between chevkinite, which are defined by a ratio of greater than 0.3, and perrierite, which are less than 0.3. A second descriminant proposed by MacDonald and Belkin (2002) for the chemical discrimination of chevkinite and perrierite uses the FeO (wt.%) vs. CaO (wt.%) content of the samples. On this diagram the Hoidas Lake chevkinites plot on the perrierite side of the divide between the chevkinite and perrierite compositional fields (Fig.6.23). Due the uncertainty as to which mineral is present at Hoidas Lake it may be more appropriate to refer to the mineral in question chevkinite-perrierite pending further definitive analysis, such as XRD.

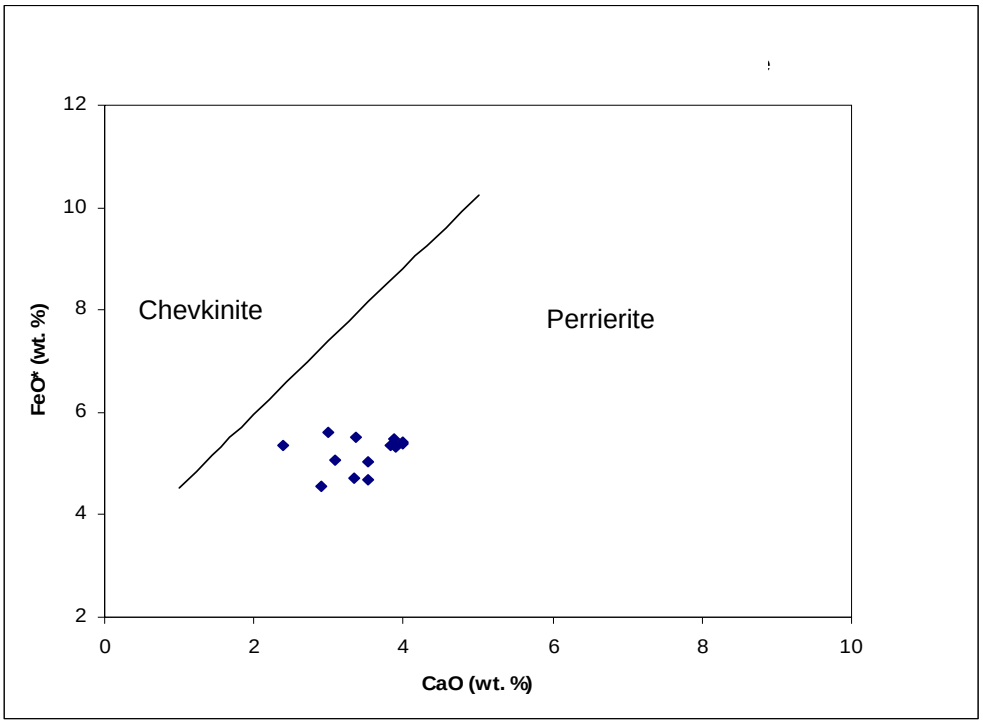

Figure 6.23 Chevkinite-Perrierite Discrimination as proposed by McDonald and Belkin (2002). As stated by MacDonld and Belkin (2002), “the line separating the two fields is arbitrary and may have a slightly different slope.”

Although determining which mineral is present in the veins at Hoidas Lake is not crucial, it would provide some additional information. One major difference between the two minerals is the association in which they occur; chevkinite is typically found in syenites, metaluminous or peralkaline granites, or in fenites associated with carbonatites, while perrierite is typically related to more mafic rocks such as gabbros or minettes. Whether the mineral is chevkinite or perrierite would also provide some additional insight into the range of pressure, temperature and fO_2 conditions present during the development of the vein system (MacDonald and Belkin, 2002).

6.3.4 MONAZITE

The monazite is typically found as an inclusion in the earliest apatite generations (Fig.6.24). The monazite alteration appears as small, bright inclusions surrounded by darker areas in the backscattered electron images. The textural relationships suggest that the majority of the monazite observed is of a secondary nature since it is most often found as an alteration product of the earliest apatites. In rare instances monazite can be found as primary crystals, although they still occur in close proximity to apatite. These primary monazites have only been observed in association with the green, REE-rich apatites (Fig. 6.25), and they tend to be found at the boundaries of the apatite crystals rather than in the cores of large crystals as is observed in earlier apatite generations.

Both types of monazite contain between 56.8 and 62.8 wt. % REE, with the dominate REE being Ce, as it is in the associated apatites. There are also minor amounts of Th, Ca, and Sr in the monazite, with higher concentrations of these elements found in samples with lower total REE content (Table B.9 Appendix B). The highest REE content in the monazite tends to occur in the primary monazites, with lower values found in the inclusions. The amount of Th seems to be slightly higher in the inclusion monazites; in the inclusions the ThO_2 content averages 1.2 wt. % while in the primary monazite is it only 0.4 wt. %. Although not as pronounced a difference, the SrO content of the inclusions is also slightly higher than in the primary monazites at 0.15 wt. % and 0.11 wt.%, respectively. In the primary monazites the CaO content is consistently around 0.48 wt. %, while in the inclusions it is much more erratic, ranging from 0.12 wt. % up to 1.1 wt. %.

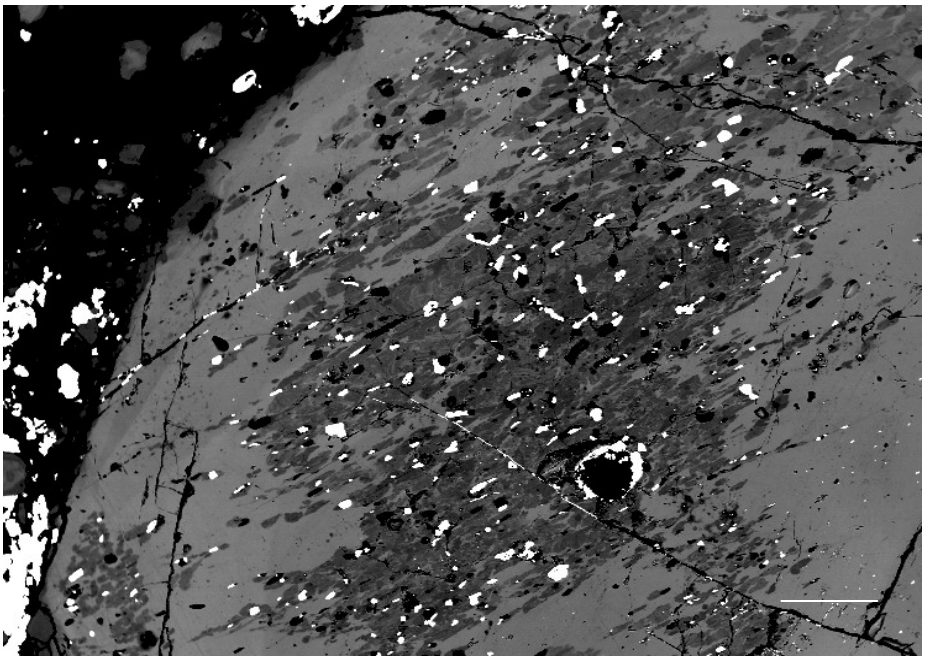

Figure 6.24 Example of monazite inclusions in a clast from the red apatite breccia in sample no 37903. Bright inclusions are typically monazite, although a minor number of thorite inclusions also exist. Dark patches surrounding the inclusion are typically REE poor Minor amounts of bastnaesite are present in the matrix, as shown by the bright patches. Scale bar is 100μm.

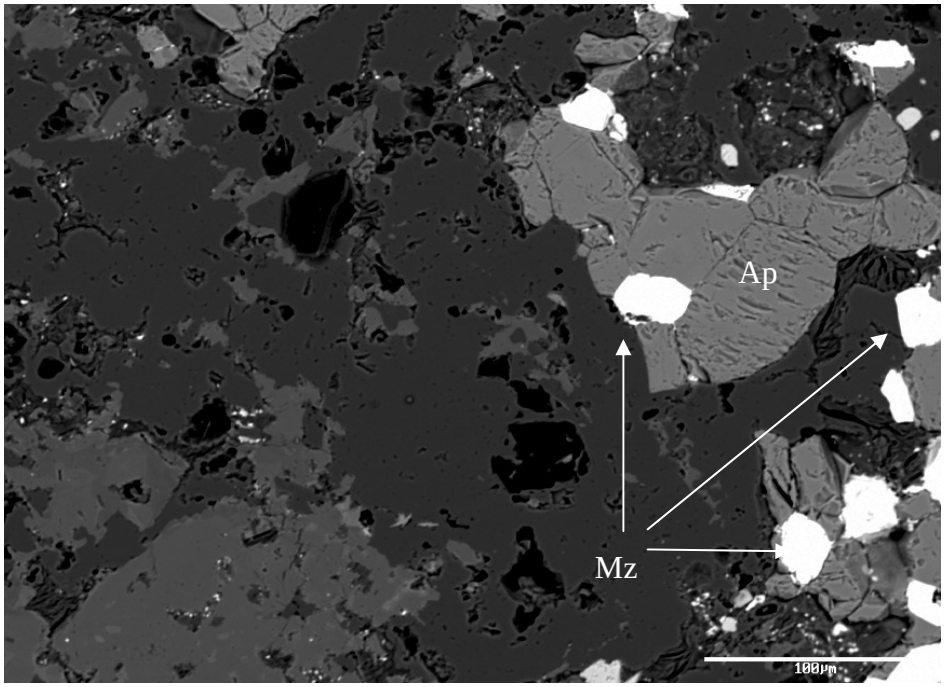

Figure 6.25 Example of monazite (Mz) with the green apatite (Ap) from sample no HL06-75. The matrix is dominated by quartz, calcite, and a minor amount of amphibole. Scale bar is 100μm.

6.3.5 REE CARBONATES

Rare REE carbonates, believed to be members of the bastnaesite group, can be found in the matrix of some of the breccias and also as an alteration product in the allanites. In the breccia matrix the REE carbonates appears as small, irregular patches of randomly oriented crystals. In allanite, the bastnaesite is concentrated in areas immediately adjacent to fracture surfaces, although in rare instances more pervasive alteration can also be observed. There are also rare REE-carbonate filled fractures which cross-cut the major vein generations. The amount of REE in the carbonates varies from 26.9% to 67.9% TREO. In almost all instances the most abundant REE is Ce, follow by La and Nd. In some cases there are trace amounts of Y, although the maximum observed Y_2O_3 content is less than 0.16 wt. % and there are a very limited number of samples where Nd is the most abundant REE.

In addition to the abundant REE there are also significant amounts of F, as would be expect in bastnaesite group minerals. Other than these major elements the exact composition of the REE carbonates is highly variable. Most contain some Ca and Sr, although the exact concentrations vary between samples. The samples typically range between bastnaesite and parasite in composition, with a limited number which are closer to synchysite (Fig. 6.26).The concentration of Th in the REE carbonates is low, with a maximum amount of 0.19 wt. % ThO_2 (See Table B.10 in Appendix B).

6.4 CHEMICAL COMPOSITION OF THE GANGUE MINERALS

6.4.1 CLINOPYROXENE

The vast majority of the clinopyroxene is diopside, although there are rare augites (Fig 6.27). In addition to Ca, Fe and Mg, most of the clinopyroxenes contain minor to trace amounts of Mn, Ti and Cr. The amount of MnO in the clinopyroxenes reaches a maximum of 0.7 wt. %, while the TiO_2 and Cr_2O_3 only reach 0.27 wt.% and 0.05 wt. %, respectively (Table B.11 Appendix B). The clinopyroxenes also contain minor amounts of Al_2O_3, consistently less than 3 wt. %, and entirely lack Na. The composition is fairly homogenous and does not display the zonation found in other minerals of this vein generation. In most pyroxenes there is minor alteration to amphibole and chlorite, particularly along fractures and cleavage planes (Fig. 6.28).

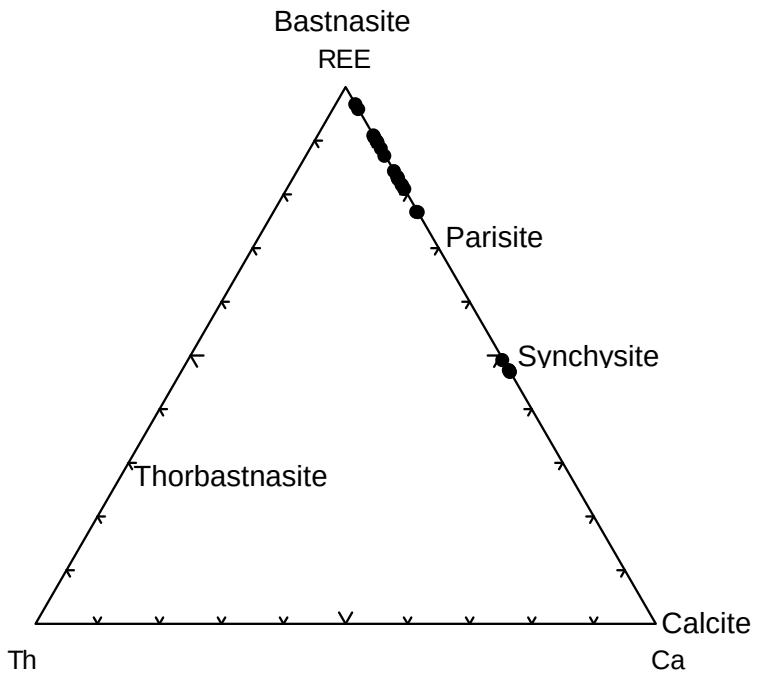

Figure 6.26 Compositional variation of the REE-carbonates from Hoidas Lake in terms of Ca, REE and Th (after Berger et al., 2008).

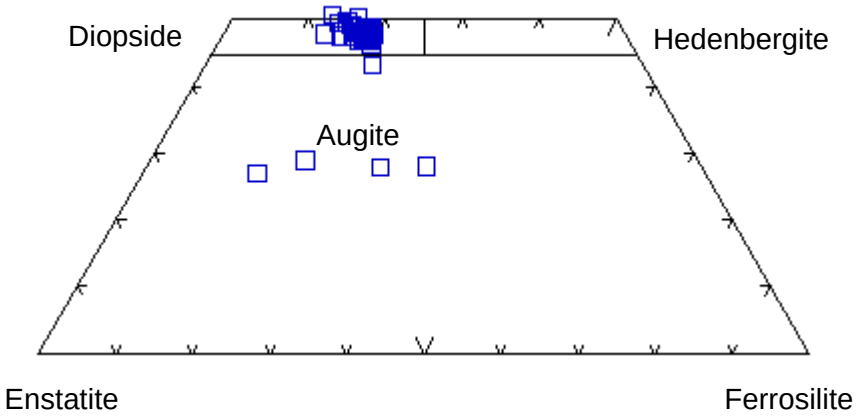

Figure 6.27 Composition of the clinopyroxene found in association with the allanite in the Hoidas Lake vein system (after Morimoto, 1988).

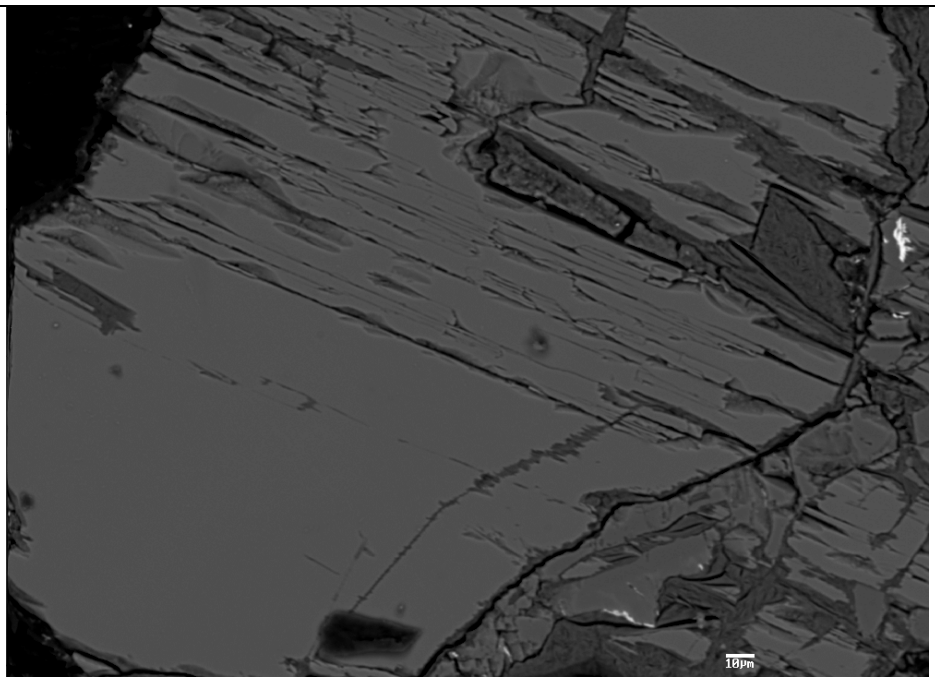

Figure 6.28 Typical clinopyroxene from the diopside-allanite vein generation from sample no. 881216. Note the darker patches which represent replacement of diopside by amphibole along fractures, cleavage planes and crystal boundaries. Scale bar is 10 µm.

6.4.2 AMPHIBOLE

Although there are rare examples of what appear to be primary amphiboles in the thin sections the vast majority of the amphibole observed in these samples appears as an alteration product, typically associated with the clinopyroxene. The amphiboles range in composition from hornblende to tremolite to rare actinolite.

6.4.3 FELDSPAR

The feldspars observed with the diopside-allanite veins at Hoidas Lake are typically hyalophane, which is a Ba-bearing feldspar, although both celsian and more typical K-feldspars can be found in the vein system (Fig. 6.29). Additional analysis of the samples reveals that there are also trace amounts of anorthite present in the diopside-allanite veins. The amount of Ba present in the feldspars varies from below the detection limit to 16.9 wt. % BaO. In addition to the K and Ba found in these feldspars there are

also minor amounts of Na and Sr. The amount of Na_2O ranges from below the detection limit to 2.3 wt.% while the amount of SrO varies from below the detection limit to 1.8 wt.% in the Ba-rich samples (Table B.12 in Appendix B).

The vast majority of the feldspars are of a uniform chemical composition, with only the rare anorthites showing any sort of zonation in backscattered electron images. In some instances the edges of the feldspars appear to be altered to barite, although the presence of Sr suggests the composition lies somewhere between the barite and celestine end members (Fig. 6.30).

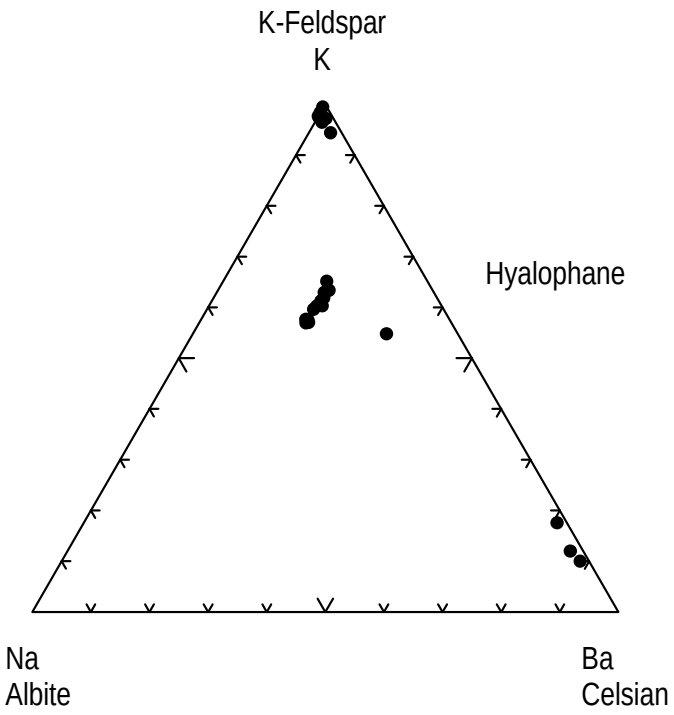

Figure 6.29 Composition of the feldspar found in the vein system at Hoidas Lake (after Essene et al., 2005).

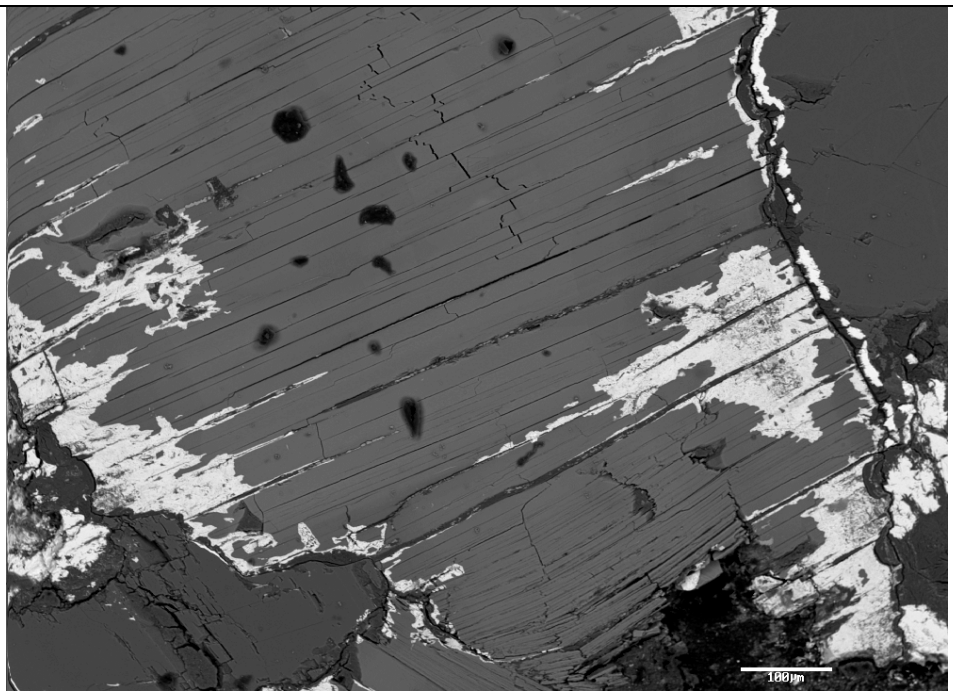

Figure 6.30 Hyalophane altering to Ba-Sr Sulphate around the margins and along cleavage planes (bright patches) in sample no. 881216. Dark grey minerals to the top right and bottom left are small crystals of calcite. Scale bar is 100 μm.

6.5 SUMMARY

The mineralization at the Hoidas Lake REE deposit consists mainly of LREE-enriched fluorapatite and allanite-(Ce), both of which lack an Eu anomaly in chondrite normalized plots. There are also minor amounts of other REE-rich minerals such as monazite, bastnaesite and chevkinite which, despite their relatively rare nature, are significant due to the high concentrations of REE they contain. These minerals are also dominated by LREE, and it appears as though monazite and bastnaesite are predominantly the result of alteration of the apatite and allanite. The most intense alteration is concentrated in the earliest vein generations suggesting that these veins were affected by the later periods of mineralization.

The complexly zoned crystals, and the multiple vein generations, indicate multiple episodes of crystal growth and alteration. Examination of the different vein generations reveals that the chemical composition of the system changed through time. The diopside-allanite veins show the largest variations in chemistry, as is reflected by

the relatively complex mineralogy of this vein generation compared to the apatite veins. The diopside-allanite veins contain abundant REE found in the allanite, titanite and chevkinite and also high amounts of Ba found mainly in the hyalophane. In the apatites there is significantly less REE than found in the allanite, although between apatite generations the REE content steadily increased with each subsequent generation to reach a maximum average REE concentration of 5.5% TREO in the green apatite. In the youngest generation of apatite the REE content drops to the lowest levels observed in the system. The key compositional difference between the coarse red apatite, which is the most recent apatite, and the other apatites in the system is that Nd, rather than Ce, is the dominant REE, and the MREE are relatively more abundant than in the other analyzed apatites.

Overall the vein system as a whole shows an unusual concentration of not only REE, but also Sr, Ba, and F. Although the majority of the Ba is found in the hyalophane or barite it is also present in trace amounts in many of the other minerals in the veins. The Sr is found dispersed throughout the majority of the minerals in the vein system rather than concentrating into select minerals. Surprisingly there is no evidence of Na in the apatites, as the substitution of Na in REE rich apatite is a common method of maintaining the charge balance

CHAPTER 7
CONSTRAINTS ON THE ORIGIN OF THE MINERALIZATION AND THE SOURCE OF THE RARE EARTH ELEMENTS

7.1 INTRODUCTION

Many of the initial questions regarding the Hoidas Lake mineralization focused on the topics addressed in the proceeding chapters, including the field relationships and paragenesis, as well as the mineralogical, textural, and compositional features of the mineralization. The detailed examination of the field relationships and mineralogy of the veins allowed the identification of the four main REE-bearing vein generations and the construction of a paragenetic sequence for the Hoidas Lake mineralization. The fieldwork also identified an unusual peralkaline pegmatite and several lamprophyres which were previously unknown, although the timing of these igneous units remains poorly constrained. The compositional and textural data obtained for the major minerals present in the veins helped to identify not only additional REE minerals, but also confirmed multiple episodes of veining and alteration as shown by the internal complexity typical of the apatite and allanite. Although this initial work answered many of the important questions about the mineralization, and provides a framework for additional analysis, some key questions remain.

One of the major unanswered questions surrounding the Hoidas Lake REE deposit is the origin of the mineralization and the source of the REE. In the past the REE mineralization has largely been assumed to be magmatic in origin, although there have also been suggestions that the Hoidas Lake mineralization is metamorphic or metasomatic in origin (Gunning and Card, 2005; Harvey et al., 2002; Hogarth, 1957). The potential for hydrothermal REE mineralization may have been overlooked in the past, as historically the REE have been assumed to be essentially immobile, which recently has proved to be untrue (Morteani, 1991). Both experimental and observational data indicated that under the appropriate conditions REE are mobile (de Hoog and van Bergen, 2000).

As the amount of available information on the behavior of REE under hydrothermal conditions increases, it becomes apparent that REE can be concentrated into economic deposits by hydrothermal processes (Samson and Wood, 2005). Some

of the most important REE deposits in the world are now believed to have a hydrothermal component in their petrogenesis (Giere, 1996). It should be noted that due to the interaction between magmas and fluids in the formation of REE mineralization it is often difficult, if not impossible, to attribute the mineralization to either a purely magmatic or purely hydrothermal source (Salvi and Williams-Jones, 2005).

7.2 EXISTING THEORIES ON THE ORIGIN OF THE HOIDAS LAKE MINERALIZATION

Gunning and Card (2005) suggested that the zonation of the veins, as well as the petrographic features of the mineralization, is reminiscent of a hydrothermal vein system. Despite the presence of what appears to be hydrothermal features, Gunning and Card (2005) concluded that the REE-mineralized occurrences are best interpreted as magmatic features due to the large amounts of clinopyroxene and feldspars in the earliest stages of mineralization, which they believe are unlikely to have originated from an aqueous solution. Gunning and Card (2005) suggest that as the dikes largely lack quartz they are more similar to alkaline rocks rather than a more traditional pegmatite. Due to the composition of the REE-bearing dikes Gunning and Card (2005) concluded that the magma was likely mantle sourced, although they do not rule out some mixing with granitic material.

Harvey et al. (2002) also favored an initially magmatic origin for the Hoidas Lake REE mineralization, with extensive alteration of the original dikes. In this scenario dikes of ultramafic to lamprophyric composition were emplaced along late faults and fractures and then subjected to further metamorphism or possibly chlorine metasomatism. Harvey et al. (2002) believed that the clinopyroxene-rich occurrences at Hoidas could be related to a larger late ultramafic event in the Ena Domain, as there has been mention of peridotite and pyroxenite dikes to the southwest of the Hoidas Lake vein system. To explain the unusual REE enrichment at Hoidas Lake Harvey et al. (2002) proposed that the REE may have been leached from the surrounding host rocks, which are known to contain allanite as a trace mineral.

The earliest examination of the veins, completed by Hogarth (1957), concluded that the veins likely represent a mix of igneous and hydrothermal origin, with the

earliest zones the result of magmatic formation evolving later to a largely hydrothermal system with some late remobilization. Hogarth attributed only the late calcite and rare quartz veins to hydrothermal formation, with all the earlier generations assumed to be magmatic. Although Hogarth does not relate the REE mineralization to a specific type of igneous rock, the source magma is suggested to be rich in REE, Ca, Ba, K, and volatiles. It should be noted that as a direct result of Hogarth's investigation of the vein system, and his reported mineralogy of the veins, the Hoidas-Nisikkatch showings have been mentioned in a number of additional publications related to carbonatites. For example *The Geology of Carbonatites* by Heinrich (1966) lists the Hoidas Lake veins as bearing a strong resemblance to occurrences of a carbonatitic affinity.

7.3 RELATION TO THE HOST ROCKS

One issue at Hoidas Lake is what influence, if any, do the host rocks or other igneous occurrences in the area have on the mineralization? In many examples worldwide there is often a clear relationship between the host rocks and the REE mineralization. An excellent example of this is where the REE mineralization consists of a primary magmatic phase which is part of the larger intrusive complex. For example, the REE mineralization at Mountain Pass, USA, is considered to be of primary magmatic origin, as is the Kangerlaursuk area in the Ilimaussaq Complex, which as part of a cumulate sequence, is undeniably magmatic (Mariano, 1989; Salvi and Williams-Jones, 2005).

In other cases the relationship between the host rocks and the REE mineralization is not as direct, such as at the Mont Blanc Massif where the REE are leached from the surrounding host rock and reconcentrated into shear zones (Rolland et al., 2003). At Rodeo de Los Molles deposit in Argentina, the REE mineralization is the result of hydrothermal alteration of an igneous intrusion. In this deposit the mineralization is found in a fenitized area of a monzogranite (Lira and Ripley, 1992). There are also many examples where there has been considerable discussion as to whether the mineralization is magmatic or hydrothermal, e.g. the Strange Lake Complex in Quebec (Salvi and Williams-Jones, 2005). In many cases there is no clear distinction between magmatic and hydrothermal mineralization in REE deposits (Pollard, 1995).

7.3.1 GRANITIC ROCKS

Although many of the rocks in the immediate vicinity of Hoidas Lake, as well as in the Ena Domain in general, contain trace amounts of REE-bearing minerals, such as allanite (Koster, 1965; Ashton and Hunter, 2003; Ashton et al., 2005; Ashton et al., 2007), the REE-mineralized veins at Hoidas Lake do not appear to be directly linked to the host rocks. This is due to a number of reasons, both compositional and textural. Texturally, it is unlikely that the mineralization is directly related to the crystallization of the surrounding granitic host rocks due to the sharp linear contacts and the crosscutting relationship between the host rocks and the veins. Also, the majority of the veins lack any evidence of deformation and are slightly discordant to the prevailing fabric of the host rocks. The distinct crosscutting nature of the veins, and the lack of deformation in the majority of the veins, suggest that the mineralization post dates the formation and subsequent deformation of the granitoids.

Chemically the veins are also quite distinct when compared to the host rocks. Despite the presence of REE-rich minerals, such as allanite, in many of the granitic rocks in the region any sort of genetic relationship between the host monzogranites and granodiorites at Hoidas Lake and the REE-mineralized veins seems unlikely. The fact that the granitic rocks in the area all contain relatively low concentrations of Ca, Sr, Ba, Ti, Fe, Mg, P and REE make it difficult to envision any sort of extensive contribution to the formation of the veins by the granitic host rocks as the veins are relatively enriched in all these elements. The composition of the Hoidas Lake apatites indicates that they are unlikely to have been derived from a highly fractionated source rock. Apatites associated with highly fractionated source rocks, such as granites or pegmatites, typically have a Sr concentration of less than 100 ppm, and therefore it is very improbable that the Hoidas Lake apatites, which typically contain several thousand ppm Sr, are associated with the granitoids or granitic pegmatites in the area. This is reinforced by the high amounts of Th and LREE in these apatites, which would be more typical of a carbonatitic or possibly syenitic source. If these apatites were related to a granitoid source there should be very low amounts of Th and they would normally display a relatively flat chondrite normalized REE pattern, with a $(La/Yb)_N$ ratio of less

than 10, often with a pronounced negative Eu anomaly. The observed LREE-enriched pattern, with an average $(La/Yb)_N$ ratio of 211, and the absence of an Eu anomaly in the apatite-rich samples is again much more typical of carbonatitic apatites (Belousova et al., 2002).

There is also little to no evidence of alteration in the host rocks immediately adjacent to the veins; the host rocks are surprisingly fresh, suggesting only limited involvement in the formation of the veins. The only visual evidence of alteration is a narrow, typically no more than a few tens of centimeters wide, zone of weak potassic and hematitic alteration and rare 1 to 2 cm wide gradational contact. The relative absence of alteration in the host rocks makes it highly unlikely that the REE have been leached from the wall rocks and redeposited in the veins. In cases where the REE and other essential elements are locally derived from the host rocks there is typically a strong alteration halo with highly gradational contacts surrounding the mineralization which is clearly absent in this case (Lira and Ripley, 1992; Rolland et al., 2003), suggesting that the bulk of the material required for the formation of the veins came from a source other than the wall rocks.

The relative lack of alteration associated with the vein system also indicates that there was little interaction between the mineralizing system and the wall rocks, suggesting that fluid-rock interactions did not strongly influence the location of the mineralization. Similar to what is discussed above, if the presence of highly reactive wall rocks controlled the location of the mineralization there should be evidence of reaction between the fluid and the wall rocks. The rare gradational contacts do suggest some small scale interactions, however their restricted occurrence suggests that other factors such as fluctuation in the temperature, pressure or fluid composition were likely more important to the formation of the veins than the fluid-rock interactions.

7.3.2 PEGMATITES

Similar arguments as proposed for the granitoid host rocks also apply to many of the granitic pegmatites in the area. Based on the limited relative age relationships in the field it is possible that some of the pegmatite generations could be broadly contemporaneous with the mineralizing system, which implies that they could be linked

to the mineralization in some manner. In particular, the rare peralkaline hyalophane-bearing pegmatites are intriguing.

Similar to the veins, these unusual pegmatites also appear to postdate the majority of deformation and metamorphism in the area, as they display little to no deformation or alteration and occur as sharp-sided linear features which are steeply dipping. The overall mineralogy of the veins and these pegmatites are also quite similar and, although the relative major mineral content varies, the pegmatite contain at least minor to trace amounts of all the essential minerals found in the REE-mineralized veins. Chemically, the hyalophane pegmatites contain much higher Sr, REE, Ca, and Fe concentrations and lower Na concentrations than the other more granitic pegmatites and most of the granitic host rocks. They are also the only sample which plots in the within plate field on the discrimination diagrams proposed by Pearce et al. (1984). This suggests an extensional environment, which is a prominent feature associated with many REE deposits. Finally, although the overall concentrations are lower, the REE pattern of this pegmatite generation is remarkably similar to that observed from the vein samples, including the lack of Eu anomaly and the unusual negative Tb anomaly (Fig. 7.1).

7.3.3 MAFIC OCCURENCES IN THE ENA DOMAIN

Koster (1965, 1970) mentions a number of mafic veins and dikes in the Ena Domain. Southwest of Nisikkatch Lake there are rare peridotite dikes which are rich in pyroxenes, olivine and amphibole. Lamprophyre dikes are also quite common in the Ena domain and can be concordant or discordant to the local structure. The “Mafelsic phase” of Koster (1965) in the Northern Complex at Ena Lake contains variable amounts of pyroxene in addition to plagioclase, biotite, and amphibole, with trace amounts of apatite, zircon, titanite, and allanite. The mineralogy in this case is interesting, as it shows many similarities to the Hoidas Lake veins. Rare massive pyroxenite dikes up to 30 m thick are also found at Ena Lake, although they are not described in detail by either Koster (1965) or Ashton et al., (2005). Unfortunately, as observed in the Hoidas Lake area, in most instances these dikes do not display any cross cutting relationships and

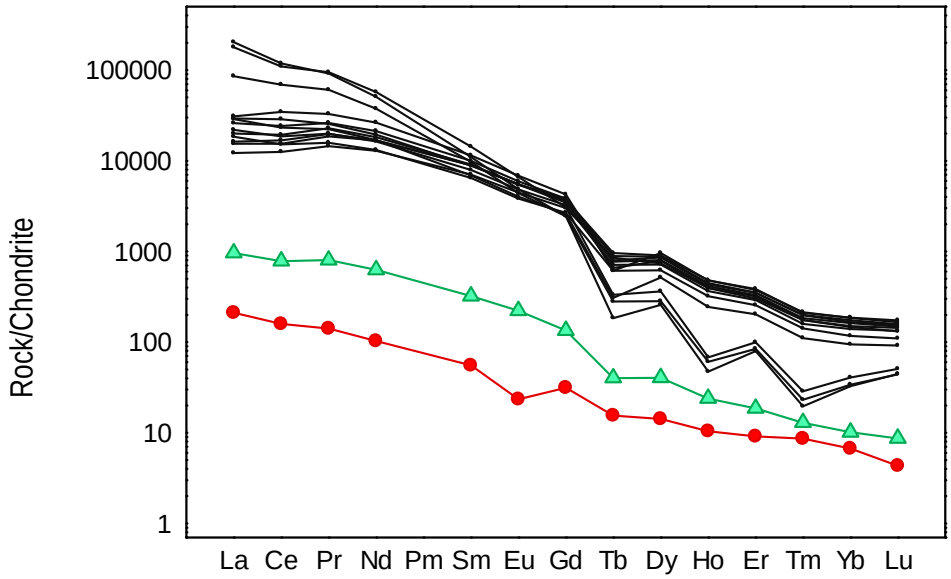

Figure 7.1 REE content of the veins compared to the peralkaline pegmatite and lamprophyre. All samples normalized to chondrite (Sun and McDonough, 1989). Vein samples shown by the black lines, pegmatite by the green triangles, and lamprophyre by the red circles.

therefore their relative age is unknown. In some cases even the timing of emplacement of the dikes relative to deformation and metamorphism is unclear. There is little geochronological data for these volumetrically minor phases, which limits attempts to determine their relation to other lithologies (Ashton et al., 2005). This lack of even relative age relationships makes it difficult to determine with any certainty what, if any, their relationship to the mineralization at Hoidas Lake may be.

One of the suggestions put forward by Harvey et al. (2002) is that the mineralization at Hoidas Lake is the result of either metamorphism or metasomatism of a pyroxenite. Metasomatism has been associated with slight REE and LILE enrichments in some mafic to ultramafic rocks (Jahn et al., 2003; Kempton et al., 1995; Stone et al., 1994). Although the alteration results in the formation of REE-rich minerals, such as apatite and allanite, the overall REE content of rock remains relatively low, much less than what is observed in the vein system at Hoidas Lake. In these situations the REE-bearing apatite is believed to be the result of alteration of pre-existing late magmatic apatite and the allanite is the result of the breakdown of plagioclase (Stone et al., 1994). In mineralization resulting from the alteration of a plagioclase-rich rock there is

typically a distinct chemical signature which often includes a positive Eu anomaly (Python et al., 2007). If the allanite at Hoidas Lake was the result of alteration of igneous plagioclase there would typically be an Eu anomaly, which is not observed. Harvey et al. (2002) also proposed that the association of Ca-scapolite and apatite in the veins is evidence of chlorine metasomatism; if this were the case the apatite should be predominantly chlorapatite, which it is not.

The idea that the vein system represents a metamsomatized lamprophyre is also unlikely as this would require either the presence of two distinct lamprophyre generations, with one generation experiencing intense metamorphism or metasomatism while the other, younger, lamprophyres are relatively fresh, or the preferential alteration of a lamprophyre in close proximity to the fault system. Although either of these situation is theoretically possible, and there are mentions of multiple lamprophyre generations in the region (e.g. Ashton et al., 2006), all the lamprophyres in the region appear to be relatively young and seem to postdate the bulk of the metamorphism and deformation (Ashton et al., 2006; Ashton and Card, 1998; Koster, 1965).

Overall, available evidence suggests that the REE-bearing veins are not the result of metamorphism or metasomatism of a preexisting mafic dike but, without more detailed information regarding the timing and composition of the various mafic dikes in the area, this relationship is impossible to fully evaluate. The major issue with idea that the veins are a metamorphosed version of a mafic dike is that in most cases the mafic dikes in the area seem to postdate the bulk of the deformation and metamorphism. Also, the multiple vein generations at Hoidas Lake, with complex variations in composition and chemistry, are unlikely to represent the metamorphism or metasomatism of a single dike. The sharp, although typically brecciated, contacts and crosscutting relationships observed in the vein system are different than the more continuous zonation which would be expected if the veins were the result of metasomatism alone. If metasomatism of a preexisting clinopyroxenite or lamprophyre dike played any role in the formation of the veins it would only be the earliest diopside-hyalophane-allanite-rich sections that would have been generated as it is difficult to envision the apatite-rich veins, which form the bulk of the vein system, resulting from a clinopyroxenite or lamprophyre protolith.

7.3.4 RELATION TO OTHER ROCK TYPES

The composition of the veins at Hoidas Lake is distinctly different than the granitic to tonalitic rocks which dominate the surrounding area and many features in the veins suggest that they are not affiliated with the nearby host lithologies. Enrichments of Si in the apatite, in addition to the high REE and Sr, have been associated with either syenites or lamprophyres (Chakhmouradian et al., 2002), although the relationship between the lamprophyres and the REE-bearing veins at Hoidas Lake is not convincing. It has also been suggested, largely based on the description provided by Hogarth (1957) that the veins at Hoidas Lake have a carbonatitic affinity. This reasoning is also supported by the chemistry of the veins, which are strongly enriched in LREE, Ba, and Sr. The strong LREE enrichment, combined with the high Sr levels, is indicative of a relationship to either a carbonatitic or alkaline source (Belousova et al., 2002; Chakhmouradian et al., 2002).

The mineralogy of the veins is also somewhat reminiscent of what would be observed with a carbonatite. The minerals found in the vein can all be found in carbonatites or related igneous rocks; the issue is the relative amount of each mineral. The problem with calling the veins a carbonatite dike is the general lack of carbonate minerals. Although minor amounts of calcite can be found in almost every vein generation, the concentrations are quite low relative to typical carbonatites (Mitchell, 2005).

The large amount of apatite present in the veins is also somewhat problematic due to the fact that, despite being a very common igneous mineral, apatite rarely reaches significant concentrations in igneous rocks (Deer et al., 1992). Phoscorites are one of the few igneous rocks that contain the required high concentration of apatite, however, they also typically contain large amounts of magnetite and either olivine or diopside. Besides the near absence of magnetite, the diopside-apatite-rich mineralogy at Hoidas Lake is similar to that found in some examples of olivine poor, diopside-rich phoscorites (e.g. Balaganskaya et al., 2007; Karchevsky and Moutte, 2004). The difference between the veins at Hoidas Lake and a typical phoscorite is underlined by the variations in the trace minerals present (Yegorov, 1993). The most notable difference is the absence of Nb

minerals, such as pyrochlore or perovskite, at Hoidas Lake (Krasnova et al., 2004; Balaganskaya et al., 2007). Also, although the high concentration of apatite is typical of phoscorites, the composition of the apatite is not. Apatite from phoscorites typically contains relatively low levels of REE_2O_3, SrO and SiO_2, usually less than 1 wt.%, 0.7 wt.% and 0.2 wt. %, respectively (Krasnova et al., 2004). This is inconsistent with the composition of the Hoidas Lake apatites, which contain high levels of REE, Sr and Si, especially in the later generations of apatite.

It is interesting to note that the apatite from Hoidas Lake does not fit neatly into any of the categories present on the discrimination plots proposed by Belousova et al. (2002). The Hoidas Lake apatites are most closely associated with the carbonatitic range, except that the Hoidas Lake apatites have a higher Y content (Fig. 7.2). The Y concentrations found in apatite ranges from tens of ppm, in carbonatites and lherzolites, to over 1% in those from granitic pegmatites, with an average of Y concentration of approximately 1500 ppm (Belousova et al., 2002). As Y tends to preferentially partition into an aqueous fluid phase relative to magma the high Y signature of the Hoidas Lake apatites may indicate a late magmatic to hydrothermal influence (Buhn et al., 2001).

Overall, the mineralogy and chemistry of the veins suggests that there may be additional lithologies in the area which have not yet been identified. The chemistry suggests that the mineralization is related to either a carbonatitic, syenitic or lamprophyric source. It is worth noting that all these rock types can occur in association with one another in carbonatite complexes; in many carbonatite complexes there are late syenite or lamprophyre dikes (Bulakh et al., 2004). If the mineralization observed at Hoidas Lake does have a carbonatitic affinity, as is implied by many of the compositional features, the carbonatitic rocks have yet to be found. This could be due to the presence of a carbonatitic intrusion at depth which has not been intersected by drilling or alternatively, if present at surface, a carbonatite would likely be covered by glacial till, lakes or swamps as carbonatites are comparatively soft and may weather preferentially. The restriction of carbonatites to relatively low lying areas would hinder attempts at identification and may explain why they have not been discovered during any of the mapping programs in the area (e.g. Mumin, 2002).

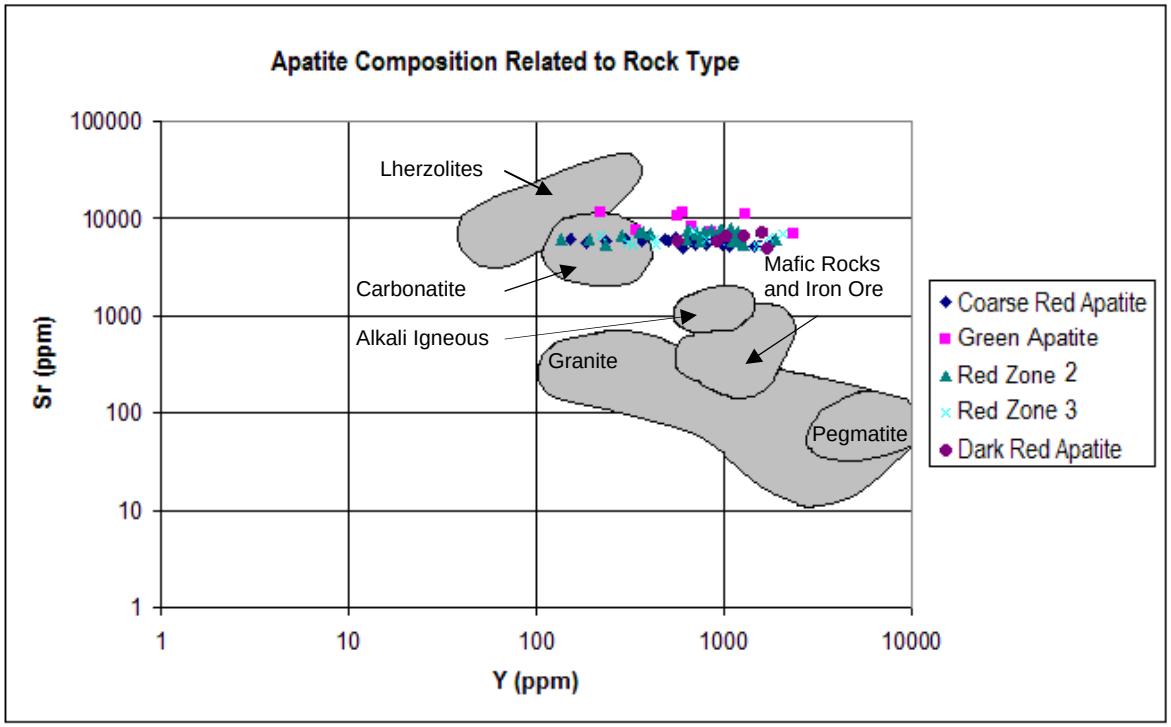

Figure 7.2 Apatite discrimination plot, as proposed by Belousova et al., (2002), showing the analyses of apatite from the Hoidas Lake deposit.

7.4 VEIN COMPOSITIONAL AND TEXTURAL CONSIDERATIONS

Many of the minerals in the veins display evidence which suggests that the vein system is late magmatic to hydrothermal in origin. The evidence of hydrothermal mineralization consists of both compositional and textural features, which are particularly prevalent in the REE-bearing minerals. It is worth noting that the extensive brecciation of many of the vein generations has largely obscured the primary textural features, limiting analysis of the initial formation of the veins. Particularly for the earliest vein generation there remains some uncertainty as to the origin of the minerals, as it is unclear whether the observed mineralogy is the result of extensive metasomatism of an originally igneous dike or if the vein is the result of primary formation from a hydrothermal fluid. Unfortunately, in some cases a definitive answer to this problem may not be available. Due to the potential interactions between hydrothermal and magmatic components it is often difficult, if not impossible, to attribute the

mineralization to either a purely magmatic or purely hydrothermal source (Salvi and Williams-Jones, 2005).

7.4.1 CHEVKINITE

The origin of the chevkinite is slightly more problematic than many of the other minerals in the veins. Chevkinite is most commonly encountered in magmatic systems and is typically not reported as a hydrothermal mineral, although in rare instances chevkinite has been found in some metasomatites (Jiang, 2006). This suggests that the earliest portion of the vein system may be more magmatic in character, although it is unclear whether chevkinite is truly restricted to a purely magmatic phase or if this is simply a result of the limited information available on this mineral. The fact that chevkinites are often found in volatile-rich rocks and that they crystallize late, at relatively low temperatures, has led to speculation that the chevkinite group minerals can crystallize hydrothermally given the appropriate conditions (Zhuming et al., 2008). This is supported by the fact that both chevkinite and perrierite have formed under hydrothermal conditions in a laboratory setting, at temperatures between 400^{o}C and 750^{o}C (Ito, 1967).

What is clearly apparent is that the chevkinite at Hoidas Lake has been exposed to hydrothermal fluids. Chevkinite which has undergone hydrothermal alteration is often mantled by a combination of both allanite and REE-rich titanite, as is observed in the Hoidas Lake chevkinites. The rim of hydrothermal allanite and titanite on the chevkinite crystals suggests that the chevkinite formed earlier and was not in equilibrium with the later fluid phase. During the alteration Si and Ti appear to be largely immobile, while the REE and Th are leached from the chevkinite. This can be seen in the dark, REE-depleted regions at the edge of the chevkinites in backscattered images. In most cases the Ca, Fe, Mg and Al in the allanite seem to have been supplied from an external source by the fluid (Vlach and Gualda, 2007; Jiang, 2006).

7.4.2 HYALOPHANE

The origin of the hyalophane in the REE-rich veins is somewhat problematic, as there is no firm evidence to suggest either a purely magmatic or hydrothermal origin.

One of the main issues Gunning and Card (2005) had with a hydrothermal origin for the veins was due, in part, to the abundant feldspar in the early veins. The presence of feldspar-rich layers or veins in many hydrothermal or exhalative deposits suggests that the crystallization of feldspars from a hydrothermal fluid is possible and therefore does not automatically exclude a hydrothermal origin for the veins (Orberger et al., 2005; Moro et al, 2001; Rao, 1976). The feldspar at Hoidas Lake is largely Ba-bearing and, although these feldspars are relatively rare, they have been found to form in a diverse range of settings including pegmatites and hydrothermal veins, as well as at a wide range of metamorphic or metasomatic conditions (Essene et al., 2005; Chakhmouradian and Mitchell, 2002).

On compositional plots compiled by Essene et al. (2005) there is a difference in the Na content of Ba-bearing feldspars from igneous and metamorphic or hydrothermal occurences (Fig. 7.3). Although there is an extensive region of overlap, the igneous Ba-feldspars tend to cluster along the Ab-Or axis, with the majority of igneous feldspars containing a relatively limited Cn component of less than Cn_{20}, with rare examples of up to Cn_{40}. For hydrothermal or metamorphic Ba-feldspars the Na substitution is a much more limited, with the amount of Na present largely a function of temperature (Essene et al., 2005). These feldspars tend to lie along the Or-Cn axis, and can contain an albite component of up to Ab_{35}. The hyalophane from Hoidas Lake plots in the region of overlap between these two fields, suggesting that a magmatic-hydrothermal origin may be appropriate (Fig. 7.3). If there is a hydrothermal component to the formation of the hyalophane it likely occurred at relatively high temperatures, as the Ab component in Ba-bearing feldspars increases with increasing temperature. However, due to the amount of overlap with the igneous field, a purely igneous origin cannot be ruled out.

An interesting feature of the Hoidas Lake hyalophane is that they are remarkably homogeneous in backscattered electron images. Hyalophane that is the result of protracted and progressive alteration often displays complex or erratic zonation patterns (Essene et al., 2005; Pan and Fleet, 1991). This suggests that either the hyalophane are primary or that the alteration or metasomatism completely eliminated any evidence of the original texture. In either case the presence of hyalophane requires an external source of Ba.

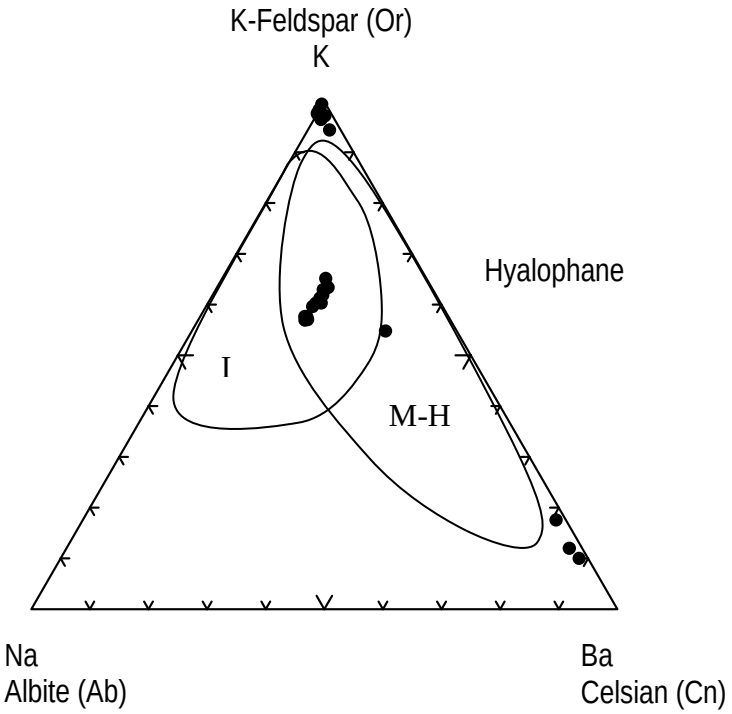

Figure 7.3 Composition of the feldspar found in the vein system at Hoidas Lake, shown by the black circles, compared to the composition of igneous (I) and metamorphic or hydrothermal (M-H) Ba-bearing feldspars (after Essene et al., 2005).

7.4.3 DIOPSIDE

As with the hyalophane, the origin of the diopside is also somewhat contentious. Gunning and Card (2005) believed that the large amount of pyroxene, which is almost entirely diopside, found in the early stages of the veins was evidence of an igneous origin. Harvey et al. (2002), in contrast, suggested that the presence of diopside is evidence of a metamorphic or metasomatic origin of the mineralization due to the fact that diopside is typically found as part of a skarn assemblage. Although each of these theories has some merit, neither is an ideal fit for what is observed in the veins at Hoidas Lake.

The composition of the pyroxenes at Hoidas Lake suggests a hydrothermal origin rather than a primary igneous pyroxene. Although the composition varies between hydrothermal and igneous pyroxenes it cannot be used to distinguish between

metamorphic or metasomatic and hydrothermal pyroxenes. Secondary or hydrothermal diopside tends to have high Ca and Si contents and low abundances of Al, Cr, Ti and Na compared to magmatic clinopyroxene (Python et al., 2007; Good et al., 1997; Manning and Bird, 1986). As Cr and Na are essentially absent and there are only limited amounts of Al and Ti present in the Hoidas Lake diopside a hydrothermal or metasomatic origin is favored over an igneous mode of formation.

If the initial vein generation was the result of replacement of a pre-existing pyroxenite, as proposed by Harvey et al. (2002), there is no evidence of the primary magmatic phase. Almost all the pyroxenes are diopside and there is no zonation or alteration observed in any of the diopside crystals which might suggest that they are the result of alteration of a pre-existing magmatic clinopyroxene. In cases where the diopside is the result of alteration of pre-existing pyroxenes by a hydrothermal fluid there may be a zonation from primary magmatic pyroxene in the cores of crystals to the diopside-rich rims or patchy, irregular alteration of the primary pyroxene to diopside (Good et al., 1997). The Hoidas Lake diopsides are homogenous in composition, with only slight alteration of the diopside to amphibole or rare chlorite; there is no evidence of a pre-existing pyroxene of a different composition. As is noted for the hyalophane, the homogenous appearance could simply be the result of complete replacement of the original magmatic mineral.

Although relatively rare, there are a number of diopside-rich dikes or veins which are believed to have formed in a late magmatic hydrothermal setting, and in several instances these examples share many common features with the mineralization at Hoidas Lake. One of the best examples is a set of diopside-titanite veins hosted by a Mesoproterozoic granite in the northern Finders Range, Australia (Bakker and Elburg, 2006). These veins appear to be controlled by late brittle structures and display sharp contacts with no wall rock interaction, similar to what is observed at Hoidas Lake. The diopside present in these veins is homogeneous in composition, with a minor amount of local replacement by actinolite and is found associated with REE-rich allanite and titanite. These veins are considered to be of late magmatic origin due to the presence of both melt and fluid inclusions in the early minerals. The highly saline fluid found in both the diopside and titanite is believed to have been exsolved from a mantle-derived

magmatic source, potentially a calcium-rich syenitic system (Bakker and Elburg, 2006; Elburg et al., 2003).

Although the example given above shares the most similarities to what is observed at Hoidas Lake, there are also a number of other examples where the pyroxene is believed to be hydrothermal in origin. At the Eden Lake carbonatite complex, Manitoba, there are late magmatic-hydrothermal veins of coarse grained aegirine-augite and K-feldspar (Mumin, 2002). The pyroxene associated with REE-enriched apatite veins at Bayan Obo, China, is believed to have formed from a hydrothermal fluid, although in this case the pyroxene is aegirine rather than diopside (Campbell and Henderson, 1997). There are also diopside-rich veins which are believed to have been precipitated directly from a hydrothermal fluid at Mount Elliot, Australia. In this example the diopside is found as a coarse-grained infill in open veins and fractures. The veins at Mount Elliot also include minor amount of allanite and REE-rich apatite. The fluids responsible for the vein formation are believed to be derived, at least in part, from a magmatic source (Wang and Williams, 2001).

7.4.4 ALLANITE

Compositionally, the allanite at Hoidas Lake is moderately to strongly enriched in LREE, although the composition varies throughout the zoned crystals with the rims typically closer to epidote in composition than they are to allanite. On the compositional plot devised by Petrik et al. (1995) the majority of the Hoidas Lake allanites cluster near the region of overlap between the igneous and hydrothermal fields, suggesting that the allanites are late magmatic to hydrothermal in origin (Fig. 7.4). The majority of the analyzed allanites show a wide range of compositional variation, with many exhibiting features typical of hydrothermal allanite. Only one sample, 782076, displays a relatively restricted range; this relatively limited compositional range may be due to the chevkinite providing some sort of compositional control as much of the allanite in this sample is a product of alteration of the chevkinite.

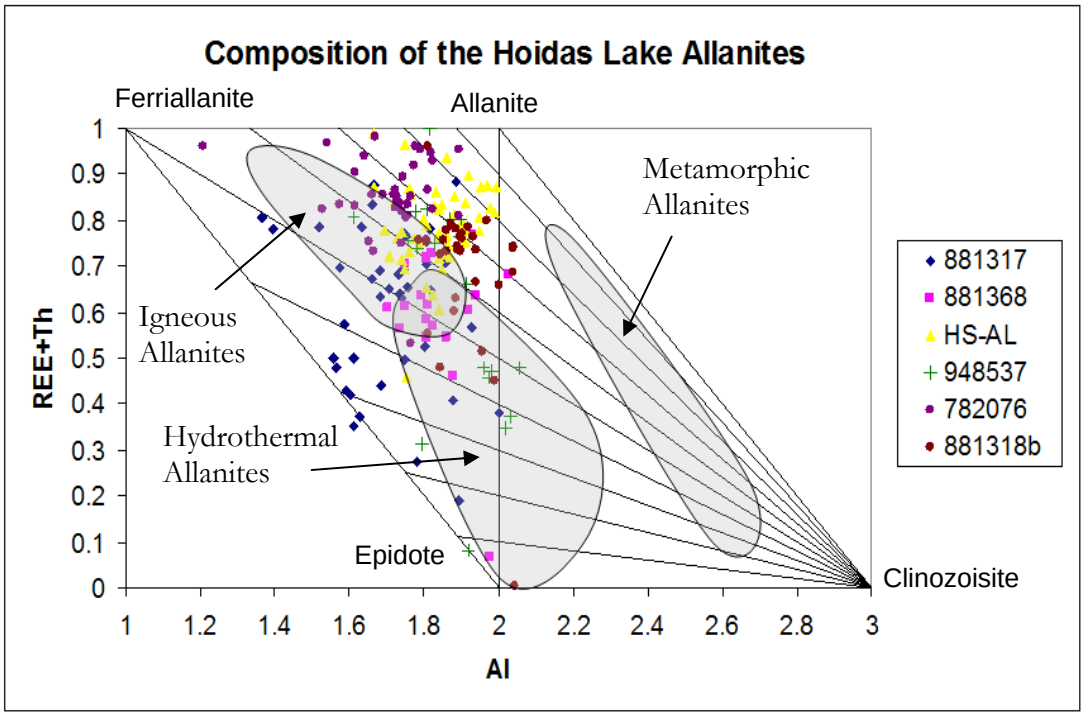

Figure 7.4 Compositional variations observed in the Hoidas Lake allanites. Shaded fields are adapted from Petrik et al. (1995). The majority of the Hoidas Lake allanites plot in or near the region of overlap between the Igneous and Hydrothermal allanite fields.

The REE, Ti, Ca and Mg content of allanite has been used by Jiang et al. (2003) to separate magmatic, late magmatic and hydrothermal allanites. Although the late magmatic and hydrothermal allanites are essentially indistinguishable based on chemistry alone, the trend of increasing REE and Ti from magmatic to hydrothermal allanites can be used to separate these two broad categories. The high REE and Ti content typical of the majority of the Hoidas Lake allanites are similar to the hydrothermal allanite of Jiang et al (2003) (Fig 7.5). The relation of Ca and Mg in the Hoidas Lake allanites is somewhat more ambiguous. The hydrothermal allanites of Jiang et al. (2003) have a CaO content of around 10 wt.% and an MgO content of less than 0.5 wt.% and, although the CaO content of the Hoidas lake allanites is similar, the MgO content in the Hoidas Lake allanites can be as high as 2.5%, again suggesting an intermediate origin between the purely magmatic or hydrothermal endmembers.

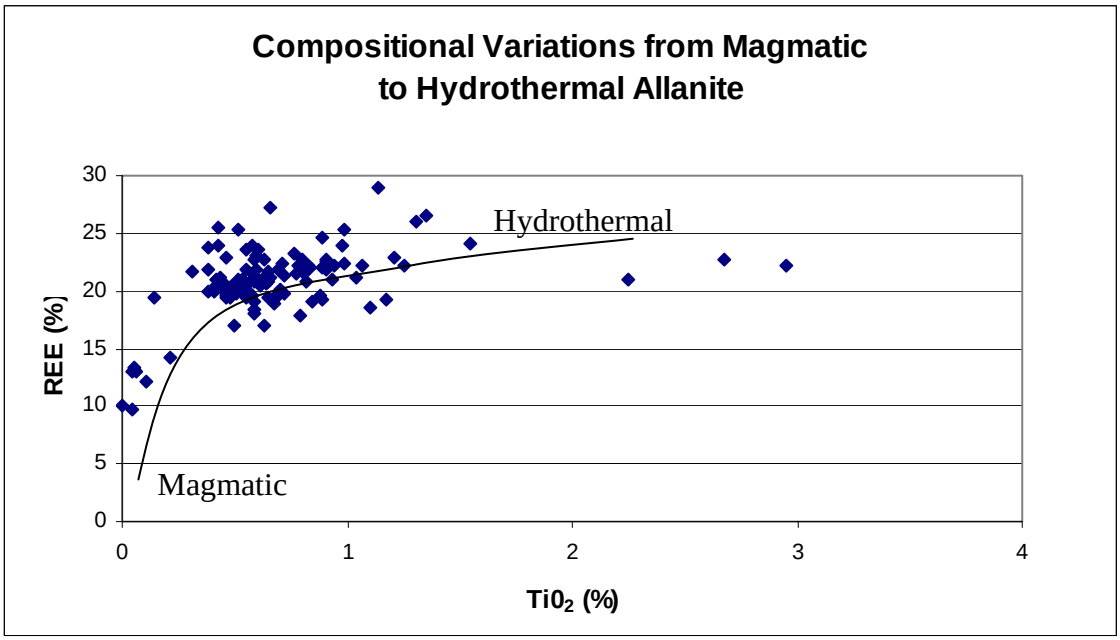

Figure 7.5 Variation in REE and Ti content of the Hoidas Lake apatites. Line shows the trend from magmatic to hydrothermal allanites defined by Jiang et al., (2003).

The low analytical totals associated with many of the Hoidas Lake allanites can be associated with hydrothermal alteration. Although in many cases the low totals appear to be related to metamict portions of the crystal there are other analyses where the low total do not seem to be the result of metamictization; in these cases the low totals may be the result of incorporation of water into the structure, which can be the result of exposure to hydrothermal fluids (Poitrasson, 2002)

The textural features of the Hoidas Lake allanites also imply a largely hydrothermal origin. Magmatic allanite is typically euhedral and any zonation, if present, typically displays clean, straight boundaries as opposed to the subhedral to anhedral hydrothermal allanites which often display irregular to mottled zonation (Poitrasson, 2002; Jiang, 2006). Also, primary magmatic allanites do not typically form as overgrowths of other minerals, such as observed on the chevkinite at Hoidas Lake (Jiang, 2006). The zonation in the hydrothermal allanites is a combination of growth zonation, alteration, and replacement textures.

As the allanite is a relatively early mineral in the paragenesis, it does display some evidence of alteration, with many of the alteration products considered as indicative of ongoing hydrothermal alteration. The fluid involved largely controls which

of the variety of possible alteration products forms; REE-fluorocarbonates are the most commonly encountered REE-bearing alteration type. Epidote is another common alteration product, although in this case the REE have largely been removed (Wood and Ricketts, 2000). The presence of bastnaesite alteration in many of the Hoidas Lake allanites supports the theory of continued interaction with hydrothermal fluid, as does the epidote-rich rims observed on many of the crystals (Smith et al, 2002; Stone, 1994; Exley, 1980).

7.4.5 TITANITE

Like many of the other minerals in the earliest vein generation the formation of the titanite is subject to debate. There are a small number of euhedral titanites which are found with diopside and can, in rare instances, be surrounded by allanite. The titanite in this case, like the chevkinite, could potentially be of magmatic origin as there is no firm evidence to suggest otherwise. Although a magmatic origin is possible, a single hydrothermal generation is more plausible. Both the homogenous appearance of individual crystals and the lack of compositional variation between crystals of different textural associations suggest a hydrothermal origin. The homogeneous composition of the Hoidas Lake titanite is unusual as there is often some irregular zonation caused by the secondary leaching of REE or secondary overgrowths (Bakker et al., 2006). Even in situations where the titanite is rimmed by the allanite there is no evidence of alteration, suggesting that the titanite was in equilibrium with the fluid phase.

More commonly encountered than the euhedral titanites are subhedral titanites which are closely related to the allanite, although no consistent relationship exists. The association of titanite with the hydrothermal allanite, particularly as a mantle surrounding the chevkinite, indicates that the majority of the REE-bearing titanite at Hoidas Lake is a hydrothermal mineral. Although Ti is typically assumed to be an immobile element there are a number of examples of titanite from hydrothermal settings (Giere, 1996 and references therein). Hydrothermal allanite and titanite are commonly associated due to the fact that Ti and REE are transported by fluids with similar compositions (Jiang et al., 2003).

7.4.6 APATITE

The origin of the earliest generations of apatite are somewhat uncertain, as they occur in association with minerals for which a large degree of uncertainty exist and the apatite itself contains no definitive features which would confirm either igneous or hydrothermal formation. One feature in the apatites which suggests that the apatite may be magmatic is the F content. Typically, primary magmatic apatite has a composition close to the stoichiometry of fluorapatite, with a F content of between 1.3 to 2.3 wt. %, and the F content of the apatite increasing with increasing differentiation. Fluorapatite is also the dominantly encountered apatite in samples related to carbonatites (Buhn et al., 2001; Liferovich and Mitchell, 2006). In less fractionated igneous rocks there is typically between 0.5 and 2 wt. % Cl (Belousova et al., 2002). The high F content of the apatite from Hoidas Lake, combined with the very low Cl values, is the only chemical feature present which indicates that the apatite could be related to a highly differentiated igneous rock. Due to the strong evidence discussed earlier that the mineralization is not related to a granitic source, a relation to a carbonatitic source may be a reasonable option if the apatite is magmatic.

An alternative explanation for the high F content present in the Hoidas Lake apatites is that they are derived from a F-rich hydrothermal fluid, as the halogen content of hydrothermal apatites is strongly dependent upon the prevailing fluid composition. At hydrothermal conditions both hydroxylapatite and chlorapatite are readily converted to fluorapatite when exposed to F-rich fluids, suggesting that even if the initial apatite composition contained slightly more Cl, a change in the composition of the fluid could potentially alter the composition of the apatite. Under similar conditions chlorapatite is much more reactive than hydroxylapatite, and therefore hydroxylapatite is more likely to be preserved after a change in fluid composition (Rendon-Angeles et al., 2000).

The theory of a hydrothermal origin of the apatite is also supported by the increase in REE content in the paragenetically late green apatites. The increased enrichment of REE in late apatites may be the result of the destruction of earlier formed, more moderately REE-enriched apatites during subsequent hydrothermal alteration or due to an increase in the REE budget of the fluid (Gleason et al., 2000). A similar

increase in REE content in paragenetically late apatites is also observed for apatite in carbonatites and related rocks.

As the structure of apatite has a high tolerance for substitutions it can serve as a sink for a number of incompatible and volatile elements in late-magmatic, pegmatitic, and postmagmatic mineral parageneses (Stoppa and Liu, 1995; Liferovich and Mitchell, 2006). This often results in the enrichment of not only REE, but also elements such as Ba or Sr (Chakhmouradian et al., 2002). At Bayan Obo, which also contains multiple generations of hydrothermal apatite, the increase in Sr content in the paragenetically late apatites is believed to be the result of the continued fractionation of the carbonatitic source (Campbell and Henderson, 1997). Similar evolutions toward Sr-rich compositions are also observed in apatites associated with peralkaline complexes, with the composition of the apatites largely a function of the fluid composition (Liferovich and Mitchell, 2006). This type of enrichment in Sr content is observed in the Hoidas Lake apatites generations, with the highest Sr content found in the REE-rich green apatites.

Texturally, there are also indications of extensive interactions with hydrothermal fluids, particularly in the earliest generations. An unusual feature in the apatite veins is that the later generations of apatite are essentially inclusion free, while the earliest generations are riddled with inclusions, the most commonly encountered inclusion being monazite. The presence of monazite inclusions in apatite can be the result of exposure to hydrothermal fluids. As REE are primarily incorporated into the apatite by the coupled substitution of

$$SiO_4^{4-} + REE^{3+} \leftrightarrow Ca^{2+} + PO_4^{3-},$$

the removal of Si without decreasing the REE content allows the REE to react with the surrounding P to produce monazite. These inclusions typically have REE signatures similar to the host apatite, with minor fluctuations depending on other influencing variables such as fluid composition, temperature, or pressure (Harlov and Forster, 2003).

As the monazite inclusions are most prevalent in the older apatite generations it is possible that the repeated exposure of the apatite to hydrothermal fluids was the trigger for the formation of the monazite inclusions, and would explain their relative absence in the younger generations. This is further supported by the fact that in

experimental studies, such as those conducted by Harlov and Forster (2003), the formation of monazite inclusions is most common in apatites which have been metasomatized by dissolution-reprecipitation, as this typically increases the micro-porosity in these apatites, which facilitates the required fluid flow necessary for inclusion formation.

The leaching, or depletion of REE in the reacted regions also helps explain the mottled appearance present in the older apatite generations; the inclusions are typically located in, or adjacent to, regions which are slightly darker than the unaltered host crystal in the backscattered electron images (Fig. 7.6). The darker regions represent areas where Si, Na, Cl, Y, and REE have been depleted relative to the original fluorapatite composition, with the REE re-concentrating into the bright monazite inclusions (Harlov et al., 2005).

There are also rare primary monazites associated with the green apatite generation. In this case the composition of the monazite suggests formation from a hydrothermal fluid rich in REE. The ThO_2 content of monazite can be used to distinguish whether monazite is igneous or hydrothermal in origin as igneous monazites typically contain more than 3 wt.% ThO_2 while hydrothermal monazites generally contain less than 1 wt.% (Schandl and Gorton, 2004). The relatively low Th content of the monazite in this vein generation, combined with its homogeneous appearance in the backscattered images is indicative of hydrothermal formation.

Overall, it is only the origin of the earliest apatites which are uncertain. Although the composition of the apatites does not clearly indicate the origin the textural features suggests extensive interactions with hydrothermal fluids. The evolution in REE and Sr concentrations in the apatites also suggests that they may be part of a hydrothermal system, although similar trends can be observed in apatite with a carbonatitic affiliation. It seems reasonable that the youngest generations of apatite, the green apatite and the coarse red apatite, are related to hydrothermal activity, even if the earlier generations are not.

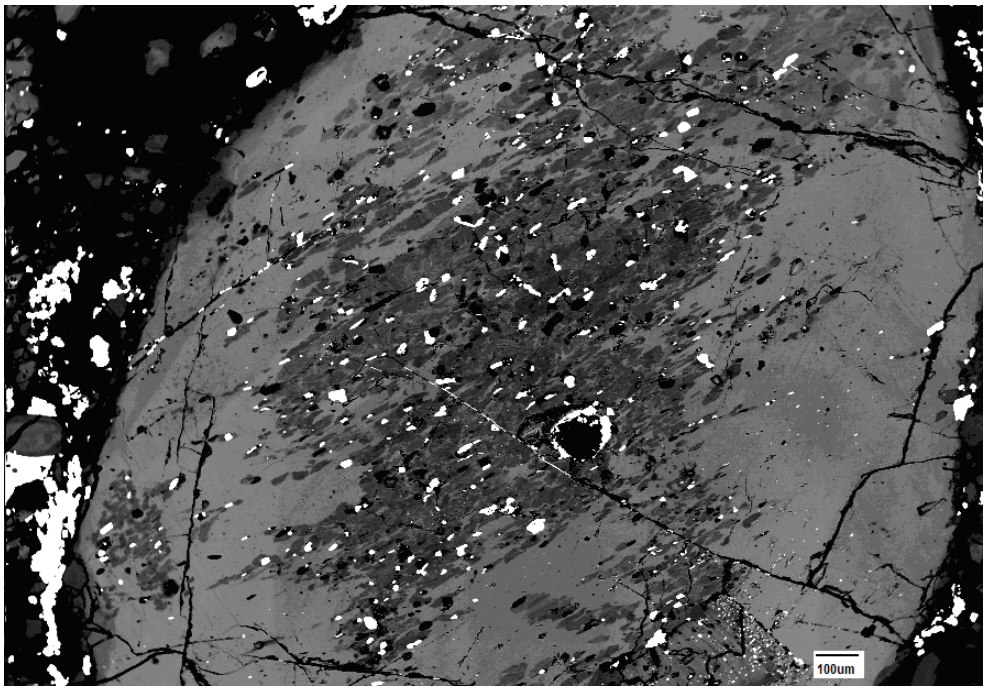

Figure 7.6 Monazite inclusions in apatite .Backscattered electron image shows a typical example of the monazite inclusion in an apatite clast from one of the red apatite breccia. The dark grey area surrounding the bright white monazite inclusions represents a leached area. Light grey areas are unaltered regions of the clast. Bright patches in the matrix are bastnaesite.

7.5 EVOLUTION OF THE MINERALIZING SYSTEM

REE deposits in general often display complex histories, and may feature multiple stages of mineralization. Late magmatic to hydrothermal deposits are often characterized by complex fluid histories, with multiple fluid migrations (Smith et al., 2000; Lira and Ripley, 1992), and Hoidas Lake appears to be no exception. The mineralization at Hoidas Lake seems to have evolved from an early late magmatic-hydrothermal phase through to REE-rich hydrothermal mineral precipitation to late REE-poor hydrothermal veins. In addition to the multiple, compositionally diverse vein generations, the extensive alteration present in the paragenetically early minerals suggests that the composition of the mineralizing system varied through time, with the early phase no longer in equilibrium with the later fluid. Although in some instances more detailed work will be required to fully delineate these trends some general features are discussed below.

7.5.1 COMPOSITIONAL VARIATIONS IN THE MINERALIZING SYSTEM

The changes in mineral composition, as well as the types of alteration present, allow for a very general examination of changes in the mineralizing system at various points during the development of the veins. One of the most obvious large scale trends is the presence of dominantly silicate minerals in the earliest mineralized vein generation with the later mineralized veins composed mainly of phosphates and carbonates with relatively minor amounts of silicates. There are also more minor variations in the chemical composition of the vein generations and of some individual minerals species.

Although the exact origin of the early diopside-allanite veins is somewhat contentious, there are still some general chemical features which can be discussed. Even if the veins are the result of metasomatism of a pre-existing igneous dike the mineralizing system would still have to contain abundant REE, Ba, and Ca, as well as Ti to result in the observed mineral compositions. The REE-bearing allanite and titanite in particular would require significant concentrations of Ca, REE and Ti. As the available evidence suggests that these are both hydrothermal minerals, the early fluid was likely enriched in these elements. The formation of the diopside and hyalophane would also require the presence of abundant Ca and Ba, respectively (Python et al., 2007). The uncertainty in this vein generation is whether the necessary elements were provided from an external source by the fluid phase or locally from the breakdown of other minerals. In some cases the observed mineralogy is at least partly derived from earlier minerals, as shown by the presence of allanite and titanite mantles on the chevkinite. In this example the REE are likely derived from the chevkinite, although many of the other elements essential for the formation of the allanite are from an external source (Jiang, 2006).

The major change in composition between the diopside-allanite veins and the subsequent apatite vein generations is the switch from dominantly silicate minerals to dominantly phosphate minerals with minor amounts of carbonates and rare silicates. The Ba and Ti are minor elements in the apatite vein generation, although there are still significant amounts of Ca and REE. Sr is also present in many of the apatite vein generations, although the concentration of Sr present varies between generations. In the various generations of the red apatite breccia and in the coarse red apatite the Sr content

is fairly constant while the green apatite breccia displays significantly higher Sr concentrations. The presence of high amounts of Sr in the green apatite generation, which also contains the highest concentrations of REE, suggests that fluid composition likely controls the mineral composition rather than any sort of crystal-chemical control, despite the fact that both Sr and REE preferentially occupy the Ca(2) site in apatite.

The REE content of the apatites also varies between the vein generations. The early apatites contain a moderate level of REE and are consistently Ce dominant, with the REE content increasing to maximum levels observed in the green apatite. The largest change in REE concentration and content is between the green apatite and the coarse red apatite. The REE concentration drops from the average of 5.5 % TREO in the green apatite to less than 1.5 % TREO in the coarse red apatite. The coarse red apatite is also the only apatite to be Nd-dominant rather Ce-dominant and contain a higher concentration of MREE than the earlier apatites.

Evolution of the fluid composition is also indicated by the alteration of the minerals present in the earlier vein generations. The alteration of these minerals suggests that they were no longer in equilibrium with the later fluid. The type of alteration present can provide some insight into the compositional changes responsible for the alteration. The two main varieties of alteration present in the allanite are an earlier epidote alteration and a later alteration to bastnaesite. The epidote rims present on the majority of the allanite crystals suggest either a reduction of the available REE or a change in the fO_2 of the system or a combination of these factors, as will be discussed below in section 7.5.2. Alteration of the allanite by later hydrothermal fluids may leach REE and Th, although the presence of phosphate in the fluid would limit transport distances as it would facilitate the precipitation of stable phosphate minerals, such as either monazite or REE-rich apatite, as is observed at Hoidas Lake (Smith et al., 2002). The formation of the monazite inclusions in the apatite provides some information about the composition of the fluid; in order for the inclusions to form the fluid cannot contain NaCl or $CaCl_2$ as the presence of Na^+ or Ca^{2+} would be expected to help maintain the apatite structure and charge balance (Harlov et al., 2005). The later alteration of the allanite to bastnaesite, rather than monazite which is another common alteration product, suggests that during the later period of alteration the fluid did not contain significant

amounts of phosphate as this would favor the formation of monazite (Woods and Ricketts, 2000).

7.5.2 CHANGE IN REDOX CONDITIONS

The composition of the early minerals, and their subsequent alteration, suggests that the responsible fluids were relatively reducing in nature and that the fluid evolved towards more oxidizing conditions with time. The presence of epidote rims on the majority of the allanite crystals may be related to changes to the fO_2 of the system. The relative stabilities of allanite and epidote are largely a function fO_2, as well as the presence or absence of REE, temperature and pressure (Smith et al., 2002). Although more information is needed to confirm relatively constant temperatures and pressures throughout the formation of the allanite-epidote crystals, as the system becomes more oxidizing epidote will form rather than allanite.

It is possible that the formation of epidote is partially a function of a reduction in the REE budget of the fluid. This theory, however, does not explain the change from magnetite to hematite as the dominant iron oxide in later vein generations or presence of hematite rims on the early magnetite found in the veins. Magnetite typically forms under low fO_2 conditions, with alteration to hematite occurring with increasing fO_2. The alteration of magnetite to hematite due to oxidation clearly shows that the early magnetite was no longer in equilibrium with the later fluids (Ramasamy et al., 2001). The initial formation of Ba feldspars, as opposed to barite, also suggests that the early fluids were relatively reducing, as in relatively oxidizing environments barite would be expected to form preferentially (Oberger et al., 2005). The presence of barite at the margins of the majority of the hyalophane crystals, and as late remobilized vein fill, is indicative of the progression to a more oxidizing environment with time (Moro et al., 2001).

7.5.3 TRANSPORTATION OF THE REE

The REE tend to exist as complexes in all but the most acidic or very dilute solutions and at the lowest temperatures. As the pH, as well as temperature and pressure, increase the proportion of REE^{3+} in solution decline sharply and therefore the tendency for REE to form aqueous complexes increases with rising temperature, pressure, and

pH. For this reason REE complexes are important as, at the conditions found in most geological environments, they are likely the predominant species and the formation of these complexes is essential for the transportation of REE (Haas et al, 1995). The strongest complexes are formed with ligands such as F^-, SO_4^{2-}, CO_3^{2-}, PO_4^{3-}, and OH^-. The REE may also complex with Cl^-, although this complex is somewhat weaker than those formed with the other ligands (Samson and Wood, 2005). Based on the composition of the minerals in the vein system at Hoidas Lake F^- and PO_4^{3-} are probably the most important complexing agents, although minor amounts of either OH^- or CO_3^{2-} may have also had an effect (Jiang et al., 2003). The fluid in these situations is often reducing, and relatively rich in HF and phosphorus (Giere and Williams, 1992). The presence of Th in many of the minerals in the vein system further supports the presence of F in the fluid as Th has been inferred to be relatively immobile in pure water or Cl-rich fluids (Woods and Ricketts, 2000).

7.5.4 TEMPERATURE OF FORMATION

Although there is no direct data from the veins at Hoidas Lake, numerous studies from other similar occurrences show considerable consistency in the estimated temperature of formation. Fluid inclusion studies from other diopside-allanite occurrences indicate the formation of diopside from saline brines at approximately 600 to 700^{o}C, with the allanite and amphibole forming from similar brines at slightly lower temperatures, typically 500 to 600^{o}C (Bakker et al., 2006; Smith et al., 2002). Diopside of low temperature (defined as less than 500^{o}C) hydrothermal origin usually has a composition close to the diopside-hedenbergite join, as is found for some of the Hoidas Lake diopsides. This suggests that the formation of diopside continued at lower temperatures (Madge et al., 1995).

Other hydrothermal veins rich in titanite and apatite are believed to have formed from a relatively water-rich environment at temperatures of 500-600^{o}C (Giere and Williams, 1992). The initial dark red apatite likely formed at similar conditions to the titanite, allanite and diopside with which it is associated. The temperature of formation of the other apatite generations is less certain, as the commonly reported temperatures for apatite formation range from over 500^{o}C to below 100^{o}C (Rankin, 2005). The

presence of monazite inclusions in many of the earlier apatite generations suggests that the fluid present during the formation of these inclusions is likely above 300^{o}C. Experimentally, the formation of monazite inclusions in apatite has been confirmed to occur over a wide range of temperatures, with a low of about 300^{o}C. These same studies indicate a pressure of between 500 to 1,000 MPa during the formation of the monazite inclusions (Harlov et al., 2005).

7.6 KEY CHARACTERISTICS OF THE HOIDAS LAKE REE MINERALIZATION

There are several key characteristics which define the mineralization at Hoidas Lake and which may be essential to the formation of the REE-mineralized veins. The REE-mineralized veins at Hoidas Lake are clearly structurally controlled and appear to have formed in a late magmatic-hydrothermal setting. There is also some evidence of a potential mantle link to the mineralization. One of the remaining questions is the source of the fluid responsible for the mineralization; although further research is needed to define the exact composition and source of the fluid, some generalizations can be made based on the composition of the veins. All of these features will be discussed in more detail below.

7.6.1 LATE MAGMATIC-HYDROTHERMAL MINERALIZATION

Although it is a relatively new concept, in many REE-rich deposits hydrothermal fluids are essential to the genesis of the deposit, with the mineralization resulting from a late to post-magmatic, often polyphase hydrothermal event (Morteani, 1991; Gleason et al., 2000), and this seems to be the case for the Hoidas Lake mineralization (Morteani, 1991; Gleason et al., 2000). The majority of the REE-mineralized veins at Hoidas Lake appear be of late magmatic hydrothermal origin, although the origin of the minerals in the earliest vein generation is somewhat enigmatic. In particular it is the origin of the diopside, hyalophane and chevkinite that is somewhat ambiguous, with a magmatic, metasomatic or hydrothermal origin being possible for these minerals. There is, however, evidence to support a late magmatic hydrothermal origin for the allanite which is found in association with the other minerals, suggesting that all these minerals may also be late magmatic hydrothermal. The work by Python et al. (2007) suggests that

minerals such as pyroxenes and feldspars, which are largely assumed to be anhydrous and typically associated with magmatic formation, can crystallize from high temperature fluids. Even if these early minerals are magmatic, they have undoubtedly been affected by exposure to later hydrothermal fluids, as is clearly shown by the mantling of the chevkinite and the presence of monazite inclusion in older apatite generations.

7.6.2 IMPORTANCE OF STRUCTURES

The presence of structural features is important to the mineralization at Hoidas Lake. The REE-mineralized veins at Hoidas Lake are clearly structurally controlled and are associated with long lived, structural features in the area. The structures likely served as fluid conduits, facilitating fluid transport and serving to focus the REE mineralization. The continuing brittle deformation along these features may also be important, as it ensured that the fluid conduit remained open for subsequent pulses of mineralizing fluid. The mineralization was broadly synchronous with the movement on the fault, although it postdates the bulk of the ductile deformation and peak regional metamorphism. The multiple brecciation events indicate that these structures remained active during the period of formation of the veins. It seems likely that the movement along the Hoidas-Nisikkatch fault was associated with that of the Black Bay Fault which was active between 2.3 to 1.7 Ga with the brittle deformation occurring between 1.95 and 1.70 Ga (Bergeron, 2001). This is broadly synchronous with the estimated age of the mineralization (Gunning and Card, 2005). The last mineralized vein generation, which consists of the coarse red apatite, does display brecciation. The fragments tend to be still in place, which is typical of hydraulic brecciation (Jebrak, 1997).

7.6.3 POTENTIAL RELATION TO MANTLE-DERIVED MAGMATISM

The close spatial and temporal association between the mineralization at Hoidas Lake and some of the other geological features of the region suggest that there is potential for an association with mantle sourced materials. Many REE deposits are associated with mantle-derived magmatic activity, as demonstrated by the number of carbonatite-associated REE deposits (Rankin, 2005; Wall and Mariano, 1996). In particular there is evidence that the Miaoniuping REE deposit, Sichuan Province, China, formed from fluids associated with a mantle-derived carbonatite (Huang et al., 2006).

Although there are no known carbonatites in the Hoidas Lake area, there are several other features which are indicative of a potential mantle link or a possible relation to a carbonatitic source. Huang et al. (2006) list a number of characteristics typical of mineralization by mantle fluids and, although the data needed to confirm the presence of several of these features at Hoidas Lake is beyond the scope of this study, some of the initial features suggest that this may be an area deserving additional examination. One of the key features is the presence of mantle derived magmatic activity (Huang et al., 2006), which is fulfilled in the Hoidas Lake area by the presence of the lamprophyres, even if they are not directly related to the mineralization. Lamprophyres are often related to continental rifting and are believed to be primary, mantle derived magmas. There is also an interesting association between carbonatites and lamprophyres, with lamprophyres grading into carbonatites or found in association with many carbonatite complexes (Bulakh et al., 2004; Le Roex and Lanyon, 1998; Rock, 1986).

The minette dikes of the Christopher Island Formation, to which the Hoidas Lake lamprophyres may be related, appear to have originated from an enriched lithospheric-mantle source beneath the Rae Domain. Although the Dubawnt minettes were only emplaced at 1.83 Ga, the reservoir of enriched lithospheric mantle was available well before their emplacement; the presence of the Hoidas Lake lamprophyres may be more important than the absolute timing of emplacement, as they indicate the presence of an enriched mantle source (Cousens et al., 2001). This may be important to the formation of the Hoidas Lake deposit, as many other REE-rich deposits are believed to be associated with an enriched, metasomatized mantle source (Hou et al., 2006).

Another key feature noted by Huang et al. (2006) is the presence of deep structural features. The presence of these deep structural features seems to influence mantle-derived magmatic activity and the related mineralization, with the magmatic activity largely controlled by the presence of faults (Hou et al., 2006; Huang et al., 2006). Although the exact extent of the Black Bay Fault is unknown, it may represent a deep structural feature, particularly considering the presence of mantle derived magmatic rocks in the vicinity of the fault, such as the lamprophyres, and also the potential history of rifting in the region, as both the Murmac Bay Group and the Martin

Group have been inferred to be rift related (Hartlaub et al., 2004; Heaman et al., 2003). In any cases, the Black Bay fault is a major structure with a protracted deformational history, which is broadly contemporaneous with the period of mineralization, and therefore may be related to the mineralization, even if it is not a crustal scale feature.

Finally, some of the compositional features of the mineralization suggest a potential relation to a carbonatitic source. The composition of the veins, with the enrichment in LREE, Ba, and Sr, combined with a relative depletion in HFSE such as Nb, Ta, Zr, Hf and Ti, is typical of what is observed in many carbonatites or carbonatite-associated REE deposits (Fig. 7.7)(Chakhamouradian et al., 2008; Hou et al., 2006). This is reinforced by the chondrite normalized REE pattern observed for the Hoidas Lake REE-mineralized veins, which is very similar to that of many carbonatites, exhibiting a strong enrichment in LREE and no Eu or Ce anomaly (Belousova et al, 2002).

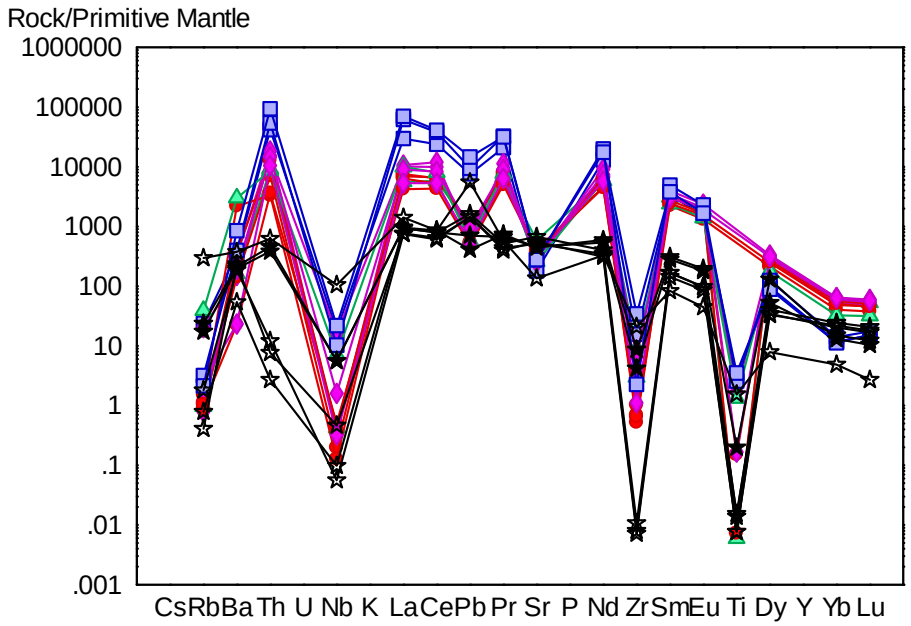

Figure 7.7 Trace element composition of the REE-bearing vein generations at Hoidas Lake normalized to that of the primitive mantle (Sun and McDonough, 1989). Diopside-allanite veins shown by squares, red apatite breccias by diamonds, green apatite breccias by triangles and the coarse red apatites by circles. Values from Eden Lake (filled stars) and Maoniuping (open stars) for comparison (Chakhamouradian et al., 2008; Hou et al., 2006)

7.7 ORIGINS OF THE HOIDAS LAKE MINERALIZATION

At Hoidas Lake the fluid responsible for the mineralization is likely derived from a magmatic source at depth (Fig. 7.8). Typically, there is a multistage devolatization which is responsible for REE liberation from magmas, with REE typically mobilized only during the later stages of fluid evolution, not in the initial fluid release (de Hoog and van Bergen, 2000). Vapor-liquid immiscibility during late stage crystallization in magmatic-hydrothermal systems may also serve to enrich the REE content of the fluids. As a vapor phase boils off the remaining fluid will be a highly saline brine, which is much more favorable for the complexation of REE. Aqueous fluids with high Cl and F contents are much more successful at fractionating the REE, in addition to lithophile elements such as Ba and Sr, from melts and therefore these fluids are significant to the transport and deposition of magmatically-derived REE deposits (de Hoog and van Bergen, 2000; Samson and Wood, 2005). The composition of the mineralized veins implies that the fluid was likely related to some sort of alkali or carbonatitic magmatic source, rich in Ca, PO_4, Sr, Ba, REE and F.

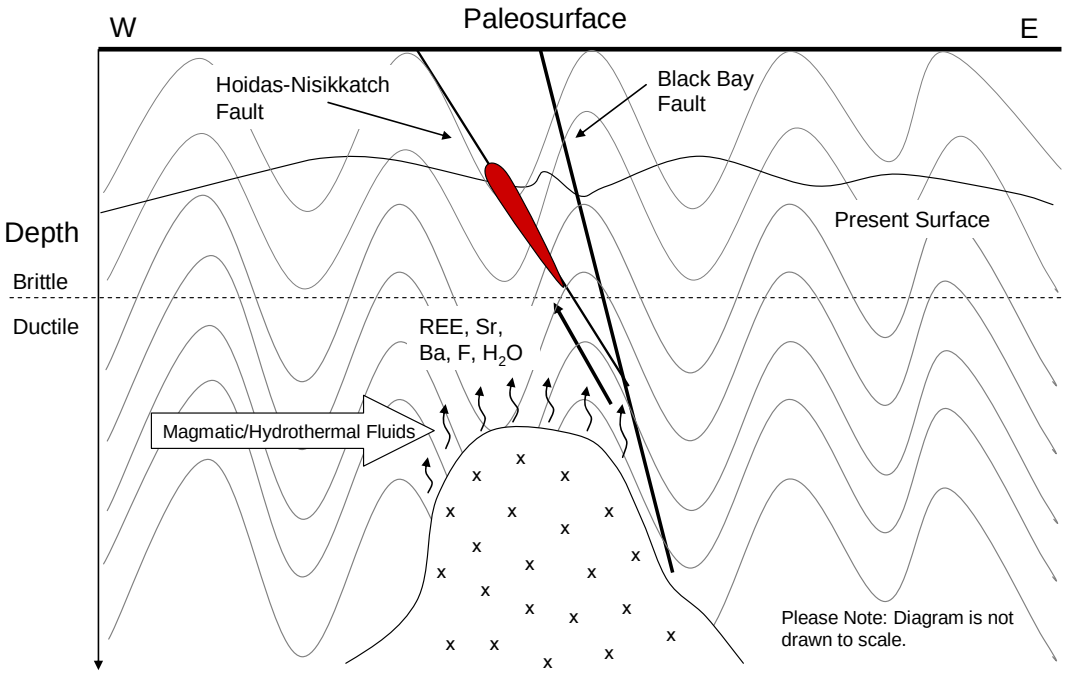

Figure 7.8 Schematic diagram showing the potential origin of the mineralization at Hoidas Lake.

The structures in the area likely served as fluid conduits, facilitating the transport of REE-rich fluids and exerting some influence on the deposition of the REE-rich minerals. All the known mineralized showings in the area are concentrated along lower order structures, such as the Hoidas-Nisikkatch fault and smaller, cross-cutting structures; to date no mineralized occurrences have been found along the Black Bay Fault. Although this may be a function of exploration history, rather than a true absence, there is evidence of preferential mineralization along secondary structures in other deposit types, such as orogenic gold deposits (e.g. Cox, 1999; Groves et al., 1998).

One major remaining question is what triggered the formation of the REE-bearing minerals. The degree of mobility of the REE in any aqueous environment is controlled by a number of factors including pH, ligand availability, temperature, and pressure. Other important factors are the fluid rock ratios, reaction kinetics, and various other crystal-chemical influences (Giere, 1996; Rolland et al., 2003). Unfortunately, detailed analysis of many of these factors is still somewhat lacking in the literature and the relative importance of each of these factors at Hoidas Lake is largely unknown.

Despite this some basic conclusions can be drawn. The lack of associated alteration indicates that fluid-rock interactions played only a minor role in the formation of the mineralized veins, while the structural setting of the veins suggest that changes in temperature or pressure could have influenced the formation of the veins. Also, the composition of the mineralizing fluid changed through time, although whether this is due to the evolution of the fluid, fluid mixing or a combination of these factors is uncertain.

7.8 RELATION TO OTHER REE SHOWINGS IN THE REGION

In addition to the REE showings at Hoidas Lake are a number of additional REE occurrence in Northern Saskatchewan, most of which were originally discovered as a result of intensive uranium exploration. The showing at Norwest Lake, although not well documented, is likely directly related to the Hoidas Lake showings. The description of the allanite-bearing veins at Norwest Lake is quite similar to what is observed at Hoidas Lake (Koster, 1965). The showing at Norwest Lake is approximately 6 km north

of the JAK Zone and is broadly along strike from the other showings on the Hoidas-Nisikkatch fault which, when combined with similar mineralogy, suggests that it may be part of the same mineralizing system. There are also a number of minor allanite showings and weak radioactive anomalies in the region around the Tazin River fault which, due to the limited data, are difficult to fully assess but may be similar to what is observed at Hoidas Lake (Koster, 1965).

Some of the other occurrences in the region are the Alces Lake and the Archie Lake REE showings, both of which seem distinctly different than the Hoidas Lake REE veins. The Alces Lake showing is reported to be a monazite-bearing pegmatite with minor amounts of allanite, apatite and zircon believed to have formed by anatectic processes. Similar pegmatites can be found at both Kulyk Lake and the Jahala prospect, although in these cases the pegmatites appear to be zoned. The Archie Lake REE showing consists of stratabound heavy mineral lenses hosted by a metasedimentary rock, suggesting a metadetrital origin (Harper, 1987).

To the southwest in the Zemlak Domain there are a number of shear host uranium veins (Beck, 1969). Any potential relation to the REE showings is difficult to evaluate due to the limited information available for most of these showings. Similar to the REE showings the uranium showings are typically structurally controlled and can be brecciated. The uranium veins are likely hydrothermal in origin, although the timing and source of the veins is poorly constrained.

There are also significant concentrations of REE associated with the uranium found in the Athabasca basin, although in these cases the occurrences are typically HREE dominant with xenotime, or possibly goyasite, hosting the REE. The REE-bearing minerals are believed to have formed from chloride-rich basinal brines as a result of fluid mixing with basement fluids along fault zones. The source of the REE in the fluids is either from interactions with heavy detrital minerals in the sandstone or possibly from garnets in the basement rocks (Quirt et al.,1991). The association of these REE enrichments with many of the unconformity deposits in the Athabsca basin has led to the theory that “unconformity-type” diagenetic-hydrothermal REE deposits may exist (Harper, 1987).

CHAPTER 8
SUMMARY

8.1 CONCLUSIONS

The REE deposit at Hoidas Lake consists of several generations of mineralogically and compositionally distinct REE-bearing veins hosted by Archean to Paleoproterozoic granitoids. There appears to be little relation between the granitoid host rocks and the mineralization; the lack of alteration associated with the veins suggest limited fluid-rock interaction and the composition of the granitoid host rocks is inconsistent with the expected igneous source composition, based on the chemistry of the veins. The strong LREE enrichment, as well as Ba and Sr, and reduce HFSE suggests the relation to either an alkali or carbonatitic source. Although there are no known carbonatites in the area there are lamprophyres and an unusual hyalophane-bearing peralkaline pegmatite. The exact relationship of the lamprophyres and pegmatites to the mineralization remains uncertain, although their presence indicates an unusual geological environment in the region which is broadly contemporaneous with the formation of the deposit.

The earliest vein generation is mineralogically the most complex, consisting of varying amounts of diopside, allanite, titanite, hornblende and hyalophane with minor amounts of apatite and chevkinite. The following vein generations are dominated by apatite, although the composition of the apatite in each generation is distinct. The earliest vein generations are extensively altered while the younger vein generations display little to no evidence of alteration. Both the allanite and the early apatites are internally complex, with alteration and zonation common.

The veins appear to be magmatic-hydrothermal in origin, as opposed to magmatic or metamorphic as proposed by previous investigations, with the structures acting as fluid conduits. The veins are clearly structurally controlled and the multiple breccia generations suggest that the Hoidas-Nisikkatch fault remained active throughout the development of the deposit, which helped ensure the continuing fluid flow necessary for mineralization.

8.2 RECOMMENDATIONS FOR FURTHER RESEARCH

Although the existing research provides a basic framework for the understanding of the mineralization, with particular focus on the identification of the REE-bearing phases and their distribution in the vein system, there are still a large number of questions which remain unanswered. Although many of these questions are essential for a full understanding of the mineralization at Hoidas Lake, they are beyond the scope of the current project.

8.2.1 REGIONAL GEOLOGICAL MAPPING

Of particular interest would be a more comprehensive regional mapping program, as the regional understanding in the area is lacking. Geological mapping in the area is limited to what has been completed by Great Western Minerals and brief visits by the Saskatchewan Geological Survey (Normand et al., 2009;Gunning and Card, 2005; Harvey et al., 2002; Koster, 1965). The limited mapping in the area is largely restricted to the region immediately surrounding both Hoidas and Nisikkatch Lakes, with the bulk of the mapping effort focused on the area surrounding known showings. A more comprehensive geological mapping program would enhance the general knowledge of the region and may reveal previously unrecognized rock types and relationships. Overall, additional regional mapping would help fill in some of the gaps in the regional framework for this area of the Rae Province, as much of the information about this area is inferred from the more comprehensively mapped areas to the north and south (e.g. Ashton and Card, 1998; Ashton et al., 2005; Ashton et al., 2006; Ashton et al., 2007; Bethune et al., 2006; Ashton and Hunter, 2003; Rainbird and Davis, 2007, Rainbird et al., 2003; Peterson et al., 2002) , and would enhance the general knowledge of the Ena Domain (Ashton and Card, 1998).

8.2.2 GEOCHRONOLOGY

Although Gunning and Card (2005) reported an age of mineralization of approximately 1.87 Ga, based on unpublished U-Pb monazite data, further geochronology would be useful to help resolve the relationship between the late pegmatites, lamprophyres and the REE-mineralized veins at Hoidas Lake. Although the date provided gives the approximate age of the mineralization it is unclear whether the

monazite is one of the rare primary monazites or if it was part of the more widespread alteration assemblage. Dating monazite of a known position in the paragenetic sequence using either U-Pb geochronology or CHIME dating would help to resolve the age of the mineralization and potentially the timing of the alteration. An attempt to determine the age of the allanite would also be interesting, as this seems to be one of the earliest major REE-bearing phases and therefore denotes the initial stage of mineralization. Although there are some issues with allanite geochronology, particularly the presence of common Pb, the potential for loss of elements with metamictization, and the internal complexity of the mineral, there has been some success with Th-Pb geochronology (Cox et al., 2003; Catlos et al., 2000; Barth et al., 1994).

In addition to determining the age of the mineralization it would also be useful to determine the age of the late igneous phases in the area, particularly the lamprophyres and some of the more unusual pegmatites in the region. Geochronology on the Hoidas Lake lamprophyres would help to determine if they are synchronous with the Dubawnt lamprophyres, as suggested by Gunning and Card. Determining the timing of both the lamprophyres and the pegmatites would help determine not only their position in the paragenetic sequence for the area but would also address what, if any, relation they may have to the mineralizing system. Once the age of the mineralization is accurately known it may also be possible to relate the mineralization to larger scale geological processes occurring at that time.

8.2.3 FLUID COMPOSITION

Fluid inclusion data would help to eliminate many of the remaining questions, such as the composition of the mineralizing fluid, the temperature and pressure at which the mineralization formed, and may help track the evolution of the fluid through time. Unfortunately, any attempts to collect fluid inclusion data may be hindered by a number of factors. One key issue is the condition of the crystals; due to the high amount of radioactive elements in the veins many of the minerals show some degree of metamictization and intense fracturing of the surrounding minerals. Also, the presence of suitable minerals is somewhat limited as many of the minerals in the veins are fairly intensely colored, which could hinder observations. Of the major minerals in the

mineralized vein generations either the hyalophane or apatite may provide the best chance at finding usable fluid inclusions. Apatite in particular seems to be a popular choice for fluid inclusion studies in REE deposits (Rankin, 2005 and references therein; Vapnik et al., 2007; Smith and Henderson, 2000). Other studies from similar systems have also had some success with the titanite and diopside in the early portions of the veins (Bakker and Elburg, 2006).

The source, temperature and evolution of the mineralizing fluids could also be tracked using a combination of stable and radiogenic isotopic data (e.g. Sr, Nd, O, C) from appropriate minerals, such as allanite, apatite, monazite and calcite. However, this must be accompanied by a similar study of regional rocks so that potential source rocks, or rocks with which the fluid may have interacted with, can be identified.

REFERENCES

Ansdell, K.M., (2005): Tectonic evolution of the Manitoba-Saskatchewan segment of the Paleoproterozoic Trans-Hudson Orogen, Canada. Canadian Journal of Earth Sciences, v. 42, p. 741-759.

Aspler, L.B., Chiarenzelli, J.R., McNicoll, V.J., (2002): Paleoproterozoic basement-cover infolding and thick-skinned thrusting in Hearne domain, Nunavut, Canada: intracratonic response to Trans-Hudson orogen. Precambrian Research, v. 116, p. 331–354.

Ashton, K.E., Card, C.E., (1998): Rae Northeast; A Reconnaissance of the Rae Province Northeast of Lake Athabasca; in Summary of Investigations 1998, vol. 2, Saskatchewan Geological Survey, Sask. Energy and Mines, Misc. Rep. 98-4.

Ashton, K.E., Boivin, D., Heggie, G., (2001): Geology of the southern Black Bay Belt, west of Uranium City, Rae Province; in Summary of Investigations 2001, v. 2, Saskatchewan Geological Survey, Misc. Rep. 2001-4.2

Ashton, K.E., Hunter, R.C., (2003): Geology of the LeBlanc-Wellington lakes area, eastern Zemlak Domain, Rae Province; in Summary of Investigations 2003, v. 2, Saskatchewan Geological Survey, Sask. Industry and Resources, Misc. Rep. 2003-4.2.

Ashton, K.E., Card, C.D., Modeland, S., (2005): Geological Reconnaissance of the Northern Tazin Lake Map Area (NTS 74N), Including Parts of the Ena, Nolan, Zemlak and Taltson Domains, Rae Province, in Summary of Investigations 2005, v. 2, Saskatchewan Geological Survey, Sask. Industry and Resources, Misc. Rep. 2005-4.2.

Ashton, K.E., Knox, B., Bethune, K.M., Marcotte, J., (2006): Bedrock geology along the northern margin of the Athabasca Basin west of Fond-du-Lac (NTS 74O-5 and -6), south-central Beaverlodge Domain, Rae Province, Fond-du-Lac Project, in Summary of Investigations 2006, v. 2, Saskatchewan Geological Survey, Saskatchewan Industry and Resources, Misc. Rep. 2006-4.2.

Ashton, K.E., Card, C.D., Davis, W., Heaman, L.M., (2007): New U-Pb Zircon Age Dates from the Tazin Lake Map Area (NTS 74N), in Summary of Investigations 2007, v. 2, Saskatchewan Geological Survey, Saskatchewan Ministry of Energy and Resources, Misc. Rep. 2007-4.2.

Bakker, R.J., Elburg, M.A., (2006): A magmatic-hydrothermal transition in Arkaroola (northern Flinders Ranges, South Australia): from diopside-titanite pegmatites to hematite-quartz growth. Contributions to Mineralogy and Petrology, v. 152, 541-569.

Balaganskaya, E.G., Downes, H., Demaiffe, D., (2007): REE and Sr-Nd isotope compositions of clinopyroxenites, phoscorites and carbonatites of the Seblyavr Massif, Kola Peninsula, Russia. Mineralogia Polonica, v. 38, 29-44.

Baldwin, J.A., Bowring, S.A., Williams, M.L., (2003): Petrological and Gechronological constraints on high pressure high temperature metamorphism in the Snowbird tectonic zone, Canada. Journal of Metamorphic Geology, v. 21, p. 81 – 98.

Banks, D.A., Yardley, B.W.D., Campbell, A.R., Jarvis, K.E., (1994): REE composition of an aqueous magmatic fluid: a fluid inclusion study from the Capitan Pluton, New Mexico. Chemical Geology, v. 113, 259-272.

Barth, S., Oberli, F., Meier, M., (1994): Th-Pb versus U-Pb isotope systematics in allanite from co-genetic rhyolite and granodiorite: implication for geochronology. Earth and Planetary Science Letters, v. 124, 149-159.

Barton, P.B., (1993): Problems and opportunities for mineral deposits, in Kirkham, R.V., Sinclair, W.D., Thorpe, R.I., and Duke, J.M., eds., Mineral Deposit Modeling: Geological Association of Canada Special Paper 40, 7-13.

Beck, L.S., (1969): Uranium Deposits of the Athabasca Region. Saskatchewan Mineral Resources Report No. 126.

Belolipetskii, A.P., Voloshin, A.V., (1996): Yttrium and rare earth element minerals of the Kola Peninsula, Russia, in Jones, A.P., Wall, F., Williams, C.T., eds., Rare Earth Minerals; Chemistry, Origin and Ore deposits, Mineralogical Society Series, v. 7, 311-326.

Belousova, E.A., Griffin, W.L., O'Reilly, S.Y., Fisher, N.I., (2002): Apatite as an indicator mineral for mineral exploration: trace-element compositions and their relationship to host rock type. Journal of Geochemical Exploration, v. 76, 45-69.

Berger, A., Gnos, E., Janots, E., Fernandez, A., Giese, J., (2008): Formation and composition of rhabdophane, bastnasite and hydrated thorium minerals during alteration: Implications for geochronology and low temperature processes. Chemical Geology, v. 254, 238-248.

Bergeron, J., (2001): The Deformational History of the Black Bay Structure Near Uranium City, Northern Saskatchewan. Unpublished M.Sc. Thesis, University of Saskatchewan.

Berman, R.G., Sanborn-Barrie, M., Stern, R.A., Carson, C.J., (2005): Tectonometamorphism at ca. 2.35 and 1.85 Ga in the Rae Domain, Western Churchill Province, Nunavut, Canada: Insights from Structural, Metamorphic and In-Situ Geochronological Analysis of the Southwestern Committee Bay Belt, The Canadian Mineralogist, v. 43, p. 409-442.

Berman, R.G., Davis, W.J., Pehrsson, S.,(2007): Collisional Snowbird tectonic zone resurrected: Growth of Laurentia during the 1.9 Ga accretionary phase of the Hudsonian orogeny. Geology, v. 35, p. 911-914.

Bethune, K.M., Scammell, R.J., (2003): Geology, geochronology, and geochemistry of Archean rocks in the Eqe Bay area, north-central Baffin Island, Canada: constraints on the depositional and tectonic history of the Mary River Group of northeastern Rae Province. Canadian Journal of Earth Sciences, v. 40, p. 1137-1167.

Bethune, K.M., Hunter, R.C., Ashton, K.E., (2006): Age and Provenance of the Paleoproterozoic Thluicho Lake Group Based on Detrital Zircon SHRIMP Geochronology: A Record of Tectonic Activity in the Southwest Rae Province, Saskatchewan, in Summary of Investigations 2006, vol. 2 Saskatchewan Geological Survey, Sask. Industry Resources, Misc. Rep. 2006-4.2.

Buhn, B., Wall, F., Le Bas, M.J., (2001): Rare-earth element systematics of carbonatitic fluorapatites, and their significance for carbonatite magma evolution. Contributions to Mineralogy and Petrology, v. 141, 572-591.

Bulakh, A.G., Ivanikov, V.V., Orlova, M.P., (2004): Overview of carbonatite-phoscorite complexes of the Kola Alkaline Province in the context of a Scandinavian North Atlantic Alkaline Province; in Wall, F., Zaitsev, A.N., eds., Phoscorites and Carbonatites from Mantle to Mine. Mineralogical Society Series, v. 10, 1-36.

Campbell, L.S., Henderson, P., (1997): Apatite paragenesis in the Bayan Obo REE-Nb-Fe ore deposit, Inner Mongolia, China. Lithos, v. 42, p.89-103.

Card, C., (2001): Basement Rocks to the Western Athabasca Basin in Saskatchewan; in Summary of Investigations 2001, vol. 2, Saskatchewan Geological Survey, Sask. Energy and Mines, Misc. Rep. 2001-4-2.

Castor, S.B., (2007): Rare Earth Deposits of North America. Resource Geology, v. 58, 337-347.

Catlos, E.J., Sorensen, S.S., Harrison, T.M., (2000) Th-Pb ion microprobe dating of allanite. American Mineralogist, v. 85, 633-648.

Chakhmouradian, A.R., Reguir, E.P., Mitchell, R.H., (2002): Strontium-Apatite: New occurrences, and the extent of Sr-for-Ca substitution in apatite group minerals. The Canadian Mineralogist, v. 40, 121-136.

Chakhmouradian, A.R., Mitchell, R.H., (2002): The mineralogy of Ba- and Zr- rich alkaline pegmatites from Gordon Butte, Crazy Mountains (Montana, USA):

comparisons between potassic and sodic agpaitic pegmatites. Contributions to Mineralogy and Petrology, v. 143, 93-114.

Chakhmouradian, A.R., Mumin, A.H., Demeny, A., Elliot, B., (2008): Postorogenic carbonatites at Eden Lake, Trans-Hudson Orogen (northern Manitoba, Canada): Geological setting, mineralogy and geochemistry. Lithos, v. 103, 503-526.

Chao E. C. T, Back J. M., Minkin J. A., Tatsumoto M., Wang Junwen, Conrad J. E., McKee E. H., Hou Zonglin, Meng Qingrun, and Huang Shengguang, (1997): The sedimentary carbonate-hosted giant Bayan Obo REE-Fe-Nb ore deposit of Inner Mongolia, China: A cornerstone example for giant polymetallic ore deposits of hydrothermal origin. *USGS Bulletin 2143*.

Cousens, B.L., Aspler, L.B., Chiarenzelli, J.R., Donaldson, J.A., Sandeman, H., Peterson, T.D., LeCheminant, A.N., (2001): Enriched Archean lithospheric mantle beneath western Churchill province tapped during Paleoproterozoic orogenesis. Geology, v. 29, p. 827-830.

Cox, R.A., Wilton, D.H.C, Kosler, J., (2003): Laser-ablation U-Th-Pb in situ dating of zircon and allanite: an example from the October harbour granite, central coastal Labrador, Canada. The Canadian Mineralogist, v. 41, 273-291.

Cox, S.F., (1999): Deformational controls on the dynamics of fluid flow in mesothermal gold systems. Geological Society, London, Special Publication, v. 155, 123-140.

Crocker, C.H., Collerson, K.D., Lewry, J.F., Bickford, M.E., (1993): Sm-Nd, U-Pb, and Rb-Sr geochronology and lithostructural relationships in the southwestern Rae province: constraints on crustal assembly in the western Canadian Shield. Precambrian Research, v. 61, p. 27 – 50.

Davis, W.J., Hanmer, S., Sandeman, H.A., (2005): Temporal evolution of the Neoarchean Central Hearne supracrustal belt: rapid generation of juvenile crust in a suprasubduction zone setting. Precambrian Research, v. 134, p. 85-112.

Deer, W.A., Howie, R.A., Zussman, J., (1992): *An Introduction to the Rock Forming Minerals.* Pearson Education Limited.

De Hoog, J.C.M., van Bergen, M.J., (2000): Volatile-induced transport of HFSE, REE, Th and U in arc magmas: evidence form zirconolite-bearing vesicles in potassic lavas of Lewotolo volcano, Indonesia. Contributions to Mineralogy and Petrology, v. 139, 485 – 502.

De Jong, G., Rotherham, J., Phillips, G.N., Williams, P.J., (1998): Mobility of rare-earth elements and copper during shear-zone related retrograde metamorphism. Geologie en Mijnbouw, v. 76, 311-319.

Elburg, M.A., Bons, P.D., Foden, J., Brugger, J., (2003): A newly defined Late Ordovician magmatic-thermal event in the Mt Painter Province, northern Flinders Range, South Australia. Australian Journal of Earth Sciences, v. 50, 611-631.

Essene, E.J., Claflin, C.L., Giorgetti, G., Mata, P.M., Peacor, D.R., Arkai, P., Rathmell, M.A., (2005): Two, three-, and four-feldspar assemblages with hyalophane and celsian: implications for phase equilibria in BaAl2Si2O8-CaAl2SiO8-NaAlSi3O8-KAlSi3O8. European Journal of Mineralogy, v. 17, 515-535.

Exley, R.A., (1980): Microprobe studies on REE rich accessory minerals; implications for Skye granite petrogenesis and REE mobility in hydrothermal systems. Earth and Planetary Science Letters, v. 48, 97-110.

Flowers, R.M., Bowring, S.A., Williams, M.L., (2006): Timescales and Significance of High Pressure, High Temperature Metamorphism and Mafic Dike Anatexis, Snowbird Tectonic Zone, Canada. Contributions to Mineralogy and Petrology, v. 151, p. 558 – 581.

Giere, R., Williams, C.T., (1992): REE-bearing minerals in a Ti-rich vein from the Adamello contact aureole, Italy. Contributions to Mineralogy and Petrology, v. 112, 83-100.

Giere, R., (1996): Formation of rare earth minerals in hydrothermal systems, in Jones, A.P., Wall, F., Williams, C.T., eds., Rare Earth Minerals; Chemistry, Origin and Ore deposits, Mineralogical Society Series, v. 7, 104-150.

Giere, R., Sorensen, S.S., (2004) Allanite and other REE-rich epidote group minerals. Reviews in Mineralogy and Geochemistry, v. 56, 431- 493.

Gleason, J.D., Marikos, M.A., Barton, M.D., Johnson, D.A., (2000): Neodymium isotopic study of rare earth element sources and mobility in hydrothermal Fe oxide (Fe-P-REE) systems. Geochimica et Cosmochimica Acta, v. 64, 1059-1068.

Good, D.J., Crocket, J.H., Barnett, R.L., (1997): A secondary clinopyroxene-chlorite-spinel assemblage in clinopyroxenite of the Mann Complex, Abitibi Belt, Ontario: an unusual hydrothermal alteration suite. Mineralogy and Petrology, v. 59, 69-90.

Grauch, R.I., (1989): Rare Earth Elements in Metamorphic Rocks: in Lipin, B.R., and McKay, G.A., eds., Geochemistry and Mineralogy of Rare Earth Elements, Reviews in Mineralogy, v. 21, 147-167.

Great Western Minerals Group Ltd., (2009): http://www.gwmg.ca/projects/hoidas-lake

Gregory, C.J., Rubatto, D., Herman, J., (2006): Exploring the potential of allanite as a geochronometer of high grade crustal processes. Geochemica et Cosmochemic Acta, v. 70, p. A216.

Grover, T.W., Pattison, D.R.M., McDonough, M.R., McNicoll, V., (1997): Tectonometamorphic Evolution of the Southern Taltson Magmatic Zone and Associated Shear Zones, Northeastern Alberta. The Canadian Mineralogist, v. 35, p. 1051-1067.

Groves, D.I., Goldfarb, R.J., Gebre-Mariam, M., Hagemann, S.G., Robert, F., (1998): Orogenic gold deposits: A proposed classification in the context of their crustal distribution and relationship to other gold deposit types. Ore Geology Reviews, v.13, 7-27.

Gunning, M.H., and Card, C.D., (2005): Transects across the Black Bay Shear Zone and Hoidas-Nisikkatch Rare-element Trend, northwest Saskatchewan; Sask. Industry Resources, Open File Rep. 2004-2.

Haas, J.R., Shock, E.L., Sassani, D.C., (1995): Rare earth elements in hydrothermal systems: estimates of standard partial molal thermodynamic properties of aqueous complex of the rare earth elements at high pressures and temperatures. Geochimica et Cosmochimica Acta, v. 59, 4329 – 4350.

Hanmer, S., Williams, M., Kopf, C., (1995): Striding-Athabasca mylonite zone: implications for the Archean and Early Proterozoic tectonics of the western Canadian Shield. Canadian Journal of Earth Sciences, v. 32, p. 178-196.

Harlov, D.E., Forster, H.J., (2003): Fluid-induced nucleation of (Y+REE)-phosphate minerals within apatite: Nature and experiment. Part II. Fluorapatite. American Mineralogist, v. 88, p. 1209-1229.

Harlov, D.E., Wirth, R., Forster, H.J., (2005): An experimental study of dissolution-reprecipitation in Fluorapatite: fluid infiltration and the formation of monazite. Contributions to Mineralogy and Petrology, v. 150, 268-286.

Harper, C.T., (1987): Rare earth elements and their occurrence in northern Saskatchewan; in Summary of Investigations 1987, Saskatchewan Geological Survey; Saskatchewan Energy and Mines, Miscellaneous Report 87-4.

Hartlaub, R.P., Heaman, L.M., Ashton, K.E., Chacko, T., (2004): The Archean Murmac Bay Group: evidence for a giant Archean rift in the Rae Province, Canada. Precambrain Research, v. 131, p. 345-372.

Hartlaub, R.P., Chacko, T., Heamana, L.M., Creaser, R.A., Ashton, K.E., Simonetti, A., (2005): Ancient (Meso- to Paleoarchean) crust in the Rae Province, Canada: Evidence from Sm–Nd and U–Pb constraints. Precambrian Research, v. 141, p. 137-153.

Hartlaub, R.P., Heaman, L.M., Chacko, T., Ashton, K.E.,(2007): Circa 2.3 Ga Magmatism of the Arrowsmith Orogeny, Uranium City Region, Western Churchill Craton, Canada. Journal of Geology, v. 115, p. 181-195.

Harvey, S.E., Young, I., and Billingsley, G. (2002): Geology of the Hoidas Lake Area, Ena Domain, northwestern Saskatchewan; in Summary of Investigations 2002, vol. 2, Saskatchewan Geological Survey, Sask. Industry and Resources, Misc. 2002-4.2.

Haxel, G.B., Hendrick, J.B., Orris, G.J., (2002): Rare Earth Elements – Critical Resources for High Technology. USGS Fact Sheet 087-02.

Heaman, L.M., Hartlaub, R.P., Ashton, K.E., Harper, C.T., Maxeiner, R.O., (2003): Preliminary Results of the 2002-2003 Saskatchewan Industry and Resources Geochronology Program, in Summary of Investigations 2003, vol. 2, Saskatchewan Geological Survey, Sask. Industry and Resources, Misc. Rep. 2003-4.2.

Heinrich, E.W., (1966): *The Geology of Carbonatites*, Rand McNally & Company.

Henderson, P., (1996): The rare earth elements: introduction and review; in Jones, A.P., Wall, F., Williams, C.T., eds., Rare Earth Minerals; Chemistry, Origin and Ore deposits, Mineralogical Society Series, v. 7, 1-17.

Hoffman, P.F., 1988, The United Plates of America, The Birth of a Craton: Early Proterozoic Growth and Assembly of Lauentia. Annual Review Earth and Plantary Science, v. 16, p. 543-603.

Hoffman, P.F., 1990, Subdivision of the Churchill Province and Extent of the Trans-Hudson Orogen, in Lewry and Stauffer, eds., The Early Proterozoic Trans-Hudson Orogen of North America: Geological Association of Canada, Special Paper 37, p. 15-39.

Hogarth, D.D., (1957): The Apatite Bearing Veins of Nissikatch Lake, Saskatchewan. Canadian Mineralogist, v. 6, p. 140-150.

Hussey, K.J., (2003): Rare earth element mineralisation in the eastern Arunta Region. Northern Territory Geological Survey, Record 2003-004.

Hou, Z., Tian, S., Yuan, Z., Xie, Y., Yin, S., Yi, L., Fei, H., Yang, Z., (2006): The Himalayan collision zone carbonatites in western Sichuan, SW China: Petrogenesis, mantle source and tectonic implication. Earth and Planetary Science Letters, v. 244, 234-250.

Huang, Z.L., Yan, Z.F., Xu, C., Zhang, Z.L. Liu, C.Q., (2006): Mineralization by mantle fluids in the Miaoniuping REE deposit, Sichuan Province, China. Journal of Geochemical Exploration, v. 89, 165-169.

Ito, J. (1967): A study of chevkinite and perrierite. The American Mineralogist, v. 52, 1094-1104.

Jackson, W.D., Christiansen, G., (1993): International strategic minerals summary report – rare-earth oxides. United States Geological Survey, circular 930-N.

Jahn, B., Fan, Q., Yang, J., Henin, O., (2003): Petrogenesis of the Maowu pyroxenite-eclogite body from the UHP metamorphic terrane of Dabieshan: chemical and isotopic constraints. Lithos, v. 70, 243-267.

Jebrak, M., (1997): Hydrothermal breccias in vein-type ore deposits: A review of mechanisms, morphology and size distribution. Ore Geology Reviews, v. 12, 111-134.

Jefferson, C.W., Thomas, D.J., Gandhi, S.S., Ramaekers, P., Delaney, G., Brisbin, D., Cutts, C., Quirt, D., Portella, P., Olson, R.A., (2007): Unconformity-Associated Uranium Deposits of the Athabasca Basin, Saskatchewan and Alberta, in Goodfellow, W.D., ed., Mineral Deposits of Canada: A Synthesis of Major Deposit Types, District Metallogeny, the Evolution of Geological Provinces, and Exploration Methods. Geological Association of Canada, Mineral Deposits Division, Special Publication no. 5, p. 273-305.

Jiang, N., (2006): Hydrothermal alteration of chevkinite-(Ce) in the Shuiquangou syenitic intrusion, northern China. Chemical Geology, v. 227, 100-112.

Jiang, N., Sun, S., Chu, X., Mizuta, T., Ishiyama, D., (2003): Mobilization and enrichement of high-field strength elements during late- and post-magmatic processes in the Shuiquangou syenitic complex, Northern China. Chemical Geology, v. 200, 117-128.

Kempton, P.D., Downes, H., Sharkov, E.V., Vetrin, V.R., Ionov, D.A., Carswell, D.A., Beard, A. (1995): Petrology and geochemistry of xenoliths from the Northern Baltic shield: evidence for partial melting and metasomatism in the lower crust beneath an Archean terrane. Lithos, v. 36, 157-184.

Koster, (1970): The Geology of the Burchnall Lake Area. Saskatchewan Department of Mineral Resources. Rep. 131.

Koster, (1965): The Geology of the Dardier Lake Area (West Half). Saskatchewan Department of Mineral Resources, Rep. 101.

Koster, (1965): The Geology of the Ena Lake Area (East Half): Saskatchewan Department of Mineral Resources, Rep. 92.

Krasnova, N.I., Petrov, T.G., Balaganskaya, E.G., Garcia, D., Moutte, J., Zaitsev, A.N., Wall, F., (2004): Introduction to phoscorites: occurrence, composition, nomenclature and petrogenesis; in Wall, F., Zaitsev, A.N., eds., Phoscorites and Carbonatites from Mantle to Mine. Mineralogical Society Series, v. 10, 45-69.

Kraus, J., Ashton, K.E., (2000): New insights into the structural geology and tectonic setting of the Uranium City area, northwestern Saskatchewan; in Summary of Investigations 2000, v. 2, Saskatchewan Geological Survey, Misc. Rep. 2000-4.2, p. 16-25.

Larsen, A.O., (1996): Rare earth minerals from the syenite pegmatites in the Oslo Region, Norway, in Jones, A.P., Wall, F., Williams, C.T., eds., Rare Earth Minerals; Chemistry, Origin and Ore deposits, Mineralogical Society Series, v. 7, 151-164.

LeMaitre, R.W., (1989): A Classification of Igneous Rocks and Glossary of Terms. Recommendations of the International Union of Geological Sciences Subcommission on the Systematics of Igneous Rocks. Blackwell Scientific Publications.

Lentz, D., (1991): Radioelement distribution in U, Th, Mo, and rare-earth-element pegmatites, skarns, and veins in a portion of the Grenville Province, Ontario and Quebec. Canadian Journal of Earth Science, v. 28, 1-12.

Le Roex, A., Lanyon, R. (1998): Isotope and Trace Element Geochemistry of Cretaceous Damaraland Lamprophyres and Carbonatites, Northwestern Namibia: Evidence for Plume-Lithosphere Interactions. Journal of Petrology, v. 39, 1117-1146.

Liferovich, R.P., Mitchell, R.H., (2006): Apatite-group minerals from nepheline syenite Pilansberg alkaline complex, South Africa. Mineralogical Magazine, v. 70, 463-484.

Lira, R., Ripley, E.M., (1992); Hydrothermal alteration and REE-Th mineralization at the Rodeo de Los Molles deposit, Las Chacras batholith, central Argentina. Contributions to Mineralogy and Petrology, v.110, 370-386.

Macdonald, R., (1987): Update on the Precambrian Geology and Domainal Classification of Northern Saskatchewan; in Summary of Investigations 1987, Saskatchewan Geological Survey; Saskatchewan Energy and Mines, Misc. Rep. 87-4.

MacLachlan, K., Davis, W.J., Relf, C., (2005): Paleoproterozoic reworking of an Archean thrust fault in the Hearne domain, Western Churchill Province: U-Pb

geochronological constraints. Canadian Journal of Earth Sciences, v. 42, p. 1313-1330.

Madge, L.S., Dick, H.J., Hart, S.R., (1995): Tectonics, alteration and the fractal distribution of hydrothermal veins in the lower ocean crust. Earth and Planetary Science Letters, v. 129, 103-119.

Mahan, K.H., Williams, M.L., Baldwin, J.A., (2003): Contractional uplift of deep crustal rocks along the Legs Lake shear zone, western Churchill Province, Canadian Shield. Canadian Journal of Earth Science, v. 40, p. 1085-1110.

Mahan, K.H., Williams, M.L., (2005): Reconstruction of a large deep-crustal terrane: Implications for the Snowbird tectonic zone and early growth of Laurentia. Geology, v. 33, p. 385-388.

Maniar, P.D., Piccoli, P.M., (1989): Tectonic Discrimination of Granitoids. Geological Society of America Bulletin, v. 101, 635-643.

Manning, C.E. Bird, D.K., (1986): Hydrothermal clinopyroxenes of the Skaergaard intrusion. Contributions to Mineralogy and Petrology, v. 92, 437-447.

Mariano, A.N., (1989): Economic geology of rare earth minerals; in Lipin, B.R., McKay, G.A., eds., Geochemistry and Mineralogy of Rare Earth Elements. Reviews in Mineralogy, v. 21, 308-337.

Mariano, A.N., (1989): Nature of economic mineralization in carbonatites and related rocks. In Bell, K.,(ed), Carbonatites: Genesis and Evolution, p. 149-176.

Martel, E., van Breemen, O., Berman, R., Pehrsson, S., (2008): Geochronology and tectonometamorphic history of the Snowbird Lake area, Northwest Territories, Canada: New insights into the architecture and significance of the Snowbird tectonic zone. Precambrian Research, v. 161, p. 201-230.

McNicoll, V.J., Theriault, R.J., McDonough, M.R., (2000): Taltson basement gneissic rocks: U-Pb and Nd isotopic constraints on the basement to the Paleoproterozoic Taltson magmatic zone, northeastern Alberta. Canadian Journal of Earth Sciences, v. 37, p. 1575-1596.

Meyer, M.T., Bickford, M.E., Lewry, J.F.,(1992): The Wathaman batholith: An Early Proterozoic continental arc in the Trans-Hudson orogenic belt, Canada. Geological Society of America Bulletin, v. 104, p. 1073-1085.

Mitchell, R.H., (2005): Carbonatites and carbonatites and carbonatites. The Canadian Mineralogist, v. 43, 2049-2068.

Morelli, R.M., Hartlaub, R.P., Ashton, K.E., Ansdell, K.M., (2009): Evidence for enrichment of subcontinental lithospheric mantle from Paleoproterozoic intracratonic magmas: Geochemistry and U-Pb geochronology of Martin Group igneous rocks, western Rae Craton, Canada. Precambrian Research, article in press, doi: 10.1016/j.precamres.2009.04.005.

Morimoto, M., (1988): Nomenclature of pyroxenes. Mineralogical Magazine, v. 52, 535-550.

Moro, M.C., Cembranos, M.L., Fernandez, A., (2001): Celsian, (Ba,K)-feldspar and crymrite from sedex barite deposits of Zamora, Spain. The Canadian Mineralogist, v. 39, 1039-1051.

Morteani, G., (1991): The rare earths: their minerals, production and technical use. European Journal of Mineralogy, v. 3, 641-650.

Morteani, G., Preinfalk, C., (1996): REE distribution and REE carriers in laterites formed on the alkaline complexes of Araxa and Catalao, Brazil; in Jones, A.P., Wall, F., Williams, C.T., eds., Rare Earth Minerals; Chemistry, Origin and Ore deposits, Mineralogical Society Series, v.7, 227-252.

Mumin, A.H., (2002): Discovery of a carbonatite complex at Eden Lake (NTS 64C9), Manitoba; in Report of Activities 2002, Manitoba Industry, Trades and Mines, Manitoba Geological Survey, 187-197.

Neary, C.R., Highley, J.E., (1984): The economic importance of the rare earth elements, in Henderson, P., ed., Rare Earth Element Geochemistry, 423-466.

Normand, C., McEwan, B., Ashton, K.E., (2009): Geology and REE mineralization of the Hoidas Lake – Nisikkatch Lake area revisited; in Summary of Investigations 2009, Saskatchewan Geological Survey, Saskatchewan Ministry of Energy and Resources, Misc. Rep. 2009-4.2.

Oliver, N.H.S., Pearson, P.J., Holcombe, R.J., Ord, A., (1999): Mary Kathleen metamorphic–hydrothermal uranium – rare-earth element deposit: ore genesis and numerical model of coupled deformation and fluid flow. Australian Journal of Earth Sciences, v. 46, 467–484.

Orberger, B., Gallien, J., Pinti, D.L., Fialin, M., Daudin, L., Grocke, D.R., Pasava, J., (2005): Nitrogen and carbon partitioning in diagenetic and hydrothermal minerals from Paleozoic Black Shales, Selwyn Basin, Yukon Territories, Canada. Chemical Geology, v. 218, 249-264.

Orrell, S.E., Bickford, M.E., Lewry, J.F., (1999): Crustal evolution and age of thermotectonic reworking in the western hinterland of the Trans-Hudson Orogen, northern Saskatchewan. Precambrian Research, v. 95, p. 187-223.

Orris, G.J., Grauch, R.I., (2002): Rare Earth Mine, Deposits and Occurrences, United States Geological Survey, Open-File Report 02-189.

Pan, Y., Fleet, M.E. (1991): Barian feldspar and barian-chromian muscovite from the Hemlo area, Ontario. Canadian Mineralogist, v. 29, 481-498.

Pan, Y., Fleet, M.E., (1996): Rare earth element mobility during prograde granulite facies metamorphism: significance of fluorine. Contributions to Mineralogy and Petrology, v. 123, 251 – 262.

Pan, Y., Fleet, M.E., (2002): Composition of the Apatite-Group minerals; substitution mechanisms and controlling factors, in Phosphates: geochemical, geobiological and materials importance, Kohn, M.J., Rakovan, J., Hughes, J.M., (eds.), Reviews in Mineralogy and Geochemistry, v. 48, 13 – 40.

Pearce, J.A., Harris, N.B.W, Tindle, A.G., (1984): Trace Element Discrimination Diagrams for the Tectonic Interpretation of Granitic Rocks. Journal of Petrology, v. 25, 956-983.

Pearson, J., (2006): Great Western Minerals Group Ltd. Assessment Report on the 2005-2006 Work Program, Hoidas Lake Rare Earth Project. Submitted to Saskatchewan Industry and Resources.

Pehrsson, S.J., van Breemen, O., (1994): Tackling the last true northern frontier: towards a modern tectonostratigraphic framework for the Western Churchill Province. Western Churchill Metallogeny Project. Manitoba Mining and Minerals Convention Presentation.

Peterson, T.D., Esperanca, S., LeCheminant, A.N., (1994): Geochemistry and Origin of the Proterozoic Ultrapotassic rocks of the Churchill Province, Canada. Mineralogy and Petrology, v. 51, 251-276.

Peterson, T.D., van Breemen, O., (1999): Review and progress report of Proterozoic granitoid rocks of the Western Churchill Province, Northwest Territories (Nunavut). Current Research 1999-C, Geological Survey of Canada, p. 199-127.

Peterson, T.D., Van Breemen, O., Sandeman, H., Cousens, B., (2002): Proterozoic (1.85 to 1.75 Ga) igneous suites of the Western Churchill Province: granitoid and ultrapotassic magmatism in a reworked Archean hinterland. Precambrian Research, v. 119, p. 73-100.

Petrik, I., Broska, I., Lipka, J., Siman, P., (1995): Granitoid Allanite-(Ce): Substitution relations, redox conditions and REE distributions. Geologica Carpathica, v. 46, 79-94.

Poitrasson, F., (2002): In situ investigations of allanite hydrothermal alteration: examples from calc-alkaline and anorogenic granites of Corsica, southeast France. Contributions to Mineralogy and Petrology, v. 142, 485-500.

Pollard, P.J., (1995): Geology of rare metal deposits; An introduction and overview. Economic Geology, v. 90, 489-494.

Python, M., Ceuleneer, G., Ishida, Y., Barrat, J., Arai, S., (2007): Oman diopsidites: a new lithology diagnostic of very high temperature hydrothermal circulation in mantle peridotite below oceanic spreading centres. Earth and Planetary Science Letters, v. 255, 289-305.

Quirt, D., Kotzer, T., Kyser, T.K., (1991): Tourmaline, Phosphate Minerals, Zircon, and Pitchblende in the Athabasca Group: Maw Zone and McArthur River Areas, Saskatchewan, in Summary of Investigations 1991, Saskatchewan Geological Survey, Sask. Energy and Mines, Misc. Rep. 91-4.

Ramasamy, R. Gwalani, L.G., Subramanian, S.P., (2001): A note on the occurrence and formation of magnetite in the carbonatites of Sevvattur, North Arcot district, Tamil Nadu, Southern India. Journal of Asian Earth Sciences, v. 19, 297-304.

Ramsden, A.R., French, D.H., Chalmers, D.I., (1993): Volcanic hosted rare metal deposits at Brockman, Australia. Mineralium Deposita, v. 28, 1-12.

Rainbird, R.H., Hadlari, T., Aspler, L.B., Donaldson, J.A., LeCheminant, A.N., Peterson, T.D., (2003): Sequence stratigraphy and evolution of the Paleoproterozoic intracontinental Baker Lake and Thelon basins, western Churchill Province, Nunavut, Canada. Precambrian Research, v. 125, p. 21-53.

Rainbird, R.H., Davis, W.J., Stern, R.A., Peterson, T.D., Smith, S.R., Parrish, R.R., Hadlari, T., (2006): Ar-Ar and U-Pb Geochronology of a Late Paleoproterzoic Rift Basin: Support for a Genetic Link with Hudsonian Orogenesis, Western Churchill Province, Nunavut, Canada. Journal of Geology, v. 114, p, 1-17.

Rankin, (2005): Carbonatite-Associated Rare Metal Deposits: Composition and Evolution of Ore-Forming Fluids – The Fluid Inclusion Evidence, in Linnen, R.L. Samson, I.M., eds., Rare Element Geochemistry and Mineral Deposits, GAC Short Course Notes 17, 299-314.

Rao, A.T., (1976): Study of the Apatite-Magnetite Veins Near Kasipatnam Visakhapatnam District, Andhra Pradesh, India. Tschermaks Min. Petr. Mitt., v. 23, 87-103.

Rendon-Angeles, J.C., Yanagisawa, K., Ishizawa, N., Oishi, S., (2000): Topotaxial conversion of chlorapatite and hydroxyapatite to Fluorapatite by hydrothermal ion exchange. Chemical Materails, v. 12, 2143-2150.

Rock, N.M.S., (1987): The nature and origin of lamprophyres: and overview, in Fitton, J.G. and Upton, B.G.J., eds., Alkaline Igneous Rocks, Geological Society Special Publication No. 30, 191-226.

Rolland, Y., Cox, S., Boullier, A.M., Pennacchioni, G., Mancktelow, N., (2003): Rare earth and trace element mobility in mid-crustal shear zones: insights from the Mont Blanc Massif, Western Alps. Earth and Planetary Science Letters, v. 214, 203 – 219.

Ross, G.M., (2002): Evolution of Precambrian continental lithosphere in Western Canada: results from Lithoprobe studies in Alberta and beyond. Canadian Journal of Earth Sciences, v. 39, p. 413-437.

Ross, G.M., Eaton, D.W., (2002): Proterozoic tectonic accretion and growth of western Laurentia: results from Lithoprobe studies in northern Alberta. Canadian Journal of Earth Science, v. 39, p. 313-329.

Salvi, S., Williams-Jones, A.E., (2005): Alkaline Granite – Syenite Deposits, in Linnen, R.L. Samson, I.M., eds., Rare Element Geochemistry and Mineral Deposits, GAC Short Course Notes 17, 315-341.

Samson, I.M., Wood, S.A., (2005): The rare earth elements: behavior in hydrothermal fluids and concentration in hydrothermal mineral deposits, exclusive of alkaline settings, in Linnen, R.L. Samson, I.M., eds., Rare Element Geochemistry and Mineral Deposits, GAC Short Course Notes 17, 269-297.

Schandl, E.S., Gorton, M.P., (2004): A textural and geochemical guide to the identification of hydrothermal monazite: criteria for selection of samples for dating epigenetic hydrothermal ore deposits. Economic Geology, v. 99, 1027-1035.

Smith, M.P., Henderson, P., (2000): Preliminary Fluid Inclusion Constraints on Fluid Evolution in the Bayan Obo Fe-REE-Nb Deposit, Inner Mongolia, China. Economic Geology, v. 95, 1371-1388.

Smith, M.P., Henderson, P., Campbell, L.S., (2000): Fraction of the REE during hydrothermal processes: Constraints from the Bayan Obo Fe-REE-Nb deposit, Inner Mongolia, China. Geochimica et Cosmochimic Acta, v. 64, 3141-3160.

Smith, M.P., Henderson, P., Jeffries, T., (2002): The formation and alteration of allanite in skarn from the Beinn an Dubhaich granite aureole, Skye. European Journal of Mineralogy, v. 14, 471-486.

Stone, W.E., Crocket, J.H., Fleet, M.E., (1994): Light-rare earth element-rich minerals associated with platinum-group element mineralization in the Archean Boston Creek Flow, Ontario. Mineralogy and Petrology, v. 51, 85-109.

Stoppa, F., Liu, Y., (1995): Chemical composition and petrogenetic implications of apatites from some ultra-alkaline Italian rocks. European Journal of Mineralogy, v. 7, 391-402.

Sun, S., McDonough, W.F., (1989): Chemical and isotopic systematics of oceanic basalts: implications for mantle composition and processes; in Saunder, A.D. and Norry, M.J., eds., Magamtism in the Ocean Basins, Geological Society Special Publication No. 42, 313-345.

Van Breeman, O., Peterson, T.D., Sandeman, H.A., (2005): U–Pb zircon geochronology and Nd isotope geochemistry of Proterozoic granitoids in the western Churchill Province: intrusive age pattern and Archean source domains. Canadian Journal of Earth Sciences, v. 42, p. 339 – 377.

Van Middlesworth, P.E., Wood, S.A., (1998): The aqueous geochemistry of the rare earth element and yttrium. Part 7. REE, Th and U content in thermal springs associated with the Idaho batholith. Applied Geochemistry, v. 13, 861 – 884.

Vapnik, Y., Bushmin, S., Chattopadhyay, A., Dolivo-Dobrovolsky, D., (2007): Fluid inclusion and mineralogical study of vein-type apatite ores in shear zones from the Singhbhum metallogenetic province West Bengal, India. Ore Geology Reviews, v. 32, 412-430.

Vlach, S.R.F., Gualda, G.A.R., (2007): Allanite and chevkinite in A-type granites and syenites of the Graciosa Province, southern Brazil. Lithos, v. 97, 98-121.

Wall, F., Mariano, A.N., (1996): Rare earth minerals in carbonatites: a discussion centred on the Kangankunde Carbonatite, Malawi, in Jones, A.P., Wall, F., Williams, C.T., eds., Rare Earth Minerals; Chemistry, Origin and Ore deposits, Mineralogical Society Series, v. 7, 193-225.

Wang, S., Williams, P.J., (2001): Geochemistry and origin of Proterozoic skarns at the Mount Elliot Cu-Au(-Co-Ni) deposit, Cloncurry district, NW Queensland, Australia. Mineralium Deposita, v. 36, 109-124.

Wood, S.A., Ricketts, A., (2000): Allanite-(Ce) from the Eocene Casto Granite, Idaho: Response to Hydrothermal Alteration. The Canadian Mineralogist, v. 38, 81-100.

Woolley, A.R., 1989. The spatial and temporal distribution of carbonatites: in Carbonatites, Bell, K. (ed). Unwin Hyman Ltd.

Wu, C., Yuan, Z., Bai, G., (1996): Rare earth deposits in China; in Jones, A.P., Wall, F., Williams, C.T., eds., Rare Earth Minerals; Chemistry, Origin and Ore deposits, Mineralogical Society Series, v.7, 281-306.

Yegorov, L., (1993): Phoscorites of the Maymecha-Kotuy Ijolite-Carbonatite Association. International Geology Review, v. 35, 346-358.

Zhao, G., Cawood, P.A., Wilde, S.A., Sun, M., (2002): Review of global 2.1–1.8 Ga orogens: implications for a pre-Rodinia supercontinent. Earth Science Reviews, v. 59, p. 125 – 162.

Zhuming, Y., Pertlik, F., Fleck, M., (2008): Hydroxyl groups in nonmetamict chevkinite-(Ce): a crystal chemical discussion. Journal of Rare Earths, v. 26, 609-613.

APPENDIX A

PETROGRAPHIC DESCRIPTIONS

Sample No. HL0907-1

Hand Specimen Description

- Deformed granite with slightly blue colored quartz.

Mineralogy

K-feldspar	57%	4 mm to 0.5 mm
Quartz	30%	4 mm to 1 mm
Epidote	8%	< 0.2 mm
Plagioclase	2%	< 0.5 mm
Chlorite	2%	< 0.5 mm
Muscovite	1%	< 0.5 mm

QAP – 34-64-2

Description

- Highly deformed sample with strong undulose extinction in quartz and common suturing at crystal boundaries
- Broadly gneissic texture to the sample
- Late dextral movement offsets the gneissic bands along late fractures
    - A minor number display sinstral movement
    - Less than 2 mm of movement
    - Fractures are typically filled with anhedral to subhedral epidote
    - Some fractures remain open
    - Minor number of fractures have late opaque core – too fine to identify with certainty, but the opaque is likely hematite
- Rare primary epidote can be found with the feldspar
- Majority of the K-feldspar appear altered, particularly in areas adjacent to veining
    - Seritization is common
    - Mix of microcline and perthite

Sample No. HL0907-2

Hand Specimen Description

- Relatively undeformed granodiorite with minor amounts of biotite and amphibole.

Mineralogy

K-feldspar	35%	0.5 mm to 4 mm
Quartz	15%	1 mm to 2 mm
Plagioclase	24%	0.5 mm to 2 mm
Hornblende	8%	0.5 mm to 2 mm
Biotite	8%	~ 1 mm
Actinolite	4%	< 0.2 mm
Epidote	2%	< 0.2 mm
Myrmekite	2%	< 0.5 mm
Magnetite	2%	< 0.5 mm
Hematite	Tr	< 0.2 mm
Chalcopyrite	Tr	< 0.2 mm

QAP – 20-47-33

Description

- Weakly deformed, with minor undulose extinction in quartz and rare deformation twins in plagioclase
- Biotite is randomly oriented although it tends to concentrate into weak bands of more mafic compostion
    - Hornblende also most common in these bands
    - Epidote, chlorite and tremolite-actinolite are common alteration produces in the mafic band
- Weak seritization and saussuritization of the feldspars
- Major minerals are typically anhedral to subhedral and roughly equigranular
- Rare myrmekite
- Microcline to perthitic K-feldspar
- Clots of magnetite are essentially fresh – they lack the hematitic rims observed in other samples

Sample No. HL0907-3

Hand Specimen Description

- Weakly deformed granite with minor biotite.

Mineralogy

K-feldspar	55%	3 mm to 0.5 mm
Quartz	30%	2 mm to 0.5 mm
Biotite	5%	< 0.5 mm
Chlorite	3%	< 0.5 mm
Myrmekite	2%	< 0.5 mm
Magnetite	2%	< 1 mm
Plagioclase	1%	< 0.5 mm
Hematite	1%	< 0.5 mm
Epidote	1%	< 0.2 mm

QAP – 35-64-1

Description

- Weakly deformed sample with undulose extinction in quartz and irregular sutured boundaries present on the major minerals
- Seritization common on the feldspar
- Abundant perthitic feldspar and microcline
    - Rare symplectitic to myrmekitic intergrowths
- Minerals are roughly equigranular and most minerals are subhedral to anhedral
- Biotite is variably chloritized
- Epidote appears to be primary
- Magnetite clots are altering to hematite along rims and fracture surfaces

Sample No. HL0907-4

Hand Specimen Description

- Weakly gneissic granodiorite.

Mineralogy

K-feldspar	35%	2 mm to 0.5 mm
Plagioclase	25%	2 mm to 0.5 mm
Quartz	15%	2 mm to 0.5 mm
Biotite	15%	2 mm to 0.5 mm
Chlorite	3%	< 0.5 mm
Epidote	1%	< 0.5 mm
Magnetite	1%	2 mm to 0.2 mm
Chalcopyrite	1%	< 0.5 mm
Hematite	Tr	< 0.5 mm

QAP – 20-47-33

Description

- Weakly deformed, slightly gneissic sample
- Biotite is randomly oriented within the more mafic bands
    - Subhedral crystals are variably chloritized
    - Opaques are much more common in these bands
    - No hematite alteration of the magnetite
- Epidote occurs as small subhedral primary crystals
- Slightly irregular, sutured boundaries are common in the quartz and feldspars
    - Quartz commonly displays undulose extinction
    - Plagioclase contains rare deformation twins
    - Feldspars are relatively unaltered compared to many of the other samples
    - K-feldspar a fairly even mix of microcline and perthite

Sample No. HL0907-5

Hand Specimen Description

- Slightly magnetic granodiorite. Rare biotite compared to previous sample.

Mineralogy

Quartz	30%	4 mm to 0.1 mm
K-feldspar	30%	~ 1 mm
Plagioclase	25%	~ 1 mm
Chlorite	5%	< 0.5 mm
Magnetite	5%	< 0.5 mm
Epidote	1%	< 0.2 mm
Biotite	1%	< 0.5 mm
Hornblende	1%	< 0.5 mm
Hematite	1%	< 0.2 mm
Chalcopyrite	1%	< 0.2 mm

QAP – 35-35-30

Description

- Majority of the slide consists of weakly deformed quartz and feldspar
    - Feldspars are extensively altered
    - Quartz displays weak undulose extinction
    - Quartz rich segregations/stringers are common
    - Minor microperthitic feldspar and rare rod-shaped antiperthite
    - Rare myremekite
    - Feldspars and quartz are subhedral to anhedral
    - Feldspars are roughly equigranular while quartz shows significant variation in crystal size
    - Large, anhedral clots of magnetite occur in association with the quartz rich areas
    - Little to no hematitic alteration present
    - Rare subhedral chlorite, biotite, epidote and hornblende in the feldspar rich areas
    - Biotite and hornblende show little alteration – some chloritization of the biotite
- Chlorite-rich band with a much smaller average crystal size present in one corner of the slide
    - This band contains the majority of the chlorite, epidote and hornblende
    - Average crystal size is less than 0.5 mm
    - Strong alignment of the chlorite in the fine grained section
    - Chlorite is concentrated along small shears and fractures

Sample No. HL0907-6

Hand Specimen Description

- Granodiorite with abundant biotite and amphibole. Slightly magnetic.

Mineralogy

Plagioclase	30%	< 2 mm
Biotite	15%	< 2 mm
Hornblende	15%	< 2 mm
K-feldspar	14%	< 2 mm
Quartz	12%	< 2 mm
Magnetite	5%	< 0.5 mm
Myrmekite	3%	< 1 mm
Epidote	3%	< 0.5 mm
Apatite	2%	< 0.5 mm
Chalcopyrite	1%	< 0.5 mm
Chlorite	Tr	< 0.5 mm
Calcite	Tr	< 0.1 mm
Hematite	Tr	< 0.1 mm

Description

- Weakly deformed sample with minor undulose extinction in quartz and rare deformation twins in plagioclase
- Inequigranular with a maximum crystal size of 2 mm
- Quartz and feldspars are anhedral to subhedral
    - Weak to moderate seritization and saussuritization of the feldspars
    - Minor myrmekite present
    - Rare subhedral to euhedral inclusions of apatite in some of the larger feldspars
    - Minor occurrence of perthitic k-feldspar
- Biotite and hornblende are typically subhedral evenly distributed throughout the sample
    - Biotite are randomly oriented
    - Weak chloritic alteration present on some biotite
    - Small clots of magnetite found near the biotite or hornblende or as rare inclusion
- Small, primary subhedral epidote found throughout the slide

Sample No. HL0907-7

Hand Specimen Description

- Pink (altered?) granite close to the veins. Quartz ribbons and augen common.

Mineralogy

K-feldspar	56%	< 3 mm
Quartz	30%	< 2 mm
Plagioclase	5%	< 1.5 mm
Epidote	3%	< 0.2 mm
Chlorite	2%	< 0.2 mm
Hornblende	2%	< 1 mm
Clinopyroxene	2%	< 1 mm
Hematite	2%	< 0.2 mm
Magnetite	Tr	< 0.2 mm
Apatite	Tr	< 0.1 mm
Calcite	Tr	< 0.1 mm

Description

- Variably altered, inequigranular feldspars
    - Mild to moderate seritization of the K-feldspars
    - Intense alteration of the plagioclase – in some areas the saussuritization esstentially obscures the plagioclase
    - Hematitic overprint of the feldspars gives a pinkish color in plane polarized light
    - Abundant perthitic k-feldspar and microcline
    - Irregular, sutured boundaries are common
    - Rare inclusions of subhedral apatite
- Anhedral quartz shows weak undulose extinction
    - Occurs in elongated patches
- Sample cross-cut be small monomineralic veinlet of epidote
- Irregular clots of hematite appear to be the result of alteration
    - Larger clots have small magnetite cores
    - Smaller clots are entirely hematite
- Hornblende and clinopyroxene are restricted to a small, irregular patch
    - Both subhedral to anhedral and are typically altered
    - Possible alteration related to the mineralization?
    - Abundant opaques present in this area
    - Epidote and chlorite common alteration products it this area
    - Rare calcite appears to be associated with the alteration

Sample No. Lamp-1

Hand Specimen Description

- Porphyritic lamprophyre dike. Large phenocrysts of biotite in a fine grayish groundmass.

Mineralogy

K-feldspar	55%	1 mm to 0.2 mm
Biotite	12%	< 6 mm
Actinolite	10%	< 0.5 mm
Plagioclase	4%	1 mm to 0.2 mm
Apatite	3%	< 0.2 mm
Hornblende	3%	2 mm to 0.5 mm
Hematite	3%	< 0.1 mm
Clinopyroxene	3%	1 mm to 0.2 mm
Magnetite	2%	< 0.2 mm
Quartz	2%	< 0.2 mm
Titanite	1%	< 0.2 mm
Epidote	1%	< 0.2 mm
Chlorite	1%	< 1 mm
Olivine	Tr	< 0.2 mm

Description

- Phenocrysts in this lamprophyre are predominantly subhedral to euhedral biotite, or possibly phologopite, with rare subhedral hornblende phenocrysts
    - Biotite phenocrysts are typically cracked and kink banded
    - Some minor alteration to chlorite at the boundaries of some crystals
    - Rare hornblende phenocryts are variably altered to tremolite – actinolite giving a somewhat fibrous appearance
    - Loose alignment of the biotite crystals
    - Rarely cumuloporphyritic
- Groundmass is dominated by K-feldspars
    - Most are slightly perthitic, with rare microcline
    - Some minor plagioclase present as well
    - Small eudhedral needles of tremolite-actinolite occur throughout the groundmass
    - Euhedral apatite occurs throughout the groundmass and as a rare inclusion in the larger feldspars
    - Opaques in the groundmass are typically subhedral magnetite surrounded by a rim of hematite – small magnetite crystals can be entirely alterted to hematite
    - Clinopyroxene and Olivine are consistently smaller than the phenocrysts but otherwise seriate and are variably altered

Sample No. Lamp-2

Hand Specimen Description

Porphyritic Lamprophyre similar to Lamp-1 in appearance.

Mineralogy

K-feldspar	66%	0.5 mm to 0.1 mm
Biotite	15%	< 8 mm
Hornblende	15%	2 mm to 0.2 mm
Clinopyroxene	4%	< 0.2 mm
Tremolite	4%	< 0.2 mm
Plagioclase	2%	0.5 mm to 0.1 mm
Hematite	2%	< 0.1 mm
Magnetite	2%	< 0.1 mm
Titanite	1%	< 0.2 mm
Apatite	1%	< 0.2 mm
Epidote	1%	< 0.1 mm
Pyrite	1%	< 0.1 mm
Quartz	1%	< 0.2 mm
Zoisite (?)	Tr	< 0.1 mm

Description

- Similar to Lamp-1, the phenocrysts are mainly subhedral to euhedral biotite, or possibly phlogopite, and subhedral to anhedral hornblende
    - Biotite crystals can be larger the 4mm in size while the hornblende is typically less than 2.5 mm in size
    - Biotite shows signs of deformation – cracked or kink banded crystals are common
    - Hornblende is slightly altered to tremolite-actinolite
    - Rare phenocrysts of altered, anhedral clinopyroxene, typically less than 2mm in size
    - Rarely cumuloporphyric
- Groundmass is dominated by finely crystalline, felty K-feldspar
    - Perthite and microcline are common
    - Some minor plagioclase, apatite, titanite, epidote, amphiboles and rare zoisite
    - With the exception of apatite, which is euhedral, the minerals in the groundmass are subhedral to anhedral
    - Amphiboles in the groundmass tend to be more equant than observed in the previous lamprophyre
    - Minor amounts of magnetite, typically rimmed by hematite and pyrite can also be found in the groundmass
    - Rare hematitic fractures

Sample No. Pegm-2

Hand Specimen Description

Pinkish K-feldspar rich pegmatite with relatively minor quartz.

Mineralogy

K-feldspar	85%	8 mm to 1 mm
Quartz	8%	3 mm to 0.5 mm
Muscovite	2%	< 0.2 mm
Plagioclase	2%	< 1 mm
Epidote	1%	< 0.2 mm
Hematite	1%	< 0.1 mm
Magnetite	1%	< 0.1 mm
Chalcopyrite	Tr	< 0.1 mm

Description

- Large, essentially undeformed subhedral crystals of K-feldspar and quartz dominate the slide
    - Minor undulose extinction in the quartz
    - K-feldspar is mainly perthitic although small crystals of microcline can be found
    - Minor seritization present
    - Hematite common along fractures and at crystal boundaries
- Rare muscovite occurs as small subhedral to euhedral crytals
- Magnetite and Chalcopyrite are frequently rimmed by hematite
    - Hematite also common along late cross-cutting fractures
- The epidote is typically subhedral and appears to be primary

Sample No. BSP-Pegm

Hand Specimen Description

Deformed pegmatite near the mineralized veins in the bulk sample pit. Quartz ribbons common. Minor amounts of clinopyroxene and amphibole.

Mineralogy

K-feldspar	50%	3 mm to 0.1 mm
Quartz	20%	< 0.5 mm
Plagioclase	10%	< 0.2 mm
Clinopyroxene	5%	4 mm to 2 mm
Hornblende	4%	< 0.5 mm
Calcite	3%	< 0.5 mm
Titanite	2%	2 mm to 0.5 mm
Biotite	2%	< 0.2 mm
Chlorite	2%	< 0.2 mm
Epidote	1%	< 0.1 mm
Tremolite-actinolite	1%	< 0.1 mm
Pyrite	Tr	< 0.1 mm

Description

- Abundant evidence of deformation through the slide
  - Deformed nature of the sample has resulted in some reduction of crystal size
  - Crushed, sutured crystals common
  - Quartz shows strong undulose extinction
  - Plagioclase commonly contains deformations twins
  - Alignment of biotite -chlorite
- Samples is slightly gneissic to schistose
- Most major minerals are inequigranular and subhedral to anhedral
- K-feldspar is mainly orthoclase with minor perthite
- Epidote, chlorite and tremolite-actinolite appear to be the result of metamorphism of the clinopyroxene, hornblende and biotite
- Calcite occurs as a late alteration mineral or in small cross-cutting veinlets
- Anhedral pyrite also occurs in late veins.

Sample No. HS-Pegm

Location Hoidas South Main showing

Hand Specimen Description

Deformed Hornblende-Hyalophane-bearing pegmatite from Hoidas South.

Mineralogy

K-feldspar	78%	< 8 mm
Hornblende	10%	4 mm to 1 mm
Quartz	5%	3 mm to 1 mm
Plagioclase	25	< 0.5 mm
Apatite	2%	< 0.5 mm
Titanite	1%	3 mm to 0.5 mm
Magnetite	1%	2 mmt to 0.5 mm
Fluorite	1%	< 0.1 mm
Biotite	Tr	< 0.5 mm
Allanite	Tr	< 0.1 mm
Monazite	Tr	< 0.1 mm
Tremolite	Tr	< 0.2 mm

Description

- Sample is dominated by large subhedral perthitic K-feldspar
    - Scale of the exolution varies, even with in a single crysts
    - Microperthite most common
    - Most feldspars show moderate seritization
    - Minor myrmekitic intergrowths found at some boundaries
- Some evidence of deformation – crushed, sutured boundaries are common and quartz typically shows strong undulose extinction
- Rare plagioclase occurs as small, typically less than 1 mm, subhedral crystals
- Inequigranular euhedral titanite, ranging from 2.5mm to less than 1mm, can be found throughout the slide
    - The color in plane polarized light varies from the typical brown to the bright orange typically observed in the mineralized veins
    - Rare crystals appear to be zoned, with orange centres surrounded by brownish rims
    - Small titanites are entirely of the brown variety
- Large subhedral hornblende and clinopyroxene
    - Some of the hornblende have optical properties similar to arfedsonite
    - Minor alteration to tremolite-actinolite
- Rare subhedral apatite found throughout
- Single, subhedral allanite with strong concentric zonation
    - The regular boundaries suggest magmatic zonation
- Large clots of magnetite, up to 2.5 mm in size
    - No hematite rims present

Sample No. 37903 – Apatite Breccia

Location DDH HL05-43 at 121.7m

Hand Specimen Description

- Rounded clasts of pale green to pink apatite and rare feldspar in a fine grained, friable carbonate-bearing matrix. Clasts are typically smaller than 1 cm in size. Reddish color to matrix.

Mineralogy

Apatite	45%	7 mm to 2 mm
Fe-oxide rich matrix	35%	< 0.1 mm
Hyalophane	10%	5 mm to 2 mm
Calcite	6%	< 0.1 mm
Quartz	2%	< 0.1 mm
Allanite	1%	< 0.1 mm
Pyrite	1%	< 0.1 mm

Description

- Matrix supported breccia consisting of well rounded clasts of apatite and rare feldspars which is believed to be hyalophane.
- Matrix is composed of calcite with abundant fine-grained apatite and opaques
    - Fine grained nature of the matrix, and the poor polish on the opaque phases makes identification of individual minerals impossible in most cases
- Most common clast type is apatite, although rare clasts of altered host granitoid and earlier vein generations also occur.
    - Alteration in the granitic clasts consists of weak hematization and sericitic alteration of the feldspars.
    - Feldspar clasts appear to be hyalophane
- Many of the apatite clasts are poikiolitic
    - Two common varieties of inclusions
    - Small, bright inclusions are randomly oriented and tend to occur in the centres of the clasts – possibly monazite, although the inclusions are too fine to identify with any certainty
    - Reddish-brown inclusions are also common and seem to display a preferred orientation. Again identification is tentative, but they appear to be some sort of iron oxide – possibly hematite?
    - Rare inclusions of what appears to be highly metamict allanite
- Clasts are also cross-cut by late fractures which seem to be coated in a reddish opaque mineral – likely hematite.
- At least two, possibly three, generations of apatite are present in this sample.
- Pyrite can be found throughout the matrix as discrete crystals

Sample No. 37906 – Apatite Breccia

Location DDH HL05-48 at 57m
Hand Specimen Description

- Largely clast supported breccia with zoned apatite clasts and carbonate rich matrix. Some apatite clasts show green centres with pinkish rims.

Mineralogy

Apatite	63%	6 mm to 1 mm
Quartz	25%	< 2 mm
Calcite	5%	< 3 mm
Epidote	2%	< 0.2 mm
Hornblende	2%	< 0.5 mm
Chlorite	1%	< 0.1 mm
Pyrite	1%	< 0.1 mm
Hematite	1%	< 0.1 mm
Allanite	Tr	< 0.1 mm

Description

- Clast supported to matrix supported breccia consisting of apatite clasts in a quartz and calcite rich matrix.
    - The matrix minerals appear strained with the quartz displaying slight undulose extinction.
    - Possibly two separate generation of quartz based on variations in strain
    - Second generation of quartz occurs as late cross-cutting veins
    - Calcite appears to be the latest mineral in the slide
- Minor amounts of chlorite, epidote and hornblende can also be found in the matrix
- Apatite clasts are typically quite angular and in many places have a crackle breccia appearance with little to no rotation of the clasts – the result of hydraulic fracturing?
- Clasts display a variation in color ranging from pinkish rims to pale green cores in some crystals
- Apatite appears be zoned, with a patchy, irregular distribution of inclusions
    - Multiple types of inclusions, including opaqes, xenoliths of earlier vien generations and what might be monazite.
    - Rare inclusions of euhedral apatite in the larger clasts
- Epidote most commonly occurs as subhedral crystals at the contacts between the apatite clasts and the quartz
- Hornblende occurs as small euhedral to subhedral crystals in the matrix or as larger altered patches associated with chlorite and epidote.
- Pyrite and hematite can also be found throughout the matrix although they are particularly common at crystal boundaries

Sample No. 37920 – Red Apatite Breccia

Location DDH HL05-68 at 75.3m.
Hand Specimen Description

- Matrix supported red apatite breccia with a reddish matrix. Minor carbonate present in the matrix. Rare, rounded clasts of granitoid host rocks.

Mineralogy

Apatite	40%	15 mm to 1 mm
Calcite	10%	< 0.2 mm
Quartz	6%	< 0.2 mm
Feldspar	2%	< 0.2 mm
Biotite	2%	< 1 mm
Amphibole	2%	< 0.2 mm
Allanite	1%	< 0.2 mm
Chlorite	Tr	< 0.1 mm
Pyrite	1%	< 0.5 mm
Fe-oxides	1%	< 0.1 mm
Matrix	35%	(cryptic)

Description

- Matrix supported breccia dominated by sub-angular to sub-rounded clasts of apatite.
- Matrix as a whole consists of apatite, calcite, opaques, amphiboles, biotite and chlorite – the exact composition varies on a small scale throughout the sample with small patches enriched in a particular mineral
    - All the matrix minerals are anhedral to subhedral with the exception of the biotite and chlorite which rarely occur distinct euhedral crystals
    - Much of the matrix has a very fine, earthy appearance with the individual minerals too small to identify
    - Matrix varies from fibrous to granular in appearance
- Wide range of clast sizes with clasts from 1.5 cm in diameter to less than 0.5mm in size
- Larger clasts typically display inclusion rich cores
    - Inclusions are often oriented and elongate in shape
    - Some inclusions a reddish color in plane polarized light – possibly some sort of iron oxide such as hematite or possibly goethite
    - Rare inclusions of what appears to be metamict allanite
- Smaller apatite clasts are typically inclusion free
- Rare quartz rich clasts are likely from host granitoids and tend to be sub-round to round
- Rare crystals of subhedral hornblende occur in the matrix

Sample No. 37933 – Apatite-Allanite Vein

Location DDH HL06-90 at 31.45m
Hand Specimen Description

- Zoned apatite-allanite vein cross-cutting feldspathic host rock. Ragged, irregular contact between the vein and host rock.

Mineralogy

K-feldspar	60%	3 mm to 1 mm
Apatite	25%	7 mm to 1 mm
Allanite	5%	<3 mm
Pyrite	4%	< 1 mm
Plagioclase	3%	<1 mm
Epidote	2%	< 0.3 mm
Muscovite	Tr	< 0.3 mm

Description

- Majority of the slide consists of highly altered feldspars (syenite)
    - The K-feldspar shows some possible evidence of exsolution although this is almost entirely masked by the alteration
    - Some minor hematization of the feldspars and seritization
    - Plagioclase mildly affected by saussuritization
    - All feldpars are anhedral
- Associated with the syenitic interval are minor amounts of subhedral muscovite and epidote and what may be rare primary allanites
- Secondary allanite can also be found in the granitic rock in small veinlets, often associated with small euhedral pyrite
- The majority of the allanite in this slide is subhedral and occurs at the contact of the vein with the granitoid wall rocks
    - Allanite contains rare angular xenoliths of the wall rock
    - Rare patches of allanite in the wall rock immediately adjacent to the contact – some localized alteration in the first few mm of the wall rock
    - Allanite displays weak, irregular, often roughly concentric zonation
    - Clast of the allanite can be found in the later apatite vein
- Cross-cutting apatite vein consists of coarse subhedral crystals
    - Only a minor number of inclusion in this apatite
    - Inclusions are typically a reddish color although they do not show the preferred orientation as has been observed in other samples
    - Apatite vein is cross-cut by late veinlets and fractures similar to what is observed in the granitoids – veinlets filled with pyrite
    - Rare iron oxide coated fractures are common – likely hematite

Sample No. 782076 – Allanite-rich Vein

Location NIS-A (J22-08-5)
Hand Specimen Description

- Coarsely crystalline allanite dominant vein with minor feldspar.

Mineralogy

Allanite	41%	20 mm to 2 mm
Hyalophane	30%	< 1mm
Scapolite	15%	< 0.7 mm
Chevkinite	10%	< 2 mm
Fe-Oxides	3%	< 0.1 mm
Pyrite	1%	< 0.5 mm

Description

- Sample dominated by coarse, cm sized, anhedral to subhedral allanite crystals
    - Allanite is typically intensely zoned, with a single crystal containing up to 5 visually distinct zones
    - Although roughly concentric the zonation is highly irregular, with variations in the thickness within a single zone and ragged, uneven boundaries between zones
    - Zonation can be distinguished in plane polarizaed light by the variations in pleochroism
    - Under crossed polars the cores of the large allanites are often almost isotropic in appearance- possibly due to metamicitization
    - From the core to the rim the optical propeties vary from those of allanite towards what is more typical of epidote
    - Allanites can be surrounded by radiating fracture sets
- Closely associated with the allanite crystals are large orange to reddish crystals believed to be titanite and chevkinite
    - Both of these minerals are typically found either as inclusion in the allanite or at the margins of the allanite crystals
    - Both are subhedral but the chevkinite displays some roughly concentric zonation while the titanite is unzoned
- Associated with the allanite, chevkinite and titanite are minor amounts of opaques which could not identified due to the previous carbon coating of this slide to confirm the identity of the chevkinite
    - Some of the opaques may be pyrite based on the shape of euhedral crystals
- The remaining portion of the slide consist of a mix of feldspar and scapolite
    - These crystals are distinctly smaller than the allanite, with an average size of 0.5 mm.
    - The feldspar, which is likely hyalophane, is most common in areas adjacent to the REE-bearing minerals

- Due to proximity to the allanite many of these feldspars are heavily fractured, with the fractures often displaying a reddish coated which is likely some sort of iron oxide
- Alteration to scapolite is common, with the optical properties suggesting a meionitic composition
- Minor clay alteration is also common

Sample No. 881317 – Diopside-Allanite Vein

Location DDH BH09 at 20m
Hand Specimen Description

- Diopside-allanite vein cross cut by a small vein of coarse red apatite. Allanite common at the contact between the two vein types. Rare brecciated clasts of the diopside-allanite material present in the later vein. Minor amphibole alteration of the diopside.

Mineralogy

Diopside	25%	< 8 mm
Apatite	25%	3 mm to 0.1 mm
Allanite	15%	20 mm to 1 mm
Hornblende	10%	< 1 mm
Titanite	5%	1 mm to 0.2 mm
Biotite	5%	4 mm to 0.5 mm
Hematite	4%	< 0.2 mm
Pyrite	1%	< 0.1 mm
Monazite	Tr	< 0.1 mm

Description

- The diopside rich interval consists of diopside, allanite, titanite, hornblende, biotite
- The diopside is subhedral, highly fractured and turbid looking
    - Small, less than 2 mm, inclusions of allanite and titanite are common in the diopside crystsal, with the allanites often surrounded by radiating fracture sets
- Biotite displays some evidence of alteration and deformation
    - Cracked and bent crystals are common and biotite is often surrounded by hornblende
- The majority of the allanite occurs at the contact between the diopside-allanite vein and the cross-cutting coarse red apatite vein
    - Allanite present along the entire length of the contact on one side of the apatite vein but occurs only sporadically on the other side
    - Allanite is strongly zoned, with the zonation roughly concentric, althought the boundaries between zones tend to be ragged and the thickness of the zones is somewhat inconsistent
    - Rims of the crystals have optical properties similar to epidote –may range towards epidote in composition instead of endmember allanite
    - Contact between the allanite and apatite vein seems brecciated and, in some areas, almost gradational
- Apatite vein is composed almost entirely of coarse subhedral crystals of apatite
    - Apatite is fractures, with the fractures typically coated with a reddish opaque which is likely hematite
    - Fracturing particularly prevalent in areas adjacent to the allanite

- Apatites are essentially inclusion free
- Some minor brecciation present in the apatite vein, although the resulting clasts are quite angular and seem to be essentially still in place, with very little rotation evident

Sample No. 881346 – Apatite Breccia

Location DDH BH08 at 99.4m

Hand Specimen Description

- Red apatite breccia with rare interstitial allanite. Rounded clasts in a fine grained reddish matrix. Sample is cross cut by fine carbonate veinlets.

Mineralogy

Apatite	92%	8 mm to 1 mm
Allanite	4%	< 2 mm
Hornblende	2%	1 mm to 0.5 mm
Calcite	1%	< 0.1 mm
Hematite	1%	< 0.1 mm
Pyrite	Tr	< 0.1 mm

Description

- Clast supported red apatite breccia in a matrix composed largely of very fine apatite, with minor calcite and hematite
    - Large variation in clast size with the largest clasts over 4 mm in size ranging to less than 1 mm
    - Apatite clasts also range from inclusion rich examples to essentially inclusion free
    - The inclusions are often aligned and display a faint yellowish color in plane polarized light and high birefringence under crossed polars
    - Inclusions range from slightly elongate to rounded in shape
- Allanite in this sample is commonly small, less than 1mm clasts from the earlier vein generations and is typically quite metamict
    - Small amounts of anhedral hornblende are often associated with these clasts
    - Rare hornblende and allanite can be found in the matrix which may be primary
- Sample is cross-cut by a number of small veinlets and hematitic fractures
    - Veins typically contain calcite although remobilized veinlets of what appears to be allanite also occur, although the small size of the vein makes definitive identification difficult

Sample No. 881368 – Diopside-Allanite Vein

Location DDH BH09 at 38m
Hand Specimen Description

- Diopside-allanite vein which dominated by slightly altered diopside. Diopside in this sample is variably altered to amphibole. Slightly vuggy appearance to this sample. Rare dark red apatite crystals.

Mineralogy

Diopside	60%	5 mm to 0.5 mm
Allanite	30%	30 mm to 0.5 mm
Hornblende	4%	< 1 mm
Hyalophane	4%	3 mm to 0.5 mm
Hematite	1%	< 0.5 mm
Epidote	1%	< 0.5 mm

Description

- Diopside rich example of a diopside allanite vein
- Diopside crystals, up to 6 mm in size, are highly fractures and turbid looking
    - Associated with the diopside is a minor amount of hornblende which most commonly occurs as an alteration product of the diopside
    - Subhedral crystals of what appears to be primary hornblende can also be found
    - Rare inclusions of allanite, surrounded by radiating fractures can be found in the diopside
- Small, late epidote can also be found with the diopside and, like the hornblende appear to be the result of alteration
- Small interstial magnetite and hematite crystals occur between the larger crystals and are the most common opaque minerals
    - The magnetite is typically completed surrouned by a reaction rim of hematite
    - Smaller hematite crystals are likely the result of complete alteration of the magnetite as opposed to primary hematite
- Allanite in this slide consists of large, up to 1 cm in size, zoned crystals
    - As observed in other slides, the zonation is roughly concentric, and ranges from a slightly metamict core through relatively fresh allanite towards an epidote rich rim
    - Up to five visually distinct zones in some of the larger crystals
    - Pleochroism and birefringence varies with the zonation
    - Allanite can be surrounded by radiating fracture sets which are likely due to a volume change associated with metamictization
    - Minor opaques appear to be associated with some of the allanite
    - Rare inclusions of hyalophane and diopside can be found in the allanite

- Some minor hyalophane which is typically highly fractured, turbid and hematized, especially adjacent to the allanite crystals or where allanite occurs as inclusions

Sample No. 881056 – Red Apatite Breccia

Location DDH HL05-22 at 67 m.

Hand Specimen Description

- Red apatite breccia with a dark matrix. Sub-rounded clasts of apatite in a dominantly clast supported breccia. The sample is cross-cut by a vein of the coarse red apatite, with sharp linear contacts between the two vein types. The late vein shows no evidence of deformation.

Mineralogy

Apatite	70%	6 mm to 0.2 mm
Allanite	10%	< 1 mm
Hematite	10%	< 0.1 mm
Calcite	5%	< 0.2 mm
Chlorite	5%	< 0.1 mm

Description

- Monomictic, clast supported apatite breccia
- Difficult to determine the composition of the matrix due to the extremely fine grain size but it seem to consist largely of apatite, chlorite, hematite and calcite
- Clasts range from 5 mm in diameter down to less than 0.1 mm in the matrix and range from subrounded to subangular
    - Large clast are typically inclusion rich, especially in the cores
    - Smaller clasts are generally inclusion free
    - Two common types of inclusions – randomly oriented opaque inclusions are likely hematite
    - Light yellow inclusions with high birefringence may be monazite although they are too fine to identify with certainty
    - Rare xenoliths of metamict allanite in some apatite clasts, surrounded by the typical radiating fractures
- Sample is cross-cut by a number of small, late hematite coated fractures and calcite filled veinlets

Sample No. 948537 – Massive Allanite Vein

Location DDH BH02 at 76.2 m.

Hand Specimen Description

- Massive allanite dominated vein with minor amounts of diopside and feldspar. Allanite is very coarsely crystalline, with the maximum size up to 7 cm. Minor alteration of the diopside to hornblende.

Mineralogy

Allanite	75%	> 20 mm to 1 mm
Apatite	4%	3 mm to 0.5 mm
Calcite	4%	< 0.2 mm
Diopside	2%	4 mm to 0.5 mm
Epidote	2%	< 0.2 mm
Titanite	2%	2 mm to 0.5 mm
Pyrite	2%	< 0.1 mm
Scapolite	1%	< 0.1 mm
Hematite	1%	< 0.1 mm
Green Mineral	Tr	< 1 mm

Description

- Sample is dominated by large, subhedral to anhedral allanite crystals
- Allanite in this slide is not as intensely zone as what is observed in many of the other samples
    - Only the edges of the crystals show some minor zonation
    - Zonation in plane polarized light does not correspond with what is observed under crossed polars
    - Rims of the allanite crystal are similar to epidote in composition
    - Allanite is realatively inclusion free, although small inclusion of diopside, titanite and hornblende can be found
- Large subhedral diopside crystals with minor hornblende alteration
- Allanite is cross cut by a small vein containing euhedral apatite, and anhedral calcite, scapolite, and an unidentified dark green isotropic mineral
    - Allanite at the contact with the veins show a similar zonation to what is observed at the boundaries of crystals
- Allanite is cross cut by a small vein filled with euhedral apatite and subhedral calcite, scapolite, opaques and an unidentified green mineral
    - Unidentified mineral is a deep green, almost opaque, in color and is isotropic – possibly a spinel?

Sample No. 881318B – Allanite-rich Vein

Location DDH BH09 at 25.9 m.
Hand Specimen Description

- Massive allanite vein.

Mineralogy

Allanite	67%	> 20 mm to 1 mm
Titanite (+/-Chevkinite)	25%	20 mm to 1 mm
Diopside	3%	2 mm to 1 mm
Epidote	2%	< 0.5 mm
Calcite	1%	< 0.5 mm
Hornblende	1%	2 mm to 1 mm
Pyrite	1%	< 0.1 mm
Green Mineral	Tr	< 0.1 mm

Description

- Slide is dominated by large anhedral allanite
    - In some cases the cores of the allanite crystals are essentially isotropic, suggesting metamictization
    - Allanite is essentially unzoned except for narrow, less than 0.5 mm, rims at the crystal boundaries or surrounding inclusions
    - Rims may be closer to epidote in composition
    - Inclusions of titanite, hornblende, diopside and pyrite are common
    - Most inclusions are subhedral to euhedral
- Titanite forms large subhedral to euhedral crystals
    - Bright orange and strongly pleochroic
    - Relatively inclusion free
    - Possibly some minor chevkinite
    - Rare dark green mineral similar to that observed in slide no. 948537 occurs along the margins of the larger titanite crystals
- Bright yellow mineral found at the contact between the titanite and the allanite – possibly a distinct zone in the allanite rather than a separate mineral

Sample No. 881216 – Diopside-Allanite Vein

Location DDH HL05-58 at 25.9 m.
Hand Specimen Description

- Diopside-allanite vein cross cut by coarse red apatite.

Mineralogy

Apatite	20%	8 mm to 0.5 mm
Diopside	20%	4 mm to 0.2 mm
Barite	17%	5 mm to 0.5 mm
Calcite	15%	2 mm to 0.5 mm
Allanite	10%	10 mm to 0.5 mm
Hornblende	6%	4 mm to 0.2 mm
Hematite	4%	< 0.1 mm
Feldspar	3%	2 mm to 0.2 mm
Chlorite	2%	< 0.1 mm
Pyrite	2%	< 0.1 mm
Fluorite	1%	< 0.1 mm

Description

- Diopside-allanite section of the vein is highly fractured and somewhat altered
    - Irregular, vuggy spaces are common and are frequently filled or lined with calcite or opaques
    - Alteration of the diopside to hornblende is common, particularly along fractures and crystal boundaries
    - Rare subhedral to euhedral primary hornblende
    - Allanit in this vein occurs as large, typically greater than 4 mm, anhedral, zoned crystals
    - Allanite is often poikiolitic with inclusions of diopside, hornblende and opaques
    - Centers of allanites often show an odd yellowish color with anomalous birefringence
- Contact between the diopside-allanite vein and the cross cutting apatite vein is not as clean as in other samples
    - Boundary is ragged and almost brecciated in appearance
    - Lacks the allanite at the contact as observed in other samples- instead a red bladed to fibrous radiating mineral tentatively identified as barite
    - Clusters of radiating minerals often greater than 4 mm in size
- Apatite occurs as large subhedral crystals which often have a slightly rounded or resorbed appearance
    - Inclusion of allanite and hornblende, possible xenoliths from the earlier vein generation
- Apatite vein also contains euhedral to subhedral calcite and minor amounts of fluorite and chlorite

- Entire sample is cross cut by hematitic fractures or small veinlets of calcite

Sample No. 881275B -

Location DDH HL05-32 at 54.2 m.

Hand Specimen Description

- Diopside-allanite vein cross cut by a late apatite vein. Allanite common at the contact between the two vein generations.

Mineralogy

Diopside	65%	20 mm to 1 mm
Apatite	10%	4 mm to 0.2 mm
Hornblende	10%	1 mm to 0.5 mm
Allanite	8%	> 10 mm to 1 mm
Titanite	2%	3 mm to 0.5 mm
Calcite	2%	< 0.1 mm
Epidote	1%	< 0.2 mm
Pyrite	1%	< 0.1 mm
Hematite	1%	< 0.1 mm

Description

- Sample is dominantly subhedral diopside with some minor alteration to hornblende
    - Diopside is mildly poikiolitic with inclusions of allanite, titanite, and pyrite
    - Some open, vuggy spaces in the diopside appear to be due to fracturing and are often filled with calcite or epidote
    - Rare allanite inclusions appear embayed and show strong, euhedral concentric zoning
- Large, anhedral allanites are strongly zoned
    - Concentric zoning is distinctly different than that observed in the allanite inclusion – the zonation is much more irregular and ragged in appearance
    - Small inclusions of titanite and diopside are common
- Large, subhedral hornblende crystals, rarely up to 4 mm in size, occur in the diopside rich areas
    - These crystals do not appear to be the result of alteration
- Hornblende and allanite line the contact between the diopside-allanite section of the sample and the cross cutting apatite vein
- The apatite is coarsely crystalline, typically around 2.5 mm in size, and contains few if any inclusions
    - The inclusions which are present appear to be hematite
    - Apatite is cross-cut by an anastomosing zone of small apatite crystals which appears to be a late vein
- The sample is cross cut by late hematitic fractures

Sample No. 881237 – Diopside-Allanite Vein

Hand Specimen Description

Diopside allanite vein

Mineralogy

Allanite	40%	10 mm to 1 mm
Apatite	15%	3 mm to 1 mm
Hyalophane	14%	2 mm to 0.5 mm
Diopside	12%	3 mm to 1mm
Hornblende	8%	< 1 mm
Titanite	5%	6 mm to 1 mm
Hematite	4%	< 0.2 mm
Pyrite	1%	< 0.2 mm
Epidote	1%	< 0.2 mm

Description

- Apatite in this slide is of the dark red variety and occurs in close association with the allanite and titanite
    - The apatite is inclusion rich with two distinct varieties of inclusion
    - Reddish inclusions appear to be hematite
    - The small bright inclusions are likely monazite
- Titanite occurs as subhedral crystals and is commonly found as an inclusion in allanite
- Majority of the hornblende present in the slide is the result of alteration to the diopside and occurs as anhedral patches within the diopside
    - Some subhedral to euhedral hornblende appear to be primary
- Hyalophane is typically turbid in appearance
    - Hematitic fractures and crystal boundaries are common
    - Moderate sericitization
    - Hyalophane rich sections display a mosaic texture with small interstial allanites present
- Allanite varies from euhedral to anhedral and from greater than 4 mm to less than 0.5 mm in size
    - Many allanites show a strong concentric zonation while in others the zonation is patchy or irregular
    - Some allanite are essentially unzoned except for epidote-like rims
    - In some areas the allanite occurs as masses of small interlocking crystals
    - Larger crystals contain inclusions of titanite
    - Rare allanite as late, remobilized vein fill
- Cross cutting veinlets of anhedral pyrite are common

Sample No. HL06-75 – Green Apatite Breccia

Location DDH HL06-75 at 67 m.

Hand Specimen Description

- Bright green apatite breccia. Largely clast supported in a fine grained, reddish, carbonate-bearing matrix. Clasts vary from sub-angular to subrounded.

Mineralogy

Apatite	80%	12 mm to 1 mm
Quartz	5%	< 1 mm
Monazite	4%	< 0.1 mm
Epidote	3%	< 0.2 mm
Fluorite	3%	< 0.1 mm
Tremolite	2%	< 0.2 mm
Pyrite	2%	< 0.1 mm
Chlorite	1%	< 0.2 mm

Description

- Sample is dominated by angular to sub-angular clasts of apatite
    - Crackle breccia – in many instances the clasts appear essentially in place with little to no rotation of the clasts
    - Breccia ranges from clasts supported to matrix supported
    - Clasts are typically large, often over 4 mm in size, although there is almost a continous zonation in clast size
    - Rare inclusions of what appears to be metamict allanite can be found in some of the apatites
    - Most apatite clasts are basically inclusion free compared to many of the other samples
    - Rare inclusion rich cores are present in a minor number of clasts
    - The most common inclusion in these clasts appears to be monazite
- Rare crystals of what appears to be subhedral monazite can be found along the edges of the apatite clasts or in the matrix
- Euhedral pyrite also occur at the edges of the clasts and in the matrix and can be up to 2 mm in size
- The matrix of this samples is dominated quartz with minor amounts of fluorite
- Sample is cross-cut by small veins of either pyrite or epidote
- Reddish, iron stained fractures are commmon
- Rare brownish-red radiating mineral appear to be growing into the open vuggy spaces – possibly fine grained barite or some sort of sheet silicate?

Sample No. HS-AL – Diopside-Allanite Vein

Location Hoidas South Main Showing
Hand Specimen Description

- Diopside-allanite vein from Hoidas South cross cut by an apatite-biotite vein.

Mineralogy

Allanite	40%	12 mm to 1 mm
Apatite	25%	8 mm to 1 mm
Feldspar	10%	3 mm to 1 mm
Biotite	10%	3 mm to 0.5 mm
Diopside	10%	4 mm to 1 mm
Titanite (chevkinite)	5%	3 mm to 0.2 mm
Pyrite	Tr	< 0.5 mm

Description

- Diopside-allanite rich section also contains minor amounts of feldspar
    - Feldspars tend to be highly fractured, particularly in crystals near the allanite, and often somewhat iron stained
    - Titanite, and possibly minor chevkinite, occur mainly as inclusions in the allanite
- Contact between the diopside-allanite-hyalophane section and the late apatite vein lined with allanite
    - Minor rounded clasts of allanite occur in the apatite vein near the contact
    - Allanite clasts often surrounded by weak radiating fractures
- Apatite in the vein is quite coarse and typically inclusion free
- Center of the late apatite vein is filled with a mix of biotite, allanite and titanite
    - Biotite is roughly aligned parallel to the vein contacts and shows minor evidence of deformation
    - Allanite is zoned and can contain small subhedral inclusions of titanite and biotite

APPENDIX B

ANALYTICAL TECHNIQUES AND ASSOCIATED DATA

B.1 X-RAY FLUORESCENCE SPECTROMETRY (XRF)

Samples were sent to the Laboratory at SGS Canada Inc. in Lakefield, Ontario for determination of major and minor element concentrations using x-ray fluorescence spectrometry on a fused disc. The detection limit for all major and minor oxides is 0.01%. Trace element concentrations were obtained by x-ray fluorescence spectrometry on a pressed powder pellet. Results of these analyses are provided in Chapter 4 in Tables 4.1 and 4.2. Detection limits for the trace elements are provided below in Table B.1.

Table B.1

Element	Reporting Limits (ppm)		Element	Reporting Limits (ppm)	
	Lower	Upper		Lower	Upper
Ba	10	10000	Rb	2	10000
Sr	2	500	Y	2	500
Nb	2	500	Zr	2	1000

B.2 ELECTRON MICROPROBE TECHNIQUES

Prior to the quantitative WDS the paragenesis of the veins was determined by the observation of macroscopic relationships present in both outcrop and drill core. Polished thin sections of each vein generation were prepared for further petrographic and microprobe analysis. WDS microanalyses of the various ore and gangue minerals was performed at the University of Saskatchewan on a JEOL JXA-8600 Superprobe. On each sample multiple points were analyzed. The results for each of the minerals can be found below.

The minerals were analyzed using an accelerator voltage of 15 kV and a probe current of 50nA. Appropriate preventative measures and procedures, as proposed by Pyle et al. (2002) were utilized to avoid many of the potential problems associated with the analysis of the REE in phosphate. To avoid potential damage to the apatites the beam diameter was set to 10 μm, when crystal size allowed. Comparisons between the relatively unfocused beam used for the majority of the analyses and spot beam analyses showed that no statistically significant variation exist between the two beam diameters. For the analysis of most minerals, except the apatites, 30 s count times were used for all elements; for the apatites the major elements were analyzed using 30 s count times with the count time increasing to 60 s for analysis of the REE. Mineral standards were used for

all major elements and the Smithsonian Reference Standards synthetic REE phosphates were used as standards for the analyses of the REE. When possible, interference free peaks were selected for measurements. The only potential peak overlap which required correction was for that of the Pr L-α_1 peak with the La L-β_1 peak. This correction was conducted in the fashion proposed by Amli and Griffin (1975); this involves subtracting 12.72% of the net counts measured from the La L-α_1 peak position from the net counts recorded from the Pr L-α_1 peak position.

Table B.3 Coarse Red Apatite

Slide #	37933	37933	37933	37933	37933	37933	37933	37933	37933	37933	37933
Point #	89	90	91	92	93	94	95	96	97	98	99
SiO_2	0.50	0.46	0.52	0.16	0.36	0.48	0.84	0.56	0.67	0.57	0.60
ThO_2	0.27	0.03	bdl	0.08	bdl	0.31	bdl	0.25	0.03	bdl	0.24
Y_2O_3	0.12	0.07	0.09	0.10	0.04	0.12	0.08	0.13	0.06	0.20	bdl
La_2O_3	0.07	0.06	0.01	0.05	0.06	bdl	0.23	0.04	0.15	0.14	0.03
Ce_2O_3	0.18	0.24	0.26	0.24	0.48	0.20	0.42	0.09	0.37	0.34	0.40
Pr_2O_3	0.08	0.06	0.09	bdl	0.03	0.16	0.12	bdl	bdl	0.01	0.12
Nd_2O_3	0.51	0.47	0.42	0.01	0.39	0.25	0.63	0.53	0.55	0.45	0.45
Sm_2O_3	0.09	0.17	0.11	0.12	0.04	bdl	0.12	0.08	0.09	0.02	0.12
Gd_2O_3	bdl	0.11	0.17	0.23	0.06	0.04	0.10	bdl	0.11	0.04	0.10
Dy_2O_3	0.11	0.06	bdl	0.07	bdl	0.15	0.02	0.04	0.04	bdl	0.04
CaO	54.10	54.10	54.80	56.83	54.66	53.93	54.30	54.04	52.93	52.81	52.67
SrO	0.74	0.75	0.63	0.74	0.72	0.62	0.59	0.70	0.68	0.76	0.65
BaO	bdl	0.01	bdl	bdl	bdl	bdl	0.01	bdl	bdl	0.08	bdl
P_2O_5	39.95	39.79	40.11	41.02	41.24	40.94	39.38	39.80	39.44	40.12	40.28
SO_3	0.11	0.05	0.14	0.10	0.06	0.08	0.13	0.10	0.12	0.12	0.07
F	3.81	2.27	3.89	3.76	3.67	3.17	2.82	3.69	3.28	3.73	3.13
Cl	0.08	0.01	bdl	0.04	0.03	0.02	0.08	0.02	0.06	bdl	0.09
Total	100.71	98.70	101.25	103.54	101.85	100.48	99.89	100.08	98.58	99.40	98.98

Table B.3 cont.

Slide #	37933	37933	37933	37933	37933	37933	37933	37920	37920	37920	37920
Point #	100	101	102	103	104	105	106	7	13	16	18
SiO_2	0.52	0.50	0.42	0.60	0.54	0.69	0.65	0.65	0.23	0.45	0.31
ThO_2	0.03	bdl	0.14	bdl	bdl	0.10	0.19	0.13	0.11	bdl	bdl
Y_2O_3	0.07	0.14	0.02	0.13	0.15	0.10	0.13	0.15	bdl	bdl	bdl
La_2O_3	0.07	0.03	bdl	bdl	0.02	0.15	0.03	0.18	0.04	bdl	0.02
Ce_2O_3	0.26	0.23	0.11	0.23	0.27	0.42	0.28	0.58	0.14	0.33	0.12
Pr_2O_3	0.04	bdl	0.04	0.06	bdl	0.12	bdl	bdl	0.10	0.16	0.06
Nd_2O_3	0.54	0.37	0.21	0.44	0.35	0.36	0.39	0.36	0.11	0.56	0.31
Sm_2O_3	0.02	0.02	0.02	0.05	0.09	0.06	0.09	0.09	bdl	0.07	bdl
Gd_2O_3	0.18	0.04	0.06	0.15	0.13	0.03	0.05	bdl	0.04	bdl	0.01
Dy_2O_3	0.05	0.05	0.02	0.03	bdl	0.03	0.02	0.07	bdl	0.16	0.24
CaO	53.57	55.93	57.94	54.89	54.29	53.83	53.56	53.16	54.42	54.61	55.01
SrO	0.62	0.61	0.67	0.76	0.68	0.62	0.66	0.67	0.70	0.84	0.72
BaO	bdl	bdl	bdl	bdl	bdl	bdl	bdl	bdl	bdl	bdl	0.05
P_2O_5	40.47	39.56	36.99	40.24	40.22	40.30	40.27	40.17	41.61	40.85	41.36
SO_3	0.17	bdl	0.03	0.19	0.15	0.10	0.10	0.16	0.03	0.27	0.06
F	3.56	2.38	2.57	2.42	2.72	2.32	2.87	2.71	2.65	3.83	3.59
Cl	bdl	0.03	0.07	0.03	0.04	0.04	bdl	0.16	0.05	0.07	0.05
Total	100.19	99.87	99.31	100.22	99.65	99.27	99.29	99.23	100.25	102.22	101.91

Table B.3 cont.

Slide #	37920	37920	37920	37920	37920	37920	37920	37920	37920	37920	37920
Point #	21	23	30	32	28	14	22	29	33	31	24
SiO_2	0.57	0.60	0.27	0.38	0.09	0.64	0.59	0.59	0.63	0.51	0.94
ThO_2	0.12	0.08	bdl	bdl	0.03	0.23	0.07	bdl	0.16	0.05	0.06
Y_2O_3	0.06	bdl	0.05	0.09	0.03	0.17	0.09	0.11	0.11	0.02	0.19
La_2O_3	0.09	0.09	0.08	bdl	0.03	bdl	bdl	0.14	0.04	0.19	0.03
Ce_2O_3	0.37	0.29	0.21	0.29	bdl	0.52	0.49	0.37	0.41	0.20	0.53
Pr_2O_3	0.26	bdl	0.08	0.08	0.03	bdl	0.07	0.08	0.10	0.02	0.26
Nd_2O_3	0.27	0.23	0.21	0.58	0.36	0.41	0.47	0.38	0.54	0.51	0.74
Sm_2O_3	bdl	bdl	0.05	0.12	0.04	0.08	bdl	0.08	0.07	0.04	bdl
Gd_2O_3	0.14	0.02	bdl	0.04	bdl	0.16	0.01	bdl	bdl	bdl	bdl
Dy_2O_3	0.02	bdl	0.27	bdl	0.04	0.16	0.31	0.02	0.01	bdl	0.04
CaO	55.25	53.37	56.87	54.10	54.64	54.63	54.94	54.79	53.73	54.24	52.91
SrO	0.72	0.68	0.70	0.76	0.70	0.68	0.66	0.78	0.73	0.71	0.62
BaO	bdl	bdl	bdl	bdl	0.01	bdl	bdl	0.06	bdl	bdl	bdl
P_2O_5	40.55	39.52	39.58	40.83	40.45	40.34	40.57	40.13	39.83	39.88	39.59
SO_3	0.12	0.18	0.05	0.05	0.15	0.32	0.08	0.12	0.31	0.24	0.13
F	2.20	2.56	2.64	3.61	3.72	2.98	2.50	3.41	3.30	2.38	3.01
Cl	0.10	0.09	0.07	0.11	0.08	0.11	0.08	0.11	0.12	0.12	0.11
Total	100.84	97.72	101.13	101.05	100.39	101.42	100.94	101.18	100.10	99.11	99.15

Table B.4 Green Apatite

Slide #	37906	37906	37906	37906	37906	37906	37906	37906	37906	37906
Point #	3	7	8	22	24	28	31	33	35	36
SiO_2	2.39	2.38	2.10	2.53	2.17	2.33	2.38	2.44	2.22	1.88
ThO_2	0.22	0.16	0.34	0.09	0.42	bdl	bdl	bdl	0.12	0.47
Y_2O_3	0.07	0.03	0.16	0.04	0.11	0.30	0.08	bdl	0.09	bdl
La_2O_3	1.23	1.14	0.97	1.15	0.57	0.49	1.24	0.83	1.41	bdl
Ce_2O_3	3.71	3.03	2.44	3.11	2.69	2.84	3.25	2.01	0.99	1.87
Pr_2O_3	0.36	0.29	0.37	0.23	0.36	0.26	0.39	0.11	0.43	0.25
Nd_2O_3	1.39	1.04	1.46	2.26	1.87	1.59	1.23	0.74	0.99	0.84
Sm_2O_3	bdl	0.08	0.02	0.12	0.13	0.18	bdl	0.15	0.43	0.08
Gd_2O_3	bdl	0.14	0.02	0.24	0.13	0.12	bdl	0.12	0.04	bdl
Dy_2O_3	bdl	0.03	0.05	0.38	bdl	bdl	bdl	0.05	bdl	0.03
CaO	48.38	48.86	49.06	47.61	49.72	49.90	48.49	49.84	50.07	50.15
SrO	1.30	1.42	1.37	0.88	0.85	0.82	1.39	1.05	0.99	1.02
BaO	bdl	bdl	bdl	bdl	bdl	bdl	bdl	bdl	0.02	bdl
P_2O_5	36.78	37.26	36.61	36.87	38.06	38.17	36.96	37.73	37.21	38.99
SO_3	0.56	0.32	0.51	0.28	0.13	0.12	0.24	0.14	0.20	0.10
F	3.54	3.83	3.57	3.35	3.51	3.48	3.22	2.56	2.78	3.58
Cl	0.30	0.26	0.29	0.12	0.07	0.13	0.30	0.16	0.16	0.14
Total	100.24	100.26	99.34	99.27	100.79	100.74	99.16	97.94	98.15	99.39

Table B.4 cont.

Slide #	HL06-75	HL06-75	HL06-75	HL06-75	HL06-75	HL06-75	HL06-75	HL06-75	HL06-75	HL06-75
Point #	4	5	6	7	8	9	10	11	12	13
SiO_2	1.14	1.63	1.57	0.99	0.69	1.42	1.29	1.50	1.01	0.91
ThO_2	0.13	0.02	0.29	bdl	bdl	bdl	bdl	bdl	bdl	bdl
Y_2O_3	0.02	0.14	0.05	0.24	0.21	0.26	0.11	0.10	0.17	bdl
La_2O_3	0.23	0.58	bdl	0.49	0.87	0.38	1.51	0.68	0.56	bdl
Ce_2O_3	1.29	1.80	1.77	1.32	1.42	1.94	1.71	1.81	1.01	3.35
Pr_2O_3	0.22	0.27	0.64	0.15	0.18	0.35	0.02	bdl	0.09	bdl
Nd_2O_3	1.24	1.89	2.27	1.41	2.10	2.06	1.43	2.31	2.41	0.03
Sm_2O_3	0.16	0.19	bdl	0.05	bdl	0.70	0.32	bdl	0.05	bdl
Gd_2O_3	-	-	-	-	-	-	-	-	-	-
Dy_2O_3	0.06	bdl	0.07	bdl	bdl	0.30	0.04	bdl	bdl	0.77
CaO	52.37	51.16	50.65	52.02	40.95	52.82	52.56	52.90	54.13	54.48
SrO	1.01	1.04	0.84	1.03	0.61	0.73	0.79	0.80	0.90	0.81
BaO	-	-	-	-	-	-	-	-	-	-
P_2O_5	37.67	36.00	37.72	38.58	37.91	37.05	36.51	37.80	37.73	38.68
SO_3	-	-	-	-	-	-	-	-	-	-
F	4.05	3.88	4.00	4.36	3.39	3.64	3.51	3.53	3.56	3.13
Cl	0.23	0.32	0.26	0.15	0.27	0.15	0.11	0.17	0.09	0.10
Total	99.94	99.03	100.21	100.87	88.77	101.89	100.07	101.74	101.80	102.32

Tabel B.4 cont.

Slide #	HL06-75	HL06-75	HL06-75	HL06-75	HL06-75	HL06-75	HL06-75
Point #	14	15	16	17	18	21	22
SiO_2	0.94	1.35	1.43	1.41	1.31	1.52	1.57
ThO_2	0.06	bdl	bdl	0.17	0.10	0.04	0.01
Y_2O_3	0.02	0.20	0.02	0.14	0.13	0.10	bdl
La_2O_3	1.30	0.50	2.83	0.10	0.39	0.64	1.86
Ce_2O_3	0.93	1.94	1.70	2.95	1.15	2.12	2.47
Pr_2O_3	0.17	bdl	bdl	0.07	0.16	bdl	0.29
Nd_2O_3	1.45	1.59	1.37	1.47	1.79	1.56	1.65
Sm_2O_3	0.12	bdl	bdl	0.04	bdl	0.42	bdl
Gd_2O_3	-	-	-	-	-	-	-
Dy_2O_3	0.01	bdl	bdl	0.27	0.02	2.61	bdl
CaO	53.81	53.17	52.85	51.32	53.07	51.76	50.16
SrO	0.88	0.87	0.91	0.99	0.92	1.14	1.15
BaO	-	-	-	-	-	-	-
P_2O_5	37.83	31.59	32.09	32.93	36.10	37.45	35.71
SO_3	-	-	-	-	-	-	-
F	3.97	4.73	3.15	3.48	3.28	3.96	4.11
Cl	0.10	0.14	0.14	0.14	0.10	0.33	0.31
Total	101.73	96.24	96.61	95.63	98.66	103.81	99.45

Table B.5 Red Apatite Breccia

Slide #	37903	37903	37903	37903	37903	37903	37903	37903	37903	37903	37903	37903
Point #	35	37	38	39	40	54	55	56	57	58	59	63
SiO_2	1.94	1.83	1.80	1.92	2.08	1.98	1.93	1.96	1.78	1.31	1.86	1.67
ThO_2	0.18	0.06	0.18	0.08	0.14	0.23	0.21	0.02	bdl	0.07	0.04	0.14
Y_2O_3	0.11	bdl	0.15	bdl	0.20	0.14	0.08	0.16	0.05	0.10	0.02	0.10
La_2O_3	0.50	0.75	0.49	0.52	0.54	0.49	0.84	0.38	0.72	0.43	0.66	0.72
Ce_2O_3	1.92	1.87	1.71	1.75	1.99	1.25	1.96	1.48	1.85	0.89	1.81	1.79
Pr_2O_3	0.24	0.16	0.28	0.26	0.20	0.17	0.12	0.12	0.07	0.11	0.27	0.38
Nd_2O_3	1.17	1.09	1.10	1.18	1.67	1.11	1.32	1.25	1.33	0.66	1.39	1.44
Sm_2O_3	bdl	0.18	0.08	0.10	0.10	0.16	0.09	0.17	0.12	bdl	0.09	0.09
Gd_2O_3	0.14	bdl	0.13	0.03	0.10	bdl	0.07	0.07	Bdl	bdl	0.18	0.02
Dy_2O_3	bdl	bdl	0.01	bdl	0.07	0.15	0.09	0.03	0.06	0.01	0.03	0.04
CaO	49.47	50.69	51.57	50.70	50.33	51.34	51.67	52.17	51.99	53.49	52.06	52.49
SrO	0.86	0.81	0.85	0.82	0.82	0.69	0.71	0.74	0.84	0.86	0.70	0.68
BaO	bdl	bdl	bdl	bdl	bdl	bdl	bdl	bdl	Bdl	bdl	bdl	bdl
P_2O_5	36.85	37.15	37.24	37.28	37.12	36.85	37.28	36.66	37.70	38.38	36.64	38.42
SO_3	0.39	0.46	0.58	0.49	0.42	0.25	0.24	0.22	0.29	0.21	0.33	0.18
F	3.56	3.56	3.88	3.61	3.82	2.77	3.23	3.35	3.03	3.66	3.08	2.65
Cl	0.22	0.22	0.20	0.14	0.21	0.16	0.15	0.23	0.15	0.16	0.19	0.13
Total	97.53	98.84	100.27	98.88	99.82	97.76	100.03	99.01	99.97	100.33	99.36	100.95

Table B.5 cont.

Slide #	37903	37903	37903	37903	37903	37903	37903	37903	37903	37903	37903	37903
Point #	66	67	69	71	73	74	75	76	77	81	82	84
SiO_2	1.64	1.54	1.63	2.21	1.92	1.72	1.58	1.66	1.41	1.36	1.37	1.77
ThO_2	0.20	bdl	bdl	bdl	0.13	0.11	bdl	bdl	0.07	0.28	0.13	0.03
Y_2O_3	0.16	0.24	0.09	0.04	0.04	0.03	0.10	bdl	0.05	0.13	0.12	0.21
La_2O_3	0.42	0.61	0.42	0.71	0.69	0.40	0.61	0.41	0.57	0.47	0.40	0.43
Ce_2O_3	1.23	1.68	1.79	2.10	1.95	1.19	1.70	1.22	1.70	1.28	1.00	1.62
Pr_2O_3	0.25	0.26	0.29	0.12	0.23	0.29	0.11	0.14	0.05	0.23	0.16	0.16
Nd_2O_3	1.25	1.32	1.29	1.44	1.37	0.79	1.11	0.63	0.89	0.84	0.70	1.14
Sm_2O_3	0.21	0.05	0.23	0.08	0.16	0.13	0.07	0.07	0.12	0.16	0.22	0.12
Gd_2O_3	bdl	0.04	0.10	0.13	0.03	bdl	0.07	bdl	bdl	0.04	0.13	bdl
Dy_2O_3	0.01	0.09	0.01	0.04	0.01	0.04	0.06	0.08	bdl	0.04	bdl	0.04
CaO	54.21	52.83	53.80	50.21	50.17	52.01	52.08	52.93	52.66	52.39	51.91	52.96
SrO	0.73	0.73	0.88	0.64	0.66	0.78	0.72	0.77	0.71	0.74	0.73	0.83
BaO	bdl	bdl	bdl	bdl	0.25	bdl	bdl	bdl	bdl	0.07	0.12	bdl
P_2O_5	37.52	38.18	38.15	36.22	36.74	37.99	37.42	38.08	37.65	38.82	37.96	37.40
SO_3	0.08	bdl	0.14	0.33	0.35	0.39	0.21	0.23	0.38	0.19	0.12	0.31
F	3.43	3.73	2.83	3.13	2.98	3.03	3.23	3.06	3.33	2.89	2.78	3.94
Cl	0.19	0.14	0.11	0.15	0.15	0.18	0.10	0.12	0.13	0.13	0.13	0.18
Total	101.53	101.45	101.74	97.56	97.82	99.08	99.18	99.38	99.72	100.07	97.95	101.12

Table B.5 cont.

Slide #	37903	37903	37903	37903	37903	37903	37920	37920	37920	37920	37920	37920
Point #	85	87	88	36	50	34	3	5	4	9	10	11
SiO_2	1.76	1.47	1.50	2.03	1.54	1.65	1.27	1.12	1.07	1.05	1.21	1.12
ThO_2	bdl	bdl	bdl	0.02	0.19	bdl	0.27	bdl	0.05	0.19	bdl	bdl
Y_2O_3	0.09	0.09	0.13	0.16	bdl	0.14	0.08	0.06	0.25	0.08	0.01	0.06
La_2O_3	0.60	0.39	0.58	0.43	0.48	0.44	0.30	0.27	0.23	bdl	0.21	0.17
Ce_2O_3	1.68	1.34	1.47	1.94	1.52	1.52	0.87	0.85	0.92	0.67	1.19	0.80
Pr_2O_3	0.31	0.02	0.35	0.32	0.08	0.07	0.26	0.20	0.17	bdl	0.17	0.05
Nd_2O_3	1.10	0.98	1.03	1.54	1.24	1.02	0.71	0.56	0.79	0.58	0.81	0.64
Sm_2O_3	0.20	0.10	0.13	0.13	0.15	0.20	0.04	0.11	bdl	0.05	0.10	bdl
Gd_2O_3	0.03	0.09	0.12	bdl	0.14	0.16	0.04	bdl	0.06	0.02	0.01	bdl
Dy_2O_3	0.01	0.03	bdl	bdl	0.09	0.07	0.04	0.01	0.05	bdl	0.11	bdl
CaO	52.82	52.46	52.05	50.39	51.04	51.36	53.48	55.18	52.61	51.75	53.38	53.22
SrO	0.87	0.65	0.78	0.81	0.80	0.76	0.74	0.75	0.70	0.68	0.68	0.70
BaO	bdl	0.10	bdl	bdl	bdl	bdl	bdl	0.03	0.17	bdl	bdl	bdl
P_2O_5	37.76	38.29	38.38	36.65	38.10	38.05	30.50	39.06	38.72	38.26	38.20	38.85
SO_3	0.36	0.26	0.17	0.66	0.14	0.34	0.37	0.21	0.11	0.19	0.06	0.23
F	3.69	2.65	3.53	3.50	3.93	3.57	1.78	2.63	2.81	2.89	2.84	2.32
Cl	0.15	0.14	0.08	0.19	0.15	0.20	0.09	0.13	0.09	0.10	0.11	0.18
Total	101.42	99.06	100.30	98.77	99.59	99.54	90.84	101.15	98.80	96.50	99.10	98.35

Table B.5 cont.

Slide #	37920	37920	37920	37920	37920	37920	37920	37920	37920	37920	37920
Point #	20	26	8	17	19	15	25	1	2	27	6
SiO_2	0.59	1.00	1.16	0.93	1.24	1.27	1.17	0.75	0.71	0.63	0.44
ThO_2	bdl	0.03	bdl	bdl	bdl	0.21	bdl	0.13	0.14	0.13	bdl
Y_2O_3	bdl	0.08	0.08	0.05	0.12	0.20	0.23	0.04	0.07	0.12	0.02
La_2O_3	bdl	bdl	0.33	0.29	0.34	0.22	0.18	0.14	0.33	0.19	0.13
Ce_2O_3	0.32	0.80	1.18	0.80	0.78	0.43	0.60	0.72	0.60	0.30	0.46
Pr_2O_3	0.07	0.13	0.14	0.08	0.04	0.09	0.03	0.15	0.19	0.08	bdl
Nd_2O_3	0.83	0.87	0.83	0.68	0.96	0.66	0.81	0.54	0.35	0.45	0.50
Sm_2O_3	0.15	0.10	0.15	bdl	0.07	bdl	0.07	0.07	bdl	0.25	bdl
Gd_2O_3	0.01	bdl	bdl	bdl	0.17	0.17	0.10	bdl	0.03	0.06	0.02
Dy_2O_3	0.18	0.03	0.11	0.03	0.04	0.07	0.14	0.02	bdl	0.04	bdl
CaO	55.20	53.20	51.61	53.11	53.92	53.24	54.17	55.90	54.42	53.85	55.44
SrO	0.84	0.69	0.71	0.80	0.75	0.59	0.65	0.82	0.79	0.67	0.70
BaO	bdl	bdl	bdl	bdl	bdl	bdl	bdl	bdl	bdl	bdl	bdl
P_2O_5	40.53	38.91	38.14	39.50	39.26	38.02	38.38	33.83	32.14	40.19	41.09
SO_3	0.17	0.24	0.18	0.36	0.14	0.11	0.32	0.03	0.19	0.17	bdl
F	3.56	2.80	2.86	3.26	3.31	2.94	2.77	1.80	1.69	2.87	2.83
Cl	0.09	0.09	0.13	0.19	0.11	0.09	0.13	0.14	0.11	0.09	0.12
Total	102.52	98.97	97.62	100.06	101.23	98.32	99.74	95.09	91.77	100.10	101.75

Table B.6 Allanite

Pt#	HS-AL 1	HS-AL 2	HS-AL 3	HS-AL 4	HS-AL 5	HS-AL 6	HS-AL 7	HS-AL 8	HS-AL 9	HS-AL 10	HS-AL 11
SiO_2	32.61	33.34	33.13	30.58	32.77	32.68	33.13	33.57	32.43	32.66	33.10
TiO_2	0.59	0.39	0.58	0.59	0.55	0.42	0.63	0.46	0.38	0.59	0.68
ThO_2	0.27	0.51	0.84	0.67	0.71	0.60	0.30	0.63	0.42	0.64	0.77
Al_2O_3	17.07	16.91	16.67	15.56	17.01	16.89	17.03	15.88	15.82	16.05	15.41
La_2O_3	4.92	5.49	5.29	5.26	5.27	5.42	5.31	5.02	5.08	4.69	3.92
Ce_2O_3	11.88	12.21	12.38	11.89	11.95	12.19	11.70	11.95	11.15	10.84	10.14
Pr_2O_3	1.67	1.38	1.49	1.15	1.76	1.43	1.35	1.23	1.26	1.46	0.98
Nd_2O_3	4.23	4.59	4.72	4.71	4.65	4.83	4.44	4.67	4.39	4.28	3.72
Sm_2O_3	bdl	bdl	bdl	bdl	bdl	bdl	bdl	bdl	bdl	bdl	0.22
Dy_20_3	0.01	0.02	0.03	0.07	bdl	0.09	bdl	0.06	bdl	bdl	bdl
FeO	11.62	12.32	11.62	8.61	8.10	9.35	8.46	12.19	10.56	10.37	11.06
MgO	2.34	1.93	2.49	1.49	1.31	1.32	1.64	1.11	0.85	0.72	1.17
MnO	0.20	0.19	0.21	0.16	0.15	0.16	0.12	0.32	0.20	0.18	0.28
CaO	11.29	11.03	11.16	11.05	11.28	11.04	11.18	11.13	11.61	11.67	9.60
SrO	bdl	bdl	bdl	0.13	0.26	0.21	0.34	0.49	0.47	0.61	0.11
BaO	bdl	bdl	bdl	bdl	bdl	bdl	bdl	bdl	bdl	bdl	bdl
SO_3	0.05	0.01	0.05	bdl	bdl	0.06	0.02	0.05	0.07	0.11	0.06
P_2O_5	bdl	0.09	bdl	0.15	bdl	0.05	0.04	bdl	0.06	bdl	0.04
Cl	0.03	bdl	0.01	0.79	0.80	0.72	0.72	0.39	0.45	0.73	0.33
F	bdl	bdl	bdl	bdl	bdl	bdl	bdl	bdl	bdl	bdl	bdl
Total	98.76	100.39	100.69	92.89	96.57	97.47	96.41	99.15	95.22	95.58	91.60

Table B.6 cont.

Pt#	HS-AL 12	HS-AL 14	HS-AL 15	HS-AL 16	HS-AL 17	HS-AL 18	HS-AL 19	HS-AL 20	HS-AL 22	HS-AL 23	HS-AL 26
SiO_2	34.67	30.53	31.75	32.09	31.70	32.48	33.52	30.81	32.55	31.81	29.48
TiO_2	0.65	0.48	0.59	0.58	0.55	0.65	0.72	0.42	0.63	0.59	31.38
ThO_2	1.17	0.38	0.62	0.37	0.59	0.50	0.42	0.18	0.38	0.49	bdl
Al_2O_3	17.17	13.95	14.45	15.27	13.94	15.19	14.85	14.57	15.27	14.34	3.69
La_2O_3	5.99	4.28	4.46	3.91	4.56	4.71	4.19	4.57	3.24	4.09	0.23
Ce_2O_3	14.28	10.21	9.88	9.95	10.22	11.34	10.23	10.69	8.73	9.36	1.03
Pr_2O_3	1.64	1.24	0.84	0.31	1.19	1.27	1.33	1.20	1.20	1.04	0.29
Nd_2O_3	5.21	4.00	3.89	3.94	3.38	4.22	3.78	3.84	3.72	3.53	1.95
Sm_2O_3	0.14	0.02	0.05	0.15	0.05	0.15	0.05	0.22	0.15	0.09	0.43
Dy_20_3	0.02	bdl	bdl	0.04	bdl	bdl	0.10	bdl	bdl	bdl	0.22
FeO	6.37	12.76	11.13	11.36	11.08	10.71	10.00	10.69	12.25	12.44	1.91
MgO	0.51	0.56	0.83	1.07	1.18	1.54	1.68	1.94	1.09	0.72	0.19
MnO	0.14	0.36	0.21	0.27	0.29	0.17	0.18	0.22	0.18	0.15	0.04
CaO	5.17	11.93	11.48	11.46	11.58	9.19	11.86	10.91	12.21	12.12	24.58
SrO	bdl	0.70	0.25	0.45	0.40	0.19	0.11	0.37	0.52	0.49	bdl
BaO	0.16	bdl	bdl	bdl	bdl	bdl	bdl	bdl	bdl	bdl	0.91
SO_3	0.10	0.03	bdl	0.17	0.02	bdl	0.10	0.08	0.15	0.12	bdl
P_2O_5	0.05	0.12	0.05	bdl	bdl	0.06	bdl	0.09	bdl	0.29	0.18
Cl	0.07	0.63	0.60	0.67	0.60	0.54	0.34	0.45	0.47	0.53	0.01
F	bdl	bdl	bdl	bdl	bdl	bdl	bdl	bdl	bdl	bdl	0.91
Total	93.51	92.17	91.07	92.07	91.36	92.90	93.46	91.26	92.73	92.20	97.40

Table B.6 cont.

Pt#	HS-AL 27	HS-AL 30	HS-AL 31	HS-AL 32	HS-AL 33	HS-AL 34	HS-AL 35	HS-AL 37	HS-AL 38	HS-AL 40	HS-AL 41
SiO_2	31.17	32.34	33.82	29.27	33.01	34.93	34.29	31.80	30.67	32.41	32.16
TiO_2	0.51	1.07	0.98	1.14	0.82	1.18	1.21	0.70	0.51	0.60	0.57
ThO_2	0.10	0.48	0.61	0.74	0.53	0.63	0.44	0.43	0.21	0.40	0.36
Al_2O_3	14.59	14.40	14.43	12.86	15.47	14.87	13.70	14.68	13.31	15.72	15.75
La_2O_3	4.26	4.94	5.65	7.34	6.22	5.30	6.38	5.04	6.74	6.40	4.79
Ce_2O_3	11.08	11.54	13.29	15.09	11.54	10.20	12.10	10.34	13.31	12.25	10.85
Pr_2O_3	0.58	1.16	1.44	1.46	1.07	0.78	1.07	0.98	1.35	1.20	1.29
Nd_2O_3	3.75	4.41	4.73	4.91	3.39	2.93	3.35	3.59	3.95	3.74	3.79
Sm_2O_3	0.17	0.13	0.21	0.22	bdl	0.04	bdl	0.10	0.02	0.01	0.07
Dy_2O_3	bdl	bdl	bdl	bdl	bdl	bdl	bdl	bdl	bdl	bdl	bdl
FeO	12.51	11.06	9.29	8.29	11.59	11.56	9.47	11.03	12.82	11.11	11.81
MgO	1.11	0.61	0.88	1.66	0.87	1.55	0.43	1.02	0.83	1.97	2.08
MnO	0.25	0.45	0.39	0.32	0.60	0.63	0.54	0.34	0.26	0.08	0.16
CaO	11.58	9.25	7.09	6.57	7.85	8.25	8.33	12.75	9.67	11.49	11.25
SrO	0.29	0.17	bdl	bdl	0.10	0.08	0.10	0.27	0.08	bdl	bdl
BaO	bdl	0.54	0.94	0.58	1.33	1.13	0.99	bdl	bdl	bdl	bdl
SO_3	bdl	bdl	0.05	0.02	0.27	0.07	bdl	0.09	0.14	0.02	bdl
P_2O_5	bdl	bdl	0.09	bdl	0.09	0.04	0.12	bdl	bdl	0.06	0.03
Cl	0.44	0.13	0.06	0.08	0.16	0.10	0.07	0.69	0.30	bdl	0.04
F	bdl	bdl	bdl	0.60	bdl	bdl	bdl	bdl	bdl	bdl	bdl
Total	92.40	92.70	93.96	91.13	94.89	94.28	92.59	93.85	94.18	97.49	95.00

Table B.6 cont.

Pt#	HS-AL 42	HS-AL 44	HS-AL 45	HS-AL 46	HS-AL 47	HS-AL 48	HS-AL 49	HS-AL 53	HS-AL 54	HS-AL 55	948537 59
SiO_2	32.51	33.18	32.81	32.24	32.25	32.50	31.13	32.73	31.52	31.36	32.00
TiO_2	0.64	0.64	0.66	0.71	0.56	0.56	0.69	0.64	0.61	0.44	0.72
ThO_2	0.31	0.29	0.59	0.32	0.71	0.46	0.91	0.67	0.53	0.13	0.61
Al_2O_3	15.78	16.21	16.16	15.69	16.05	15.87	14.17	16.21	15.35	14.74	14.74
La_2O_3	5.14	5.15	5.38	5.20	4.81	4.45	5.09	4.82	4.92	4.72	6.04
Ce_2O_3	10.98	10.71	10.93	11.81	10.66	10.41	11.19	11.12	10.61	10.92	10.99
Pr_2O_3	0.98	1.10	1.12	1.08	1.00	0.98	1.25	1.41	0.99	1.34	1.08
Nd_2O_3	3.64	3.72	3.54	4.22	3.43	3.68	4.09	3.79	3.79	4.04	3.13
Sm_2O_3	0.10	0.08	0.04	0.11	0.11	0.05	0.16	0.17	0.09	0.16	bdl
Dy_2O_3	bdl	bdl	0.07	bdl	bdl	bdl	bdl	bdl	bdl	bdl	0.11
FeO	12.55	11.83	6.37	6.05	9.88	11.25	13.41	9.95	11.65	12.36	10.90
MgO	1.89	2.15	0.36	0.28	2.23	1.80	1.33	1.44	2.14	1.17	0.72
MnO	0.12	0.14	bdl	bdl	0.09	0.15	0.08	0.12	0.08	0.17	0.19
CaO	11.24	11.50	10.59	10.67	11.23	11.99	11.19	11.49	11.23	11.10	10.17
SrO	bdl	bdl	0.16	0.12	0.09	0.34	0.11	0.17	bdl	0.21	0.25
BaO	bdl	bdl	bdl	bdl	bdl	bdl	bdl	bdl	bdl	bdl	bdl
SO_3	bdl	bdl	0.11	0.16	bdl	bdl	0.15	0.07	0.04	bdl	0.19
P_2O_5	0.09	bdl	bdl	bdl	bdl	bdl	bdl	0.11	0.02	0.10	0.08
Cl	bdl	bdl	0.62	0.92	0.81	0.53	0.54	0.73	0.03	0.50	0.44
F	bdl	bdl	bdl	bdl	bdl	bdl	bdl	bdl	bdl	bdl	bdl
Total	95.99	96.70	89.51	89.57	93.91	95.00	95.49	95.64	93.60	93.45	92.36

Table B.6 cont.

Pt#	948537 60	948537 63	948537 64	948537 65	948537 66	948537 74	948537 75	948537 76	948537 80	948537 81	948537 82
SiO_2	32.74	30.57	34.27	30.84	35.22	32.58	32.77	33.50	31.69	30.27	33.01
TiO_2	0.11	0.46	0.05	0.14	0.88	bdl	0.06	0.50	0.55	0.54	0.05
ThO_2	0.57	0.52	0.28	0.28	0.51	0.26	0.08	0.67	0.44	0.53	0.27
Al_2O_3	16.60	14.21	17.77	14.84	14.81	17.27	16.89	15.67	14.85	15.24	17.70
La_2O_3	3.59	5.49	3.22	5.73	5.50	2.92	3.62	4.64	6.33	5.92	4.04
Ce_2O_3	6.07	10.30	4.68	10.01	9.83	5.32	6.66	8.78	11.11	10.75	6.67
Pr_2O_3	0.74	0.90	0.48	0.71	1.17	0.32	0.80	1.04	1.02	1.22	0.53
Nd_2O_3	1.66	2.74	1.32	3.02	3.02	1.53	1.85	2.51	3.31	2.92	1.83
Sm_2O_3	bdl	bdl	bdl	bdl	bdl	bdl	bdl	0.09	0.02	bdl	bdl
Dy_2O_3	0.06	bdl	bdl	bdl	bdl	bdl	bdl	bdl	bdl	bdl	bdl
FeO	12.28	13.28	13.74	12.71	9.63	12.76	13.11	10.65	12.84	11.21	12.80
MgO	0.42	1.21	1.03	0.52	0.52	0.22	0.27	0.49	1.66	1.27	0.25
MnO	0.27	0.23	0.25	0.26	0.37	0.25	0.17	0.20	0.12	0.12	0.15
CaO	13.79	11.22	13.91	12.11	7.67	15.72	14.60	8.68	11.16	12.26	13.92
SrO	1.12	0.50	1.59	0.55	0.14	1.26	1.12	0.18	bdl	0.36	1.03
BaO	0.58	bdl	bdl	bdl	2.08	bdl	bdl	2.01	bdl	bdl	0.15
SO_3	0.04	0.28	0.11	0.16	0.04	0.05	0.09	0.08	bdl	0.03	0.21
P_2O_5	0.04	0.08	0.07	0.07	0.04	0.01	0.04	bdl	0.01	0.08	bdl
Cl	0.39	0.61	0.54	0.62	0.10	0.66	0.46	0.29	0.02	0.67	0.40
F	bdl	bdl	bdl	bdl	bdl	bdl	bdl	bdl	bdl	bdl	bdl
Total	91.06	92.59	93.31	92.56	91.52	91.14	92.61	89.98	95.14	93.41	92.99

Table B.6 cont.

Pt#	948537 87	782076 1	782076 5	782076 8	782076 11	782076 12	782076 17	782076 21	782076 22	782076 23	782076 24
SiO_2	29.81	31.57	27.08	30.43	31.22	30.96	30.17	32.00	32.23	32.07	31.11
TiO_2	0.59	0.81	2.95	1.55	2.24	0.31	0.43	8.14	0.93	0.84	0.95
ThO_2	0.36	0.18	1.07	0.60	0.47	bdl	0.02	0.34	0.49	0.43	0.58
Al_2O_3	15.39	14.47	8.92	12.06	12.14	15.65	15.63	8.42	14.38	14.29	14.67
La_2O_3	6.32	6.61	7.23	6.85	5.22	5.98	6.11	7.28	6.07	6.37	6.28
Ce_2O_3	10.58	11.14	10.80	12.46	10.97	11.01	12.82	14.73	11.11	11.20	11.77
Pr_2O_3	0.88	0.75	1.12	1.23	1.12	1.10	1.32	1.18	0.84	1.03	1.07
Nd_2O_3	2.97	2.92	2.91	3.52	3.59	3.45	4.91	4.79	3.00	3.31	3.05
Sm_2O_3	bdl	bdl	bdl	0.03	bdl	0.09	0.25	0.12	bdl	0.05	bdl
Dy_2O_3	bdl	bdl	0.20	bdl	bdl	bdl	bdl	bdl	bdl	bdl	0.05
FeO	12.01	12.71	17.50	12.21	11.78	15.15	14.05	7.93	10.32	11.17	9.86
MgO	1.75	1.79	1.37	0.63	0.54	1.20	0.50	0.42	0.33	0.86	0.51
MnO	0.17	0.10	0.16	0.31	0.25	0.43	0.24	0.29	0.23	0.16	0.18
CaO	11.30	10.43	8.32	9.70	11.13	9.02	10.34	5.03	11.92	11.24	11.49
SrO	bdl	bdl	0.28	0.16	0.18	0.02	bdl	bdl	0.38	0.39	0.25
BaO	bdl	bdl	bdl	bdl	bdl	bdl	bdl	0.83	bdl	bdl	bdl
SO_3	0.01	bdl	bdl	bdl	bdl	0.04	0.01	bdl	0.10	0.02	0.04
P_2O_5	bdl	bdl	bdl	bdl	0.03	0.02	0.10	bdl	0.05	bdl	0.13
Cl	0.64	0.03	0.36	0.50	0.47	0.07	0.01	0.11	0.84	0.62	0.68
F	bdl	bdl	bdl	bdl	bdl	bdl	bdl	bdl	bdl	bdl	bdl
Total	92.78	93.51	90.26	92.21	91.34	94.50	96.90	91.61	93.22	94.06	92.66

Table B.6 cont.

Pt#	782076 25	782076 26	782076 27	782076 28	782076 29	782076 31	782076 38	782076 39	782076 40	782076 41	782076 43
SiO_2	30.26	36.89	31.42	30.63	37.93	31.07	31.61	31.73	31.43	32.10	39.08
TiO_2	0.98	1.25	0.77	0.89	1.35	0.69	0.83	0.79	0.78	0.78	1.31
ThO_2	0.14	0.68	0.26	0.46	1.02	0.51	0.39	0.34	0.09	0.25	0.87
Al_2O_3	14.29	15.49	14.46	14.12	14.25	13.53	14.28	14.36	14.19	14.64	15.20
La_2O_3	7.22	6.08	7.52	6.89	6.52	5.66	6.45	6.32	6.34	6.21	6.08
Ce_2O_3	12.11	11.35	11.28	11.29	13.30	9.62	11.34	11.32	10.87	11.43	13.37
Pr_2O_3	1.20	1.08	1.30	1.07	1.82	1.06	1.09	0.91	0.88	1.18	1.48
Nd_2O_3	3.41	3.59	3.07	bdl	4.64	3.26	3.28	3.46	3.45	3.45	4.80
Sm_2O_3	bdl	0.09	0.05	bdl	0.22	bdl	0.07	bdl	0.01	bdl	0.16
Dy_2O_3	bdl	bdl	bdl	bdl	0.03	bdl	bdl	bdl	bdl	bdl	0.12
FeO	7.96	7.23	13.39	13.54	5.60	12.51	13.04	13.25	10.83	11.05	3.85
MgO	0.68	1.04	1.94	1.85	0.49	1.14	1.89	1.89	1.66	1.63	0.19
MnO	0.03	0.06	0.10	0.14	0.05	0.17	0.12	0.49	0.09	0.04	bdl
CaO	11.24	6.42	11.00	10.76	6.57	11.53	10.16	10.19	11.30	11.08	4.94
SrO	0.11	bdl	bdl	bdl	bdl	0.20	bdl	bdl	0.08	0.14	bdl
BaO	bdl	bdl	bdl	bdl	bdl	bdl	bdl	bdl	bdl	bdl	bdl
SO_3	bdl	0.04	0.04	0.08	bdl	1.00	bdl	bdl	bdl	bdl	0.10
P_2O_5	0.04	0.02	0.02	0.06	0.18	0.09	bdl	0.08	0.05	0.24	0.24
Cl	0.83	0.42	bdl	0.21	0.20	0.73	bdl	0.04	0.63	0.55	0.29
F	bdl	bdl	bdl	bdl	bdl	bdl	bdl	bdl	bdl	bdl	bdl
Total	90.50	91.72	96.62	91.97	94.15	92.76	94.54	95.18	92.69	94.77	92.07

Table B.6 cont.

Pt#	782076 44	782076 46	782076 47	782076 48	782076 49	782076 51	782076 52	782076 53	782076 55	782076 57	782076 58
SiO_2	31.54	31.42	30.83	29.93	31.51	31.42	30.72	31.64	36.76	32.74	30.76
TiO_2	0.91	0.80	0.59	0.82	0.84	0.90	0.98	1.04	2.68	0.89	0.89
ThO_2	0.24	0.26	0.17	0.54	0.43	0.34	0.58	0.69	0.93	0.46	0.31
Al_2O_3	14.17	13.78	13.74	12.73	13.63	14.29	12.61	12.59	14.25	14.45	14.01
La_2O_3	6.05	6.35	6.08	5.56	5.38	7.00	5.80	5.33	5.66	7.58	6.90
Ce_2O_3	11.49	11.79	11.49	10.94	9.88	11.70	11.44	10.70	11.50	12.30	11.22
Pr_2O_3	0.93	1.06	1.09	1.12	0.94	0.94	1.24	1.28	1.29	1.11	0.85
Nd_2O_3	3.35	3.36	3.26	3.22	2.88	3.05	3.97	3.69	4.12	3.49	3.00
Sm_2O_3	0.06	0.12	bdl	bdl	bdl	bdl	bdl	0.13	0.20	0.05	0.05
Dy_2O_3	bdl	bdl	bdl	bdl	bdl	bdl	bdl	bdl	bdl	0.02	0.09
FeO	9.51	8.99	11.68	12.71	14.41	13.27	9.67	11.36	8.12	9.24	11.12
MgO	0.33	0.39	0.67	0.47	0.83	1.77	0.69	1.00	0.64	0.51	1.51
MnO	0.29	0.19	0.25	0.43	0.28	0.10	0.12	0.46	0.12	0.16	0.18
CaO	11.56	10.76	11.35	12.40	11.27	10.38	11.35	11.25	5.17	8.16	11.69
SrO	0.22	0.32	0.43	0.35	0.43	bdl	0.21	0.15	bdl	bdl	0.20
BaO	bdl	bdl	bdl	bdl	bdl	bdl	bdl	bdl	bdl	bdl	bdl
SO_3	0.05	0.08	0.05	0.17	0.11	bdl	0.02	bdl	bdl	0.02	0.06
P_2O_5	bdl	bdl	bdl	bdl	0.14	0.07	0.11	0.02	0.14	0.14	bdl
Cl	0.98	0.84	0.74	0.59	0.53	0.04	0.67	0.63	0.02	0.22	0.47
F	bdl	bdl	bdl	bdl	bdl	bdl	bdl	bdl	bdl	bdl	bdl
Total	91.68	90.51	92.41	91.97	93.48	95.27	90.18	91.96	91.58	91.53	93.31

Table B.6 cont.

Pt#	782076 59	881318b 61	881318b 62	881318b 63	881318b 64	881318b 65	881318b 66	881318b 67	881318b 71	881318b 72	881318b 73
SiO_2	31.28	31.41	31.63	32.81	32.15	35.50	31.36	40.31	32.93	32.06	32.65
TiO_2	0.91	0.42	0.52	0.51	0.46	0.79	0.70	1.10	0.45	0.53	0.46
ThO_2	0.54	0.14	0.14	0.30	0.02	0.30	0.54	0.23	0.38	0.33	0.18
Al_2O_3	13.73	16.08	16.55	16.42	15.42	16.28	14.50	17.65	16.13	16.20	16.23
La_2O_3	6.59	5.51	5.54	5.22	5.02	4.50	4.99	4.45	5.38	5.76	5.57
Ce_2O_3	11.53	10.57	10.73	10.36	9.91	9.19	10.18	9.76	10.22	10.32	10.28
Pr_2O_3	0.99	1.05	1.04	0.96	0.81	0.86	1.02	0.76	0.91	1.27	1.00
Nd_2O_3	3.36	3.63	3.36	3.59	3.78	3.22	3.18	3.45	3.49	3.55	3.48
Sm_2O_3	bdl	0.08	0.21	0.06	0.02	0.07	0.17	0.11	0.04	0.01	0.19
Dy_2O_3	bdl	0.06	0.09	0.08	bdl	bdl	bdl	bdl	bdl	bdl	bdl
FeO	13.49	12.39	12.23	12.44	11.94	9.64	11.90	4.46	10.56	12.35	12.44
MgO	1.94	1.53	1.60	1.56	1.22	0.74	1.10	0.38	1.32	1.67	1.60
MnO	0.13	0.15	0.13	0.09	0.18	0.28	0.62	0.22	0.22	0.10	0.06
CaO	10.66	12.38	12.20	11.96	11.96	7.35	10.71	4.88	12.15	11.61	11.76
SrO	bdl	0.03	0.12	0.09	0.24	0.16	0.20	bdl	0.42	0.08	0.02
BaO	bdl	bdl	bdl	bdl	bdl	0.88	bdl	3.73	bdl	bdl	bdl
SO_3	0.11	bdl	0.16	bdl	0.04	bdl	bdl	bdl	0.05	bdl	0.07
P_2O_5	bdl	0.03	0.03	0.07	0.12	bdl	0.08	0.08	0.10	0.10	bdl
Cl	0.06	bdl	0.01	0.05	0.61	0.07	0.38	bdl	0.54	0.03	bdl
F	bdl	bdl	bdl	bdl	bdl	bdl	bdl	bdl	bdl	bdl	bdl
Total	95.31	95.47	96.30	96.57	93.92	89.84	91.63	91.58	95.29	95.96	95.99

Table B.6 cont.

Pt#	881318b 74	881318b 75	881318b 76	881318b 79	881318b 80	881318b 81	881318b 82	881318b 83	881318b 87	881318b 89
SiO_2	32.14	32.13	32.18	32.28	31.91	30.79	29.80	29.22	30.76	32.75
TiO_2	0.48	0.60	0.65	0.46	0.41	0.49	0.54	0.38	0.48	0.06
ThO_2	0.49	0.35	0.26	0.35	0.33	0.26	0.60	0.27	0.10	0.04
Al_2O_3	15.65	15.50	14.61	15.81	16.05	15.79	14.87	15.15	14.99	16.58
La_2O_3	5.42	5.55	5.14	5.26	5.46	5.65	5.56	5.12	5.17	3.03
Ce_2O_3	10.71	10.53	9.87	10.23	9.97	10.40	10.15	10.42	9.87	6.61
Pr_2O_3	0.89	0.87	1.16	1.06	1.00	1.16	0.90	0.97	1.06	0.70
Nd_2O_3	3.24	3.80	3.23	3.26	3.48	3.32	3.14	3.18	3.24	2.63
Sm_2O_3	0.05	bdl	0.11	bdl	bdl	bdl	0.13	0.22	0.08	0.15
Dy_2O_3	bdl	bdl	bdl	bdl	bdl	bdl	bdl	bdl	bdl	bdl
FeO	12.41	10.51	10.48	12.39	12.63	9.23	9.51	10.81	11.79	12.43
MgO	1.61	1.41	0.81	1.52	1.51	0.71	0.89	1.08	0.78	0.43
MnO	0.10	0.10	0.41	0.14	0.16	0.05	0.10	0.20	0.25	0.27
CaO	11.55	11.53	10.77	12.25	11.89	11.11	12.53	11.98	12.42	14.32
SrO	0.02	0.21	0.22	0.05	0.10	0.30	0.46	0.54	0.57	0.83
BaO	bdl	bdl	bdl	bdl	bdl	bdl	bdl	bdl	bdl	bdl
SO_3	0.04	bdl	0.01	0.04	bdl	0.12	0.20	0.11	0.04	0.12
P_2O_5	bdl	0.08	0.03	bdl	bdl	0.07	0.08	bdl	0.02	0.16
Cl	0.02	0.35	0.60	0.07	0.04	1.05	0.72	0.51	0.72	0.68
F	bdl	bdl	bdl	bdl	bdl	bdl	bdl	bdl	bdl	bdl
Total	94.81	93.52	90.56	95.17	94.92	90.49	90.17	90.16	92.34	91.79

Table B.7 Titanite

Slide	881257	881257	881257	881257	881257	881237	881237
Pt#	1	2	3	4	5	1	2
SiO_2	30.28	30.55	31.70	30.34	28.91	30.79	30.02
TiO_2	32.24	32.60	33.29	31.96	30.99	31.95	31.20
ThO_2	bdl	0.12	bdl	bdl	0.08	0.21	bdl
Al_2O_3	2.92	3.07	2.76	2.93	2.81	3.47	3.55
La_2O_3	bdl	0.53	0.14	0.47	bdl	0.57	0.33
Ce_2O_3	3.23	1.76	1.37	1.72	1.63	1.17	0.82
Pr_2O_3	0.60	0.29	bdl	0.33	0.34	0.04	0.31
Nd_2O_3	1.86	2.69	1.17	2.66	3.27	1.87	2.49
Sm_2O_3	0.27	0.89	0.32	0.61	0.33	0.32	0.55
Dy_2O_3	bdl	bdl	bdl	0.11	0.10	bdl	bdl
FeO	1.84	1.96	1.39	1.93	2.02	1.79	1.79
MgO	0.09	0.09	0.84	0.10	0.48	0.15	0.15
MnO	bdl	0.01	0.05	bdl	bdl	0.04	bdl
CaO	26.04	26.21	26.52	26.08	24.38	26.45	26.66
Na_2O	0.02	bdl	0.07	bdl	0.88	bdl	bdl
F	0.58	0.87	0.45	0.71	0.21	1.13	1.06
Total	99.98	101.65	100.07	99.96	96.45	99.94	98.92

Table B.7 cont.

	881237	881237	881237	881237	881237	881237
Pt#	3	4	5	6	7	8
SiO_2	30.85	30.63	30.77	31.34	30.60	30.47
TiO_2	30.73	31.17	32.86	37.04	32.08	31.20
ThO_2	bdl	0.11	0.02	bdl	bdl	bdl
Al_2O_3	3.78	3.49	2.83	1.42	2.80	3.28
La_2O_3	0.06	0.16	0.17	bdl	0.25	0.33
Ce_2O_3	1.19	1.20	0.84	0.42	1.16	1.44
Pr_2O_3	0.27	0.22	0.16	bdl	0.02	0.22
Nd_2O_3	1.94	2.10	2.34	1.82	1.79	2.46
Sm_2O_3	0.31	0.80	0.52	0.75	0.46	0.86
Dy_2O_3	bdl	0.23	0.06	0.23	0.01	bdl
FeO	2.30	1.58	1.69	0.89	1.62	1.69
MgO	0.84	0.14	0.09	0.01	0.12	0.17
MnO	bdl	0.07	0.05	0.10	bdl	bdl
CaO	23.70	26.36	26.68	28.29	26.27	25.44
Na_2O	0.21	bdl	0.03	bdl	0.03	bdl
F	0.36	1.01	0.85	0.34	0.87	0.96
Total	96.55	99.29	99.96	102.65	98.08	98.52

Table B.8 Chevkinite

Slide	782076	782076	782076	782076	782076	782076	782076
Pt#	2	3	4	6	9	13	14
SiO_2	20.56	20.29	20.20	18.85	20.01	20.23	20.30
TiO_2	18.60	18.44	17.90	18.35	18.36	19.25	18.06
ThO_2	0.79	0.89	0.77	0.72	1.02	1.04	1.20
Al_2O_3	3.80	3.79	3.73	2.82	3.41	3.42	3.74
La_2O_3	10.05	10.82	10.47	9.45	8.99	9.97	9.97
Ce_2O_3	19.00	19.28	18.43	18.51	17.77	19.46	19.39
Pr_2O_3	2.00	2.06	1.92	1.74	2.06	2.10	1.96
Nd_2O_3	6.34	6.07	6.16	6.31	6.53	6.57	6.50
Sm_2O_3	0.23	0.14	0.27	0.22	0.28	0.24	0.16
Dy_2O_3	bdl	0.02	bdl	bdl	bdl	bdl	bdl
FeO	6.87	6.86	6.47	7.20	6.04	5.87	7.06
MgO	0.69	0.69	0.66	0.65	0.58	0.54	0.67
CaO	5.35	5.46	4.93	4.19	4.93	4.07	5.41
SrO	0.56	0.52	0.52	0.70	0.55	0.39	0.48
BaO	bdl	bdl	bdl	bdl	bdl	bdl	bdl
P_2O_5	bdl	0.08	0.03	bdl	0.01	0.06	0.20
Cl	0.01	0.08	0.10	0.09	0.08	0.09	0.01
F	bdl	bdl	bdl	bdl	bdl	bdl	bdl
Total	94.84	95.50	92.55	89.81	90.61	93.30	95.10

Table B.8 cont.

Slide	782076	782076	782076	782076	782076	782076	782076
Pt#	15	19	33	34	35	36	56
SiO_2	18.69	20.45	19.46	20.47	20.43	19.53	18.45
TiO_2	17.64	18.64	17.39	18.11	18.56	18.70	18.97
ThO_2	0.07	0.93	0.80	1.06	0.83	0.66	1.72
Al_2O_3	3.02	3.77	3.50	3.48	3.85	3.48	3.30
La_2O_3	10.90	10.81	10.08	10.18	10.09	9.29	8.93
Ce_2O_3	21.24	19.88	18.86	19.41	19.23	18.15	22.93
Pr_2O_3	2.27	1.95	2.05	2.12	1.82	1.88	2.09
Nd_2O_3	7.16	6.57	6.39	6.63	6.59	6.34	6.73
Sm_2O_3	0.21	0.25	0.15	0.25	0.13	0.10	0.17
Dy_20_3	bdl	0.23	bdl	bdl	bdl	bdl	bdl
FeO	6.91	6.99	6.51	7.08	6.95	6.08	1.91
MgO	0.79	0.64	0.70	0.70	0.65	0.55	0.06
CaO	3.36	5.60	4.33	4.71	5.60	4.66	2.46
SrO	0.84	0.48	0.63	0.62	0.48	0.41	bdl
BaO	bdl	bdl	bdl	bdl	bdl	bdl	0.03
P_2O_5	bdl	0.05	bdl	0.02	0.11	0.13	0.13
Cl	0.08	0.05	0.13	0.13	0.01	0.14	0.13
F	bdl	bdl	bdl	bdl	bdl	0.07	1.08
Total	93.19	97.28	90.98	94.96	95.33	90.17	89.09

Table B.9 Monazite

Pt#	HL06-75 1	HL06-75 2	HL06-75 3	HL06-75 4	HL06-75 5	39703 14	39703 15	39703 4
SiO_2	0.72	0.74	0.72	1.57	1.02	0.91	1.03	1.57
ThO_2	0.26	0.40	0.63	1.51	0.48	1.21	1.90	1.51
Y_2O_3	bdl	0.03	0.05	0.17	0.01	bdl	bdl	0.17
La_2O_3	19.03	20.29	19.37	11.83	18.40	19.97	18.81	11.83
Ce_2O_3	37.08	35.18	36.60	32.05	35.93	34.64	35.90	32.05
Pr_2O_3	4.43	2.83	3.84	4.34	3.73	2.75	3.41	4.34
Nd_2O_3	12.35	11.18	12.98	16.42	12.90	9.88	10.48	16.42
Sm_2O_3	0.38	bdl	bdl	1.23	0.26	bdl	bdl	1.23
Dy_2O_3	0.24	bdl	bdl	0.44	bdl	bdl	bdl	0.44
CaO	0.44	0.57	0.46	1.14	0.48	0.13	0.26	1.14
SrO	bdl	0.07	0.07	0.26	0.19	0.08	0.12	0.26
Cl	0.05	0.12	0.09	0.21	bdl	0.01	0.23	0.21
F	0.87	0.86	0.74	0.69	0.54	0.47	0.17	0.69
P_2O_5	24.80	24.73	24.70	23.96	24.43	27.62	26.49	23.96
Total	100.66	97.00	100.25	95.83	98.37	98.45	99.62	95.83

Table B.10 Bastnaesite

Pt#	881216 1	881216 2	881216 3	881216 4	881216 5	881257 7	881257 8	881237 1	881237 2	881237 3	881237 5
SiO_2	1.56	bdl	0.08	1.10	2.46	0.65	0.82	bdl	1.57	0.19	0.36
ThO_2	bdl	bdl	0.20	bdl	0.01	bdl	0.04	bdl	bdl	bdl	bdl
Al_2O_3	0.17	bdl	bdl	bdl	0.04	bdl	0.01	bdl	0.04	bdl	0.15
Y_2O_3	bdl	bdl	bdl	bdl	bdl	bdl	bdl	0.02	0.16	bdl	bdl
La_2O_3	15.83	17.66	18.10	15.08	14.88	20.67	20.36	26.17	26.86	24.73	23.38
Ce_2O_3	31.80	32.76	32.43	30.48	28.65	31.74	31.84	36.01	35.03	34.83	30.66
Pr_2O_3	2.50	3.23	2.88	3.14	2.61	2.45	2.50	3.36	3.24	2.99	2.35
Nd_2O_3	12.69	14.09	13.48	14.22	11.69	11.74	11.55	14.41	12.46	13.68	7.78
Sm_2O_3	0.18	0.23	0.12	bdl	0.12	bdl	bdl	0.25	0.21	bdl	bdl
Dy_2O_3	0.53	bdl	0.15	0.11	0.18	bdl	bdl	bdl	bdl	0.41	bdl
FeO	0.34	bdl	bdl	0.06	bdl	bdl	bdl	bdl	bdl	bdl	bdl
CaO	1.63	2.36	2.31	1.69	7.46	1.56	1.57	1.07	0.92	1.77	8.31
SrO	0.02	0.05	0.19	0.05	0.03	0.13	0.18	0.07	0.11	0.03	3.53
Na_2O	bdl	bdl	bdl	bdl	bdl	bdl	bdl	bdl	bdl	0.02	0.05
P_2O_5	0.21	0.01	0.13	0.11	0.04	0.04	bdl	bdl	0.03	bdl	bdl
Cl	0.13	0.12	0.11	0.04	0.17	0.07	0.13	0.11	0.08	0.27	0.09
F	2.37	2.91	3.18	2.27	2.99	4.19	4.29	2.31	3.25	3.66	0.88
Total	69.96	73.42	73.37	68.34	71.31	73.23	73.29	83.78	83.96	82.59	77.52

Table B.10 cont.

Pt#	881237 6	881237 7	881237 8	881237 9	881237 10	881237 12	881237 13	881237 15	881237 16	HL06-75 17	HL06-75 19
SiO_2	0.13	0.15	0.41	2.54	4.32	0.99	0.35	0.13	1.21	0.04	0.02
ThO_2	0.19	bdl	bdl	bdl	bdl	bdl	0.01	0.02	0.09	bdl	bdl
Al_2O_3	0.03	0.03	0.05	0.52	1.13	0.12	0.02	bdl	0.16	bdl	bdl
Y_2O_3	bdl	0.03	0.19	0.12	0.16	bdl	0.16	0.13	bdl	bdl	0.01
La_2O_3	25.70	24.16	25.84	23.31	25.16	29.99	27.50	28.72	32.80	23.92	21.76
Ce_2O_3	31.94	32.12	36.95	33.74	34.53	36.87	38.46	34.25	38.28	40.25	40.18
Pr_2O_3	3.13	2.81	3.20	3.50	2.83	3.00	2.12	2.64	3.06	2.99	3.03
Nd_2O_3	10.10	8.15	13.47	13.57	10.56	13.35	11.61	10.43	12.19	12.13	11.70
Sm_2O_3	bdl	bdl	bdl	bdl	bdl	bdl	bdl	bdl	bdl	bdl	bdl
Dy_2O_3	bdl	0.20	bdl	0.44	bdl	bdl	1.23	0.06	bdl	bdl	bdl
FeO	bdl	bdl	bdl	bdl	bdl	bdl	bdl	bdl	bdl	bdl	bdl
CaO	8.37	8.62	1.19	1.59	0.96	0.96	1.04	1.94	1.45	0.31	0.39
SrO	0.05	2.19	0.04	0.11	bdl	0.16	0.01	0.06	0.09	0.04	0.08
Na_2O	bdl	0.01	bdl	0.02	0.05	bdl	0.01	bdl	0.06	0.04	0.06
P_2O_5	0.03	0.01	bdl	0.10	0.03	bdl	0.07	bdl	bdl	0.05	bdl
Cl	0.12	0.06	0.13	0.10	0.22	0.09	0.11	0.29	0.13	0.05	0.04
F	3.95	1.00	4.08	4.03	4.33	3.84	2.78	4.63	3.85	2.26	2.57
Total	83.74	79.54	85.55	83.69	84.28	89.37	85.49	83.30	93.37	82.08	79.85

Table B.11 Pyroxenes

Pt#	881216 1	881216 2	881216 3	881216 4	881216 6	881216 7	881216 11	881216 12	881216 13	881216 15
SiO_2	52.93	53.03	52.33	52.73	52.13	51.77	52.41	51.84	55.68	50.54
TiO_2	0.02	0.03	0.09	0.04	0.03	0.11	bdl	0.11	0.08	0.26
Al_2O_3	0.77	0.58	1.18	1.14	1.17	1.39	1.25	1.49	1.40	2.80
Cr_2O_3	0.05	bdl	0.04	bdl	bdl	0.01	0.01	bdl	bdl	0.03
FeO	9.22	8.74	9.65	9.27	9.92	9.86	10.09	10.13	8.53	11.16
MgO	11.93	12.40	11.76	12.35	11.70	11.56	11.78	11.53	18.75	10.94
MnO	0.41	0.46	0.34	0.38	0.38	0.39	0.41	0.38	0.36	0.41
CaO	23.43	23.57	23.15	22.09	22.46	22.70	22.42	24.17	12.10	22.42
SrO	bdl	bdl	bdl	bdl	bdl	bdl	bdl	bdl	bdl	bdl
Na_2O	bdl	bdl	bdl	bdl	bdl	bdl	bdl	bdl	bdl	bdl
K_2O	0.07	0.07	0.05	0.05	0.02	0.11	bdl	0.04	0.28	0.05
Cl	0.01	bdl	0.07	bdl	bdl	0.01	0.90	0.02	0.06	0.02
F	bdl	bdl	bdl	bdl	bdl	bdl	bdl	bdl	bdl	bdl
Total	98.84	98.88	98.64	98.06	97.82	97.94	99.28	99.71	97.24	98.62

Table B.11 cont.

Pt#	881216 17	881216 18	881216 19	881216 20	881216 21	881216 22	881216 23	881257 24	881257 25	881257 26
SiO_2	50.97	51.25	51.41	51.25	51.52	50.07	51.10	48.97	51.82	51.63
TiO_2	0.25	0.17	0.21	0.17	0.19	0.21	0.22	0.22	0.19	0.23
Al_2O_3	2.38	2.13	2.33	2.35	2.22	2.24	2.20	3.12	2.19	2.29
Cr_2O_3	bdl	0.03	bdl	0.03	bdl	0.03	0.03	bdl	bdl	bdl
FeO	10.79	10.56	10.80	10.82	10.75	11.04	10.96	12.53	9.73	11.36
MgO	10.81	11.51	11.13	11.09	10.99	11.30	10.99	11.42	11.69	11.39
MnO	0.45	0.43	0.39	0.29	0.39	0.40	0.39	0.39	0.35	0.38
CaO	22.20	23.08	22.65	22.27	21.93	22.71	22.48	19.52	22.63	22.06
SrO	bdl	bdl	bdl	bdl	bdl	bdl	bdl	bdl	bdl	bdl
Na_2O	bdl	bdl	bdl	bdl	bdl	bdl	bdl	bdl	bdl	bdl
K_2O	0.10	0.06	0.09	0.05	0.03	bdl	0.02	0.09	0.11	0.01
Cl	0.03	bdl	bdl	0.01	bdl	0.01	0.03	0.33	0.02	0.01
F	bdl	bdl	bdl	bdl	bdl	bdl	bdl	bdl	bdl	bdl
Total	97.98	99.22	99.03	98.34	98.03	98.01	98.41	96.60	98.73	99.36

Table B.11 cont.

Pt#	881257 27	881257 28	881257 29	881257 30	881257 31	881257 32	881257 34	881257 35	881257 36	881257 39
SiO_2	51.16	52.50	51.08	50.98	50.68	54.53	53.55	51.45	52.74	53.37
TiO_2	0.20	bdl	0.25	0.26	0.26	bdl	bdl	0.20	0.08	0.03
Al_2O_3	2.12	1.39	2.52	2.61	2.26	0.23	0.44	2.18	1.33	0.80
Cr_2O_3	0.04	0.01	bdl	0.02	bdl	bdl	bdl	0.03	0.01	bdl
FeO	11.28	7.56	11.37	11.62	bdl	11.07	8.41	11.10	10.42	10.36
MgO	11.25	12.19	10.92	11.16	10.55	15.77	13.76	11.46	11.79	12.32
MnO	0.37	0.42	0.43	0.42	bdl	0.37	0.50	0.41	0.47	0.38
CaO	22.22	23.49	21.81	21.86	22.60	12.45	23.54	22.77	23.29	23.24
SrO	bdl	bdl	bdl	bdl	bdl	bdl	bdl	bdl	bdl	bdl
Na_2O	bdl	bdl	bdl	bdl	0.62	bdl	bdl	bdl	bdl	bdl
K_2O	bdl	bdl	0.05	0.03	0.09	0.01	0.10	0.09	0.03	0.05
Cl	0.06	0.03	bdl	0.03	0.07	0.01	0.08	0.02	bdl	0.03
F	bdl	bdl	bdl	bdl	bdl	bdl	bdl	bdl	bdl	bdl
Total	98.70	97.60	98.44	98.98	87.12	94.45	100.38	99.70	100.17	100.57

Table B.11 cont.

Pt#	881237 1	881237 2	881237 3	881237 4	881237 5	881237 6	881237 7	881237 8	881237 9	881237 10
SiO_2	52.03	51.88	50.50	52.56	51.14	53.85	53.91	50.78	49.96	50.85
TiO_2	0.17	0.12	0.18	0.10	0.13	0.03	bdl	0.21	0.15	0.20
Al_2O_3	1.53	1.62	2.12	1.34	1.33	0.07	0.13	1.92	1.52	2.09
Cr_2O_3	bdl	bdl	bdl	bdl	bdl	bdl	bdl	0.08	bdl	bdl
FeO	10.87	11.25	11.46	10.43	10.25	20.51	17.02	11.33	10.94	11.67
MgO	11.87	11.64	11.17	12.04	12.10	11.28	13.06	11.47	11.41	10.89
MnO	0.55	0.50	0.53	0.54	0.56	0.71	0.48	0.58	0.51	0.57
CaO	22.11	22.14	22.12	22.43	22.38	12.32	12.17	21.99	22.56	22.15
SrO	bdl	bdl	bdl	bdl	bdl	bdl	bdl	bdl	bdl	bdl
Na_2O	bdl	bdl	0.66	bdl	0.92	bdl	0.64	bdl	0.83	bdl
K_2O	bdl	0.04	bdl	0.07	bdl	bdl	bdl	0.07	bdl	0.07
Cl	bdl	bdl	bdl	bdl	0.06	bdl	0.02	0.03	bdl	0.02
F	bdl	bdl	bdl	bdl	bdl	bdl	bdl	bdl	bdl	bdl
Total	99.14	99.20	98.73	99.58	98.86	98.77	97.43	98.47	97.89	98.50

Table B.11 cont.

Pt#	881237 11	881237 12	881237 13	881237 14	881237 15	881237 16	881237 17	881237 18	881237 19	881237 20
SiO_2	49.82	51.38	51.15	50.82	49.41	50.94	51.16	49.68	51.35	49.20
TiO_2	0.27	0.19	0.08	0.16	0.18	0.21	0.18	0.25	0.22	0.24
Al_2O_3	2.26	1.79	1.75	2.14	2.24	2.20	1.86	2.35	2.42	2.29
Cr_2O_3	0.02	0.03	bdl	bdl	0.01	bdl	0.01	bdl	bdl	bdl
FeO	11.39	11.12	11.09	11.05	11.39	11.10	10.94	11.55	11.93	11.64
MgO	11.26	11.09	11.62	11.50	10.98	11.21	11.48	11.09	11.24	11.23
MnO	0.55	0.42	0.50	0.54	0.50	0.43	0.46	0.36	0.60	0.57
CaO	21.66	21.67	21.78	21.57	21.20	21.33	21.77	21.72	21.55	22.02
SrO	bdl	0.02	bdl	bdl	bdl	0.07	0.03	0.02	bdl	bdl
Na_2O	1.04	bdl	0.80	bdl	0.73	bdl	0.93	bdl	1.23	bdl
K_2O	bdl	0.11	bdl	0.08	bdl	0.08	bdl	0.10	bdl	0.12
Cl	bdl	bdl	bdl	0.01	bdl	0.02	0.01	0.03	0.01	0.06
F	bdl	bdl	bdl	bdl	bdl	bdl	bdl	bdl	bdl	bdl
Total	98.26	97.81	98.76	97.87	96.65	97.70	98.84	97.13	100.56	97.36

Table B.12 Feldpars

Pt#	881216 1	881216 2	881216 3	881216 4	881216 5	881216 6	881216 7	881216 8	881216 9	881216 10	881216 11	881216 12
SiO_2	55.01	56.77	54.41	64.68	63.74	64.73	62.63	58.64	63.99	63.13	64.84	64.07
TiO_2	0.87	0.80	1.11	bdl	bdl	0.01	bdl	bdl	bdl	bdl	bdl	bdl
Al_2O_3	14.90	13.66	14.35	18.23	18.53	18.57	18.42	17.98	18.62	17.09	18.31	17.82
Fe_2O_3	0.27	0.59	0.27	0.12	0.30	0.37	0.22	1.10	0.88	1.24	0.20	0.38
MgO	0.03	0.09	0.03	0.02	bdl	bdl	0.01	0.07	0.02	1.16	bdl	0.01
CaO	1.78	1.16	0.81	bdl	bdl	bdl	bdl	bdl	bdl	bdl	bdl	bdl
SrO	bdl	bdl	bdl	bdl	bdl	bdl	bdl	bdl	bdl	bdl	bdl	bdl
BaO	14.11	13.56	16.97	bdl	bdl	bdl	0.06	bdl	0.26	bdl	bdl	bdl
Na_2O	0.06	0.07	0.06	0.08	0.23	0.12	0.18	0.07	0.25	0.13	0.11	0.08
K_2O	0.93	0.57	0.58	16.41	16.80	16.71	16.50	16.40	15.82	14.98	16.35	16.84
Total	87.96	87.27	88.59	99.55	99.60	100.51	98.03	94.26	99.84	97.73	99.81	99.20

Table B.12 cont.

Pt#	881237 1	881237 2	881237 3	881237 4	881237 5	881237 6	881237 7	881237 8	881237 9	881237 10	881237 11	881237 12
SiO_2	56.78	56.20	56.96	64.38	64.82	28.26	28.59	28.36	55.35	55.62	54.99	55.59
TiO_2	0.55	0.48	0.50	bdl	bdl	32.64	32.12	32.43	0.53	0.53	0.55	0.51
Al_2O_3	20.31	20.02	20.40	18.12	19.00	2.37	2.67	2.68	19.93	20.09	20.16	20.38
Fe_2O_3	0.09	0.07	0.04	0.85	0.23	1.91	1.38	1.91	0.09	0.30	0.06	0.07
MgO	0.02	bdl	bdl	1.88	0.05	0.11	0.93	0.11	bdl	0.17	bdl	bdl
CaO	bdl	bdl	bdl	bdl	bdl	25.78	24.76	25.82	bdl	bdl	bdl	bdl
SrO	0.95	1.76	1.82	bdl	bdl	bdl	bdl	bdl	1.77	1.18	1.83	1.42
BaO	8.71	8.41	8.42	0.08	0.15	1.61	1.91	1.63	8.54	8.83	8.64	8.33
Na_2O	1.69	2.29	2.31	0.23	0.23	0.02	0.12	0.03	1.97	1.80	2.10	1.70
K_2O	9.73	7.97	8.25	14.51	16.20	bdl	bdl	bdl	8.47	9.19	8.58	8.32
Total	98.82	97.20	98.71	100.05	100.67	92.69	92.48	92.98	96.66	97.69	96.90	96.33

Table B. 12 cont.

Pt#	881237 13	881237 14	881237 15	881237 16	881237 17	881237 18	881237 19	881237 21	881237 22	881237 23	881237 24
SiO_2	55.48	54.63	56.06	64.15	32.51	36.22	35.68	61.59	57.09	57.43	47.13
TiO_2	0.62	0.62	0.57	0.09	bdl	0.03	0.01	0.47	0.53	0.57	0.05
Al_2O_3	20.94	20.36	20.48	19.07	22.23	20.99	20.38	21.54	21.35	21.18	32.51
Fe_2O_3	0.12	0.05	0.12	0.10	9.70	10.99	11.84	0.07	0.22	0.10	3.29
MgO	bdl	bdl	0.01	0.03	0.02	0.03	0.02	0.01	0.01	0.01	0.46
CaO	bdl	bdl	bdl	bdl	20.01	19.66	20.48	0.02	bdl	bdl	0.22
SrO	1.23	1.72	1.54	bdl	3.85	3.90	3.20	0.54	1.26	1.64	bdl
BaO	8.96	8.67	8.66	0.74	bdl	bdl	bdl	8.25	8.69	8.96	0.51
Na_2O	1.66	2.30	2.26	0.25	bdl	0.02	bdl	0.61	1.87	1.89	0.08
K_2O	9.08	8.31	8.05	15.98	bdl	bdl	bdl	4.17	8.67	8.48	9.14
Total	98.11	96.65	97.74	100.41	88.33	91.83	91.60	97.28	99.69	100.25	93.39

B.3 INDUCTIVELY COUPLED PLASMA MASS SPECTROMETRY (ICP-MS)

Inductively coupled plasma mass spectrometry (ICP-MS) analysis of whole rock powders was completed in the ICP-MS Laboratory at the University of Saskatchewan, using a Perkin Elmer ELAN 5000. Samples of the lamprophyre, select pegmatites and representative samples of each vein generation were selected for analysis. Care was taken to try and ensure that only a single vein generation was present in each of the whole rock samples but, due to the complexity of the vein system, some minor contamination by other vein generations or wall rock may have occurred, particularly in the brecciated vein generations. Powders samples of the dikes and individual vein generations were analyzed for their trace element concentrations using the following methodology.

Approximately 100 mg of powered sample was placed in a Teflon jar and dissolved with 5 ml of HF(48-51%) and 5 ml of concentrated (16N) HNO_3. The jar was capped and heated at approximately 125^{o}C for three days, until completely dissolved. The sample was then evaporated until dry. Once the sample has cooled 2 ml of HNO_3 and 2 ml of HF were added and the sample was refluxed for an additional three days, then evaporated until dry. 2.5 ml of 8N HNO_3 were added and the sample was warmed gently to dissolve the residue. The sample was then transferred to a bottle, Milli-Q water added to make up a final weight of 100g, and were analyzed. The complete results of the ICP-MS analyses and the detection limits are provided in Table B.12

Table B.13 ICP-MS Results

Element	Det. lmt. (ppm)	HS-Pegm	Pegm-2	Lamp-1	Allanite 881318B	Allanite 948537	Allanite HS-AL	Red Ap Bx 881056	Red Ap Bx 881240R	Red Ap Bx 881318A
Li	2.54	3.19	30.40	23.87	22.52	14.97	13.99	44.56	11.95	bdl
Be	6.55	1.44	2.14	7.00	1.17	2.47	6.54	4.61	2.96	0.68
Sc	3.38	13.08	18.23	14.26	13.88	12.89	16.67	6.44	5.62	6.00
V	1.20	17.81	37.77	103.01	315.88	364.91	229.40	92.64	43.91	22.03
Rb	0.04	184.43	143.42	287.52	2.03	1.35	15.09	12.81	0.75	1.58
Sr	0.29	3365.63	489.91	1011.41	5847.51	5855.23	3806.63	5271.34	6570.90	6441.20
Y	0.07	38.67	10.24	17.66	230.02	167.63	196.57	682.75	736.63	786.07
Zr	0.07	337.43	74.94	181.80	25.30	382.84	174.12	73.83	26.02	12.47
Nb	0.04	14.26	2.13	7.19	7.29	15.54	12.88	11.47	1.14	0.23
Mo	0.12	2.96	1.04	0.69	0.98	1.61	2.33	0.90	0.56	0.24
Cs	0.01	0.82	1.58	3.87	0.12	0.27	0.17	0.08	0.02	0.01
Ba	0.07	5196.59	4685.56	3590.74	2778.88	5932.77	2443.45	1057.55	1336.92	162.10
La	0.07	227.75	26.44	50.01	42332.79	48053.80	20296.34	6928.45	6165.33	3641.21
Ce	0.01	478.18	51.32	97.00	67066.54	72459.54	42228.83	17589.20	14767.24	9422.41
Pr	0.46	76.14	7.73	13.39	8987.24	8736.44	5758.42	2424.52	2484.02	1767.61
Nd	0.11	292.60	32.20	48.15	26756.60	23704.67	17508.94	9078.15	9913.66	7839.04
Sm	0.01	49.21	5.76	8.49	2190.21	1683.27	1489.57	1349.06	1523.97	1362.65
Eu	0.14	12.87	1.16	1.36	383.55	280.49	254.69	320.26	344.50	317.63
Gd	0.01	27.55	4.33	6.45	629.15	503.31	502.97	742.97	788.18	763.87
Tb	0.12	1.50	0.32	0.58	12.43	6.88	10.49	24.60	29.82	35.88
Dy	0.01	10.27	2.30	3.61	92.03	65.37	71.82	199.71	217.15	229.45
Ho	0.07	1.35	0.39	0.59	3.85	2.68	3.43	22.45	24.55	27.19
Er	0.01	3.08	1.00	1.51	16.47	13.16	13.97	52.81	57.72	62.23
Tm	0.01	0.33	0.11	0.22	0.73	0.50	0.59	4.47	5.10	5.45
Yb	0.03	1.72	0.54	1.14	6.93	5.56	5.77	25.52	29.62	31.42
Lu	0.14	0.22	0.05	0.11	1.29	1.13	1.12	3.64	4.00	4.21
Hf	0.02	8.47	1.80	5.08	0.89	8.51	3.25	0.80	0.09	bdl
Ta	0.04	1.19	bdl	0.50	0.24	0.36	0.47	0.29	bdl	bdl
Tl	0.04	0.98	0.75	2.22	bdl	0.05	0.07	bdl	bdl	bdl

Element	Det. lmt. (ppm)	HS-Pegm	Pegm-2	Lamp-1	Allanite 881318B	Allanite 948537	Allanite HS-AL	Red Ap Bx 881056	Red Ap Bx 881240R	Red Ap Bx 881318A
Pb	0.08	80.01	60.60	35.79	670.98	1034.68	536.85	55.40	67.80	36.81
Bi	0.04	0.05	0.04	0.03	1.23	0.88	0.69	1.08	1.95	1.78
Th	0.05	40.00	1.39	26.67	4596.60	7918.13	3556.36	1299.04	1244.90	886.13
U	0.03	4.16	0.34	6.31	81.83	48.83	78.91	126.75	83.97	61.70
P	36.45	850.71	256.22	3535.09	267.21	103.05	7588.53	92394.30	124362.43	149770.75
Ti	6.90	2209.40	1186.73	3086.13	3324.99	4559.45	3520.47	2216.92	216.11	bdl
Cr	1.46	129.41	135.48	141.85	67.46	73.18	44.36	3.95	bdl	bdl
Co	0.11	4.50	6.83	19.43	15.21	16.01	21.56	17.70	6.62	1.53
Ni	0.38	4.80	7.37	48.69	9.24	7.19	13.86	15.68	6.66	4.29
Cu	3.35	8.77	24.10	11.13	5.01	5.09	bdl	10.60	5.74	bdl
Zn	1.56	75.18	105.75	115.20	213.25	259.09	252.35	98.78	38.95	28.65
Ge	0.06	1.49	0.89	0.82	11.64	6.32	5.68	8.05	5.16	6.26
As	1.81	bdl	bdl	bdl	36.31	17.79	18.32	70.17	78.85	133.26
Ag	0.05	bdl	0.31	bdl	0.19	bdl	bdl	bdl	bdl	bdl
Cd	0.12	bdl	bdl	0.26	bdl	0.51	0.43	0.17	bdl	bdl
Sn	0.09	0.82	0.84	3.81	2.38	2.35	14.94	3.86	0.19	0.32
Sb	0.05	bdl	bdl	bdl	0.06	bdl	0.07	0.14	0.07	0.06
W	0.18	0.86	1.19	0.52	0.21	0.76	0.92	1.64	0.89	0.67
Mn	0.28	400.96	597.78	723.82	2652.88	2449.03	3250.66	666.66	428.92	382.59
Ga	0.35	36.29	3.32	5.47	22.21	15.22	14.37	3.97	bdl	0.54

Element	Det. lmt. (ppm)	Green Ap HL-06-75	Green Ap 881240G	Coarse Red Ap 881176	Coarse Red Ap 881182	Coarse Red Ap 881194	Coarse Red Ap 881237	Coarse Red Ap 881317
Li	2.54	3.19	52.07	8.51	11.81	5.69	8.00	4.32
Be	6.55	0.23	4.93	0.72	1.13	1.49	0.64	1.07
Sc	3.38	4.63	11.21	3.96	4.51	4.54	4.13	5.36
V	1.20	22.72	91.94	43.85	36.47	26.04	16.87	21.42
Rb	0.04	0.61	24.78	0.50	0.71	0.56	0.96	0.66
Sr	0.29	12352.15	5419.48	6075.04	7571.63	6649.14	8759.80	7992.25
Y	0.07	794.04	441.36	790.24	651.56	660.62	520.67	641.95
Zr	0.07	101.09	33.29	30.52	5.86	7.78	7.20	11.42
Nb	0.04	0.30	5.03	0.25	0.14	0.31	0.09	0.36
Mo	0.12	0.41	3.28	0.68	0.34	0.77	0.41	0.30
Cs	0.01	0.02	0.69	0.05	0.04	0.05	0.28	bdl
Ba	0.07	1123.02	20951.06	2257.16	987.60	2599.69	15256.19	158.29
La	0.07	3851.37	6816.13	7305.48	5201.57	4744.16	4365.58	2886.25
Ce	0.01	10293.40	14215.44	21111.57	11380.04	11804.27	9258.97	7663.74
Pr	0.46	1877.44	2118.12	3117.40	1889.82	2173.80	1499.49	1379.18
Nd	0.11	7858.21	7894.86	12314.34	7620.67	8514.24	6139.67	6016.94
Sm	0.01	1368.35	1055.38	1752.57	1207.95	1386.28	987.69	1077.08
Eu	0.14	314.34	232.85	395.18	279.71	317.15	221.77	258.66
Gd	0.01	783.94	533.93	872.18	664.50	708.68	547.60	618.44
Tb	0.12	33.26	11.49	22.99	26.60	28.84	22.87	31.93
Dy	0.01	222.69	130.80	244.12	181.98	203.65	157.15	186.93
Ho	0.07	25.35	13.81	26.95	20.70	23.36	18.15	22.33
Er	0.01	58.21	33.61	63.97	48.26	54.56	42.24	50.13
Tm	0.01	5.04	2.82	5.36	4.05	4.68	3.62	4.47
Yb	0.03	28.37	16.04	31.64	23.76	27.61	19.87	25.08
Lu	0.14	3.91	2.33	4.41	3.39	3.77	2.79	3.33
Hf	0.02	1.02	0.50	bdl	bdl	bdl	bdl	bdl
Ta	0.04	bdl	0.14	bdl	bdl	bdl	bdl	bdl
Tl	0.04	0.06	0.11	bdl	bdl	bdl	bdl	bdl
Pb	0.08	69.08	41.10	40.47	76.95	71.50	37.64	33.91
Bi	0.04	1.03	1.58	3.63	0.98	1.42	1.20	1.12

Element	Det. lmt. (ppm)	Green Ap HL-06-75	Green Ap 881240G	Coarse Red Ap 881176	Coarse Red Ap 881182	Coarse Red Ap 881194	Coarse Red Ap 881237	Coarse Red Ap 881317
Th	0.05	782.71	728.39	1554.29	595.21	1080.46	282.17	306.47
U	0.03	105.28	66.96	57.54	82.87	118.97	60.93	68.66
P	36.45	120131.91	74098.82	123200.83	121061.93	118758.02	123234.02	157171.94
Ti	6.90	7.64	1715.93	bdl	194.46	9.46	bdl	bdl
Cr	1.46	bdl	7.51	2.18	41.31	bdl	bdl	bdl
Co	0.11	0.76	25.66	2.43	2.96	1.56	2.83	1.31
Ni	0.38	2.91	24.04	4.77	4.01	3.33	5.79	2.82
Cu	3.35	bdl	160.39	bdl	bdl	bdl	5.32	bdl
Zn	1.56	18.94	84.94	31.78	48.83	32.68	35.83	30.70
Ge	0.06	6.41	6.46	6.64	2.88	6.97	6.24	4.44
As	1.81	81.04	59.85	147.79	81.23	85.77	88.52	96.02
Ag	0.05	bdl	0.10	0.10	bdl	bdl	bdl	bdl
Cd	0.12	bdl	bdl	bdl	bdl	0.17	bdl	bdl
Sn	0.09	bdl	0.73	bdl	1.15	bdl	2.07	0.25
Sb	0.05	bdl	bdl	bdl	bdl	bdl	0.07	bdl
W	0.18	0.26	0.64	2.71	0.59	0.72	0.34	0.35
Mn	0.28	395.77	489.38	565.37	714.42	353.89	455.47	385.50
Ga	0.35	1.12	bdl	bdl	0.93	bdl	44.48	bdl

All values in ppm. Bdl – below detection limit.